Uppsala University
Signals and Systems

THE MULTIVARIABLE DECISION FEEDBACK EQUALIZER

Multiuser Detection and Interference Rejection

Claes Tidestav

UPPSALA UNIVERSITY 1999

Dissertation for the degree of Doctor of Philosophy
in Signal Processing at Uppsala University, 1999

ABSTRACT

Tidestav, C., 1999. The Multivariable Decision Feedback Equalizer: Multiuser Detection and Interference Rejection, 201 pp. Uppsala. ISBN 91-506-1371-5.

The multivariable decision feedback equalizer (DFE) is investigated as a tool for multiuser detection and interference rejection. Three different DFE structures are introduced. The first DFE has a non-causal feedforward filter and a causal feedback filter. We show how its parameters can be tuned to give a minimum mean-square error. The second DFE is derived under the constraint of realizability. The explicit structure and design equations for an optimum realizable minimum mean-square error DFE are obtained. The zero-forcing criterion is also considered, and conditions for the existence of a zero-forcing solution are derived. We then consider a DFE where both feedforward and feedback filters are FIR filters of predetermined degrees. We discuss the tuning procedure for obtaining the parameters of a minimum mean-square error DFE and present the conditions for the existence of a zero-forcing solution. Two specific applications are considered next. In the first scenario, an antenna array is used at the receiver in a cellular system to accomplish spatial division multiple access. We compare two DFEs, operating as multiuser detectors and interference cancellers, respectively, and it is demonstrated that the difference in performance is small when few users are active in the system. We also show that the parameter estimation problem is more complicated for interference rejection. The second application is multiuser detection in DS-CDMA. A family of minimum mean-square error detectors with different amounts of decision feedback is designed, based on a possibly rapidly time-varying linear model. The linear model includes effects of the multipath channel, pulse shaping filters and the spreading. We also show that near-far resistance of the minimum mean-square error detectors can be guaranteed if and only if the parameters of the detector can be tuned so that the zero-forcing condition is fulfilled.

Keywords: Decision feedback equalizer, multiuser detection, interference rejection, antenna arrays, DS-CDMA, near-far resistance

Claes Tidestav, Signals and Systems, Uppsala University, P O Box 528, SE-751 20 Uppsala, Sweden. Email: claes.tidestav@signal.uu.se.

ISBN 91-506-1371-5
Printed in Sweden by Elanders Digitaltryck AB, Angered 1999
Distributed by Signals and Systems, Uppsala University, Uppsala, Sweden

To my parents

CONTENTS

Acknowledgments

I want to express my sincere gratitude to my supervisors, Professor Anders Ahlén and Dr Mikael Sternad. During my five years as a Ph.D. student, I have come to appreciate their scientific curiosity and willingness to share thoughts and ideas about anything from quality of sun glasses to university politics. I have gotten used to the comforting sound of Anders' laughter, which can be heard all through the corridor. I am also grateful to Anders for introducing me to the higher levels of the university bureaucracy, thereby deterring me from pursuing an academic career. Mikael, who thinks every time has an "academic quarter of an hour" associated with it, has an attitude which is so positive, that he agrees with anything you say to him. Neither of my supervisors ever says "no" to any suggestion you approach them with.

My two closest friends during my Ph.D. studies are Jonas Öhr and Dr Lars Lindbom. Jonas has a unique ability to always understand what I say to him. He is also a person with very large practical skills, for which I envy him. I am also very impressed by his long and winding road to academic studies. I consider Lars to be my mentor. During our walks in his final year as a Ph.D. student, Lars and I shared many thoughts about life and graduate education.

Erik Lindskog has my appreciation for convincing me to work with him when neither of us had the time for it. I also thank him for proof-reading parts of this manuscript. I thank Andreas Jakobsson for his many social initiatives and Torbjörn Ekman for many calm philosophical discussions and bad jokes.

I also want to thank all the people working at Signals and Systems for providing a relaxed research environment. It has been fun to witness the formation of such a dynamic group. I am also grateful to all the current and former Ph.D. students of the Systems and Control Group. It has been a privilege to get to know so many talented individuals.

During my graduate studies, I have had the opportunity to work closely with the Antenna Systems and Propagation Research Group at Ericsson Radio Systems

AB. This has been very rewarding for me and has made me realize that it is important to study the correct problems. I am very grateful to Dr Sören Andersson, Dr Ulf Forssén, Dr Ari Kangas and Mr Henrik Damm for providing me with this opportunity.

Many years ago, my parents taught me that education is important, and that you should always try your best. I realize that without this background, it is not likely that I would have written this thesis. I am also grateful for their support and the support of my sister, although I have never quite managed to explain exactly what I have been doing during all these years.

At the very end of my graduate education, I realize how much I appreciate coming home every day. My dear wife Åsa provided me with a warm home environment, and kept my mind off research and signal processing. Åsa also taught me to get up early in the morning, a lesson I learned so well that the pupil now outshines the teacher. For these and many other things, I will always be grateful.

Claes Tidestav
Uppsala, October 1999.

Remarks on the notation

In this thesis, we will almost exclusively use linear, discrete-time filter and channel descriptions. A scalar and causal, discrete-time filter can be represented by an infinite power series in the unit delay operator q^{-1}:

$$\mathcal{T}(q^{-1}) = \sum_{n=0}^{\infty} t_n q^{-n} \, .$$

For any signal $x(k)$, $q^{-1}x(k) = x(k-1)$. The output of the linear filter $\mathcal{T}(q^{-1})$ is given by

$$y(k) = \mathcal{T}(q^{-1})x(k) = \sum_{n=0}^{\infty} t_n q^{-n} x(k) = \sum_{n=0}^{\infty} t_n x(k-n)$$

when the time series $x(k)$ is applied to its input. In general, the coefficients $\{t_n\}_{n=0}^{\infty}$ will be complex-valued. When discussing frequency domain properties of the filters, we will often replace the operator q^{-1} with the complex variable z^{-1}.

A linear filter of finite order can be described by a *ratio between two polynomials in* q^{-1}:

$$\mathcal{T}(q^{-1}) = \frac{B(q^{-1})}{A(q^{-1})} \, ,$$

where

$$\begin{aligned} A(q^{-1}) &\stackrel{\triangle}{=} 1 + a_1 q^{-1} + \cdots + a_{\delta a} q^{-\delta a} \\ B(q^{-1}) &\stackrel{\triangle}{=} b_0 + b_1 q^{-1} + \cdots + b_{\delta b} q^{-\delta b} \, . \end{aligned}$$

When the time series $x(k)$ is applied to the input of a filter described by such a rational function, the output will be given by

$$y(k) = -\sum_{n=1}^{\delta a} a_n y(k-n) + \sum_{n=0}^{\delta b} b_n x(k-n) \, .$$

The filter is called *stable* if all the roots of $A(z^{-1}) = 0$ have magnitudes which are strictly less than one.

Many important filters have finite impulse responses. Such FIR filters will be described by *polynomials in q^{-1}:*

$$y(k) = P(q^{-1})x(k) = p_0 x(k) + p_1 x(k-1) + \cdots + p_{\delta p} x(k - \delta p) \; .$$

The parameter δp is called the *degree* of the polynomial. A polynomial is said to be *monic* if $p_0 = 1$.

A causal *multiple-input multiple-output (MIMO)* filter with n_x inputs and n_y outputs can be described by the infinite series

$$\boldsymbol{\mathcal{T}}(q^{-1}) = \sum_{n=0}^{\infty} \mathbf{T}_n q^{-n}$$

where $\mathbf{T}_n$ are matrices with n_y rows and n_x columns. Proceeding as for the scalar filters, a MIMO filter of finite order will be described by the *rational matrix*

$$\boldsymbol{\mathcal{T}}(q^{-1}) = \begin{pmatrix} \mathcal{T}_{11}(q^{-1}) & \dots & \mathcal{T}_{1n_x}(q^{-1}) \\ \vdots & & \vdots \\ \mathcal{T}_{n_y 1}(q^{-1}) & \dots & \mathcal{T}_{n_y n_x}(q^{-1}) \end{pmatrix}$$

where

$$\mathcal{T}_{ij}(q^{-1}) = \frac{B_{ij}(q^{-1})}{A_{ij}(q^{-1})}$$

are scalar rational functions as described above. The rational matrix $\boldsymbol{\mathcal{T}}(q^{-1})$ is called stable if all its elements are stable. Also, an FIR MIMO filter will be described by the *polynomial matrix*

$$\boldsymbol{P}(q^{-1}) = \begin{pmatrix} P_{11}(q^{-1}) & \dots & P_{1n_x}(q^{-1}) \\ \vdots & & \vdots \\ P_{n_y 1}(q^{-1}) & \dots & P_{n_y n_x}(q^{-1}) \end{pmatrix} \; ,$$

or equivalently by the *matrix polynomial*

$$\boldsymbol{P}(q^{-1}) = \mathbf{P}_0 + \mathbf{P}_1 q^{-1} + \cdots + \mathbf{P}_{\delta P} q^{-\delta P} \; .$$

The parameter δP is called the degree of the polynomial matrix (and the matrix polynomial), and equals the highest degree of any of the elements in the polynomial

matrix. The polynomial matrix $\boldsymbol{P}(q^{-1})$ is said to be monic when $\mathbf{P}_0 = \mathbf{I}$, where $\mathbf{I}$ is the identity matrix.[1]

Special cases of MIMO filters are single-input multiple-output (SIMO) and multiple-input single-output (MISO) filters, which will be described by rational (polynomial) column vectors and rational (polynomial) row vectors, respectively.

A rational matrix may be represented by a *matrix fraction description (MFD)*, which can be either left

$$\boldsymbol{\mathcal{T}}(q^{-1}) = \boldsymbol{A}^{-1}(q^{-1})\boldsymbol{B}(q^{-1})$$

or right

$$\boldsymbol{\mathcal{T}}(q^{-1}) = \tilde{\boldsymbol{B}}(q^{-1})\tilde{\boldsymbol{A}}^{-1}(q^{-1}) \; .$$

Above, $\boldsymbol{A}(q^{-1})$, $\boldsymbol{B}(q^{-1})$, $\tilde{\boldsymbol{A}}(q^{-1})$, and $\tilde{\boldsymbol{B}}(q^{-1})$ are polynomial matrices of dimensions $n_y \times n_y$, $n_y \times n_x$, $n_x \times n_x$ and $n_y \times n_x$, respectively.

For any linear MIMO filter $\boldsymbol{\mathcal{T}}(q^{-1}) = \sum_{n=0}^{\infty} \mathbf{T}_n q^{-n}$, we define the non-causal filter

$$\boldsymbol{\mathcal{T}}_*(q) \stackrel{\triangle}{=} \sum_{n=0}^{\infty} \mathbf{T}_n^H q^n \; ,$$

where $(\cdot)^H$ denotes complex conjugate transpose. If we apply this definition to any rational matrix $\boldsymbol{\mathcal{T}}(q^{-1})$, we obtain

$$\boldsymbol{\mathcal{T}}_*(q) = \boldsymbol{B}_*(q)\boldsymbol{A}_*^{-1}(q) = \tilde{\boldsymbol{A}}_*^{-1}(q)\tilde{\boldsymbol{B}}_*(q) \; .$$

Above, we have used *conjugate polynomial matrices*, which are defined as

$$\boldsymbol{P}_*(q) \stackrel{\triangle}{=} \mathbf{P}_0^H + \mathbf{P}_1^H q + \cdots + \mathbf{P}_{\delta P}^H q^{\delta P}$$

for any polynomial matrix $\boldsymbol{P}(q^{-1}) \stackrel{\triangle}{=} \mathbf{P}_0 + \mathbf{P}_1 q^{-1} + \cdots + \mathbf{P} q^{-\delta P}$. For polynomial matrices, we will also use the *reciprocal polynomial matrix*, defined by

$$\bar{\boldsymbol{P}}(q^{-1}) \stackrel{\triangle}{=} q^{-\delta P}\boldsymbol{P}_*(q) = \mathbf{P}_{\delta P}^H + \mathbf{P}_{\delta P-1}^H q^{-1} + \cdots + \mathbf{P}_0^H q^{-\delta P} \; .$$

[1] The $n_x \times n_x$ identity matrix will often be denoted $\mathbf{I}_{n_x}$.

CHAPTER 1

Introduction

EVER since Alexander Graham Bell patented the telephone in 1876, it has been possible for people to have private communication also when they are geographically separated. With the invention of switching, households could have their own telephone connection, and when the switching was automated during the 1930s and 1940s, telephony became a mass market.

During the next few decades, although the telephone systems expanded, and the quality of the transmitted speech kept improving, the consumers noted few fundamental changes in the operation of the telephone system. However, the number of subscribers and the amount of telephone usage were constantly growing. As the demand for transmission capacity grew, it became apparent that some of the current technical solutions were becoming impractical. In particular, this was true for the multiplexing. Multiplexing is the process whereby several calls are combined and sent in parallel over a common communication link. The multiplexing of the calls was based on frequency division, a technique that was becoming increasingly complex with the growing traffic.

New solutions were based on time division multiple-access (TDMA). However, TDMA is very difficult to implement in a system where the multiplexed information is analog. Gradually, the decision was made to convert telephone systems to use digital transmission. The process was pushed forward by the development of cheap but powerful digital circuits.

The introduction of a digital transmission format brought several additional advantages. The amplifiers could be made simpler, and it became easier to maintain the quality of the transmitted signals over long distances. The digital hardware proved to be cheaper and more reliable than its analog counterpart. Also, the in-

troduction of new transmission media with very high transmission capacity was greatly simplified.

However, the most important consequence of the digitalization of the backbone network was the ability to handle new services in a flexible way. This is particularly apparent today, when the voice traffic in the "telephone" system is less than half of the total traffic. The rest is generated by various flavors of data communication, which is inherently digital. For such information, digital transmission is the only reasonable alternative.

Handling the still increasing amount of digital traffic is today a large and important research area. Also, the explosive growth of digital cellular telephony provides new research challenges.

We will now introduce some of these issues, before introducing and motivating the main theme of this thesis: the multivariable *decision feedback equalizer (DFE)*. This DFE is a tool for suppressing two special types of interference which is present in digital communication. The thesis has two main parts. Chapters 2 and 3 present the theoretical background and discuss properties common to all applications of the DFE, whereas in Chapters 4 and 5, two specific applications are investigated.

We begin, however, with an introduction which provides the necessary background about digital communication, cellular systems and multivariable channel models.

1.1 Digital communications

Figure 1.1 shows an overview of a digital communication system. In this section, we will briefly discuss each of the blocks in Figure 1.1 with emphasis on the channel descriptions.

The *source* delivers the information to be transmitted. This information may be *analog* or *digital*. Speech, audio and video are examples of information from analog sources, since they can only be exactly represented by analog waveforms. On the other hand, digital sources deliver a stream of quantized values. The most important example of such a source is a computer, but in the future we can foresee several scenarios with machine-to-machine communication.

The non-trivial task of the *source encoder* is to represent the transmitted information using as few bits as possible. For analog sources, we try to model the unquantized waveform as closely as possible. Some modeling errors are then unavoidably introduced, and the encoder design always involves a trade-off between fidelity of reproduction and the bandwidth of the transmitted signal.

For a digital source on the other hand, we cannot allow any error: The transmitted signal must be perfectly reconstructible at the receiver. The source encoding

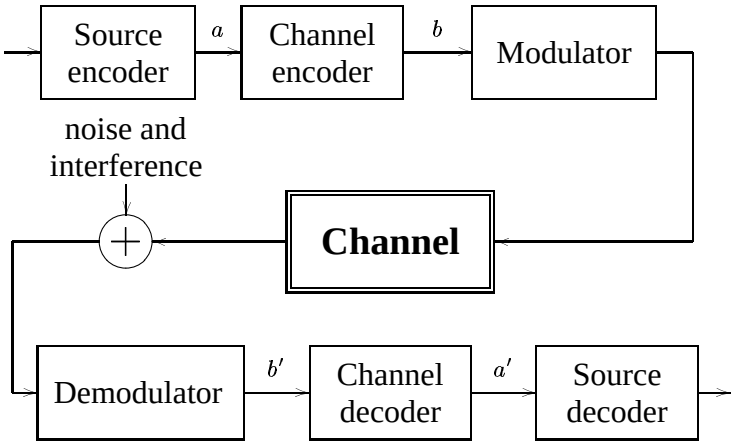

Figure 1.1: A digital communication system.

must in this case be *lossless*, and constitutes data compression. The most famous example of such data compression is the Huffman algorithm [39].

The source encoder delivers a stream of bits to the *channel encoder*, which in turn adds redundancy to the bit stream. With this redundancy, it is possible to perform error detection and error correction at the receiver.

Channel codes without memory are called *block codes*. The encoder for a block code independently maps one block of k information bits onto a block of n bits, called a *code word*. The ratio k/n is called the *code rate*. Since the encoding is memoryless, both encoding and decoding can be efficiently implemented with a combinational logic circuit. Famous block codes include the Hamming, the BCH and the Reed-Solomon codes [48].

A convolutional code on the other hand has memory. A convolutional encoder also accepts blocks of k information bits from the source encoder, and maps them onto blocks of n bits. However, the output of the encoder depends not only on the present block of information bits, but also on the m preceding blocks. The constant m is known as the *constraint length* of the code. The encoder for a convolutional code can be implemented with a sequential logic circuit, containing shift registers and exclusive-OR gates. Convolutional codes are most often decoded by means of the Viterbi algorithm [30].

The next step in the communication process is the *modulation*. The purpose of the modulator is to transform the stream of bits from the channel encoder to an analog waveform that can be transmitted over the communication channel.

The modulation can be further separated into digital and analog modulation. The digital modulator collects a block of bits from the channel encoder and uniquely maps it onto the *symbol constellation*. Each block of bits are thus transformed into

one of M *symbols*, which may be complex valued. Examples of such mappings are shown in Figure 1.2. These complex-valued symbols will be used as input in

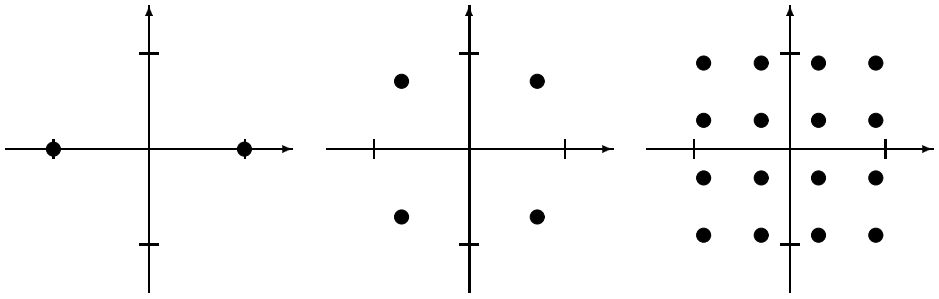

(a) Mapping for *binary phase-shift keying (BPSK)* ($M = 2$)

(b) Mapping for *quaternary phase-shift keying (QPSK)* ($M = 4$)

(c) Mapping for 16-*quadrature amplitude modulation (16-QAM)* ($M = 16$)

Figure 1.2: Examples of different mappings.

the discrete time channel models used throughout this thesis.

The purpose of the analog modulation is to superimpose these symbols on a radio frequency carrier. The modulator first splits the symbol into its real and imaginary parts. Each of these signals then pass through a *pulse shaping filter*. The continuous time signals at the output of these two pulse shaping filters are known as the *in-phase* and *quadrature* components respectively. The impulse response of the pulse shaping filter is chosen to control the bandwidth of these signals.

The in-phase and quadrature components constitute a *baseband* or *equivalent lowpass* representation of the signal. The baseband signal may also be represented by its *complex envelope.* The complex envelope is a complex-valued signal whose real part is the in-phase component and whose imaginary part is the quadrature component.

The next step in the communication process is to convert the baseband signal into a *passband* signal[1], which is real-valued and contains much higher frequencies. This is done by the last step in the analog modulation, the frequency up-conversion. By multiplying the in-phase component by $\cos 2\pi f_c t$ and the quadrature component by $\sin 2\pi f_c t$ and adding them, the center frequency of the signal is shifted from 0 to f_c. The choice of f_c depends on the application, but is often much larger than the bandwidth of the baseband signal. The passband signal is

[1]Not all communication systems use high frequency carriers. See [73, p. 186] for a discussion of system using only baseband signals.

then transmitted. The process of analog modulation is depicted in Figure 1.3.

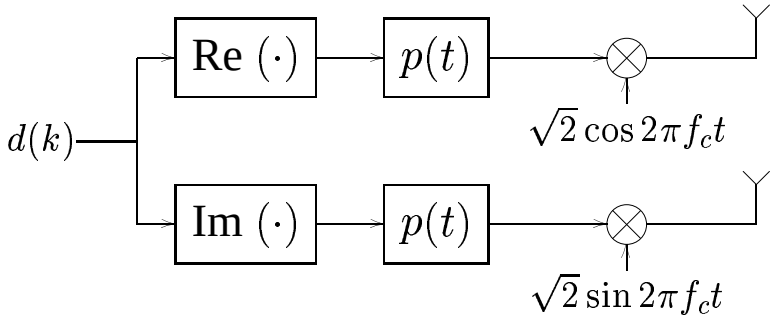

Figure 1.3: Analog modulation for linear modulation. The complex-valued symbols are separated into its real and imaginary parts and converted into a continuous-time waveform that can be transmitted.

When the baseband signal is not generated by linear filtering of the real and imaginary parts of the symbols, the modulation is called *non-linear.* The basic non-linear modulation method is *frequency-shift keying (FSK)*, where the information symbols control the carrier frequency.

The major disadvantage of FSK is that it occupies a large bandwidth. To remedy this problem, several modifications of FSK have been used. The most important is *continuous phase modulation (CPM)*. In CPM, the information symbols control the carrier phase, and the modulator parameters are tuned to trade-off bandwidth consumption for detector complexity.

When the signal travels through the channel, it experiences a damping and phase shift that is in general frequency dependent and time-varying. In a wireless channel, the frequency selectivity is caused by *multipath propagation*, that is, the signal travels via several different paths from the transmitter to the receiver. When the passband signal passes through electrical wires, various capacitances and inductances cause the frequency selective damping. Even optical communications suffer from this effect, since the propagation velocity in the optical fiber depends on the wavelength. This phenomenon is known as *chromatic dispersion.*[2]

In the time domain, the effect of the frequency selectivity is that a single transmitted pulse is received as a pulse train. The duration of this pulse train is called the *delay spread* of the channel. When a digital signal signal is sent over a frequency selective channel, the received signal is said to suffer from *intersymbol interference.*

The temporal variations in the channel are caused by the movement of the receiver or the transmitter.[3] The carrier frequency will thus experience a *Doppler*

[2]This effect can be avoided by clever design of the transmitted pulse. See [47, p. 141]

[3]Any mismatch between the carrier frequency and the frequency of the local oscillator in the

shift for which the receiver may be unable to compensate. When the transmission is distorted by severe multipath propagation in such a non-stationary scenario, the signal will even experience a Doppler *broadening.* A single sinusoid may then be received as a signal with non-zero bandwidth.

The communication is always impaired by *noise.* The stochastic noise process is described by its distribution and color. Noise is almost always assumed to contain a component that is Gaussian distributed. To describe the noise color, the power spectral density is most often used. The most common noise model assumes that the power spectral density is constant over some frequency interval and zero outside it. Such a model is appropriate for the *thermal noise*, which is caused by the thermal motion of the electrons in the material.

The communication may also be adversely affected by *co-channel interference (CCI), multiple-access interference (MAI)* or *cross-talk.* These three terms are used in different application scenarios to describe the same impairment: interference from other signals that share the same channel.

At the receiver, the steps are carried out in reversed order. The demodulator converts the signal to an equivalent lowpass representation. The in-phase and quadrature signals are sampled, and a discrete-time complex signal is formed. The demodulator must then suppress the impact of noise and interference to produce an estimate of the transmitted symbol. This estimate may be passed directly to the decoder, or it may be quantized to produce a *hard* decision on what symbol was transmitted. In the latter case, we have *detected* what symbol was transmitted.

The channel decoder then tries to find the most probable sequence of information bits, using the symbol estimates and the redundancy introduced by the channel encoder. When the decoder uses unquantized symbol estimates, the decoding is said to be *soft*, whereas with quantized symbol estimates, it is called *hard*. Finally, the source decoder restores the original information.

The performance of a digital communication system is usually expressed in terms of error rates. Two bit streams, which should ideally be identical, are compared. The number of bits that are different in the two streams is divided by the total number of bits to obtain the *Bit Error Rate (BER)*. Referring to Figure 1.1, we can for instance compare the bit streams at a and a' to obtain the *coded* BER. We may also compare the bit streams at b and b' to obtain the *uncoded* or *raw* BER. In this thesis, we will use the uncoded BER as a performance measure.

receiver will also cause a time-varying channel.

Equivalent discrete-time channels

It should be evident from the above discussion that a communication system is very complex, even if we only study the detection problem. Therefore, several simplifications are commonly used when designing and analyzing detection problems in the context of communication systems. One simplification is the consequent use of baseband signals and models. Modeling the frequency up- and down-conversion then becomes unnecessary. A disadvantage of this approach is that we have to work with systems where the transfer function parameters are *complex-valued.* This unexpected property is explained in for instance [85].

Analysis of the detection process can be further simplified if we use an equivalent discrete-time channel model to describe the transmission. This channel model relates the complex-valued symbols to the sampled version of the received complex-valued signal. This channel must then model not only the equivalent lowpass representation of the passband channel, but also effects of the modulation and the transmit and receive filters.

We will further constrain the channel model to be *linear*. At discrete-time instant k, the channel can thus be described by the infinite series

$$\mathcal{H}_k(q^{-1}) = \sum_{n=0}^{\infty} h_{n,k} q^{-n} \ . \tag{1.1}$$

This means that in general, non-linear modulation methods, such as CPM can not be accommodated. Some CPM schemes can, however, with a simple non-linear transformation at the channel output, be converted to a system that can be modeled as linear with good approximation [46].

In general, the model (1.1) is of infinite order. It is impossible to estimate the parameters of an infinite-order linear model using a finite number of data. Therefore, we will assume that the channel can be represented by a linear model of finite order. Such a model can be described by a rational function

$$\mathcal{H}_k(q^{-1}) = \frac{B_k(q^{-1})}{A_k(q^{-1})} \ , \tag{1.2}$$

where

$$\begin{aligned} B_k(q^{-1}) &\triangleq b_{0,k} + b_{1,k} q^{-1} + \cdots + b_{\delta b,k} q^{-\delta b} \\ A_k(q^{-1}) &\triangleq 1 + a_{1,k} q^{-1} + \cdots + a_{\delta a,k} q^{-\delta a} \end{aligned}$$

are polynomials of finite order in q^{-1} with complex coefficients.

Using the linear channel model (1.2), we can express the received signal as

$$y(k) = \mathcal{H}_k(q^{-1}) d(k) + v(k) \ , \tag{1.3}$$

where $y(k)$ is the received signal, sampled at the discrete time instant k. Similarly, $d(k)$ is the symbol transmitted at time k, and $v(k)$ constitutes noise and interference.

Throughout this thesis, we will use discrete-time channel descriptions to design detectors. No optimization is performed for the continuous-time filters that are inevitably present in a communication system. In particular, no continuous-time matched filter is used as an *a priori* component in the detector design. Instead, we assume that the anti-aliasing filtering and sampling is fixed, and we design detectors that optimally process the sampled signal. Since we have no control over the sampling, we cannot guarantee that the sampled signal constitutes a sufficient statistic of the received signal [72, 76]. The main reason for refraining from optimization of the continuous time filters is that in a real communication system, only fixed analog filters can be used.

The description (1.3) incorporates most channel models discussed in the literature. Below we briefly discuss the three most common, and show what additional properties the channel model (1.2) has in each case.

1. *The additive white Gaussian noise (AWGN) channel.* For the AWGN channel, the received signal can be modeled as

   $$y(k) = b_0 d(k) + v(k)$$

   where $v(k)$ is white Gaussian noise with variance σ^2. The coefficient b_0 is a fixed constant.

2. *The flat fading channel.* For the flat fading channel, the received signal can be modeled as

   $$y(k) = b_0 d(k) + v(k)$$

   where $v(k)$ is noise with variance σ^2. Often the noise is assumed to be Gaussian and white, but this is not a prerequisite for the channel model. The coefficient b_0 is no longer a fixed constant. Rather it is a stochastic variable, with a specified distribution. The two most common cases are

   - The *Rayleigh fading channel.* In this case, the channel coefficient b_0 is a zero mean complex circular Gaussian distributed stochastic variable, or equivalently

     $$b_0 \in \mathcal{CN}(0, \sigma_b) \ .$$

- The *Ricean fading channel.* In this case, the channel coefficient b_0 is a complex circular Gaussian distributed stochastic variable with non-zero mean, or equivalently

$$b_0 \in \mathcal{CN}(m_b, \sigma_b) \ .$$

For both these fading channels, the names are derived from the distribution of the absolute value of b_0: For the Rayleigh fading channel, $|b_0|$ is Rayleigh distributed, whereas it for the Ricean fading channel has a Rice distribution. See [37].

3. *The frequency selective fading channel.* A general frequency selective channel is described by (1.2) with $\delta a > 0$ or $\delta b > 0$. However, especially in wireless communications, it is common to use a model with a finite, rather than an infinite, impulse response, in which case $\delta a = 0$. The channel coefficients in a frequency selective channel are frequently modeled as stochastic variables with Rayleigh or Ricean distributed amplitudes.

For the two last channels, the channel coefficients will in general be time-varying.

Remark 1. Note that the term *fading* can mean two things:

- A channel is said to be fading if it *varies* either with time or frequency.
- A channel is also said to be fading if the parameters which describe the channel are *stochastic variables*, drawn from a specific distribution.

In this thesis, all considered channels will be frequency selective. The process of combating the effects of frequency selective fading is the topic of the next section.

1.2 Equalization and the decision feedback equalizer

Suppressing intersymbol interference, or equivalently removing the effect of a frequency selective channel is known as *equalization.* In the process, the spectrum of the received signal becomes flat, hence the name equalization.

EXAMPLE 1.1

The intersymbol interference can be quite severe. As an example, consider the detection of a QPSK modulated signal, transmitted over a four-tap channel ($\delta b = 3$, $\delta a = 0$ in (1.2)). In Figure 1.4, the received complex-valued sampled signal

is displayed before and after equalization. Without intersymbol interference, the received signal should appear as small clouds, centered around the points in the symbol constellation, depicted in Figure 1.2(b).

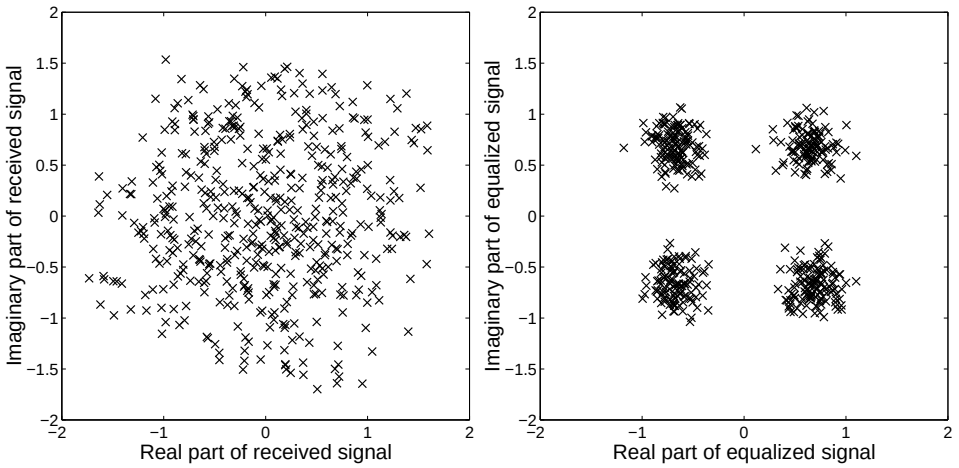

(a) Real and imaginary parts of the 500 received samples *before* equalization.

(b) Real and imaginary parts of the 500 received samples *after* equalization.

Figure 1.4: Scatter plots of the received signal before and after equalization. Prior to equalization, it is impossible to see that the transmitted signal is QPSK modulated.

We see that we have to compensate for the intersymbol interference. Any attempt to detect the transmitted symbols without such compensation would be futile: There is no trace of the QPSK constellation in Figure 1.4(a).

The first attempt to solve the equalization problem was the *linear transversal* equalizer, which is depicted in Figure 1.5. The received sampled baseband signal,

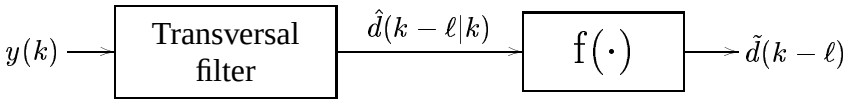

Figure 1.5: The linear transversal equalizer, in which the received signal is fed through a single FIR filter to produce an estimate of the received symbol.

corrupted by ISI and noise, is used as input to an FIR filter. The coefficients of this filter are adjusted to produce an estimate of the transmitted symbol. This esti-

mate is then quantized to produce one of the symbols in the symbol constellation. Although this equalizer is able to remove most of the ISI, its performance is poor for channels $B(q^{-1})$ for which the zeros of $B(z^{-1})$ are close to the unit circle. The linear equalizer will also tend to amplify the noise, which will lead to frequent decision errors.

Much better performance is obtained with *maximum likelihood sequence estimation (MLSE)*. The MLSE searches among all possible transmitted sequences for the sequence with which the conditional probability of the received signal is maximized. This statement can be formally expressed as follows: Consider the sequence of received sampled signals $\mathrm{Y} = \{y(k)\}_{k=1}^{N}$. Assume that a channel model and a noise description are available so that we can calculate the conditional probability $p(\mathrm{Y}|\mathrm{D})$ of the received sequence Y for any admissible input sequence $\mathrm{D} = \{d(k)\}_{k=1}^{N}$. The maximum likelihood sequence estimate is then

$$\{\tilde{d}(k)\}_{k=1}^{N} = \arg\max_{\mathrm{D}} p(\mathrm{Y}|\mathrm{D}) \ .$$

When the noise is Gaussian, maximizing the conditional probability $p(\mathrm{Y}|\mathrm{D})$ is equivalent to minimizing the sum of the squared differences between the received signals and the corresponding model outputs. Furthermore, when the impulse response of the channel is finite and the noise is white, the MLSE can be efficiently implemented using the Viterbi algorithm [29]. Still, the complexity is very high for long channels and large symbol alphabets: When M-ary modulation is used in a channel with L taps, the number of multiplications necessary for detecting one symbol is approximately equal to M^L.

An equalizer that performs almost as well as the MLSE at a complexity only slightly higher than the linear equalizer is the *decision feedback equalizer (DFE)*. Thus, the DFE — depicted in Figure 1.6 — constitutes an attractive compromise between complexity and performance. The received signal is here used as an input

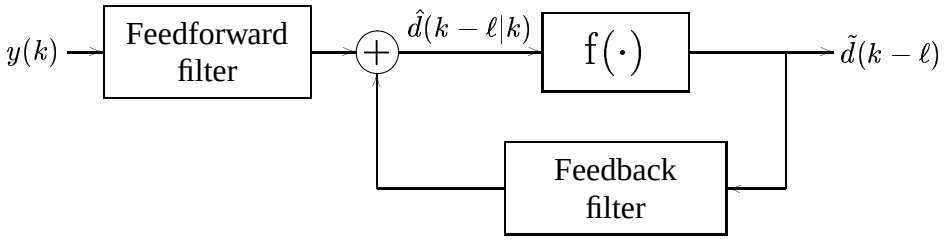

Figure 1.6: The scalar decision feedback equalizer (DFE).

to the *feedforward filter*. From the output of the feedforward filter, the interference from previously detected symbols are removed via the output of the *feedback filter*.

The difference between these two filter outputs constitutes an estimate of the transmitted symbol. This estimate is sometimes called *soft*, since it is not yet quantized. The decision device quantizes the soft estimate and the resulting *hard* estimate is used as input of the feedback filter to remove its effect on future symbol estimates. The constant ℓ is known as the *decision delay* or the *smoothing lag*. It specifies how many future measurements which are processed before a decision is made on the present symbol.

For a thorough understanding of the equalization process, we will study the impulse response between the transmitted symbols and the various signals in Figure 1.6. Starting at the channel output, we, of course, obtain the impulse response of the channel, as depicted in Figure 1.7.

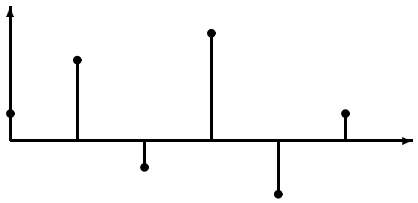

Figure 1.7: The impulse response of the channel.

The partly equalized channel at the output of the feedforward filter is depicted in Figure 1.8. The purpose of the feedforward filter in a DFE is to suppress the first $\ell - 1$ taps in the equalized channel impulse response, the so-called *precursor* ISI. The feedforward filter must also try to keep tap ℓ, the so-called *reference tap* close to unity.

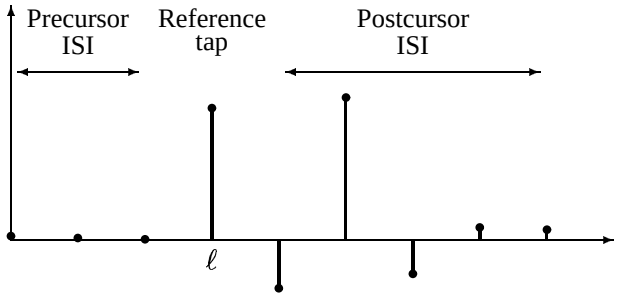

Figure 1.8: The signal at the output of the feedforward filter: The precursor has been suppressed, whereas the reference tap is close to one and the remaining taps are arbitrary.

The feedback filter will be tuned so that its impulse response matches the

postcursor ISI, that is, the taps $\ell + 1, \ell + 2$ and so forth in the partly equalized channel. When the output of the feedback filter is subtracted from the output of the feedback filter, we obtain the impulse response shown in Figure 1.9. This impulse response relates the symbol estimate to the transmitted symbols.

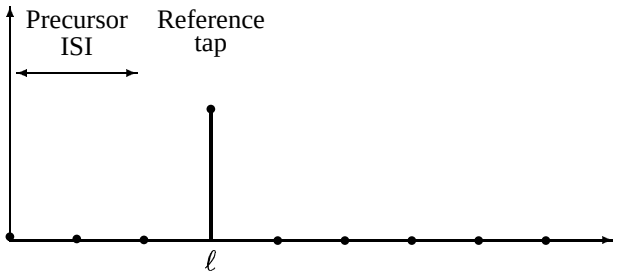

Figure 1.9: The complete equalized channel. Note that the postcursor has been obliterated.

The use of decision feedback to combat intersymbol interference was originally proposed by Austin in [10]. However, it was Monsen [63] who put the DFE on a sound mathematical and practical basis.[4] The three major contributions in the paper [63] were

- *The assumption of correct past decisions.* Monsen assumed that all previous outputs from the decision device coincide with the transmitted symbols they estimate.
- *The MMSE criterion.* Monsen suggested that the DFE coefficients should be tuned so that the mean-square error of the soft symbol estimate is minimized.
- *The structure of the DFE.* Monsen showed that the optimum DFE with infinite smoothing lag has a feedforward filter with a matched filter as a factor. Both the feedforward and the feedback filters will be IIR filters. He also suggested that in practice, a DFE with FIR filters in the feedforward and feedback paths should be used and he showed that the coefficients of these filters can be tuned from the Wiener-Hopf equations.

Most DFE derivations during the last 30 years use these three properties.

The assumption of correct previous decisions will almost surely be violated. Therefore, the performance of a DFE that is tuned assuming correct decisions but implemented using real decisions will almost always be suboptimum. However,

[4] For a comprehensive review of the first ten years of DFE research, see [13].

finding a DFE without the assumption of correct decisions is much more difficult. Also, more elaborate schemes — for instance, those that model the effect of incorrect past decisions as an additive noise term [80] — often give only minor improvements. The main reason for this is that in realistic communication scenarios, the probability of error is so small that almost all previous decisions are correct.

When an incorrect decision is made, the probability for subsequent decision errors will increase, since all postcursor ISI cannot be removed. A single erroneous decision may thus cause an *error burst*. Such *error propagation* degrades the performance of the DFE, and considerable effort has been spent on deriving bounds on the DFE error probability when the error bursts are taken into account [15, 26, 44]. However, even when error bursts are considered, the performance of the DFE is still superior to that of the linear equalizer.[5] In Chapter 3, we will see that the error propagation becomes worse, as the length of the impulse response of the feedback filter increases.

Virtually all papers about DFEs use one of the structures suggested by Monsen. This is a bit remarkable, since the optimum structure with infinite smoothing lag cannot be implemented in practice and the performance of a DFE with FIR structure is suboptimum.

This dilemma was resolved in 1990, when Sternad and Ahlén published a paper [79] that dealt with the optimization of the DFE structure under the constraint of realizability. This work has received little attention, and subsequent proposals of realizable DFEs with IIR filters are more *ad hoc* [21].

The purpose of this thesis is to provide a multivariable generalization of these scalar DFEs. Such a multivariable DFE can be used in a system, where several measurement signals are used to estimate the symbols transmitted from several sources. This situation occurs frequently in mobile telephone systems, and Chapters 4 and 5 are devoted to the study of two such scenarios. To facilitate understanding of these two chapters, we will now give a short introduction to mobile telephone, or *cellular* systems.

1.3 Cellular communications

In the last decade of the 19th century, the 21-year old Italian student Guglielmo Marconi brought the world into the era of wireless communication. He managed to transfer a message between two stations using radio waves. Only six years later, in 1901, Marconi succeeded in transmitting a message across the Atlantic. For these achievements, Marconi shared the Nobel Prize in physics in 1909.

[5] This is true for scalar channels. For channels with a single input and several outputs, the difference between a linear equalizer, a DFE and even the MLSE tends to diminish [20].

By the time Marconi received the Nobel Prize, radio transmitters had already been installed on ships all over the world. The wireless telegraph was a blessing for the maritime fleet: For the first time, it was possible to send distress calls irrespective of the weather conditions. It also became possible to receive weather reports and other messages from shore. On the Titanic in 1912, it was even possible to send personal radio messages.

During the next few decades, radio transceivers found their way into more and more areas. In 1946, the world's first [60] public mobile telephone system was introduced in St Louis. The idea with this system was to supply the same services to mobile terminals that were available in the fixed telephone network. Within a year, 25 other American cities had mobile networks in operation. Each city had one *base station*, which was designed to cover as large area as possible. Every mobile in this area communicated with the base station, which relayed the calls through its connection with the fixed network.

With this system, the number of simultaneous calls that can be handled is limited by the available spectrum. Another disadvantage is that the transmitter power of the mobile terminals must be rather high to reach the base station.

Already in 1947, a solution to these two problem was devised: the cellular system.

The cellular concept

The starting point was this: How do we provide private wireless communication services to mobile customers within a certain area? The original solution with a single powerful base station transmitter is depicted in Figure 1.10. The system has

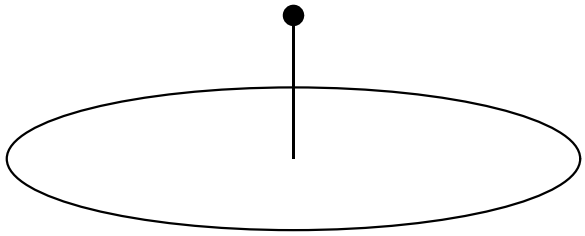

Figure 1.10: A cellular system with a single cell.

access to N frequencies, which can be used to communicate with the mobiles in its coverage area. Half of these frequencies are used for transmission from the base station to the mobiles, and the remaining frequencies are used for transmission from the mobiles to the base station. The former link is known as the *downlink* or *forward link*, and the latter is called the *uplink* or *reverse link*. In total, the system

can accommodate $N/2$ users.

Another solution is to build several base stations within the area, as depicted in Figure 1.11. Each of the base stations can now use $N/6$ frequencies to set up

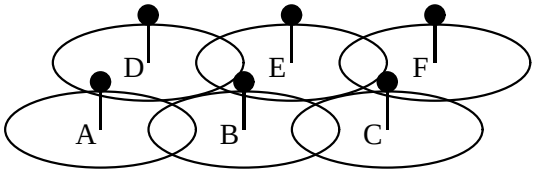

Figure 1.11: A cellular system with 6 cells.

communication with at most $N/12$ mobiles in its coverage area. The system as a whole can thus still handle (at most) $6 \times N/12 = N/2$ simultaneous calls.

However, since each base station only covers a smaller area, it is possible to reduce the antenna height and the transmitter power so that the range of the base stations is reduced. This leads to reduced interference from neighboring transmissions, making it possible to *reuse* frequencies. Taking the network in Figure 1.11 as an example, base stations A and F may use the same frequencies, and so may base stations C and D. The available frequencies can then be divided into only four groups with $N/4$ frequencies in each. The system can then handle $6 \times N/8 = 3N/4$ simultaneous calls. By building additional base stations, we have thus increased the system capacity. As a bonus, the mobiles can lower their transmit powers, and hence their power consumption, which extends the battery life time.

This is the *cellular concept.* A geographical area, which can be arbitrarily large, is divided into a number of *cells.* With each cell, we associate one base station, which provides wireless access to all mobiles in the cell. The base station is equipped with a transmitter and a receiver and is connected to a fixed network. The frequencies used by the base station for transmission and reception are reused by a base station some distance away. The smaller the reuse distance, the larger the system capacity.

When a mobile moves across a cell boundary, control of the call must be transferred from one base station to another. This process is known as *handover* or *hand off*. Making a handover without interrupting the telephone call was one of the major problems that delayed the introduction of a fully automatic commercial cellular system until the early 1980s.

Multiple-access methods

In the system we have described so far, the users are granted exclusive access to a communication channel by assigning to each user a different frequency. This method is known as *frequency division multiple-access (FDMA)*, and was used in the so-called first generation systems. These systems used analog technology and frequency modulation. Examples of such systems are the Nordic standard NMT[6], the British standard TACS[7] and the North American standard AMPS[8].

Modern cellular systems are digital and use a combination of FDMA and *TDMA/CDMA*. In a TDMA (*time division multiple-access*) system, different users are assigned different *time slots*. The duration of such a time slot differs among different standards, but is typically on the order of milliseconds. In each time slot, one user transmits a *burst* of digital data. Examples of cellular systems which use TDMA are GSM[9], the North American standards IS-54 and IS-136 which are sometimes collectively labeled D-AMPS[10] and the Japanese standard PDC[11]. All these systems belong to the second generation of cellular systems.

In a system employing *code division multiple-access* or CDMA, all users within a cell concurrently share the same bandwidth. The most common CDMA flavor is called *direct sequence* CDMA (DS-CDMA). In DS-CDMA, the signal from each user is multiplied by a unique *signature waveform* prior to transmission, a process known as *spreading*. Since the signature waveform has a much larger bandwidth than the information bearing signal from the user, the CDMA signal constitutes a *spread spectrum* signal.

At the receiver, the sum of all the transmitted broadband signals is received. Conventionally, the signals from the different users are extracted by cross-correlation with the respective signature sequences. Under ideal conditions, the spread spectrum signals corresponding to different users will be orthogonal at the receiver. The output of each correlator will then be the transmitted signal of the desired user. This correlation receiver is known as the *conventional receiver*.

In practice, the spread spectrum signals corresponding to different users will be non-orthogonal at the receiver, and the output of all correlators will have contributions from all the transmitted signals. This interference is known as *multiple-access interference (MAI)* in the CDMA literature. Still, the conventional receiver will work well under the following two conditions:

[6] Nordic Mobile Telephone
[7] Total Access Communication System
[8] Advanced Mobile Phone Service
[9] Global System for Mobile communications
[10] Digital Advanced Mobile Telephone Service
[11] Personal Digital Cellular

- The correlation between the signature sequences is small.
- The signals from different users are received with approximately the same power.

The first condition can be fulfilled by careful design of the signature waveforms. The second condition can be fulfilled by accurate *power control*, which implies that the receiver measures the received power and instructs the transmitter to adjust its output power to obtain the desired performance.[12] Without power control, the powers of the received signals may differ significantly. This is the so-called *near-far problem*: A strong signal, typically originating near the receiver, will outpower a weak (far) signal.

All major operational CDMA based cellular networks are based on the IS-95 standard [84]. For the upcoming third generation of cellular systems, CDMA is the multiple-access method chosen for most proposals.

The challenge: to increase system capacity

The goal of any cellular system must be to provide powerful and flexible wireless services of high quality to as many users and at as low a cost as possible. Needless to say, this goal is easier to accomplish the larger the system capacity is.

At this point, it important to remember that we are trying to increase the capacity of the system as a whole. The *channel* capacity is limited by the available bandwidth and the signal-to-noise ratio. The channel capacity thus provides an upper bound on the capacity of a single-cell cellular system with a single base station antenna. On the other hand, the capacity of a multi-cell cellular system is in theory infinite.

To increase the capacity of a cellular system, several routes are possible. We mention just a few:

1. *Decrease the cell size.* This is the standard way of increasing the capacity of a cellular system. An additional advantage with this approach is that the life time of the mobile batteries is increased. However, reducing the cell size is expensive. This was certainly true for the simple example described by Figures 1.10 and 1.11: The capacity increased by only 50 percent when we increased the number of base station by a factor of six. Furthermore, the number of handovers for rapidly moving terminals increases when the cells are made smaller.

[12] Power control can also be used to alleviate fading: By adjusting the transmitter power of a signal, we can control the SNR at the receiver.

2. *Hierarchical Cell Structures (HCS)* solves the handover problem, by having two sets of cells covering one area. The first set uses large cells to supply services to rapidly moving mobiles, and the other set consists of small cells that provide the wireless services to many stationary or slowly moving terminals. The large disadvantage with HCS is that the frequency planning becomes more complex.

3. *Smart antennas.* By using antennas with several antenna elements at the receiver and/or transmitter, it is possible to increase the system capacity, without reducing the cell size. In TDMA systems, the reuse distance can be reduced, whereas for CDMA systems, we can simply allow more users in each cell.

4. *Better receiver structures.* With better receiver structures, the impact of co-channel or multiple-access interference can be reduced, for a given cell planning and antenna technology. The goal is to increase the system capacity by improving the signal processing software, without having to install new hardware.

In this thesis, items three and four will be discussed, and we show that a multivariable DFE can be used as a tool for the last two capacity enhancing features. In Chapter 4, the DFE is used in conjunction with an antenna array. In Chapter 5, a multiuser detector for CDMA systems is derived based on a multivariable DFE.

The key property that makes the multivariable DFE suitable for these and other purposes is its ability to simultaneously handle signals from several measurement sensors and several data sources. To accurately describe the relation between these data sources and measurement signals, we need a *multivariable channel model.*

1.4 Multivariable channel models

A *multivariable channel* or *multiple-input multiple-output (MIMO) channel* is a channel with several inputs and/or outputs. Such channels occur frequently in models of modern communication systems. In this section, we will give five examples where MIMO models can be used to provide an accurate system description.

Channels with multiple inputs are often introduced to give a more exact description of the detection scenario. In situations where several signals were actually affecting the channel output, the channels were previously modeled with only a single input. A large amount of additive noise was then used to describe the effect of the remaining signals. Such single input modeling has previously been used in the scenarios described in all the following subsections.

In the cases described in Subsections 1.4.1 and 1.4.5, the multiple outputs of the channels originate from different sensors. These channels are "true" multiple output channels. Other channels are not truly multivariable, in the sense that the received signal is actually scalar. The multiple-output character is generated by some transformation of the received signal. The channel models described in Subsections 1.4.2–1.4.4 are examples of such channels.

Acquiring MIMO models

Channel models are rarely known *a priori.* Instead, they have to be estimated. For unambiguous estimation of the IIR models described in this thesis, a known training sequence is generally required.[13] We thus assume that a training sequence is present.

With SISO models, this assumption would be sufficient to ensure that we can estimate the channels. However, for MIMO models additional problems arise. Since multivariable models can be parametrized in many different ways, ordinary prediction error methods [54, 82] may be inappropriate, due to the large number of structural design variables involved. In this respect, *subspace identification* [68] offers a solution. With subspace identification, only one design variable is used: the order of the realization. The estimated model is a minimal state space realization, which can then be converted into any suitable form [40].

Fortunately, multivariate FIR models are still relatively easy to estimate, using least-squares methods. One remaining problem is that the number of parameters to estimate may be unnecessarily large. In particular, this is the case for the multivariable channel models described in Subsection 1.4.1. These channels can in fact often be described by a *reduced rank* model [52]. This low-rank property can also be taken into account when the channel is estimated [53, 81], leading to more accurate models. Another way to improve the channel estimates is *bootstrapping*, which is described in [91]. By letting the channel estimator work in tandem with a symbol estimator, the channel estimates can be improved iteratively, using the whole detected data burst, not only the training sequence. This method will be used both in Subsections 4.4.3 and 4.5.

In this thesis, we will assume that all models are known without error. In practice, of course, models are uncertain and better performance may be obtained with robust methods. With such methods, detectors that explicitly take the model uncertainty into account can be designed. See [80] and [110] for examples of such designs.

[13] Identification is sometimes possible even without a known training sequence. This is known as *blind* identification [59, 65, 78, 94, 97].

1.4.1 Multi-element antennas

In cellular communication systems, multi-element antennas, also known as antenna arrays or spatial diversity receivers, are frequently used to reject interference and to reduce the effect of fading and noise [6, 64]. They can also be used to increase system capacity [106].

The introduction of antennas with several elements at the receiver results in a channel with multiple outputs. Assume that the received signal is sampled at the symbol rate. The signal received at antenna i is denoted $y_i(k)$, and the additive noise received at the same antenna is denoted $v_i(k)$. Furthermore, assume that the scalar channel from the transmitter to receiver antenna i is described by the transfer operator $\mathcal{H}_i(q^{-1})$. To obtain a collective representation of the antenna signals, we form the following vectors:

$$y(k) \stackrel{\triangle}{=} \begin{pmatrix} y_1(k) & y_2(k) & \dots & y_{n_y}(k) \end{pmatrix}^T \tag{1.4a}$$

$$\boldsymbol{\mathcal{H}}(q^{-1}) \stackrel{\triangle}{=} \begin{pmatrix} \mathcal{H}_1(q^{-1}) & \mathcal{H}_2(q^{-1}) & \dots & \mathcal{H}_{n_y}(q^{-1}) \end{pmatrix}^T \tag{1.4b}$$

$$v(k) \stackrel{\triangle}{=} \begin{pmatrix} v_1(k) & v_2(k) & \dots & v_{n_y}(k) \end{pmatrix}^T , \tag{1.4c}$$

where n_y is the number of antenna elements in the array. The vector of received samples can then be expressed as

$$y(k) = \boldsymbol{\mathcal{H}}(q^{-1})d(k) + v(k) \tag{1.5}$$

where $d(k)$ is the transmitted signal. The model (1.5) is a single-input multiple-output (SIMO) model, and is depicted in Figure 1.12.

The model (1.5) can be used as a basis for design of a detector performing *interference rejection.* This approach has been thoroughly investigated, in for instance [11, 14, 64]. In all these investigations, interference rejection improves the performance significantly.

In a scenario where several users transmit simultaneously, we can modify (1.5) to explicitly incorporate multiple users. For this purpose, we assume that the signal $d_j(k)$ is transmitted from user j, and define

$$d(k) \stackrel{\triangle}{=} \begin{pmatrix} d_1(k) & d_2(k) & \dots & d_{n_d}(k) \end{pmatrix}^T . \tag{1.6a}$$

We also denote the scalar channel from transmitter j to receiver antenna i as $\mathcal{H}_{ij}(q^{-1})$ and define the matrix

$$\boldsymbol{\mathcal{H}}(q^{-1}) \stackrel{\triangle}{=} \begin{pmatrix} \mathcal{H}_{11}(q^{-1}) & \mathcal{H}_{12}(q^{-1}) & \dots & \mathcal{H}_{1n_d}(q^{-1}) \\ \mathcal{H}_{21}(q^{-1}) & \mathcal{H}_{22}(q^{-1}) & & \mathcal{H}_{2n_d}(q^{-1}) \\ \vdots & & \ddots & \vdots \\ \mathcal{H}_{n_y1}(q^{-1}) & \mathcal{H}_{n_y2}(q^{-1}) & \dots & \mathcal{H}_{n_yn_d}(q^{-1}) \end{pmatrix} . \tag{1.6b}$$

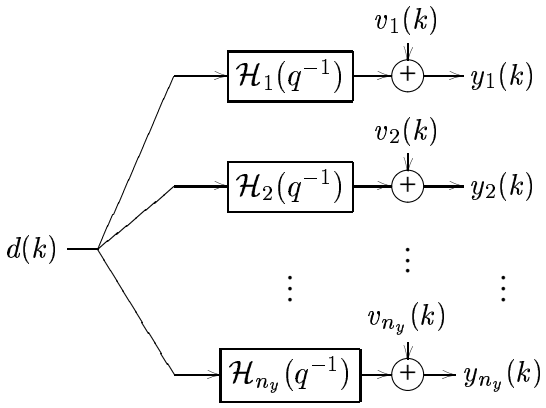

Figure 1.12: The presence of an antenna array at the receiver results in a single-input multiple-output (SIMO) model.

Using (1.4a), (1.4c), (1.6a) and (1.6b), we can now express the signal received at the antenna array by the multiple-input multiple-output model

$$y(k) = \boldsymbol{\mathcal{H}}(q^{-1})d(k) + v(k) \ . \tag{1.7}$$

Of course, the model (1.5) is a special case ($n_d = 1$) of (1.7).

The channel model (1.7) can be used as a basis for design of a *multiuser detector*, which simultaneously detects the symbols transmitted from all users. This approach was first studied by Winters in [104] and more recently by Tidestav et al. in [92], where in addition, multiuser detection and interference rejection were compared. This scenario will be investigated in detail in Chapter 4.

1.4.2 Fractionally spaced sampling

We shall now turn our attention to *fractionally spaced sampling.* Fractionally spaced sampling implies that the received signal is sampled several, say p, times during a symbol period T_s, as depicted in Figure 1.13.

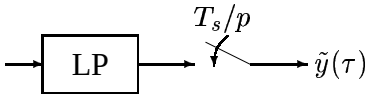

Figure 1.13: Fractionally spaced sampling leads to a stationary multiple output model.

The sampling rate of the discrete-time signal $\tilde{y}(\cdot)$ equals p/T_s. Fractionally

spaced sampling can be used to reduce the sensitivity of the receiver to synchronization errors, or simply to improve detector performance.

Since the sampling rate is not equal to the symbol rate, the signal $\tilde{y}(\cdot)$ is not stationary, but cyclo-stationary: Its moments vary periodically with a period equal to p. Since a new symbol is transmitted only once every p samples, we can express the received signal $\tilde{y}(\cdot)$ as

$$\tilde{y}(kp+r) = \tilde{H}(q^{-1})\tilde{d}(kp+r) + \tilde{v}(kp+r), \qquad \begin{matrix} k = 0, 1, \dots, \\ r = 0, 1, \dots, p-1 \end{matrix} \quad . \tag{1.8}$$

In (1.8), we have introduced a scalar discrete-time input $\tilde{d}(\cdot)$, defined by

$$\tilde{d}(kp+r) = \begin{cases} d(k) & r = 0 \\ 0 & \text{otherwise} \end{cases}$$

and a scalar channel

$$\tilde{H}(q^{-1}) = \tilde{H}_0 + \tilde{H}_1 q^{-1} + \tilde{H}_2 q^{-2} + \dots \ .$$

Note that the sampling rate of the time-series $\tilde{d}$ and the model $\tilde{H}(q^{-1})$ equals p times the symbol rate.

To transform $\tilde{y}(kp+r)$ to a stationary signal, we collect p consecutive samples of $\tilde{y}(\cdot)$ in the vector

$$y(k) \stackrel{\triangle}{=} \begin{pmatrix} \tilde{y}(kp) & \tilde{y}(kp+1) & \dots & \tilde{y}(kp+p-1) \end{pmatrix}^T \ . \tag{1.9}$$

The vector-valued stochastic process $y(k)$ is stationary and has sampling rate equal to the symbol rate $1/T_s$. To obtain the desired multivariable model, we introduce the single-input multiple-output (SIMO) transfer operator

$$\boldsymbol{\mathcal{H}}(q^{-1}) \stackrel{\triangle}{=} \mathbf{H}_0 + \mathbf{H}_1 q^{-1} + \mathbf{H}_2 q^{-2} + \dots \tag{1.10}$$

where

$$\mathbf{H}_m \stackrel{\triangle}{=} \begin{pmatrix} \tilde{H}_{mp} & \tilde{H}_{mp+1} & \dots & \tilde{H}_{mp+p-1} \end{pmatrix}^T \ .$$

Analogous to (1.9), we stack the noise samples $\tilde{v}(kp+r)$ to form the vector $v(k)$:

$$v(k) \stackrel{\triangle}{=} \begin{pmatrix} \tilde{v}(kp) & \tilde{v}(kp+1) & \dots & \tilde{v}(kp+p-1) \end{pmatrix}^T \ . \tag{1.11}$$

Using (1.10) and (1.11), we can express $y(k)$ as

$$y(k) = \boldsymbol{\mathcal{H}}(q^{-1})d(k) + v(k) \ , \tag{1.12}$$

which is a SIMO model whose inputs and outputs are stationary and sampled at the symbol rate.

When several signals are transmitted over a common channel, an oversampled version of the received signal can be used to detect all of them. This can be implemented in CDMA systems, as described in [1, 2, 86], and in xDSL systems, as described in [36, 71]. The resulting model will have multiple inputs, as well as multiple outputs.

In Chapter 5, the CDMA detection problem will be investigated in detail. The model (1.12) will be generalized to represent multiple users, and to model rapid time-variations.

1.4.3 Multiuser detection in DS-CDMA

In DS-CDMA systems, detection can be improved if we explicitly model the multiple-access interference. The resulting MIMO model will have the symbols from all the users as input. The output of the MIMO model will be the symbol rate sampled outputs from n_d filters, each matched to the signature sequence of a specific user. We thus collect the sampled outputs of the matched filters in a vector:

$$y'(k) \stackrel{\triangle}{=} \begin{pmatrix} y_1(k) & y_2(k) & \dots & y_{n_d}(k) \end{pmatrix}^T \ . \tag{1.13}$$

For a channel without delay spread, this vector is related to the vector of transmitted symbols $d(k)$ and a vector of noise samples $v'(k)$ through, see [57],

$$\begin{aligned} y'(k) = \mathbf{R}(1)\mathbf{W}d(k+1) + \mathbf{R}(0)\mathbf{W}d(k) \\ + \mathbf{R}(-1)\mathbf{W}d(k-1) + v'(k) \ . \end{aligned} \tag{1.14}$$

In (1.14), the matrices $\mathbf{R}(m)$ contain partial cross-correlations between the spreading sequences $s_i(t)$:

$$\left(\mathbf{R}(m)\right)_{i,j} \stackrel{\triangle}{=} \int_{\tau_i}^{T_s+\tau_i} s_i(t-\tau_i)s_j^*(t+mT_s-\tau_j)dt \ ,$$

where T_s is the symbol period, $\tau_i \in [0, T_s[$ is the propagation delay of user i and $(\cdot)^*$ denotes complex conjugate. It is here assumed that $s_i(t) = 0$ outside $t \in [0, T_s[$. The elements in the diagonal matrix $\mathbf{W}$ represent the amplitudes and phase shifts of the respective signals.

The model (1.14) is non-causal. To obtain a causal model, we define $y(k) \triangleq y'(k-1)$ and $v(k) \triangleq v'(k-1)$, which can be inserted into (1.14) to yield:

$$y(k) = \boldsymbol{\mathcal{H}}(q^{-1})d(k) + v(k) \ ,$$

with a MIMO FIR channel of second order:

$$\boldsymbol{\mathcal{H}}(q^{-1}) = \mathbf{R}(1)\mathbf{W} + \mathbf{R}(0)\mathbf{W}q^{-1} + \mathbf{R}(-1)\mathbf{W}q^{-2} \ .$$

Unlike the model described in the preceding subsection, this channel model assumes that the received CDMA signal is first correlated with the signature sequences of the users to obtain a new set of measurement signals. This has implications for the detector design, which will be discussed in Chapter 5.

1.4.4 Separation of I- and Q-channels

Consider a scalar channel of the form (1.3). We now separate the transmitted signal, the channel, the received signal and the noise term into their real and imaginary parts:

$$\begin{aligned} d(k) &\triangleq d^r(k) + jd^i(k) \\ \mathcal{H}(q^{-1}) &\triangleq \mathcal{H}^r(q^{-1}) + j\mathcal{H}^i(q^{-1}) \\ y(k) &\triangleq y^r(k) + jy^i(k) \\ v(k) &\triangleq v^r(k) + jv^i(k) \ . \end{aligned}$$

We realize that we can write

$$\bar{y}(k) = \boldsymbol{\mathcal{H}}(q^{-1})\bar{d}(k) + \bar{v}(k)$$

with

$$\begin{aligned} \bar{y}(k) &\triangleq \begin{pmatrix} y^r(k) & y^i(k) \end{pmatrix}^T \\ \bar{d}(k) &\triangleq \begin{pmatrix} d^r(k) & d^i(k) \end{pmatrix}^T \\ \bar{v}(k) &\triangleq \begin{pmatrix} v^r(k) & v^i(k) \end{pmatrix}^T \end{aligned}$$

and

$$\boldsymbol{\mathcal{H}}(q^{-1}) \triangleq \begin{pmatrix} \mathcal{H}^r(q^{-1}) & -\mathcal{H}^i(q^{-1}) \\ \mathcal{H}^i(q^{-1}) & \mathcal{H}^r(q^{-1}) \end{pmatrix} \ . \tag{1.15}$$

We have thus converted the complex-valued SISO channel to a real-valued MIMO channel. This approach has been investigated in [28]. For real-valued transmitted

signals, the model reduces to a SIMO model. In this case, using the multivariable real-valued formulation, rather than the original scalar complex-valued one, can be advantageous, since we get two measurement signals instead of one. See for instance [51].

This separation will be used in Chapter 5.

1.4.5 Magnetic recording channels

Information storage resembles communication. Storing the information then corresponds to transmitting the data, and the information retrieval corresponds to the reception. A data bit which cannot be read from an information storage is equivalent to a bit error in communication, and error correcting coding must be used to correct this bit.

Keeping this in mind, it is not surprising that signal processing can be used to increase the *areal density* of a magnetic storage device, such as a hard disc. The areal density describes how many bits can be stored and reliably retrieved from a given area of the hard disc.

The information bits on a hard disc are stored along concentric circles, known as *tracks*. These bits are retrieved by letting the disc rotate under a read head. The output of the read head is determined by the data bits stored below the head.

Unfortunately, the output of the read head is affected not only by the value of the data bit stored right below it: It also depends on the values of adjacent bits. Both bits on the same track and bits on neighboring tracks determine the output of the read head. The former cause intersymbol interference, whereas the latter cause *intertrack* interference. The output of the read head can thus be thought of as the output of a MISO channel: The inputs are all the stored information bits which affect the current output.

To retrieve the information, it is also possible to use an array of read heads, mounted side by side. This array can read several tracks simultaneously, thus increasing the maximum rate of data transfer. At the same time, the read process may become more reliable.

To be specific, assume that the array has N read heads, and that M tracks are read simultaneously, as depicted in Figure 1.14.

One stored information bit in track j will result in a signal $p_{ij}(t)$ at the output of read head i. The continuous time impulse response from track j to read head i is thus equal to $p_{ij}(t)$. After lowpass filtering and symbol rate sampling, the discrete time model $\mathcal{H}_{ij}(q^{-1})$ is obtained.

We can relate the information bits stored at the M tracks to the sampled output

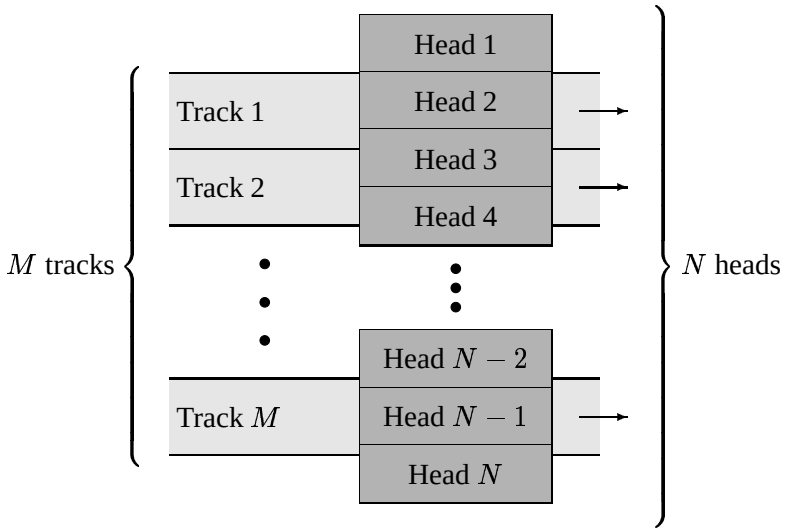

Figure 1.14: A configuration with N heads simultaneously scans M tracks of the magnetic storage device. The media moves below the heads, producing a stream of measurement vectors.

$y_i(k)$ of the ith read head:

$$y_i(k) = \sum_{j=1}^{M} \mathcal{H}_{ij}(q^{-1}) d_j(k) + v_i(k) \ ,$$

where

$$\begin{aligned} d_j(k) &\stackrel{\triangle}{=} \text{The information bit stored at track } j. \\ v_i(k) &\stackrel{\triangle}{=} \text{The noise received at read head } i. \end{aligned}$$

We can now combine the outputs from the N read heads to obtain the MIMO model

$$y(k) = \boldsymbol{\mathcal{H}}(q^{-1}) d(k) + v(k) \ ,$$

where

$$\begin{aligned} y(k) &\stackrel{\triangle}{=} \begin{pmatrix} y_1(k) & y_2(k) & \dots & y_N(k) \end{pmatrix}^T \\ d(k) &\stackrel{\triangle}{=} \begin{pmatrix} d_1(k) & d_2(k) & \dots & d_M(k) \end{pmatrix}^T \\ v(k) &\stackrel{\triangle}{=} \begin{pmatrix} v_1(k) & v_2(k) & \dots & v_N(k) \end{pmatrix}^T \end{aligned}$$

and

$$\boldsymbol{\mathcal{H}}(q^{-1}) \triangleq \begin{pmatrix} \mathcal{H}_{11}(q^{-1}) & \dots & \mathcal{H}_{1M}(q^{-1}) \\ \vdots & \ddots & \vdots \\ \mathcal{H}_{N1}(q^{-1}) & \dots & \mathcal{H}_{NM}(q^{-1}) \end{pmatrix}$$

This model has been used by Voois and Cioffi in [101] to derive a multivariable DFE, which extracts the information stored on the hard disc.

1.5 Outline of the thesis

The ambitious goal of this thesis is to give a thorough treatment of multivariable decision feedback equalizers. Properties which apply equally well to scalar DFEs are only briefly discussed or not discussed at all. These important properties include, for instance, error propagation [15, 43], combination of equalization and coding [18, 19], and performance bounds [26, 44]. Instead, this thesis focuses on the multivariable nature of the equalization problem, and, in particular, the use of the DFE as a tool for multiuser detection and interference rejection.

The thesis is divided into two major parts. The first part consists of Chapters 2 and 3, where a concise theoretical foundation is laid for the later chapters. Three multivariable DFE structures are introduced. Design equations for all three structures are presented and their relative performances are compared in a numerical example. These DFEs are all multivariable generalizations of scalar DFEs. The focus lies on minimum mean-square error and zero-forcing designs, under the assumption of correct past decisions.

The second part of the thesis treats the applications in Chapters 4 and 5. The properties of the DFE as a multiuser detector and an interference rejector are described and discussed in detail in two application scenarios. Some general conclusions can be drawn from the results in these two chapters:

1. Multivariable equalization in general, and the multivariable decision feedback equalizer in particular, is very powerful. The introduction of multiple sensors leads to an enormous interference rejection capability, far beyond than the capabilities of any scalar filter.

2. With many receivers and few transmitters, the difference between different equalizers tends to decrease. In particular, this is true for the decision feedback equalizers discussed in Chapters 4 and 5. An indication of this property is that the conditions for the existence of a zero-forcing solution to the equalization problem become less restrictive for situations where the number of transmitters is small relative to the number of receivers.

3. When the number of transmitters and/or receivers increase, the parameter estimation becomes much more difficult. This is true in particular for the estimation of the noise color. Due to an insufficient number of training data, the estimate of the noise covariance function may become so unreliable, that better detection performance is obtained if the detector is designed based on the incorrect assumption of temporally white noise. This is the case for several of the scenarios in Chapter 4.

The specific scientific contributions in the thesis are described in the following subsection.

1.5.1 Contributions

The DFEs in Sections 3.1 and 3.2 are described in

> Claes Tidestav, Anders Ahlén, and Mikael Sternad, "Realizable MIMO decision feedback equalizers: structure and design," submitted to *IEEE Transactions on Signal Processing.*

See also [90]. The DFE presented in Section 3.1 resembles the DFEs presented in [23] and [28], but differs in two aspects:

1. The DFE in Section 3.1 can be straightforwardly applied to channels with different number of inputs and outputs. Hence, it includes the DFE in [11, 12] as a special case.

2. Colored noise can be handled in an optimum way.

The DFE in Section 3.2 is a novel, multivariable generalization of the scalar DFE published in [79]. Closed form minimum mean-square error design equations are presented for this DFE. The zero-forcing criterion is also discussed and we derive conditions for the existence of a multivariable zero-forcing DFE.

The results in Section 3.3 have been published in [92]:

> Claes Tidestav, Mikael Sternad, and Anders Ahlén, "Reuse within a cell—interference rejection or multiuser detection?," *IEEE Transactions on Communications*, vol. 47, no. 10, pp. 1511–1522, Oct. 1999.

The structure of this DFE is identical to that of the DFE published by Voois and Cioffi in [101]. A special case of the DFE in [92] was independently derived in [85]. The derivation of the minimum mean-square error DFEs in [92] and [101] are equivalent, whereas the derivation of the zero-forcing DFE in [92] is novel.

The precise condition for the existence of a DFE which complies with the zero-forcing condition has not been previously published. Also, the implications of the non-existence of a zero-forcing equalizer have never been discussed.

Parts of Chapter 4 are also published in [92]. See also [88, 89, 93]. The comparison between multiuser detection and interference rejection with antenna arrays involves novel insights about structural aspects and estimation problems for both detectors.

In Chapter 5, a linear time-varying model of transmission and reception in a DS-CDMA system is introduced. A similar model was introduced by the author in [86, 87]. The model in itself is not new, but the extension to long codes is. The idea of actually using the model as a basis for detector design is also novel.

This linear model is used to derive a family of MMSE detectors with various degrees of decision feedback. As a bonus, we obtain novel design equations for a time-varying version of the FIR DFE introduced in Section 3.3. We also prove that a linear MMSE detector with or without decision feedback, is near-far resistant if and only if its parameters can be adjusted to comply with the zero-forcing condition. The results in Chapter 5 will be published in

> Claes Tidestav, "Implementation and near-far resistance of chip-spaced DS-CDMA detectors," in preparation.

In addition to the journal papers mentioned above, the author has published the following conference papers, all of which treat various aspects of the multivariable DFE:

- Claes Tidestav, Anders Ahlén, and Mikael Sternad, "Narrowband and broadband multiuser detection using a multivariable DFE," in *Proceedings of the IEEE International Symposium on Personal, Indoor and Mobile Radio Communications*, Toronto, Canada, Sept. 1995, vol. 2, pp. 732–736.

- Claes Tidestav, "Linear baseband modeling of direct-sequence code-division multiple access systems," in *Proceedings of Radiovetenskap och Kommunikation 96 (RVK96)*, Luleå, Sweden, June 1996, pp. 156–160.

- Claes Tidestav, "Designing equalizers based on explicit channel models of DS-CDMA systems," in *Proceedings of the 5th IEEE International Conference on Universal Personal Communications*, Cambridge, MA, Oct. 1996, pp. 131–135.

- Claes Tidestav, Anders Ahlén, and Mikael Sternad, "Realizable MIMO decision feedback equalizers," in *Proceedings of the 1999 International Conference on Acoustics Speech and Signal Processing*, Phoenix, AR, 1999, pp. 2591–2594.

- Claes Tidestav, Mikael Sternad, and Anders Ahlén, "Reuse within a cell—interference rejection or multiuser detection?," in *Proceedings of the 49th IEEE Vehicular Technology Conference*, Houston, TX, May 1999, pp. 1618–1621.

- Claes Tidestav, Anders Ahlén, and Mikael Sternad, "A comparison of multiuser detection and interference rejection," in *Proceedings of Radiovetenskap och Kommunikation 99 (RVK99)*, Karlskrona, Sweden, June 1999, vol. 1, pp. 446–450.

The results in the following conference papers are also briefly discussed in the thesis:

- Claes Tidestav and Erik Lindskog, "Bootstrap equalization," in *Proceedings of the 1998 IEEE International Conference on Universal Personal Communications*, Florence, Italy, Oct. 1998, pp. 1221–1225.

- Erik Lindskog and Claes Tidestav, "Reduced rank space-time equalization," in *Proceedings of the 9th IEEE International Symposium on Personal, Indoor and Mobile Radio Communications*, Boston, MA, Sept. 1998, pp. 1081–1085.

- Erik Lindskog and Claes Tidestav, "Reduced rank channel estimation," in *Proceedings of the 49th IEEE Vehicular Technology Conference*, Houston, TX, USA, May 1999, vol. 2, pp. 1126–1130.

CHAPTER 2

Problem statement

IN this chapter, we begin by giving an overview of the detection problem. We then present properties that are common to all the decision feedback equalizers discussed in the thesis. The criteria used when tuning the equalizer parameters are then introduced. Finally, we describe and discuss the channel models that will be used as basis for equalizer design in Chapter 3.

Consider the received sequence of measurement vectors $y(k)$. Each vector can be described as the sum of the output from a dispersive, linear multivariable channel and a multivariate noise term:

$$y(k) = \boldsymbol{\mathcal{H}}(q^{-1})d(k) + v(k) \ . \tag{2.1}$$

In (2.1), the channel is described by the linear MIMO operator

$$\boldsymbol{\mathcal{H}}(q^{-1}) \triangleq \begin{pmatrix} \mathcal{H}_{11}(q^{-1}) & \mathcal{H}_{12}(q^{-1}) & \dots & \mathcal{H}_{1n_d}(q^{-1}) \\ \mathcal{H}_{21}(q^{-1}) & \mathcal{H}_{22}(q^{-1}) & & \mathcal{H}_{2n_d}(q^{-1}) \\ \vdots & & \ddots & \vdots \\ \mathcal{H}_{n_y1}(q^{-1}) & \mathcal{H}_{n_y2}(q^{-1}) & \dots & \mathcal{H}_{n_yn_d}(q^{-1}) \end{pmatrix} ,$$

whereas $y(k)$ and $v(k)$ are column vectors with n_y elements and $d(k)$ is a column vector of dimension n_d. The model is depicted in Figure 2.1.[1] We saw in Section 1.4 that this model offers considerable flexibility to cope with a large number of situations occurring in digital communication. We will therefore use this model as a starting point.

[1] Note that this model can not be used to describe non-linear channels or non-additive noise.

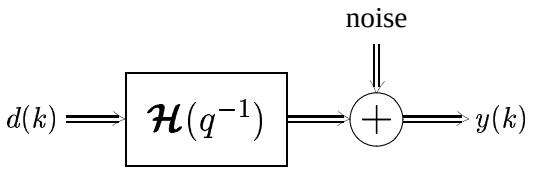

Figure 2.1: A linear model of a dispersive channel.

Our primary goal is to reconstruct the input vector $d(k-\ell)$ to the channel using the measurements $\{y(n)\}_{n=0}^{k}$. The constant ℓ is the *smoothing lag* or *decision delay*, and may be infinite.

2.1 The multivariable decision feedback equalizer

As a symbol detector, we introduce the multivariable *decision feedback equalizer (DFE)*:

$$\begin{aligned} \hat{d}(k-\ell|k) &= \boldsymbol{\mathcal{R}}(q^{-1})y(k) - \boldsymbol{\mathcal{F}}(q^{-1})\tilde{d}(k-\ell-1) \\ \tilde{d}(k-\ell) &= \mathrm{f}(\hat{d}(k-\ell|k)) \ . \end{aligned} \tag{2.2}$$

The DFE consists of two linear multiple-input multiple-output filters and a decision non-linearity. The measurement vectors $y(k)$ are used as input to the *feedforward filter* $\boldsymbol{\mathcal{R}}(q^{-1})$, and the detected symbols are fed into the *feedback filter* $\boldsymbol{\mathcal{F}}(q^{-1})$. The difference between the outputs of the feedforward and feedback filters is a soft estimate of the input vector $d(k-\ell)$. This soft estimate $\hat{d}(k-\ell|k)$ is then quantized to the closest point in the signal constellation, and the resulting hard estimate $\tilde{d}(k-\ell)$ is fed to the feedback filter to remove its effect on future symbol estimates. The DFE is shown in Figure 2.2.

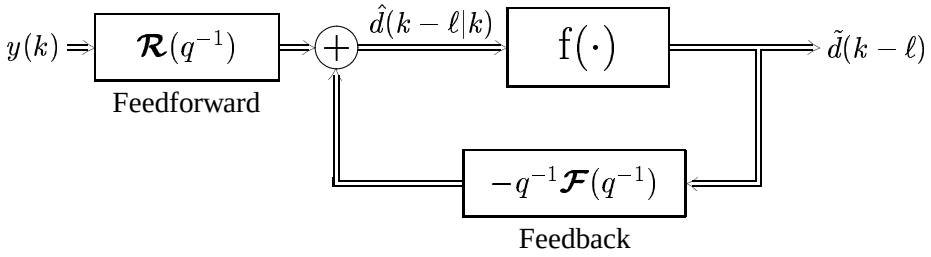

Figure 2.2: The multivariable decision feedback equalizer.

Remark 1. The output of the decision device is always bounded. Therefore, as long as the individual filter $\boldsymbol{\mathcal{R}}(q^{-1})$ and $\boldsymbol{\mathcal{F}}(q^{-1})$ are stable, the DFE will be stable

in the sense that all internal variables are bounded when $y(k)$ is bounded, despite the presence of the feedback link.

The function of this multivariable DFE is the same as that of the scalar DFE introduced in Section 1.2. The main difference is that for multiple users, both the feedforward and the feedback filters can be designed to reduce and cancel interference between users, as well as intersymbol interference.

We will consider DFEs with a decision device where the decisions for all users are made simultaneously and independently of each other. For a multivariable DFE, there is, however, a possibility to use more elaborate decision rules. For instance, if we allow decisions to be made consecutively on individual elements in the vector estimate, we can remove the interference from detected symbols not only on estimates of future symbols, but also on the estimates of the present symbols for *other* users [25]. In cases where some or all of the symbols in a transmitted vector are correlated[2], it may be advantageous to jointly map several elements in the vector symbol estimate to the closest point in the (vector) constellation. This procedure is similar to the decoding process in a system employing vector quantization [67].

Even with the simple decision device used in this thesis, closed form expressions for optimal equalizer coefficients are impossible to obtain for realistic criteria. To make the determination of useful DFE parameters possible, we adopt the common assumption that all past decisions, which affect the current estimate, are correct. Under this assumption, optimal DFE parameters can be obtained, since the symbols fed back from the decision circuit can be treated as a feedforward connection from delayed transmitted symbols, as depicted in Figure 2.3.

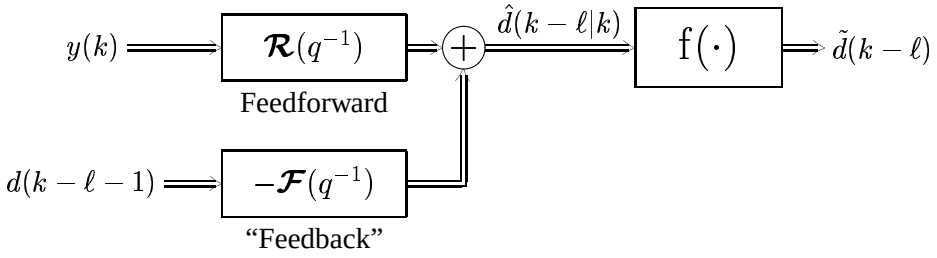

Figure 2.3: The decision feedback equalizer with the decision feedback from $\tilde{d}(k-\ell-1)$ replaced by feedforward from $d(k-\ell-1)$.

Remark 2. As discussed in Subsection 1.2, an inherent drawback with the multivariable as well as the scalar DFE structure is error propagation, a problem which is

[2]For instance, this could be the case in a DS-CDMA system, where *multicode transmission* is used in conjunction with precoding to reduce envelope variations. [67]

illuminated by the assumption on correct past decisions. When incorrect decisions are fed back, the probability of future decision errors increases, possibly causing additional decision errors and an error burst.

The parameters in the feedforward and feedback filters can now be tuned to obtain the desired properties of the soft estimate $\hat{d}$. In a digital communication system, it may seem more natural to adjust the properties of the hard estimate $\tilde{d}$, for instance to minimize the probability of error. However, controlling the properties of $\tilde{d}$ is much more difficult than controlling the properties of $\hat{d}$, and often the two approaches give essentially the same performance [63]. Also, in a digital communication system with coding, the soft rather than the hard decisions should be used in the decoding process. Controlling the properties of the soft decisions in this case makes sense.

We will now present the two schemes for parameter adjustment used in this thesis, the *zero-forcing (ZF)* criterion and the *minimum mean-square error (MMSE)* criterion.

2.2 Parameter adjustment criteria

Originally, equalizers in general and DFEs in particular were invented to suppress the channel distortion. To describe the ability of the equalizers to carry out this task, the *peak distortion* measure is commonly used. The peak distortion is defined as the absolute value of the worst case residual intersymbol interference at the output of the equalizer. Obviously, the minimum value of the peak distortion is zero. An equalizer that manages to achieve zero peak distortion, that is, to remove all intersymbol interference, is called a *zero-forcing* equalizer.

When extending the definition of a zero-forcing equalizer to a multivariable scenario, is is natural to require that both intersymbol *and* co-channel interference be removed. When this happens, the estimation error will be uncorrelated with *all* transmitted symbol vectors. A multivariable zero-forcing equalizer can thus be defined as follows:

Definition 2.1 *Consider a multivariable equalizer that produces the soft estimate $\hat{d}(k-\ell|k)$ of a transmitted symbol vector $d(k-\ell)$. If*

$$E\left[\left(d(k-\ell)-\hat{d}(k-\ell|k)\right)d^H(m)\right]=0 \;\; \forall\, m\;, \tag{2.3}$$

then the equalizer is said to be zero-forcing.

In many cases, a zero-forcing equalizer provides adequate performance, in particular when the SNR is high. In other cases, the noise enhancement caused by the

zero-forcing equalizer may be unacceptable. A design that balances interference suppression against noise amplification may be better suited for such a scenario.

This is exactly what a *minimum mean-square error (MMSE)* equalizer does. The parameters of such an equalizer are tuned so that the estimation error covariance matrix

$$\mathbf{P} \stackrel{\triangle}{=} E\varepsilon(k-\ell)\varepsilon^H(k-\ell) \tag{2.4}$$

where the estimation error $\varepsilon(k-\ell)$ is defined as

$$\varepsilon(k-\ell) \stackrel{\triangle}{=} d(k-\ell) - \hat{d}(k-\ell|k) \tag{2.5}$$

is minimized.[3] An equalizer that minimizes (2.4) also minimizes[4]

$$\begin{aligned}
\operatorname{tr}\mathbf{P} &= E\operatorname{tr}(d(k-\ell)-\hat{d}(k-\ell|k))(d(k-\ell)-\hat{d}(k-\ell|k))^H \\
&= E\operatorname{tr}(d(k-\ell)-\hat{d}(k-\ell|k))^H(d(k-\ell)-\hat{d}(k-\ell|k)) \\
&= E\sum_{i=1}^{M}|d_i(k-\ell)-\hat{d}_i(k-\ell|k)|^2 = \sum_{i=1}^{M}E|d_i(k-\ell)-\hat{d}_i(k-\ell|k)|^2 .
\end{aligned}$$

The equalizer thus minimizes the sum of the MSEs for all the transmitted signals, hence the name MMSE equalizer.

2.3 The channel models

Although it is possible to design a DFE directly from the received data and a training sequence, we will assume that a model of the channel has been made available to us prior to the equalizer design. Such model based or *indirect* design has two distinct advantages:

1. The channel model can often be described using fewer parameters than the corresponding equalizer. Given a limited amount of data, more accurate equalizer tuning is obtained by first estimating a channel model, and then performing a model-based equalizer design. See Chapter 3 in [51].

2. In time-varying scenarios, the parameters of the channel will vary more smoothly than the corresponding equalizer parameters. Tracking the channel parameters is then easier than tracking the equalizer parameters. See Chapter 2 in [49].

[3] The covariance matrix is minimized in the sense that any other admissible choice of equalizer parameters will result in an estimation error covariance matrix $\tilde{\mathbf{P}}$ such that $\tilde{\mathbf{P}}-\mathbf{P}$ is positive definite.

[4] An estimator that 'minimizes' $\mathbf{P}$ actually minimizes any non-decreasing function of $\mathbf{P}$, such as $\det\mathbf{P}$ or $\operatorname{tr}\mathbf{W}\mathbf{P}$ for any positive definite weighting matrix $\mathbf{W}$. See [82, p. 234].

In our design of decision feedback equalizers in Chapter 3, we will use two time-invariant channel models:

1. A full parametric description using an IIR channel and an ARMA noise model.
2. A description based on an FIR model of the channel and a non-parametric model of the noise.

These models will be described and motivated in the following subsections.

2.3.1 A general finite-order linear model

A general linear model of finite order is depicted in Figure 2.4. Both the channel

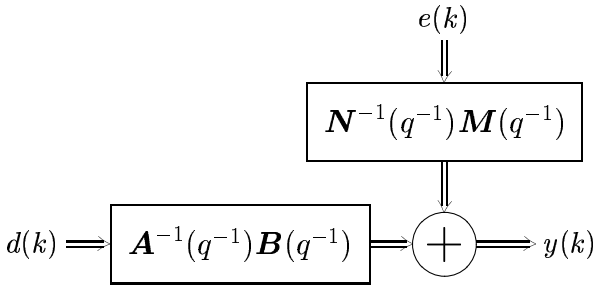

Figure 2.4: The general multivariable channel model. Both the multivariable IIR channel and the vector ARMA noise model are parametrized as left matrix fraction descriptions (MFDs).

model and the noise process are parametrized by left matrix fraction descriptions (MFDs) [40]:

$$y(k) = \boldsymbol{A}^{-1}(q^{-1})\boldsymbol{B}(q^{-1})d(k) + \boldsymbol{N}^{-1}(q^{-1})\boldsymbol{M}(q^{-1})e(k)\ . \tag{2.6}$$

The polynomial matrix $\boldsymbol{B}(q^{-1})$ has n_y rows and n_d columns, whereas $\boldsymbol{A}(q^{-1})$, $\boldsymbol{M}(q^{-1})$ and $\boldsymbol{N}(q^{-1})$ are square polynomial matrices of dimension n_y. These three matrices are assumed to have full normal rank [40] and to be *stably invertible*, that is, the roots of

$$\begin{aligned} \det \boldsymbol{A}(z^{-1}) &= 0 \\ \det \boldsymbol{M}(z^{-1}) &= 0 \\ \det \boldsymbol{N}(z^{-1}) &= 0 \end{aligned} \tag{2.7}$$

all lie inside the unit circle $|z| = 1$. For FIR channel models $\boldsymbol{A}(q^{-1}) = \mathbf{I}$, while $\boldsymbol{N}(q^{-1}) = \mathbf{I}$ for moving average noise descriptions.

In general, we assume that the leading matrix coefficient $\mathbf{M}_0$ in $\boldsymbol{M}(q^{-1})$ is non-singular.[5] The denominator matrices $\boldsymbol{A}(q^{-1})$ and $\boldsymbol{N}(q^{-1})$ are assumed to be monic. To simplify the presentation, $\boldsymbol{A}(q^{-1})$ and $\boldsymbol{N}(q^{-1})$ are also assumed to be *diagonal*. Compared to using full matrices, this will result in much less complex MMSE design equations, but might lead to unnecessarily high polynomial degrees in the matrix elements.[6] The polynomial elements in the matrices may have complex coefficients, and are assumed to be correctly estimated. The degree of $\boldsymbol{A}(q^{-1})$ is δA, whereas the matrix polynomials $\boldsymbol{B}(q^{-1})$, $\boldsymbol{M}(q^{-1})$ and $\boldsymbol{N}(q^{-1})$ have degrees δB, δM, and δN, respectively.

We will assume that each element $d_i(k)$ in the symbol vector $d(k)$ is a stochastic variable with zero mean. The vector $d(k)$ is also uncorrelated with the noise vector $e(k)$:

$$E[d(k)e^H(m)] = 0 \quad \forall k, m \,. \tag{2.8}$$

Finally, without restriction we assume that

$$Ed(k)d^H(m) = \mathbf{I}\,\delta_{km} \,, \tag{2.9}$$

where

$$\delta_{km} = \begin{cases} 1 & \text{if } k = m \\ 0 & \text{otherwise} \end{cases} \,.$$

The assumption on temporal whiteness of the transmitted symbols is generally valid in a communication system employing *interleaving* [48, Ch. 9]. Different elements in the symbol vector $d(k)$ are uncorrelated when they correspond to different users. The extension to correlated signals is straightforward.

The noise vector $e(k)$ in (2.6) has n_y elements. It is a possibly complex-valued, white stochastic process with zero mean and covariance matrix

$$E[e(k)e^H(k)] = \lambda_e \mathbf{I} \,. \tag{2.10}$$

This model is general enough to handle most scenarios of interest, and will be used as a basis for the design of two types of DFEs in Chapter 3.

2.3.2 A finite impulse response model

In cases where the general model (2.6) is considered too difficult to obtain we may consider a simpler structure. Such a structure is depicted in Figure 2.5. In this case,

[5] Since the noise model is only unique in the sense that it accurately models the noise spectral density, we can always choose an $\boldsymbol{M}(q^{-1})$ with $\mathbf{M}_0$ non-singular and still obtain the desired noise spectrum.

[6] Hence, neither $\boldsymbol{A}^{-1}(q^{-1})\boldsymbol{B}(q^{-1})$ nor $\boldsymbol{N}^{-1}(q^{-1})\boldsymbol{M}(q^{-1})$ constitute irreducible MFDs.

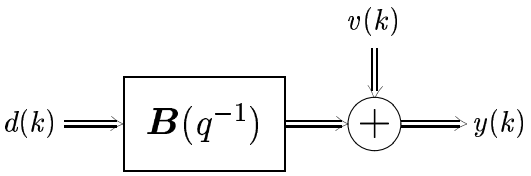

Figure 2.5: The FIR channel model. The channel is described by a polynomial matrix, whereas the noise is described by its matrix-valued covariance function.

the received signal can be described by the model

$$y(k) = \boldsymbol{B}(q^{-1})d(k) + v(k) \ , \tag{2.11}$$

where $\boldsymbol{B}(q^{-1})$ is a polynomial matrix of degree L with n_y rows and n_d columns. The properties of the signal d are described in Subsection 2.3.1, whereas the noise term is described by its matrix valued covariance function

$$\psi_{k-m} \stackrel{\triangle}{=} E[v(k)v^H(m)] \ . \tag{2.12}$$

Furthermore, v is uncorrelated with d:

$$E[d(k)v^H(m)] = 0 \quad \forall k, m \ . \tag{2.13}$$

This model is the most common model used for designing adaptive equalizers. Its structure permits an accurate description of wireless channels, and the channel $\boldsymbol{B}(q^{-1})$ can be easily estimated. However, estimation of the covariance function (2.12) can be very difficult. As we shall see, this model is closely tied to the third type of DFE that will be described in Chapter 3.

In the next chapter, we will show how to adjust the equalizer coefficients according to the criteria introduced in Section 2.2, using the channel models described in this section as a basis.

CHAPTER 3

The multivariable decision feedback equalizer

IN this chapter, three multivariable decision feedback equalizers will be presented:

1. The optimum, non-realizable DFE. The smoothing lag of this DFE is infinite, which is equivalent to allowing a non-causal feedforward filter. The scalar version of this DFE was originally derived by Monsen in [63], and the multivariable version was first derived in [28] for a channel with two inputs and two outputs, and in [23] for a more general multivariable channel with equal numbers of inputs and outputs. This DFE will be presented in Section 3.1.

2. The optimum realizable DFE, which has causal feedforward and feedback filters. The decisions on the symbols are made after a finite delay. This multivariable DFE was originally published in [90], and was a generalization of the scalar design presented by Sternad and Ahlén in [79]. This DFE will be discussed in Section 3.2.

3. The FIR DFE, where both feedforward and feedback filters are transversal filters. The degrees of the feedforward and feedback filter are design variables. This DFE was first derived in [101] and independently in [85]. See also [88, 92]. Section 3.3 will be devoted to the study of this DFE.

As mentioned in Chapter 2, we will consider two criteria for filter optimization: the *minimum mean-square error (MMSE)* criterion and the *zero-forcing (ZF)* criterion. A ZF equalizer may provide adequate performance when the noise can be neglected, but at low to moderate signal-to-noise ratios, the performance of an

MMSE equalizer will be superior. Therefore, an MMSE equalizer is often preferred for practical implementation.

However, studies of the multivariable ZF criterion can provide important information about the corresponding MMSE solution. When a ZF solution exists, the MMSE solution will approximate a ZF solution for low noise levels. In situations where *no* equalizer fulfills the ZF condition (2.3), an MMSE equalizer with the same structure will not work well. Its estimation error will not vanish for a vanishing noise level. The lack of a zero-forcing solution may be caused by an ill-posed problem and/or an inappropriate filter structure.

This effect will be most clearly visible with very disparate received signal powers. This is known as the *near-far problem* in the CDMA literature. The ability to detect a weak signal (typically originating far from the receiver) in the presence of strong (near) interfering signals is a distinguishing property of CDMA detectors. In this chapter, we will study under what conditions solutions to the multivariable zero-forcing problem exists. In Chapter 5, we will see how the non-existence of a zero-forcing equalizer will affect the near-far properties of the corresponding MMSE equalizer.

3.1 The optimum MMSE decision feedback equalizer

We will first derive the optimum MMSE DFE with no constraint on the smoothing lag. The only restriction we impose on the DFE is that the feedback filter must be strictly causal.[1]

Allowing an infinite smoothing lag is equivalent to allowing an arbitrary non-causal feedforward filter. To show this, we rewrite (2.2) as

$$\begin{aligned} \hat{d}(k|k+\ell) &= q^{\ell}\boldsymbol{\mathcal{R}}(q^{-1})y(k) - \boldsymbol{\mathcal{F}}(q^{-1})\tilde{d}(k-1) \\ \tilde{d}(k) &= \mathrm{f}(\hat{d}(k|k+\ell)) \; . \end{aligned}$$

We now let ℓ tend to infinity to obtain the optimum non-realizable MIMO DFE:

$$\begin{aligned} \hat{d}^{\infty}(k) &= \boldsymbol{\mathcal{R}}^{\infty}(q,q^{-1})y(k) - \boldsymbol{\mathcal{F}}^{\infty}(q^{-1})\tilde{d}(k-1) \\ \tilde{d}(k) &= \mathrm{f}(\hat{d}^{\infty}(k)) \; , \end{aligned} \tag{3.1}$$

[1] In [23], this assumption is relaxed. Present symbol decisions about one signal are used to improve the estimates of other signals.

where we have defined

$$\begin{aligned}\hat{d}^{\infty}(k) &\triangleq \lim_{\ell\to\infty} \hat{d}(k|k+\ell)\\ \boldsymbol{\mathcal{R}}^{\infty}(q,q^{-1}) &\triangleq \lim_{\ell\to\infty} q^{\ell}\boldsymbol{\mathcal{R}}(q^{-1})\\ \boldsymbol{\mathcal{F}}^{\infty}(q^{-1}) &\triangleq \lim_{\ell\to\infty} \boldsymbol{\mathcal{F}}(q^{-1})\ .\end{aligned}$$

Note that the filter $\boldsymbol{\mathcal{R}}^{\infty}(q,q^{-1})$ represents an arbitrary non-causal filter. The structure of the DFE now matches the structure of the DFE discussed in [23].

We introduce the following polynomial matrices:

$$\boldsymbol{\Gamma}(q^{-1}) \triangleq \boldsymbol{A}(q^{-1})\boldsymbol{M}(q^{-1}) \tag{3.2a}$$

$$\boldsymbol{\tau}(q^{-1}) \triangleq \boldsymbol{N}(q^{-1})\boldsymbol{B}(q^{-1})\ . \tag{3.2b}$$

We also define the polynomial matrices $\tilde{\boldsymbol{\Gamma}}(q^{-1})$ and $\tilde{\boldsymbol{\tau}}(q^{-1})$ by the matrix identity

$$\tilde{\boldsymbol{\tau}}(q^{-1})\tilde{\boldsymbol{\Gamma}}^{-1}(q^{-1}) = \boldsymbol{\Gamma}^{-1}(q^{-1})\boldsymbol{\tau}(q^{-1})\ , \tag{3.3}$$

which is equivalent to the linear polynomial matrix equation

$$\boldsymbol{\Gamma}(q^{-1})\tilde{\boldsymbol{\tau}}(q^{-1}) = \boldsymbol{\tau}(q^{-1})\tilde{\boldsymbol{\Gamma}}(q^{-1})\ .$$

Solving (3.3) implies finding a right MFD from a left MFD. Without restriction, we assume that, $\tilde{\boldsymbol{\tau}}(q^{-1})\tilde{\boldsymbol{\Gamma}}^{-1}(q^{-1})$ (in contrast to $\boldsymbol{\Gamma}^{-1}(q^{-1})\boldsymbol{\tau}(q^{-1})$) constitutes an irreducible MFD [40].

The coefficients of the optimum MMSE DFE can then be obtained using the following theorem:

Theorem 3.1 *Assume that a multivariable channel is described by* (2.6)*, and that the transmitted data is described by* (2.9)*. Furthermore, assume that the noise is described by* (2.10) *with* $\lambda_e > 0$ *and that* (2.8) *holds. Assuming correct past decisions, the non-causal feedforward filter* $\boldsymbol{\mathcal{R}}^{\infty}(q,q^{-1})$ *and causal feedback filter* $\boldsymbol{\mathcal{F}}^{\infty}(q^{-1})$ *of the optimum non-realizable MIMO MMSE DFE* (3.1) *are given by*

$$\boldsymbol{\mathcal{R}}^{\infty}(q,q^{-1}) = \frac{1}{\lambda_e}\tilde{\boldsymbol{\Gamma}}_0\mathbf{W}^{-1}\boldsymbol{\beta}_*^{-1}\tilde{\boldsymbol{\Gamma}}_*\boldsymbol{\tau}_*\boldsymbol{\Gamma}_*^{-1}\boldsymbol{M}^{-1}\boldsymbol{N} \tag{3.4a}$$

$$= \frac{1}{\lambda_e}\tilde{\boldsymbol{\Gamma}}_0\mathbf{W}^{-1}\boldsymbol{\beta}_*^{-1}\tilde{\boldsymbol{\tau}}_*\boldsymbol{M}^{-1}\boldsymbol{N} \tag{3.4b}$$

$$\boldsymbol{\mathcal{F}}^{\infty}(q^{-1}) = q(\tilde{\boldsymbol{\Gamma}}_0\boldsymbol{\beta}\tilde{\boldsymbol{\Gamma}}^{-1} - \mathbf{I})\ , \tag{3.4c}$$

where $\tilde{\mathbf{\Gamma}}_0$ is the leading coefficient of $\tilde{\mathbf{\Gamma}}$ and $\boldsymbol{\beta}$ is the monic and stable solution to the matrix spectral factorization

$$\boldsymbol{\beta}_* \mathbf{W} \boldsymbol{\beta} = \tilde{\mathbf{\Gamma}}_* \tilde{\mathbf{\Gamma}} + \frac{1}{\lambda_e} \tilde{\boldsymbol{\tau}}_* \tilde{\boldsymbol{\tau}} \ . \tag{3.5}$$

In (3.5), $\mathbf{W}$ *is a constant, positive definite matrix which has been introduced to make $\boldsymbol{\beta}$ monic.*

Proof: See Appendix A. ■

Remark 1. Note that since $\tilde{\mathbf{\Gamma}}_*$ and $\tilde{\boldsymbol{\tau}}_*$ have no common left factors, equation (3.5) has a unique solution $\{\boldsymbol{\beta}, \mathbf{W}\}$, where $\boldsymbol{\beta}$ is causally invertible. See [109] for a discussion.

Remark 2. The filter $\boldsymbol{\mathcal{F}}^{\infty}(q^{-1})$ will be causal, since the leading coefficient in $\tilde{\mathbf{\Gamma}}_0 \boldsymbol{\beta} \tilde{\mathbf{\Gamma}}^{-1}$ equals the identity matrix.

We can now determine the residual MSE for the optimum DFE when it is applied to the output of the channel (2.6). Assuming correct past decisions, we insert $\hat{d}^{\infty}(k)$ from (3.1) into (2.5) and use the optimum filters in Theorem 3.1 together with (3.3):

$$\varepsilon(k) = -\frac{1}{\lambda_e} \tilde{\mathbf{\Gamma}}_0 \mathbf{W}^{-1} \boldsymbol{\beta}_*^{-1} \tilde{\boldsymbol{\tau}}_* \boldsymbol{M}^{-1} \boldsymbol{N} y(k) + \tilde{\mathbf{\Gamma}}_0 \boldsymbol{\beta} \tilde{\mathbf{\Gamma}}^{-1} d(k) \ .$$

We now insert the channel model (2.6):

$$\begin{aligned} \varepsilon(k) = &-\frac{1}{\lambda_e} \tilde{\mathbf{\Gamma}}_0 \mathbf{W}^{-1} \boldsymbol{\beta}_*^{-1} \tilde{\boldsymbol{\tau}}_* \boldsymbol{M}^{-1} \boldsymbol{N} \left(\boldsymbol{A}^{-1} \boldsymbol{B} d(k) + \boldsymbol{N}^{-1} \boldsymbol{M} e(k) \right) \\ &+ \tilde{\mathbf{\Gamma}}_0 \boldsymbol{\beta} \tilde{\mathbf{\Gamma}}^{-1} d(k) \ . \end{aligned}$$

Keeping in mind that $\boldsymbol{N}$ and $\boldsymbol{A}^{-1}$ are diagonal and hence commute, we use the definitions (3.2a) and (3.2b) and rearrange:

$$\begin{aligned} \varepsilon(k) = &\left(\tilde{\mathbf{\Gamma}}_0 \boldsymbol{\beta} \tilde{\mathbf{\Gamma}}^{-1} - \frac{1}{\lambda_e} \tilde{\mathbf{\Gamma}}_0 \mathbf{W}^{-1} \boldsymbol{\beta}_*^{-1} \tilde{\boldsymbol{\tau}}_* \mathbf{\Gamma}^{-1} \boldsymbol{\tau} \right) d(k) \\ &- \frac{1}{\lambda_e} \tilde{\mathbf{\Gamma}}_0 \mathbf{W}^{-1} \boldsymbol{\beta}_*^{-1} \tilde{\boldsymbol{\tau}}_* e(k) \ . \end{aligned}$$

Making use of the identity (3.3), we can rewrite this as

$$\begin{aligned} \varepsilon(k) &= \tilde{\mathbf{\Gamma}}_0 \left(\boldsymbol{\beta} - \frac{1}{\lambda_e} \mathbf{W}^{-1} \boldsymbol{\beta}_*^{-1} \tilde{\boldsymbol{\tau}}_* \tilde{\boldsymbol{\tau}} \right) \tilde{\mathbf{\Gamma}}^{-1} d(k) - \frac{1}{\lambda_e} \tilde{\mathbf{\Gamma}}_0 \mathbf{W}^{-1} \boldsymbol{\beta}_*^{-1} \tilde{\boldsymbol{\tau}}_* e(k) \\ &= \tilde{\mathbf{\Gamma}}_0 \mathbf{W}^{-1} \boldsymbol{\beta}_*^{-1} \left(\boldsymbol{\beta}_* \mathbf{W} \boldsymbol{\beta} - \frac{1}{\lambda_e} \tilde{\boldsymbol{\tau}}_* \tilde{\boldsymbol{\tau}} \right) \tilde{\mathbf{\Gamma}}^{-1} d(k) - \frac{1}{\lambda_e} \tilde{\mathbf{\Gamma}}_0 \mathbf{W}^{-1} \boldsymbol{\beta}_*^{-1} \tilde{\boldsymbol{\tau}}_* e(k) \\ &= \tilde{\mathbf{\Gamma}}_0 \mathbf{W}^{-1} \boldsymbol{\beta}_*^{-1} \tilde{\mathbf{\Gamma}}_* \tilde{\mathbf{\Gamma}} \tilde{\mathbf{\Gamma}}^{-1} d(k) - \frac{1}{\lambda_e} \tilde{\mathbf{\Gamma}}_0 \mathbf{W}^{-1} \boldsymbol{\beta}_*^{-1} \tilde{\boldsymbol{\tau}}_* e(k) \end{aligned}$$

where we in the last equality used the spectral factorization (3.5). The final expression for the estimation error then becomes

$$\varepsilon(k) = \tilde{\mathbf{\Gamma}}_0 \mathbf{W}^{-1} \boldsymbol{\beta}_*^{-1} \left(\tilde{\mathbf{\Gamma}}_* d(k) - \frac{1}{\lambda_e} \tilde{\boldsymbol{\tau}}_* e(k) \right) .$$

Keeping in mind that $d(k)$ and $e(k)$ are uncorrelated, we use Parseval's relation for complex signals to obtain an expression for the estimation error covariance matrix (2.4):

$$\mathbf{P} = \frac{1}{2\pi j} \oint_{|z|=1} \tilde{\mathbf{\Gamma}}_0 \mathbf{W}^{-1} \boldsymbol{\beta}_*^{-1} \left(\tilde{\mathbf{\Gamma}}_* \tilde{\mathbf{\Gamma}} + \frac{1}{\lambda_e} \tilde{\boldsymbol{\tau}}_* \tilde{\boldsymbol{\tau}} \right) \boldsymbol{\beta}^{-1} \mathbf{W}^{-H} \tilde{\mathbf{\Gamma}}_0^H \frac{dz}{z} .$$

For a description on how Parseval's relation is used to evaluate these correlations, see[3]. Finally, we again use the spectral factorization (3.5):

$$\begin{aligned} \mathbf{P} &= \frac{1}{2\pi j} \oint_{|z|=1} \tilde{\mathbf{\Gamma}}_0 \mathbf{W}^{-1} \boldsymbol{\beta}_*^{-1} \boldsymbol{\beta}_* \mathbf{W} \boldsymbol{\beta} \boldsymbol{\beta}^{-1} \mathbf{W}^{-H} \tilde{\mathbf{\Gamma}}_0^H \frac{dz}{z} \\ &= \tilde{\mathbf{\Gamma}}_0 \mathbf{W}^{-H} \tilde{\mathbf{\Gamma}}_0^H . \end{aligned} \tag{3.6}$$

The filter $\boldsymbol{\tau}_* \mathbf{\Gamma}_*^{-1} \boldsymbol{M}^{-1} \boldsymbol{N}$ that appears as a right factor of (3.4a) constitutes a bank of *whitening matched filters*. This means that the received signal first is passed through a filter that whitens the noise. The noise whitened signal is then fed to a filter that is matched to an equivalent channel. To see this, we introduce the noise-whitened measurement signal

$$y_w(k) \triangleq \boldsymbol{M}^{-1}(q^{-1}) \boldsymbol{N}(q^{-1}) y(k) .$$

If we insert (2.6) into this expression, we obtain

$$\begin{aligned} y_w(k) &= \boldsymbol{M}^{-1}(q^{-1}) \boldsymbol{N}(q^{-1}) \left(\boldsymbol{A}^{-1}(q^{-1}) \boldsymbol{B}(q^{-1}) d(k) + \boldsymbol{N}^{-1}(q^{-1}) \boldsymbol{M}(q^{-1}) e(k) \right) \\ &= \boldsymbol{M}^{-1}(q^{-1}) \boldsymbol{N}(q^{-1}) \boldsymbol{A}^{-1}(q^{-1}) \boldsymbol{B}(q^{-1}) d(k) + e(k) \\ &= \boldsymbol{M}^{-1}(q^{-1}) \boldsymbol{A}^{-1}(q^{-1}) \boldsymbol{N}(q^{-1}) \boldsymbol{B}(q^{-1}) d(k) + e(k) \\ &= \mathbf{\Gamma}^{-1}(q^{-1}) \boldsymbol{\tau}(q^{-1}) d(k) + e(k) , \end{aligned}$$

since $\boldsymbol{N}(q^{-1})$ and $\boldsymbol{A}^{-1}(q^{-1})$ are diagonal and thus commute. The signal $d(k)$ has then passed through the equivalent channel

$$\mathbf{\Gamma}^{-1}(q^{-1}) \boldsymbol{\tau}(q^{-1}) ,$$

and a filter matched to this channel is equal to

$$\boldsymbol{\tau}_*(q) \mathbf{\Gamma}_*^{-1}(q) .$$

Hence, when the smoothing lag tends to infinity, there is no performance penalty associated with the introduction of such a filter prior to the optimization of the DFE. However, it is not possible to prove this when the feedforward filter is required to be causal.

Remark 3. The DFE described in this section resembles the DFE presented by Duel-Hallen in [23]. However, there are also important differences which make comparison of the resulting designs difficult:

- The DFE in [23] uses present decisions from one user to improve the estimation of the symbols for other users. The DFEs discussed in this thesis do not: only past decisions are fed back.
- The DFE in [23] assumes white noise and correlated symbols, whereas the DFE described in this section assumes colored noise and uncorrelated symbols.
- The DFE in [23] does not allow any poles in the channel description. Instead, the channel is described by an all-zero filter with infinite impulse response.

Due to the first property, we cannot choose a set of system parameters to obtain the same design equations.

Of course, an infinite smoothing lag is not admissible in practice. The only reason for studying this non-realizable DFE is that it provides a lower bound for the achievable MSE with any realizable DFE.

3.2 The optimum realizable decision feedback equalizer

If a DFE is to be implemented, it has to be realizable. One way of achieving this would be to use Theorem 3.1 to design a DFE with a non-causal feedforward filter. A suitable delay could then be introduced, and the feedforward filter could be truncated to make it causal. However, a better option would be to include the constraint of realizability already in the DFE design, as described below. The performance of such a DFE would be better than or equal to that of a DFE obtained from truncating the non-realizable DFE.

3.2.1 The MMSE design

In this case, we will use the DFE (2.2) directly, with a finite smoothing lag ℓ. The feedforward and feedback filter of the MMSE optimum realizable DFE can then be calculated using the following theorem

Theorem 3.2 *Assume that a multivariable channel is described by* (2.6)*, and that the transmitted data is described by* (2.9)*. Furthermore, assume that the noise is described by* (2.10) *with* $\lambda_e > 0$ *and that* (2.8) *holds. Assuming correct past decisions, the optimum realizable multivariable DFE* (2.2) *minimizes the estimation error covariance matrix* (2.4) *if and only if*

$$\boldsymbol{\mathcal{R}}(q^{-1}) = \boldsymbol{S}(q^{-1})\boldsymbol{M}^{-1}(q^{-1})\boldsymbol{N}(q^{-1}) \tag{3.7a}$$

$$\boldsymbol{\mathcal{F}}(q^{-1}) = \boldsymbol{Q}(q^{-1})\tilde{\boldsymbol{\Gamma}}^{-1}(q^{-1})\ . \tag{3.7b}$$

Above, $\boldsymbol{S}$ *and* $\boldsymbol{Q}$*, of dimensions* $n_d \times n_y$ *and* $n_d \times n_d$ *respectively, together with the polynomial matrices* $\boldsymbol{L}_1$ *and* $\boldsymbol{L}_2$ *of dimensions* $n_d \times n_d$ *and* $n_y \times n_d$ *respectively can be calculated as the unique solution to the two coupled polynomial matrix equations*

$$\tilde{\boldsymbol{\Gamma}} - q^{\ell}\boldsymbol{S}\tilde{\boldsymbol{\tau}} + q^{-1}\boldsymbol{Q} = \boldsymbol{L}_{1*}\tilde{\boldsymbol{\Gamma}} \tag{3.8a}$$

$$q^{-\ell}\boldsymbol{L}_{1*}\boldsymbol{\tau}_* - \lambda_e\boldsymbol{S}\boldsymbol{\Gamma}_* = q\boldsymbol{L}_{2*} \tag{3.8b}$$

where the degrees of the unknown polynomial matrices satisfy

$$\delta S = \ell \tag{3.9a}$$

$$\delta Q = \max(\delta\tilde{\Gamma}, \delta\tilde{\tau}) - 1 \tag{3.9b}$$

$$\delta L_1 = \ell \tag{3.9c}$$

$$\delta L_2 = \max(\delta\tau, \delta\Gamma) - 1\ . \tag{3.9d}$$

Proof: See Appendix B. ■

Remark 4. The degrees listed in (3.9a)–(3.9d) are sufficiently high. When τ_0 (and hence $\tilde{\tau}_0$) has full rank, these degree conditions are also necessary.

Remark 5. It is demonstrated in Appendix B that the design procedure described in Theorem 3.2 always provides a unique solution.

Remark 6. Note that the feedforward filter $\boldsymbol{\mathcal{R}}(q^{-1})$ will always contain a noise-whitening filter as a right factor. It will, however *not* contain any matched filter for $\ell < \infty$. The signal after the noise whitening

$$y_w(k) \triangleq \boldsymbol{M}^{-1}\boldsymbol{N}y(k) = \boldsymbol{M}^{-1}\boldsymbol{N}\boldsymbol{A}^{-1}\boldsymbol{B}d(k) + e(k)$$

is then equalized by an FIR feedforward filter $\boldsymbol{S}(q^{-1})$ which minimizes the precursor taps of the equalized channel and a feedback filter $\boldsymbol{\mathcal{F}}(q^{-1})$ which cancels all postcursor taps.

Remark 7. From (3.7a) and (3.7b), we see that both the feedforward and the feedback filters have the zeros of the noise description as poles. When these noise zeros are located close to the unit circle, the impulse response of both filters will be very long.

Remark 8. The two coupled *Diophantine equations* (3.8a) and (3.8b) are *unilateral*, since all the unknown polynomial matrices appear on the same (in this case left) side of their respective coefficient polynomial matrices. Solving these unilateral Diophantine equations corresponds to solving a block-Toeplitz system of linear equations, as demonstrated in Appendix B, equations (B.19)–(B.22).

Remark 9. The smoothing lag ℓ is a design variable and should be chosen as a trade-off between complexity and performance. In general, the smoothing lag should be chosen so that "enough" signal power can be collected by the feedforward filter before a decision is made. Actually, a performance close to that of the unconstrained solution in Theorem 3.1 is obtained when ℓ is chosen a few times the settling time of the impulse response of the noise-whitened channel $\boldsymbol{M}^{-1}\boldsymbol{N}\boldsymbol{A}^{-1}\boldsymbol{B} = \boldsymbol{\Gamma}^{-1}\boldsymbol{\tau}$. Also, the performance penalty of using a matched filter as an *a priori* component in the design of an optimum MMSE DFE diminishes.

Remark 10. In the next section, we will consider a DFE where feedforward and feedback filters are constrained to be FIR filters. Theorem 3.2 tells us that this *structure* is optimal only when the channel has a finite impulse response, and the noise is white or autoregressive.

When the channel is equalized using the optimum MMSE DFE, the estimate of the transmitted vector will be given by

$$\begin{aligned}\hat{d}(k-\ell|k) &= \boldsymbol{\mathcal{R}}(q^{-1})y(k) - \boldsymbol{\mathcal{F}}(q^{-1})d(k-\ell-1) \\ &= \boldsymbol{\mathcal{R}}(q^{-1})(\boldsymbol{A}^{-1}(q^{-1})\boldsymbol{B}(q^{-1})d(k) + \boldsymbol{N}^{-1}(q^{-1})\boldsymbol{M}(q^{-1})e(k)) \\ &\quad - \boldsymbol{\mathcal{F}}(q^{-1})d(k-\ell-1) \\ &= (\boldsymbol{\mathcal{R}}(q^{-1})\boldsymbol{A}^{-1}(q^{-1})\boldsymbol{B}(q^{-1}) - q^{-\ell-1}\boldsymbol{\mathcal{F}}(q^{-1}))d(k) + \boldsymbol{S}(q^{-1})e(k)\end{aligned}$$

when all previous decisions are assumed correct. We now insert (3.7a) and (3.7b) into this expression. We also use the definitions (3.2a) and (3.2b) to obtain

$$\begin{aligned}\hat{d}(k-\ell|k) = (&\boldsymbol{S}(q^{-1})\boldsymbol{\Gamma}^{-1}(q^{-1})\boldsymbol{\tau}(q^{-1}) - q^{-\ell-1}\boldsymbol{Q}(q^{-1})\tilde{\boldsymbol{\Gamma}}^{-1}(q^{-1}))d(k) \\ &+ \boldsymbol{S}(q^{-1})e(k)\ .\end{aligned}$$

We now utilize the factorization (3.3) together with (3.8a) to obtain

$$\hat{d}(k-\ell|k) = (q^{-\ell}\mathbf{I} - \bar{\boldsymbol{L}}_1(q^{-1}))d(k) + \boldsymbol{S}(q^{-1})e(k)\ , \tag{3.10}$$

where $\bar{\boldsymbol{L}}_1(q^{-1}) = q^{-\ell}\boldsymbol{L}_{1*}(q) = \mathbf{L}_{1\ell}^H + \mathbf{L}_{1,\ell-1}^H q^{-1} + \cdots + \mathbf{L}_{10}^H q^{-\ell}$. The *equivalent equalized channel* is thus given by

$$\boldsymbol{C}_{eq}(q^{-1}) = q^{-\ell}\mathbf{I} - \bar{\boldsymbol{L}}_1(q^{-1}) \; .$$

Note that the polynomial matrix $-\bar{\boldsymbol{L}}_1(q^{-1})$ represents the deviation from a zero-forcing solution.

Also, from (3.10) we can calculate the resulting estimation error covariance matrix (2.4). Using the assumptions (2.8)–(2.10), we readily obtain

$$\mathbf{P} = \sum_{n=0}^{\ell} \mathbf{L}_{1n}^H \mathbf{L}_{1n} + \lambda_e \sum_{n=0}^{\ell} \mathbf{S}_n \mathbf{S}_n^H \; . \tag{3.11}$$

The first term in (3.11) is caused by residual intersymbol and co-channel interference from the first ℓ taps in the equalized channel. The deviation of the reference tap from the identity matrix also contributes to the term. The last term in (3.11) is caused by the noise.

To illustrate the design procedure, we will consider a specific example.

EXAMPLE 3.1

We will determine an optimum realizable DFE with smoothing lag $\ell = 1$ when the channel is described by the FIR model

$$\begin{aligned} \boldsymbol{A}(q^{-1}) &= \mathbf{I} \\ \boldsymbol{B}(q^{-1}) &= \begin{pmatrix} 0.979 + 0.204q^{-1} & 0.826 + 0.563q^{-1} \\ -0.843 - 0.538q^{-1} & 0.403 + 0.915q^{-1} \end{pmatrix} \; , \end{aligned} \tag{3.12}$$

and the noise is described by the MA process

$$\begin{aligned} \boldsymbol{N}(q^{-1}) &= \mathbf{I} \\ \boldsymbol{M}(q^{-1}) &= \begin{pmatrix} -0.409 - 0.179q^{-1} & -0.535 + 0.717q^{-1} \\ -0.507 + 0.361q^{-1} & 0.761 - 0.181q^{-1} \end{pmatrix} \; . \end{aligned} \tag{3.13}$$

With $\lambda_e = 0.1$, we obtain an SNR of 10 dB at each of the channel outputs. For this system, we obtain $\boldsymbol{\tau}(q^{-1}) = \boldsymbol{B}(q^{-1})$ and $\boldsymbol{\Gamma}(q^{-1}) = \boldsymbol{M}(q^{-1})$. To determine the right MFD $\tilde{\boldsymbol{\tau}}(q^{-1})\tilde{\boldsymbol{\Gamma}}^{-1}(q^{-1})$ from the left MFD $\boldsymbol{\Gamma}^{-1}(q^{-1})\boldsymbol{\tau}(q^{-1}) = \boldsymbol{M}^{-1}(q^{-1})\boldsymbol{B}(q^{-1})$ we use the functions of the Polynomial Toolbox for use with MATLAB$^{\text{TM}}$, described in [35]. The result is

$$\begin{aligned} \tilde{\boldsymbol{\Gamma}}(q^{-1}) &= \begin{pmatrix} -0.698 + q^{-1} & -1.87 \\ 0.822 & -1.49 + q^{-1} \end{pmatrix} \\ \tilde{\boldsymbol{\tau}}(q^{-1}) &= \begin{pmatrix} -0.839 - 1.54q^{-1} & 3.1 + 3.35q^{-1} \\ 0.649 - 0.1q^{-1} & 3.35 + 1.62q^{-1} \end{pmatrix} \; . \end{aligned}$$

We now obtain the degrees of the polynomial matrices that satisfy the Diophantine equations (3.8a) and (3.8b) from (3.9a)–(3.9d):

$$\delta S = \delta L_1 = \ell = 1 \text{ and } \delta Q = \delta L_2 = 0$$

We can now insert the polynomial matrices $\boldsymbol{B}$, $\boldsymbol{M}$, $\tilde{\boldsymbol{\tau}}$, and $\tilde{\boldsymbol{\Gamma}}$ into (3.8a) and (3.8b). These Diophantine equations can be solved by first solving (B.22) in Appendix B for $\boldsymbol{S}(q^{-1})$ and $\boldsymbol{L}_1(q^{-1})$, then computing the right-hand side of (B.19) and finally obtaining $\boldsymbol{Q}(q^{-1})$ from (B.23). The solution is

$$\begin{aligned}\boldsymbol{S}(q^{-1}) &= \begin{pmatrix} 0.0331 + 0.117q^{-1} & -0.0563 - 0.662q^{-1} \\ -0.067 - 0.593q^{-1} & 0.0634 + 0.169q^{-1} \end{pmatrix} \\ \boldsymbol{Q}(q^{-1}) &= \begin{pmatrix} -1.0606 & -0.7068 \\ 0.8696 & -2.6606 \end{pmatrix} .\end{aligned}$$

With

$$\begin{aligned}\boldsymbol{M}^{-1}(q^{-1}) &= \frac{-1.715}{1 - 0.848q^{-1} + 0.388q^{-2}} \begin{pmatrix} 0.761 - 0.181q^{-1} & 0.535 - 0.717q^{-1} \\ 0.507 - 0.361q^{-1} & -0.409 - 0.179q^{-1} \end{pmatrix} \\ \tilde{\boldsymbol{\Gamma}}^{-1}(q^{-1}) &= \frac{0.388}{1 - 0.848q^{-1} + 0.388q^{-2}} \begin{pmatrix} -1.49 + q^{-1} & 1.87 \\ -0.822 & -0.698 + q^{-1} \end{pmatrix}\end{aligned}$$

we can calculate the final filters with the aid of (3.7a) and (3.7b):

$$\begin{aligned}\boldsymbol{\mathcal{R}}(q^{-1}) &= \begin{pmatrix} \frac{0.00571+0.398q^{-1}-0.373q^{-2}}{1-0.848q^{-1}+0.388q^{-2}} & -\frac{0.07-0.549q^{-1}-0.0589q^{-2}}{1-0.848q^{-1}+0.388q^{-2}} \\ \frac{0.0322+0.646q^{-1}-0.0791q^{-2}}{1-0.848q^{-1}+0.388q^{-2}} & \frac{0.106+0.646q^{-1}-0.677q^{-2}}{1-0.848q^{-1}+0.388q^{-2}} \end{pmatrix} \\ \boldsymbol{\mathcal{F}}(q^{-1}) &= \begin{pmatrix} \frac{0.838-0.412q^{-1}}{1-0.848q^{-1}+0.388q^{-2}} & \frac{-0.579-0.275q^{-1}}{1-0.848q^{-1}+0.388q^{-2}} \\ \frac{0.348+0.338q^{-1}}{1-0.848q^{-1}+0.388q^{-2}} & \frac{1.35-1.03q^{-1}}{1-0.848q^{-1}+0.388q^{-2}} \end{pmatrix} .\end{aligned}$$

We can also compute the equivalent channel from (3.10):

$$\boldsymbol{C}(q^{-1}) = \begin{pmatrix} 0.0645 + 0.946q^{-1} & -0.0235 + 0.0269q^{-1} \\ -0.0578 + 0.0269q^{-1} & 0.0694 + 0.95q^{-1} \end{pmatrix}$$

and the residual MSE from (3.11):

$$\mathbf{P} = \begin{pmatrix} 0.0539 & -0.0269 \\ -0.0269 & 0.0503 \end{pmatrix} .$$

3.2.2 The ZF design

To derive the conditions under which the optimum realizable DFE satisfies (2.3), we first need an expression for the estimation error. For this purpose, we insert (2.6) into (2.2) to obtain

$$\hat{d}(k-\ell|k) = \boldsymbol{\mathcal{R}}\left(\boldsymbol{A}^{-1}\boldsymbol{B}d(k) + \boldsymbol{N}^{-1}\boldsymbol{M}e(k)\right) - \boldsymbol{\mathcal{F}}\tilde{d}(k-\ell-1) \tag{3.14}$$

$$= \left(\boldsymbol{\mathcal{R}}\boldsymbol{A}^{-1}\boldsymbol{B} - q^{-\ell-1}\boldsymbol{\mathcal{F}}\right) d(k) + \boldsymbol{\mathcal{R}}\boldsymbol{N}^{-1}\boldsymbol{M}e(k)\,, \tag{3.15}$$

where we once again used the assumption on correct past decisions. We now insert $\hat{d}(k-\ell|k)$ into the expression for the estimation error:

$$\begin{aligned}\varepsilon(k-\ell) &= d(k-\ell) - \hat{d}(k-\ell|k)\\ &= \left(q^{-\ell}\mathbf{I} - \boldsymbol{\mathcal{R}}\boldsymbol{A}^{-1}\boldsymbol{B} + q^{-\ell-1}\boldsymbol{\mathcal{F}}\right) d(k) - \boldsymbol{\mathcal{R}}\boldsymbol{N}^{-1}\boldsymbol{M}e(k)\,.\end{aligned}$$

To ensure that the zero-forcing condition (2.3) is fulfilled, we must thus require that

$$q^{-\ell}\mathbf{I} - \boldsymbol{\mathcal{R}}\boldsymbol{A}^{-1}\boldsymbol{B} + q^{-\ell-1}\boldsymbol{\mathcal{F}} = 0$$

or, equivalently

$$\boldsymbol{\mathcal{R}}\boldsymbol{A}^{-1}\boldsymbol{B} - q^{-\ell-1}\boldsymbol{\mathcal{F}} = q^{-\ell}\mathbf{I}\,. \tag{3.16}$$

This condition is both sufficient and necessary due to the assumptions in (2.9) and (2.8).

Since the detection performance of a zero-forcing equalizer is inferior to that of a minimum mean-square error equalizer, we are usually not interested in actually finding a solution to (3.16). However, we are interested to see under what conditions a solution to (3.16) exists, since it would then represent the limit towards which an MMSE solution will converge for a vanishing noise variance. As will be discussed in Subsections 4.3.2 and 5.3.2, the existence of such a limit is an important indication for the soundness of an MMSE solution. The existence of ZF solutions is the topic of the following theorem:

Theorem 3.3 *There exists a solution to* (3.16) *if and only if every common right divisor of* $\boldsymbol{A}^{-1}\boldsymbol{B}$ *and* $q^{-\ell-1}\mathbf{I}$ *is a right divisor also of* $q^{-\ell}\mathbf{I}$*. The right divisors should be members of the ring of stable and causal rational matrices.*

Proof: The theorem follows from the general theory of Diophantine equations, see [45]. ■

The theorem can be used to find out if there exists a zero-forcing MIMO DFE for any given channel and smoothing lag. However, we can use the theorem also to find trivial channel characteristics that preclude the existence of a zero-forcing DFE. The following two corollaries are examples of such cases.

Corollary 3.1 *If* $\operatorname{rank} \boldsymbol{A}^{-1}\boldsymbol{B} < n_d$*, then* $\boldsymbol{A}^{-1}\boldsymbol{B}$ *and* $q^{-\ell-1}\mathbf{I}$ *will always have a common right divisor that is not a right divisor of* $q^{-\ell}\mathbf{I}$*.*

Proof: See Appendix D. ■

The exact procedure for finding the rank of a rational matrix can be found in [40, Sec. 6.5]. Three important situations when the rank is smaller than n_d are:

- *More channel inputs than channel outputs.* Since

  $$\operatorname{rank} \boldsymbol{A}^{-1}\boldsymbol{B} \leq \min(n_y, n_d) \leq n_y \ ,$$

  we realize that $\operatorname{rank} \boldsymbol{A}^{-1}\boldsymbol{B}$ is smaller than n_d whenever $n_y < n_d$.

- *Linearly dependent columns.* When the channels from some of the transmitters are linearly dependent, $\boldsymbol{A}^{-1}\boldsymbol{B}$ will loose rank.

- *More than* $n_y - n_d$ *linearly dependent rows.* In some cases, the channels to some of the receivers may be linearly dependent. This could happen when the multivariable channel model is obtained by excessive oversampling of a band-limited signal. When more than $n_y - n_d$ of these row channels are linearly dependent, the rank of the channel will be less than n_d.

For the second corollary, we define

$$\Delta_i \stackrel{\triangle}{=} \text{the propagation delay of user } i \text{ in any channel.} \tag{3.17}$$

Thus, Δ_i is the largest number such that the first Δ_i column taps in the matrix polynomial representation of column i in $\boldsymbol{B}(q^{-1})$ are identically zero. This leads to the following formulation:

Corollary 3.2 *If* $\Delta_i > \ell$ *for some* i*, then* $\boldsymbol{A}^{-1}\boldsymbol{B}$ *and* $q^{-\ell-1}\mathbf{I}$ *will always have a common right divisor that is not a right divisor of* $q^{-\ell}\mathbf{I}$*.*

Proof: See Appendix D. ■

Remark 11. From the perspective of a detector designer, Corollary 3.2 is enlightening. When designing a multiuser detector, it is vital to choose a smoothing lag that is guaranteed to exceed the bulk delay of *all* users.

Additional insights into the problem of finding zero-forcing DFEs can be obtained by rewriting (3.16) as

$$q^{-\ell}\mathbf{I} = (\mathbf{I} + q^{-1}\boldsymbol{\mathcal{F}})^{-1}\boldsymbol{\mathcal{R}}\boldsymbol{A}^{-1}\boldsymbol{B} \triangleq \boldsymbol{\mathcal{H}}^{L}\boldsymbol{\mathcal{H}} \ . \tag{3.18}$$

with $\boldsymbol{\mathcal{H}} = \boldsymbol{A}^{-1}\boldsymbol{B}$ and

$$\boldsymbol{\mathcal{H}}^{L} = (\mathbf{I} + q^{-1}\boldsymbol{\mathcal{F}})^{-1}\boldsymbol{\mathcal{R}} \ .$$

Here, $\boldsymbol{\mathcal{H}}^{L}$ is a left inverse of $\boldsymbol{\mathcal{H}}$ for $\ell = 0$ and it represents a generalized left inverse for $\ell > 0$. Since both $\boldsymbol{\mathcal{F}}$ and $\boldsymbol{\mathcal{R}}$ are required to be causal, $\boldsymbol{\mathcal{H}}^{L}$ must be causal. However, $\boldsymbol{\mathcal{H}}^{L}$ is not required to be stable: Even if $\boldsymbol{\mathcal{F}}$ is stable $(\mathbf{I} + q^{-1}\boldsymbol{\mathcal{F}})^{-1}$ may very well be unstable. Thus, the class of admissible $\boldsymbol{\mathcal{H}}^{L}$s is much larger for DFEs than for linear equalizers ($\boldsymbol{\mathcal{F}} = 0$): Unstable zeros of $\boldsymbol{B}$ cannot be canceled by $\boldsymbol{\mathcal{R}}$, since $\boldsymbol{\mathcal{R}}$ is required to be stable. See [33] for conditions for the existence of a multivariable zero-forcing linear equalizer.

Another reformulation of (3.16) also provides some additional insight. We realize that we can write

$$q^{-\ell}\mathbf{I} = \begin{pmatrix} \boldsymbol{\mathcal{R}} & \boldsymbol{\mathcal{F}} \end{pmatrix} \begin{pmatrix} \boldsymbol{A}^{-1}\boldsymbol{B} \\ -q^{-\ell-1}\mathbf{I} \end{pmatrix} \ . \tag{3.19}$$

We thus see that it is the properties of

$$\begin{pmatrix} \boldsymbol{A}^{-1}\boldsymbol{B} \\ -q^{-\ell-1}\mathbf{I} \end{pmatrix}$$

rather than the properties of $\boldsymbol{A}^{-1}\boldsymbol{B}$ alone that determine the existence of a zero-forcing solution.

3.3 The optimum FIR decision feedback equalizer

In practice, implementation of the optimum realizable DFE may be deemed inappropriate. This is true in particular when an adaptive implementation is considered, since, for instance, stability monitoring has to be performed. Also, acquiring a parametric model of the noise may be too computationally intensive. In the performance comparison at the end of this chapter, we will see that error propagation may severely degrade the performance of the DFE derived from Theorem 3.2, which is yet another reason to consider a different DFE structure.

An attractive alternative is to use a DFE where both feedforward and feedback filters are multiple-input multiple-output FIR filters of predetermined degrees. We

will call this equalizer the *FIR* or *conventional DFE*. In this DFE, we thus have

$$\boldsymbol{\mathcal{R}}(q^{-1}) = \boldsymbol{S}(q^{-1}) = \mathbf{S}_0 + \mathbf{S}_1 q^{-1} + \cdots + \mathbf{S}_{\delta s} q^{-\delta s} \tag{3.20a}$$

$$\boldsymbol{\mathcal{F}}(q^{-1}) = \boldsymbol{Q}(q^{-1}) = \mathbf{Q}_0 + \mathbf{Q}_1 q^{-1} + \cdots + \mathbf{Q}_{\delta Q} q^{-\delta Q} \ . \tag{3.20b}$$

where δs is a design variable, whereas δQ will be a function of δs, the channel degree L and the smoothing lag ℓ. The FIR DFE is thus implemented as

$$\begin{aligned} \hat{d}(k-\ell|k) &= \boldsymbol{S}(q^{-1})y(k) - \boldsymbol{Q}(q^{-1})\tilde{d}(k-\ell-1) \\ \tilde{d}(k-\ell) &= \mathrm{f}(\hat{d}(k-\ell|k)) \ . \end{aligned} \tag{3.21}$$

3.3.1 The MMSE design

To obtain a conventional MMSE DFE, the matrix coefficients in (3.20a) and (3.20b) are adjusted so that the MSE (2.4) is minimized. The resulting design equations are given in the next theorem.

Theorem 3.4 *Consider the multivariable DFE described by* (3.21)*, the FIR channel model* (2.11) *and the input signal statistics* (2.9)*. Assume that the noise is described by* (2.12) *with ψ_0 being non-singular, and assume that* (2.13) *holds. If all past decisions are assumed correct, then the unique matrix polynomials $\boldsymbol{S}(q^{-1})$ and $\boldsymbol{Q}(q^{-1})$ in* (3.21) *of orders δs and $\delta Q = L + \delta s - \ell - 1$ respectively, minimizing the MSE* (2.4)*, are obtained as follows:*

1. *The feedforward filter $\boldsymbol{S}(q^{-1}) = \mathbf{S}_0 + \mathbf{S}_1 q^{-1} + \cdots + \mathbf{S}_{\delta s} q^{-\delta s}$ is determined by solving the system of $n_y(\delta s + 1)$ linear equations*

$$(\mathcal{F}\mathcal{F}^H + \Psi) \begin{pmatrix} \mathbf{S}_0^H \\ \vdots \\ \mathbf{S}_{\delta s}^H \end{pmatrix} = \begin{pmatrix} \mathbf{B}_\ell \\ \vdots \\ \mathbf{B}_0 \\ \mathbf{0} \end{pmatrix} \tag{3.22}$$

   with respect to the $n_y \times n_d$ matrix coefficients $\mathbf{S}_n^H$, where $\mathcal{F}$ is the $n_y(\delta s + 1) \times n_d(\ell + 1)$ matrix

$$\mathcal{F} = \begin{pmatrix} \mathbf{B}_0 & \mathbf{B}_1 & \dots & \mathbf{B}_\ell \\ 0 & \mathbf{B}_0 & \dots & \mathbf{B}_{\ell-1} \\ \vdots & \ddots & \ddots & \vdots \\ 0 & \dots & 0 & \mathbf{B}_0 \\ \mathbf{0} & \dots\dots & & \mathbf{0} \end{pmatrix} \tag{3.23}$$

and where

$$\Psi = \begin{pmatrix} \psi_0 & \cdots & \psi_{\delta s} \\ \vdots & \ddots & \vdots \\ \psi_{-\delta s} & \cdots & \psi_0 \end{pmatrix} . \tag{3.24}$$

2. *The coefficients of the feedback filter* $\boldsymbol{Q}(q^{-1}) = \mathbf{Q}_0 + \mathbf{Q}_1 q^{-1} + \cdots + \mathbf{Q}_{\delta Q} q^{-\delta Q}$ *are given by*

$$\mathbf{Q}_n = \sum_{m=\max(0,n-L+\ell+1)}^{\min(\delta s,\ell+n+1)} \mathbf{S}_m \mathbf{B}_{\ell+1-m+n} \tag{3.25}$$

where $\delta Q = L + \delta s - \ell - 1$.

Proof: See Appendix C. ■

Remark 12. The condition that the noise covariance for lag zero, ψ_0, has full rank ensures that the matrix $\mathcal{F}\mathcal{F}^H + \Psi$ in (3.22) is non-singular. A unique MMSE solution will thus always exist.

Remark 13. For a given detection scenario, the structure of the DFE is determined by the decision delay ℓ and the degrees of the feedforward and feedback filters. The impact of these three variables is outlined below.

- The decision delay ℓ is chosen as a trade-off between complexity and performance: the larger decision delay, the better the performance. However, choosing ℓ larger than the delay spread L only leads to minor improvements in performance. This is in accordance with the rule of thumb in Subsection 3.2.1: ℓ should be chosen so that "enough" signal power can be collected by the feedforward filter before a decision is made.
- The degree δs of the feedforward filter should be chosen as large as possible, at least equal to the decision delay ℓ. When the noise is assumed to be temporally white ($\psi_n = 0,\ n \neq 0$), equation (3.22) will give $\mathbf{S}_n = 0$ for $n > \ell$. This is however *not* true when the noise is temporally colored, and choosing a feedforward filter length which is larger than the decision delay will in this case give better performance. In fact, for a fixed feedforward filter degree, performance can even be improved if the decision delay is decreased!
- The degree δQ of the feedback filter should be large enough to cancel all postcursor taps in the linearly equalized channel $\boldsymbol{S}(q^{-1})\boldsymbol{B}(q^{-1})$. A lower

degree will lead to a loss in performance, and a higher degree will not improve performance. The number of postcursor taps equals $L+\delta s-\ell$, so we conclude that $\delta Q = L + \delta s - \ell - 1$.

It is enlightening to compare the above rule of thumb for selection of δs with the degree conditions in Subsection 3.2.1. When the noise can be modeled as an MA or ARMA process, the feedforward filter of the optimum realizable DFE has an infinite impulse response. The performance of the FIR DFE will then improve with increasing δs. On the other hand, if the noise is described by an autoregressive model, the length of the feedforward filter of the optimum realizable DFE equals

$$\delta s + \delta N = \ell + \delta N$$

which is finite. In this case, the resulting MSE at the output of the FIR DFE does not decrease as δS is increased above $\ell + \delta N$.

The residual MSE at the output of the DFE described in Theorem 3.4 is given in the following corollary to Theorem 3.4:

Corollary 3.3 *When the FIR MMSE DFE designed from Theorem 3.4 is applied to the output of the channel* (2.11)*, the residual MSE is given by*

$$\mathbf{P} = \mathbf{I} - \mathcal{F}_{pres}^H \left(\mathcal{F}\mathcal{F}^H + \Psi\right)^{-1} \mathcal{F}_{pres} \tag{3.26}$$

where $\mathcal{F}$ and Ψ are defined in (3.23) *and* (3.24)*, respectively, and*

$$\mathcal{F}_{pres} \triangleq \begin{pmatrix} \mathbf{B}_\ell \\ \vdots \\ \mathbf{B}_0 \\ \mathbf{0} \end{pmatrix} .$$

Proof: See Appendix C. ■

In the next chapter, the conventional DFE will be used as a multiuser detector in conjunction with an antenna array. In Chapter 5, we will derive a time-varying version of the FIR DFE in Theorem 3.4, which will be used as a multiuser detector for DS-CDMA.

3.3.2 The ZF design

To derive the design equations for an FIR DFE that fulfills the zero-forcing condition, we proceed as in Subsection 3.2.2: We insert (2.11) into (3.21) and rearrange to obtain the equation

$$\hat{d}(k-\ell|k) = \left(\boldsymbol{S}\boldsymbol{B} - q^{-\ell-1}\boldsymbol{Q}\right) d(k) + \boldsymbol{S}v(k) \; . \tag{3.27}$$

As always, to obtain the above equation, the assumption on correct past decisions has been used. For the estimator (3.27) to be zero-forcing as defined in Defintion 2.1, we must require

$$q^{-\ell}\mathbf{I} = \boldsymbol{S}\boldsymbol{B} - \boldsymbol{Q}q^{-\ell-1} \ . \tag{3.28}$$

This condition is sufficient and necessary, due to the assumptions (2.13) and (2.9).

The solvability of (3.28) is discussed in the next theorem.

Theorem 3.5 *There exists a solution to* (3.28) *if and only if every common right divisor of* $\boldsymbol{B}(q^{-1})$ *and* $q^{-\ell-1}\mathbf{I}$ *is a right divisor also of* $q^{-\ell}\mathbf{I}$*. The right divisors should be members of the ring of polynomial matrices.*

Proof: The theorem follows from the general theory of Diophantine equations, see [45]. ■

The same two situations as in Subsection 3.2.2 cause the condition in Theorem 3.5 to be violated. For completeness, we formulate the corresponding corollaries below.

Corollary 3.4 *If* $\operatorname{rank} \boldsymbol{B} < n_d$*, then* $\boldsymbol{B}$ *and* $q^{-\ell-1}\mathbf{I}$ *will always have a common right divisor that is not a right divisor of* $q^{-\ell}\mathbf{I}$*.*

Proof: See Appendix D. ■

To determine the rank of a polynomial matrix, the procedure described in [40, Sec. 6.3] can be used. See also the MATLAB™ functions in the Polynomial Toolbox [35].

As in Subsection 3.2.2, we realize that the rank of $\boldsymbol{B}$ is smaller than n_d when

- $n_y < n_d$,
- some of the columns in $\boldsymbol{B}$ are linearly dependent, or
- more than $n_y - n_d$ of the rows of $\boldsymbol{B}$ are linearly dependent.

Corollary 3.5 *If* $\Delta_i > \ell$*, defined in* (3.17) *for some* i*, then* $\boldsymbol{B}$ *and* $q^{-\ell-1}\mathbf{I}$ *will always have a common right divisor that is not a right divisor of* $q^{-\ell}\mathbf{I}$*.*

Proof: See Appendix D. ■

The condition for the existence of a zero-forcing FIR DFE is a lot milder than the corresponding condition for a linear equalizer. For a zero-forcing linear equalizer to exist, there must be no common factor in any column of $\boldsymbol{B}(q^{-1})$ other than

$q^{-n},\ n \leq \ell$. See [34] for a discussion. Such common factors can easily be handled by the DFE.

When the condition in Theorem 3.5 is fulfilled, we know that a zero-forcing FIR DFE exists, *for some degrees of the filters* $\boldsymbol{S}$ *and* $\boldsymbol{Q}$. In Theorem 3.6, the required degree of the feedforward filter $\boldsymbol{S}$ is specified.

Theorem 3.6 *Consider the MIMO channel model* (2.11) *with* n_d *sources and* n_y *measurement signals and assume that the condition in Theorem 3.5 is fulfilled. A generically necessary*[2] *condition for the existence of a zero-forcing FIR MIMO DFE* (3.21) *with decision delay* ℓ *and feedforward filter degree* δ_S *is then that*

$$\delta_S \geq \frac{n_d(\ell+1) - \sum_{m=1}^{n_d} \Delta_m}{n_y} - 1 \ , \tag{3.29}$$

where Δ_m *is defined in* (3.17)*.*

Proof: See Appendix E. ■

When the degree of the feedforward filter is chosen smaller than the degree specified in Theorem 3.6, the DFE will have inadequate degrees of freedom to suppress all intersymbol and co-channel interference.

3.4 A comparison of the MMSE DFEs

To compare the three MMSE decision feedback equalizers introduced in this chapter, we will consider a specific example: the channel and noise description introduced in Example 3.1. To compare the performances of these DFEs, we will evaluate their respective estimation error covariance matrices. In Subsection 3.4.1, all previous decisions are assumed to be correct and the estimation error covariance matrix is evaluated from (3.6) and (3.11). In Subsection 3.4.2, we directly estimate the covariance matrix. To obtain a suitable scalar performance measure, we in both subsections use $\mathrm{tr}\,\mathbf{P}$ and normalize with the number of transmitters.

3.4.1 A comparison of the optimum and the optimum realizable DFE

We will start by comparing the optimum DFE determined from Theorem 3.1 and the optimum realizable DFE determined from Theorem 3.2. Our objective is to address the performance penalty associated with the realizability constraint, that

[2] Generic necessity of the degree condition in Theorem 3.6 should be interpreted as follows: When (3.29) is violated, a zero-forcing equalizer exists with probability zero if the channel taps $\mathbf{B}_0, \ldots, \mathbf{B}_L$ are random matrices. See also [82, p. 266]

is, how much the performance degrades when the feedforward filter is required to be causal. More specifically, we will investigate the performance of the optimum realizable DFE as a function of the smoothing lag, and compare it to that of the non-realizable DFE. As shown in Section 3.1, the non-realizable DFE can be thought of as a realizable DFE with an infinite smoothing lag.

Theorem 3.1 is thus used to determine an optimum non-realizable MMSE DFE for the channel (3.12) and the noise description (3.13). The SNR equals 0, 5 or 10 dB and is defined by

$$\mathrm{SNR}_j \stackrel{\triangle}{=} \frac{E\left[s_j^H(k)s_j(k)\right]}{E\left[v^H(k)v(k)\right]} \tag{3.30}$$

where

$$s_j(k) \stackrel{\triangle}{=} \boldsymbol{A}^{-1}(q^{-1})\boldsymbol{B}_j(q^{-1})d_j(k)\ ; \quad v(k) \stackrel{\triangle}{=} \boldsymbol{N}^{-1}(q^{-1})\boldsymbol{M}(q^{-1})e(k)\ ,$$

and $\boldsymbol{B}_j(q^{-1})$ is column j in $\boldsymbol{B}(q^{-1})$. In this section, we assume that the SNR is equal for the two users and hence independent of j.

From (3.6), we obtain the following residual MSEs:

SNR	$\frac{1}{2}\,\mathrm{tr}\,\mathbf{P}$
0 dB	0.2292
5 dB	0.1029
10 dB	0.0389

For the channel and noise description in Example 3.1, we evaluate the residual MSE also for the optimum realizable DFE using (3.11). The smoothing lag ℓ varies between 0 and 10, and the SNR is 0, 5 or 10 dB. The result is shown in Figure 3.1 together with the residual MSE for the non-realizable DFE.

It is clear from Figure 3.1 that it is sufficient to use a rather small smoothing lag in the optimum realizable DFE to obtain a performance that is very close to the performance of the non-realizable DFE: The curves are indistinguishable for $\ell \geq 6$.

The difference in performance between the two DFEs is remarkably small. Apparently, having a smoothing lag $\ell = 6$ is sufficient for the realizable DFE to be able to capture enough signal energy. Keeping in mind the rule of thumb that we introduced in Remark 9 on page 48, we realize that the smoothing lag that the optimum realizable DFE requires to obtain the performance of the non-realizable DFE grows with the settling time of the impulse response of the noise-whitened channel. In this example, the poles of the noise-whitened channel are the zeros of the

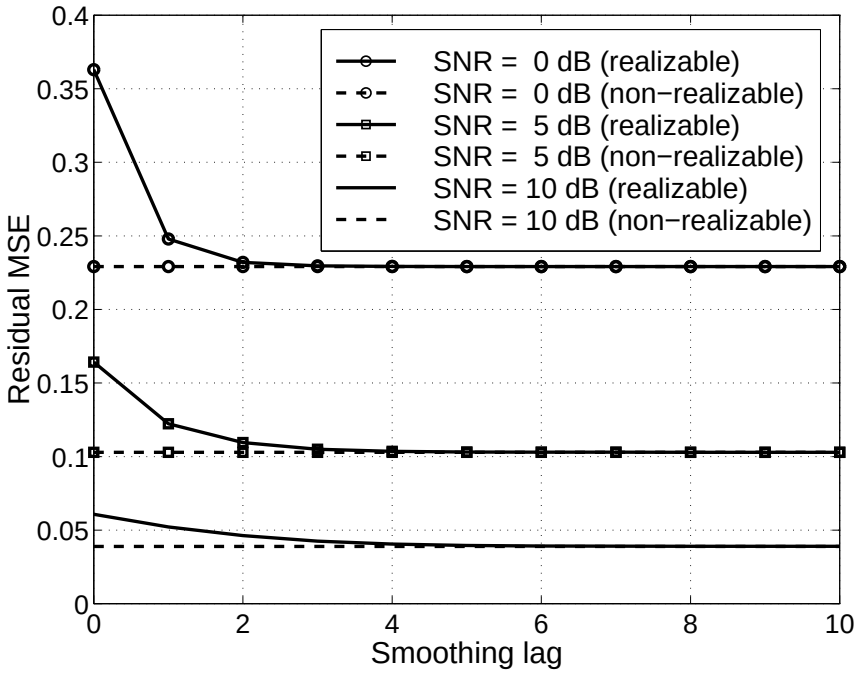

Figure 3.1: Comparison of the optimum and optimum realizable DFE as a function of the smoothing lag of the realizable DFE.

noise description $\boldsymbol{M}(q^{-1})$, which are located at $0.424 \pm 0.457j = 0.623e^{\pm 0.823j}$. The closer these zeros are to the unit circle, the larger the performance difference becomes between the optimum and the optimum realizable DFE with a fixed smoothing lag.

Finally, we compare the tuning complexities of the two DFEs. Both DFEs require one operation that the other does not:

- To determine the non-realizable DFE, the spectral factorization (3.5) must be solved.
- To determine the realizable DFE, the system of linear equations (B.22) must be solved.

The relative complexity of these two operations depends on the relation between n_y and n_d. When n_y is large in comparison to n_d, solving (B.22) is more complex, but when n_d and n_y are equal, the multivariable spectral factorization is more computationally intensive. See [38] for an efficient implementation of the multivariable spectral factorization.

3.4.2 A comparison of the optimum realizable and the FIR DFE

We will now compare the performance of the optimum realizable DFE (2.2) and the FIR DFE (3.21). Again, we are interested in how the performance is degraded by the *a priori* selection of a structure that is inappropriate for the equalization problem in this example. In this subsection, the impact of using decisions from the decision device is also investigated. Finally, we address the influence of the additional design variable δs.

Again, we use Theorem 3.2 to determine the optimum realizable DFE with $\ell = 1$ for the channel in Example 3.1. To determine the FIR DFE, we use Theorem 3.4. To compute the covariance function of the noise term $v(k)$, we use

$$v(k) = \boldsymbol{M}(q^{-1})e(k) \; .$$

This can be inserted into (2.12) to obtain

$$\begin{aligned}
\psi_0 &= \lambda_e \left(\mathbf{M}_0 \mathbf{M}_0^H + \mathbf{M}_1 \mathbf{M}_1^H \right) = \lambda_e \begin{pmatrix} 1.0000 & -0.3938 \\ -0.3938 & 1.0000 \end{pmatrix} \\
\psi_1 &= \lambda_e \mathbf{M}_1 \mathbf{M}_0^H = \lambda_e \begin{pmatrix} -0.3103 & 0.6366 \\ -0.0512 & -0.3207 \end{pmatrix} \\
\psi_n &= \mathbf{0}, \quad n > 1 \; .
\end{aligned}$$

Optimum coefficients of the MMSE FIR DFE can now be obtained.

The optimum realizable and the FIR DFE are now simulated with BPSK modulated signals. The MSE is averaged over 200 realizations, each consisting of 50000 transmitted symbols.

SNR dependence First, we address the performance of these DFEs as a function of the SNR with $\delta s = 2$. This feedforward filter degree was chosen so that both DFEs are described by the same number of parameters. The result is shown in Figure 3.2 for an SNR between 0 and 15 dB.

We see in Figure 3.2 that the optimal realizable DFE is only slightly better than the FIR DFE: With correct decisions, the difference is only 0.6 dB over the entire investigated range of SNRs. With real decisions, the FIR DFE is actually *better* than the "optimum" DFE for low SNR! Thus, the DFE determined from Theorem 3.2 seems to be more sensitive to incorrect decisions than the FIR DFE. However, for SNRs over 4 dB, the optimum realizable DFE is better. At this SNR, about three percent of the decisions are incorrect.

Dependence on location of noise zeros For the considered FIR channel, the structure of the FIR DFE is optimal when the additive noise is temporally white.

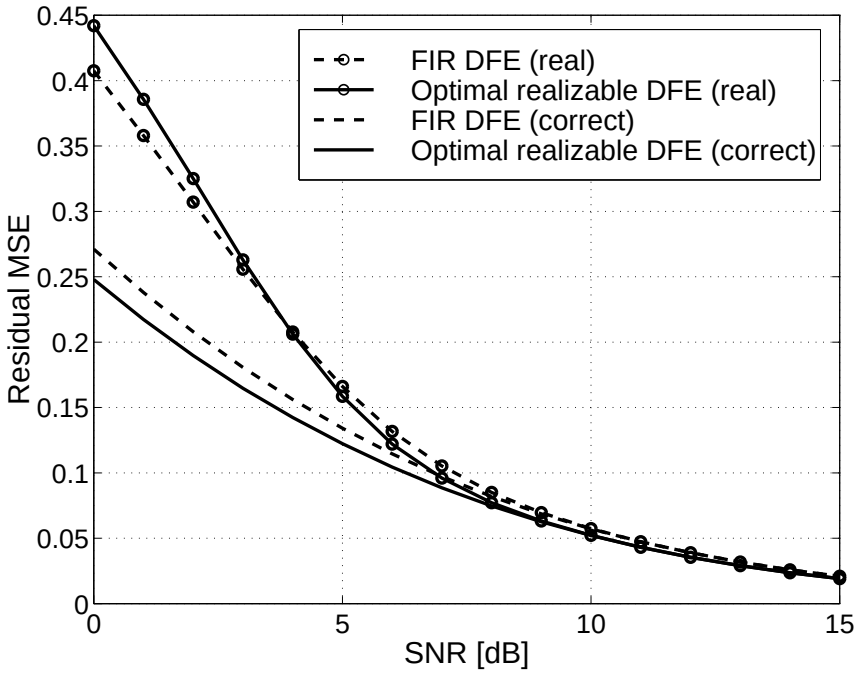

Figure 3.2: Comparison of the optimum realizable and the FIR DFE as a function of the SNR. The residual MSE is estimated over 200 realizations, each consisting of 50000 transmitted symbols. The DFEs are executed using either correct decisions (correct) or decisions from the decision device (real).

White noise corresponds to noise described by a moving average process, whose zeros are located in the origin. Therefore, the difference between the optimum realizable DFE and the FIR DFE should be smaller, the closer to the origin the noise zeros lie. Correspondingly, when the noise zeros lie close to the unit circle, the difference should be larger.

To investigate this assumption, the locations of the zeros of the noise model are varied according to

$$z_{1,2}(r) = re^{\pm j0.823},\ r = 0.01,\, 0.1,\, 0.2,\, \ldots,\, 0.9,\, 0.95,\, 0.98,\, 0.99,$$

while the SNR, as defined in (3.30), is kept constant at 5 dB. Thus, the noise model zeros are moved along a radius, from the origin towards the unit circle. All other conditions for the simulation scenario are as in Figure 3.2. The result is depicted in Figure 3.3.

The location of the noise zeros clearly affects the relative performances of the two algorithms. When the zeros are close to the origin, the performance of the

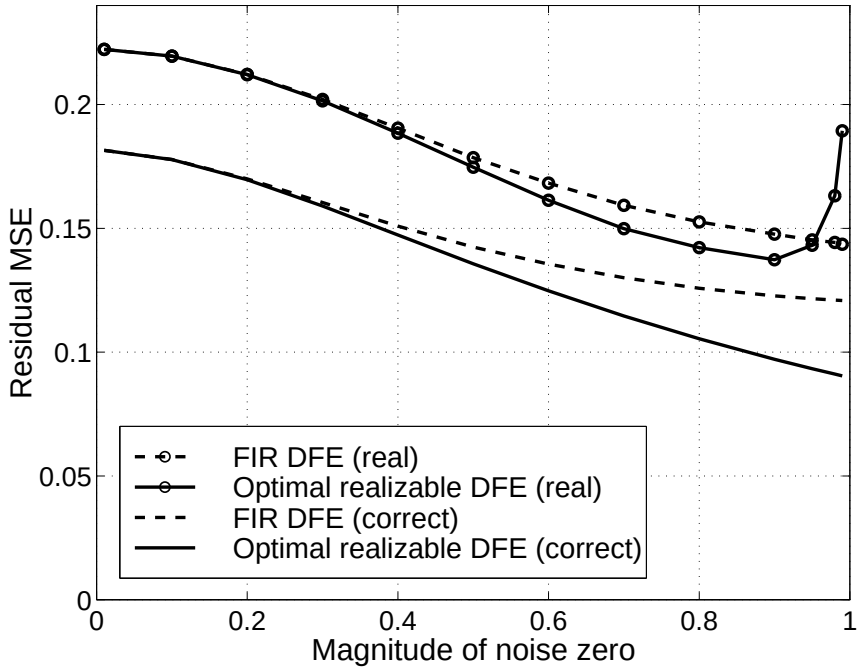

Figure 3.3: Comparison of the optimum realizable and the FIR DFE as a function of the position of the noise zero. The SNR is 5 dB. The residual MSE is estimated over 200 realizations, each consisting of 50000 transmitted symbols. The DFEs are executed using either correct decisions (correct) or decisions from the decision device (real).

two DFEs are identical, but the further out towards the unit circle the zeros are moved, the larger the difference becomes when correct decisions are used. One interesting discovery is the performance of the optimum realizable DFE with real decisions when the noise zeros are located very close to the unit circle: In this scenario, error propagation causes bad performance. The reason is that when the noise zeros are close to the unit circle, so are the poles of the feedback filter. The impulse response of the feedback filter then becomes very long, leading to a higher probability of error bursts.

Dependence on feedforward filter degree For the present example, the structure of the FIR DFE approaches the optimum structure when $\delta s \to \infty$. The performance of the FIR DFE should then approach the performance of the optimum DFE with increasing feedforward filter degree. We therefore investigate the per-

formance of the FIR DFE for feedforward filter degrees between one and ten, that is for $1 \leq \delta s \leq 10$. The result is depicted in Figure 3.4 for an SNR of 5 dB.

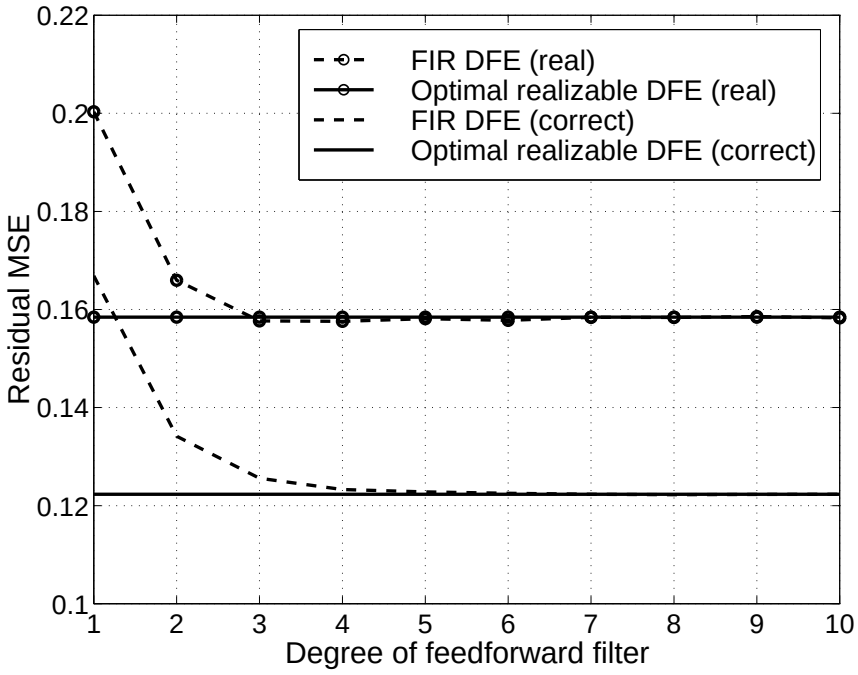

Figure 3.4: Comparison of the optimum realizable and the FIR DFE as a function of the degree of the feedforward filter of the FIR DFE. The SNR is 5dB. The residual MSE is estimated over 200 realizations, each consisting of 50000 transmitted symbols. Note the lower limit on the y-axis. The DFEs are executed using either correct decisions (correct) or decisions from the decision device (real).

For this example, the performance of the FIR DFE is good, already for rather small δs, both for correct decisions and real decisions from the decision device. For real decisions, the best performance is obtained with a feedforward filter degree of four: With a lower δs, the lower noise rejection capability degrades the performance, whereas for larger δs, the performance is (to a small degree) adversely affected by error propagation.

To conclude this subsection, we compare the complexities of the optimum realizable DFE and the FIR DFE.

Complexity To determine the optimum realizable DFE, we have to solve (3.3) and solve a system of linear equations for the $\ell + 1$ matrix coefficients of $\boldsymbol{S}(q^{-1})$.

To determine the FIR DFE, we have to solve the system of linear equations (3.22) for the $\delta s + 1$ matrix coefficients of $\boldsymbol{S}(q^{-1})$. Since $\delta s \geq \ell$, this system is larger than the corresponding system for the optimum realizable DFE. However, for realistic δs and ℓ, the additional complexity is small relative to the complexity of solving (3.3).

For the optimum realizable DFE, the noise whitening parts of the feedforward filter ($\boldsymbol{M}^{-1}\boldsymbol{N}$) and feedback filter ($\tilde{\boldsymbol{\Gamma}}$) must be executed, whereas for the FIR DFE, the feedforward and feedback filter each have $\delta s - \ell$ more taps. We conclude that the execution complexities of the two DFEs are roughly the same for a "reasonable" choice of δs.

CHAPTER 4

Reuse within cell using antenna arrays

4.1 Introduction

THE high capacity of a cellular communication system is obtained by the division of a geographical area into cells. Each communication channel[1] is used in a fraction of the cells, and by decreasing the cell size, the capacity of the system can be increased.

Reducing the cell size is however expensive and leads to increased number of handovers. Instead, multi-element antennas, also known as *antenna arrays*, can be used at the receiver to increase the capacity. Antenna arrays can enhance the desired signal and suppress the interference so that each communication channel can be used more frequently across the network, thereby decreasing the so-called *reuse factor*. When all channels are utilized in every cell, the system is said to have reuse factor one.

To increase the capacity of an FDMA or a TDMA cellular system that has reuse factor one, several users within a cell would have to share each available channel; the system must support *reuse within a cell*.[2] This will cause severe co-channel interference at the receiver. Antenna arrays are then indispensable tools for separating the signals from different users. With an antenna array, beamforming [95] can be used to suppress co-channel interference. However, in situations with frequency selective fading, beamformers that operate only in the spatial domain can suppress only a few interferers. In this chapter, we illustrate, compare and explore

[1] We use the term "communication channel" as a shorthand for a particular combination of carrier frequency, time slot and code, depending on the multiple-access scheme employed.

[2] This concept is also known as *Spatial Division Multiple-Access (SDMA)*.

two more elaborate ways of using an antenna array at the receiver to accomplish channel reuse within a cell:

1. Detect the signal from one user at a time while treating the other users as interference. In the following, this approach will be denoted *interference rejection* or *interference cancellation*.

2. Detect the signals from all users simultaneously. This approach will be called *multiuser detection*.

Interference rejection has been thoroughly studied for many different transmission environments using different detectors. In [20], interference rejection using linear receivers is studied, whereas decision feedback equalizers are used for the same purpose by Monsen in [64] and by Balaban and Salz in [11, 12]. Decision feedback equalizers are also the topic of [55], but in an adaptive setting. In [14], Bottomley and Jamal use maximum likelihood sequence estimation with spatial interference whitening to suppress intersymbol and co-channel interference. In [7], the authors provide a unified analysis of interference rejection using linear equalizers, decision feedback equalizers and maximum-likelihood sequence estimation. The reference [51] provides a comprehensive investigation of space-time processing and the associated parameter estimation problems. Interference rejection, that is, taking the covariance matrix of the interference into account, leads to substantial performance improvements in all these papers.

Multiuser detection within a cell using antenna arrays was first suggested by Winters in [103] and [104]. The emphasis of these papers is on frequency *non-selective* channels and linear detectors. In [75] extensions are made to frequency selective channels. Linear and non-linear multiuser detectors have been extensively investigated for application in CDMA systems, see, for instance, [57, 96, 99, 105] and other works discussed in Chapter 5. Most multiuser detectors for CDMA systems are block detectors. Such detectors are also becoming increasingly popular in TDMA systems for multiuser detection in conjunction with antenna arrays [83, 98]. However, block detection has limitations for time-varying channels, since the detector parameters in that case may have to be updated on a symbol-by-symbol basis. In general, block detectors are also more complex and memory consuming than their symbol-by-symbol counterparts.

As will become evident in the following sections, the performance of multiuser detectors is mostly superior to that of interference cancellers. This is due to two reasons:

1. Non-linear multiuser detectors can suppress interference more efficiently than non-linear interference cancellers. (This is in contrast to MSE optimal *linear* detectors, such as those used in [104]. An optimally tuned linear

multiuser detector is exactly the same detector as a set of optimally tuned linear interference cancellers. See Remark 5 on page 120 for a discussion.)

2. The channel estimation is improved: When utilizing training sequences from all users instead of treating all except one as noise, the estimates of channel and noise statistics will be based on more data. Therefore, the model quality is in general improved, which leads to more precise tuning of the detector.

In this chapter, we will use decision feedback equalizers to illustrate the influence of these two factors by comparing two equalizer structures:

1. The DFE presented in [55] and outlined in Section 4.3, which rejects interference.

2. The DFE of Section 3.3, which detects multiple signals simultaneously. See also [88].

These algorithms will be compared and studied by analysis in Section 4.3 and by extensive simulations in Section 4.4. In Section 4.5, we apply the algorithms to experimental data collected at an antenna array testbed.

To use the multiuser detector presented here, the channels from each user to each antenna element must be estimated. In a TDMA system, this in turn requires that bursts from all users are roughly synchronized, and that different users send different training sequences that are known at the receiver. These requirements are not hard to fulfill for users within a cell. Therefore, some form of multiuser detection seems to be a feasible tool for attaining channel reuse within a cell. Exploiting multiuser detection to reduce interference from transmitters *outside* the cell is more difficult, since the base stations in adjacent cells must in that case be synchronized.

4.2 Channel models

We shall now introduce the channel models upon which we base the derivation of the detectors. These baseband models are assumed to be linear and sampled at the symbol rate[3]. They are also assumed to include the effects of pulse shaping and analog modulation. The symbol rate is equal for all users. Finally, we assume the channel models to be *time-invariant* over the duration of a TDMA burst. The motivation for the last assumption is solely simplicity of presentation. In practice, the channels will be time-varying due to carrier frequency offsets and fading.

[3]Since the bandwidth of the signal is at least at large as the reciprocal of the symbol rate, symbol rate sampling actually constitutes *undersampling*. Some of the information in the continuous-time signals is thus inevitably lost.

The channel models, detectors and design equations presented here can easily be generalized to the time-varying case, see Chapter 5.

4.2.1 A multiple-input multiple-output baseband channel model

We consider a case with M transmitters and N receiver antennas. In the uplink, the M transmitters represent M different mobiles, each of which being equipped with one antenna. Each mobile transmits a signal to the base station, which uses an N element antenna array to detect all the signals. For downlink transmission, we assume that the base station is equipped with M antennas, each of which transmits a separate message. Each mobile has a receiver with N antennas/diversity branches, which are used to detect one (or several) of the transmitted signals.

The signal from transmitter j propagates through the discrete-time baseband channel $B_{ij}(q^{-1})$ to receiver antenna i. The channel $B_{ij}(q^{-1})$ is given by

$$B_{ij}(q^{-1}) = B_{ij}^0 + B_{ij}^1 q^{-1} + \cdots + B_{ij}^{L_{ij}} q^{-L_{ij}} \tag{4.1}$$

where B_{ij}^n are complex-valued constants.

The digital signal received at antenna i at the discrete time instant k is denoted $y_i(k)$ and can be expressed as

$$y_i(k) = \sum_{n=1}^{M} B_{in}(q^{-1}) d_n(k) + v_i(k) \ , \tag{4.2}$$

where $d_n(k)$ is the symbol transmitted from user n and the term $v_i(k)$ corresponds to noise and out-of-cell co-channel interference. Note that signals from transmitters within the cell are explicitly modeled in (4.2). The signals $d_n(k)$ and the noises $v_i(k)$ are assumed to be mutually uncorrelated, zero mean wide sense stationary stochastic signals. Furthermore, all signals $d_j(k),\ j = 1, \ldots, M$ are assumed to be mutually uncorrelated, and white with zero mean. The situation is depicted in Figure 4.1.

To obtain a MIMO model, we introduce the signal vectors

$$y(k) = \begin{pmatrix} y_1(k) & y_2(k) & \ldots & y_N(k) \end{pmatrix}^T \tag{4.3a}$$

$$d(k) = \begin{pmatrix} d_1(k) & d_2(k) & \ldots & d_M(k) \end{pmatrix}^T \tag{4.3b}$$

$$v(k) = \begin{pmatrix} v_1(k) & v_2(k) & \ldots & v_N(k) \end{pmatrix}^T \ . \tag{4.3c}$$

The vector $v(k)$ of noise samples is characterized by its matrix-valued covariance function

$$\psi_{k-m} \stackrel{\triangle}{=} E[v(k) v^H(m)] \tag{4.4}$$

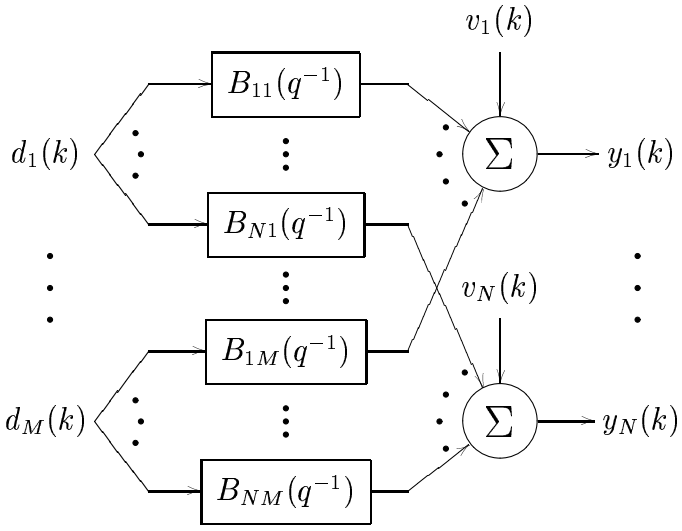

Figure 4.1: The MIMO channel model, where $d_j(k)$ is the symbol transmitted at discrete-time instant k from user number j, while $y_i(k)$ is the received sampled baseband signal at antenna i. The signal $v_i(k)$ represents additive noise and out-of-cell co-channel interference.

and can be both spatially[4] and temporally colored. The vector $y(k)$ of sampled antenna outputs can now be expressed as

$$y(k) = \boldsymbol{B}(q^{-1})d(k) + v(k) \tag{4.5a}$$
$$= \mathbf{B}_0 d(k) + \mathbf{B}_1 d(k-1) + \cdots + \mathbf{B}_L d(k-L) + v(k) \tag{4.5b}$$

where we have introduced the MIMO impulse response

$$\boldsymbol{B}(q^{-1}) = \begin{pmatrix} B_{11}(q^{-1}) & \dots & B_{1M}(q^{-1}) \\ \vdots & \ddots & \vdots \\ B_{N1}(q^{-1}) & \dots & B_{NM}(q^{-1}) \end{pmatrix} \tag{4.6}$$

with individual matrix coefficients (taps)

$$\mathbf{B}_p = \begin{pmatrix} B^p_{11} & \dots & B^p_{1M} \\ \vdots & \ddots & \vdots \\ B^p_{N1} & \dots & B^p_{NM} \end{pmatrix} . \tag{4.7}$$

[4]The noise is spatially colored when any of the off-diagonal elements of ψ_m are non-zero. When ψ_m is diagonal for all m, the noise is said to be spatially white.

In (4.5b),

$$L = \max_{i,j} L_{ij}$$

represents the maximum order of all scalar channels (4.1).

Remark 1. The model (4.5b) is rather general, in that it incorporates many different antenna configurations:

1. Phased array receivers, where the antenna elements are placed closely together.
2. Spatial diversity receivers, where the antennas are usually placed far apart. The large antenna separation helps to reduce the impact of fading.
3. Macro diversity, where multiple base stations communicate simultaneously with a single mobile. This is a special case of a diversity system, described above.
4. Polarization diversity receivers, where two orthogonal polarizations of the received signal are measured.

Remark 2. The number of measurements can be increased by other means than increasing the number of antennas. For instance, the received signal may be sampled faster than the symbol rate as described in Subsection 1.4.2. By sampling the received signal p times during a symbol period, a p-fold increase in the effective number of antennas is obtained. Excessive oversampling of a bandlimited signal will, however, lead to high correlation among consecutive samples, which in turn may lead to an ill-conditioned problem. We can also choose to handle the I- and Q-channels separately as described in Subsection 1.4.4. Each scalar complex-valued channel is then transformed to a real-valued channel with two outputs, and the number of measurements can thus be doubled. Since the real and imaginary parts of the input symbols constitute separate inputs to this real-valued channel, the number of channel inputs is also doubled when the symbols are complex-valued. However, for one-dimensional symbol constellations, such as BPSK, the number of channel inputs does not change.

Remark 3. Although the focus of this chapter will be on reuse within a cell, interferers outside the cell could be included among the M users that are explicitly modeled. The fact that transmission in adjacent cells is in general not synchronized on a burst-by-burst basis will in that case be a major problem for multiuser detectors for two reasons:

1. Channel estimation must be performed for one user at a time, since the training sequences may not overlap. This will reduce the estimation accuracy, which will lead to worse detection performance.
2. During the transmission of any single user, different users will interfere during different parts of the burst. When the interference scenario changes, the multiuser detector must be retuned.[5]

4.2.2 Reducing the MIMO model to a SIMO model with colored noise

If we explicitly model the signal from only one of the transmitters, we have to consider the remaining signals as interference. Assuming the signal of interest to be signal number 1, we define a disturbance vector $V(k)$ as the sum of all co-channel interference and noise:

$$V(k) = \sum_{n=2}^{M} \boldsymbol{B}_n(q^{-1}) d_n(k) + v(k) \tag{4.8}$$

where $\boldsymbol{B}_n(q^{-1})$ is column n in (4.6). Since all signals $d_n(k)$ are white with unit variance and mutually uncorrelated as well as uncorrelated with the interference $v(k)$, the matrix-valued covariance function of the interference $V(k)$ is given by:

$$\bar{\psi}_{k-m} \stackrel{\triangle}{=} E[V(k)V^H(m)] = \sum_{n=2}^{M} \sum_{p=\max(0,m-k)}^{\min(L,L-k+m)} \mathbf{B}_n^p (\mathbf{B}_n^{p-k+m})^H + \psi_{k-m} \tag{4.9}$$

where $\mathbf{B}_n^p$ is column n of the impulse response coefficient (4.7) for lag p:

$$\mathbf{B}_n^p = \begin{pmatrix} B_{1n}^p & B_{2n}^p & \dots & B_{Nn}^p \end{pmatrix}^T . \tag{4.10}$$

The complete single-input multiple-output channel model thus becomes

$$y(k) = \boldsymbol{B}_1(q^{-1}) d_1(k) + V(k) . \tag{4.11}$$

The DFE performing interference rejection will be based on this model.

Remark 4. If the model (4.11) is used as a basis for detector design, estimation of the matrix-valued covariance function of $V(k)$ is vital. This becomes a major problem, since direct estimation of $\bar{\psi}_m$ will provide poor accuracy for the short training sequences typically present in cellular systems. In fact, the estimates of the covariance function will be so unreliable, that we in Subsection 4.4.3 and Section 4.5 are forced to exploit only the spatial structure of $V(k)$, that is, we will assume that $E[V(k)V^H(m)] = 0$ for $k \neq m$.

[5] In fact, this is a problem also for interference rejection, see [41].

4.2.3 Antenna correlation

Spatial diversity has for a long time been used to mitigate fading. The idea is to open multiple uncorrelated channels from the transmitter to the receiver. By combining the signals received through the different channels, the effect of fading can be reduced. If the channels are correlated, the advantage of using diversity decreases.

With correlated base station antennas, the statistical properties of the uplink and downlink channels will differ. In the uplink, M mobile users transmit M separate messages, which are detected using N receiver antennas at the base station. In the scenario depicted in Figure 4.2, the channels from one transmitter to different receivers will be *correlated,* but the channels from different transmitters to a single receiver will be *uncorrelated.*

For downlink transmission, the situation is the opposite. Recall that in the downlink, M different messages are transmitted from different base station antennas. Each mobile is equipped with N receiver antennas, which are used to detect one or several of the transmitted signals. The channels from two different transmitter antennas to a single receiver antenna will now be *correlated,* but the channels from one transmitter antenna to different receiver antennas will be *uncorrelated.*

We will now derive the correlation between signals received at two base station antennas. This correlation will then be used to generate correlated uplink channels. Due to the reciprocity of the radio frequency propagation [102], we can also use the result to generate correlated downlink channels.

The actual correlation will depend on the distribution of the scatterers that cause the fading, but different scatterer distributions give similar results [8]. We will use a model first suggested in [6], which assumes a uniform linear array at the base station and a large number of scatterers located on a circle around the mobile. This situation is depicted in Figure 4.2.

Each of the scatterers that surround the mobile is treated as a secondary transmitter. Assuming that the transmitted signal is narrowband, the signal replicas originating from one such secondary transmitter and received at different antenna elements will be identical except for a phase shift. The complex correlation coefficient between the received baseband signals $y_i(k)$ and $y_{i+1}(k)$ at two antenna elements i and $i+1$ respectively is given by

$$\frac{E[y_i(k)y_{i+1}^*(k)]}{E[|y_i(k)|]E[|y_{i+1}(k)|]} \triangleq \rho(\delta, R, r, \theta) \ . \tag{4.12}$$

We insert the expression (4.2) with $M = 1$ and $v_i(k) = v_{i+1}(k) = 0$ into (4.12). We first consider the case with no intersymbol interference, that is, $L_{ij} = L_{(i+1)j} = 0$. By assuming that the channel taps are independent of the transmitted signal, the

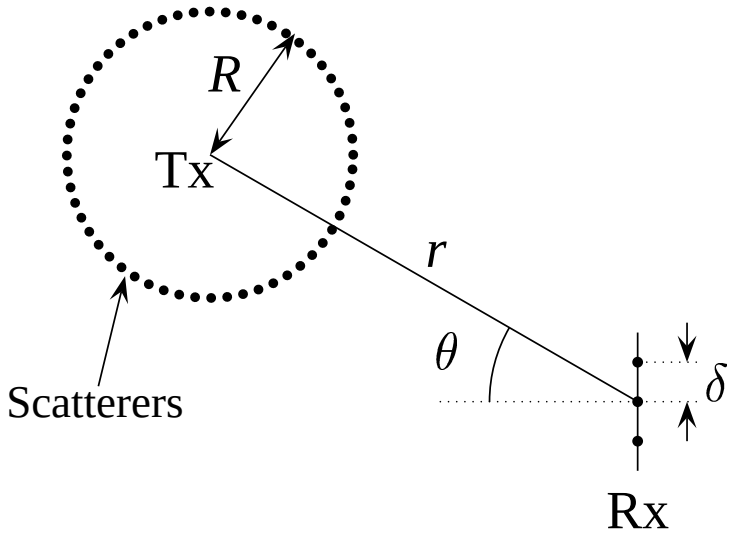

Figure 4.2: Geometry of local scatterers surrounding the mobile transmitter that results in correlation among the signals received at different antenna elements of a uniform linear array.

expression (4.12) reduces to

$$\rho(\delta, R, r, \theta) = \frac{E[B^0_{i1}(B^0_{(i+1)1})^*]}{E[|B^0_{i1}|]E[|B^0_{(i+1)1}|]} \,. \tag{4.13}$$

For the circular scatterer distribution depicted in Figure 4.2, Fulghum et al. [31] obtained the following approximation for the channel correlation:

$$\rho(\delta, R, r, \theta) = J_0\left(\frac{2\pi\delta R}{r}\cos\theta\right) e^{-j2\pi\delta\sin\theta} \tag{4.14}$$

where

δ = the antenna separation, expressed in carrier wavelengths
R = the radius of the ring of scatterers
r = the distance between the receiver and the transmitter
θ = the angle of the incoming signal with respect to antenna broadside,

and where J_0 is the Bessel function of the first kind and order zero. Equation (4.14) is a good approximation when δ and R are both small relative to r.

In a cellular system, there may be scatterers that are located far from both the transmitter and the receiver. The corresponding paths will have different propagation delays, leading to a delay spread $L > 0$. To model this frequency selective

fading, we use the model proposed in [8]. See also [27]. We will still assume that (4.14) can be used to describe the correlation within each vector tap. With each of these $L+1$ vector taps in the impulse response, we associate a separate circular cluster.

The impact of antenna correlation on the performance of the multivariable DFE will be investigated in Subsection 4.4.2.

4.3 Deployed DFEs

One of the main objectives of this chapter is to compare the performance of multiuser detection and interference rejection. Decision feedback equalizers of both kinds can be derived using Theorem 3.4 and the models in Section 4.2:

1. With the model (4.5a) and the noise description (4.4), an FIR DFE performing multiuser detection (MU-DFE) can be designed.

2. With the model (4.11) and the noise description (4.9), an FIR DFE performing interference rejection (IR-DFE) can be designed.

Theorems 3.5 and 3.6 can be used to determine whether or not a zero-forcing MU-DFE exists for a given scenario. However, we have not yet derived a corresponding condition for the IR-DFE. Also, the complexity of the two approaches should be compared. These two issues will be dealt with in the remainder of this section.

4.3.1 The ZF IR-DFE

In this subsection, we will investigate under what conditions there exists an FIR IR-DFE that completely eliminates both intersymbol and co-channel interference. In an IR-DFE, the feedforward filter has N inputs and a single output, whereas the feedback filter is a SISO filter:

$$\hat{d}_i(k-\ell|k) = \boldsymbol{S}^{(i)}(q^{-1})y(k) - Q_{ii}(q^{-1})\tilde{d}_i(k-\ell-1)\ . \tag{4.15}$$

Above, $\boldsymbol{S}^{(i)}(q^{-1})$ is a polynomial row vector with N elements, whereas $Q_{ii}(q^{-1})$ is a scalar polynomial.

To derive the zero-forcing condition for the IR-DFE, we assume that all previous decisions are correct and insert the channel model (2.11) into (4.15):

$$\begin{aligned}\hat{d}_i(k-\ell|k) = {} & \boldsymbol{S}^{(i)}(q^{-1})\boldsymbol{B}(q^{-1})d(k) \\ & - Q_{ii}(q^{-1})d_i(k-\ell-1) + \boldsymbol{S}^{(i)}(q^{-1})v(k)\ .\end{aligned} \tag{4.16}$$

We introduce the *unit row vector* $e^{(i)}$, whose kth element is given by

$$(e^{(i)})_k = \begin{cases} 1 & \text{if } k = i \\ 0 & \text{otherwise} \end{cases} .$$

The estimator (4.16) can now be rewritten

$$\begin{aligned} \hat{d}_i(k-\ell|k) &= \boldsymbol{S}^{(i)}(q^{-1})\boldsymbol{B}(q^{-1})d(k) - Q_{ii}(q^{-1})e^{(i)}d(k-\ell-1) \\ &+ \boldsymbol{S}^{(i)}(q^{-1})v(k) = d_i(k-\ell) - \varepsilon_i(k-\ell) \end{aligned}$$

with

$$\begin{aligned} \varepsilon_i(k-\ell) &= \left(q^{-\ell}e^{(i)} - \boldsymbol{S}^{(i)}(q^{-1})\boldsymbol{B}(q^{-1}) + q^{-\ell-1}Q_{ii}(q^{-1})e^{(i)}\right) d(k) \\ &- \boldsymbol{S}^{(i)}(q^{-1})v(k) \ . \end{aligned}$$

To comply with the zero-forcing condition (2.3), we have to require that

$$q^{-\ell}e^{(i)} - \boldsymbol{S}^{(i)}(q^{-1})\boldsymbol{B}(q^{-1}) + q^{-\ell-1}Q_{ii}(q^{-1})e^{(i)} = 0 \ . \tag{4.17}$$

This condition has to be fulfilled for every user, that is, for $i = 1, \ldots, M$.

We can now formulate the condition for existence of a set of M zero-forcing interference rejecting DFEs:

Theorem 4.1 *There exists a set of M zero-forcing IR-DFEs if and only if for every $i = 1, \ldots, M$, every right divisor of $\boldsymbol{B}(q^{-1})$ and $q^{-\ell-1}e^{(i)}$ is a right divisor also of $q^{-\ell}e^{(i)}$. The right divisors should be members of the ring of polynomial matrices.*

Proof: The theorem follows from the general theory of Diophantine equations, see [45]. ■

The situations described in Corollaries 3.4 and 3.5 preclude the existence also of a zero-forcing DFE performing interference rejection. In fact, the conditions in Theorem 4.1 is always at least as strict as the condition in Theorem 3.5. To see this, assume that no solution to (3.28) exists, that is, assume that $\boldsymbol{B}(q^{-1})$ and $q^{-\ell-1}\mathbf{I}$ have a common right divisor, say $\boldsymbol{R}_r(q^{-1})$ that is not a factor of $q^{-\ell}\mathbf{I}$. In this case, any row m of $\boldsymbol{R}_r(q^{-1})$ is then a right divisor of $\boldsymbol{B}(q^{-1})$ and $q^{-\ell-1}e^{(m)}$, but not of $q^{-\ell}e^{(m)}$, which means that equation (4.17) cannot have any solution for $m = i$. We thus realize that as soon there exists a right divisor that precludes the existence of a solution to (3.28), no zero-forcing IR-DFE can exist.

It remains to derive a condition corresponding to Theorem (3.6). As a prerequisite, we need the following definitions. We first factorize $\boldsymbol{B}(q^{-1})$ into three matrix polynomials:

$$\boldsymbol{B}(q^{-1}) = \bar{\boldsymbol{B}}(q^{-1})\boldsymbol{G}(q^{-1})\boldsymbol{\Delta}(q^{-1}) \; . \tag{4.18}$$

The factors of (4.18) are defined as

$$\boldsymbol{\Delta}(q^{-1}) \stackrel{\triangle}{=} \operatorname{diag}\left(q^{-\Delta_1} \quad \dots \quad q^{-\Delta_M}\right) \tag{4.19a}$$

$$\boldsymbol{G}(q^{-1}) \stackrel{\triangle}{=} \operatorname{diag}\left(G_1(q^{-1}) \quad \dots \quad G_M(q^{-1})\right) \tag{4.19b}$$

$$\bar{\boldsymbol{B}}(q^{-1}) \stackrel{\triangle}{=} \bar{\mathbf{B}}_0 + \bar{\mathbf{B}}_1 q^{-1} + \cdots + \bar{\mathbf{B}}_{\bar{L}} q^{-\bar{L}} \tag{4.19c}$$

where Δ_j is defined in (3.17), and

$$G_j(q^{-1}) \stackrel{\triangle}{=} \text{the greatest common polynomial factor other than } q^{-\Delta_j} \text{ of the channels } B_{1j}(q^{-1}), \dots, B_{Nj}(q^{-1}) \text{ from user } j \text{ to all antenna elements. Without restriction, } G_j(q^{-1}) \text{ is assumed to be monic.} \tag{4.20}$$

We also define

$$g_j \stackrel{\triangle}{=} \deg G_j(q^{-1}) \tag{4.21a}$$

$$\bar{L}_j \stackrel{\triangle}{=} \max_i L_{ij} - \Delta_j - g_j \tag{4.21b}$$

$$\bar{L} \stackrel{\triangle}{=} \max_j \bar{L}_j \tag{4.21c}$$

We are now ready to formulate Theorem 4.2.

Theorem 4.2 *Consider the MIMO channel model* (2.11) *with M sources and N measurement signals and assume that the conditions in Theorem 4.1 are fulfilled. A generically necessary condition for the existence of a zero-forcing FIR IR-DFE described by* (4.15) *with decision delay ℓ and feedforward filter degree δs is then that*

$$\delta s \geq \max_j \frac{\sum_{m=1}^{M} \bar{L}_m + \ell + 1 - \bar{L}_j - \Delta_j}{N + 1 - M} - 1 \tag{4.22}$$

where $\bar{L}_j$ is defined in (4.21b) *and Δ_j is the propagation delay for user j, defined in* (3.17)*.*

Proof: See Appendix 4.A. ■

Consider column j in (4.18). From the vector taps in the impulse response of user j, we can form the *channel matrix*

$$[\mathbf{B}_j] \stackrel{\triangle}{=} \begin{pmatrix} \mathbf{B}_j^0 & \mathbf{B}_j^1 & \dots & \mathbf{B}_j^{L_j} \end{pmatrix} \tag{4.23}$$

where $L_j \stackrel{\triangle}{=} \max_i L_{ij}$ and where $\mathbf{B}_j^p$ is defined in (4.10). The rank of the channel matrix in general equals

$$\min(N, L_j + 1) \ .$$

However, when $\bar{L}_j < L_j$, we can rewrite (4.23) as

$$[\mathbf{B}_j] = \left[\bar{\mathbf{B}}_j\right] [G_j] \tag{4.24}$$

with

$$\left[\bar{\mathbf{B}}_j\right] \stackrel{\triangle}{=} \begin{pmatrix} \bar{\mathbf{B}}_j^0 & \bar{\mathbf{B}}_j^1 & \dots & \bar{\mathbf{B}}_j^{\bar{L}_j} \end{pmatrix}$$

$$[G_j] \stackrel{\triangle}{=} \begin{pmatrix} 0 & \dots & 0 & 1 & G_j^0 & \dots & G_j^{g_j} & \dots & 0 \\ \vdots & & \vdots & \ddots & \ddots & \ddots & \ddots & \ddots & \vdots \\ 0 & \dots & 0 & \dots & 0 & 1 & G_j^0 & \dots & G_j^{g_j} \end{pmatrix}$$

where in $[G_j]$, the first Δ_j columns are identically zero.

We see that the rank of $[\mathbf{B}_j]$ is $\bar{L}_j$. This low rank property can be exploited in two ways:

1. It can be used to simplify detector tuning and execution, as described in [52].
2. It can also be used to improve the estimation accuracy, as described in [53, 81].

As has been demonstrated above, an interfering user whose channel is described by a low rank model can be more easily rejected: With a rank $\bar{L}_j$ channel, only $\bar{L}_j$ spatial nulls are necessary to completely suppress the interference.

4.3.2 The zero-forcing solution and well-posed equalization problems

An MMSE equalizer balances rejection of intersymbol and co-channel interference against noise amplification. The resulting estimation error at the input to the decision device has two components: one caused by residual intersymbol and co-channel interference and one caused by noise. This can be seen explicitly in (3.11).

For any equalizer, it is desirable that when the noise power tends to zero, the estimation error should vanish. In this situation, error free communication is possible when the SNR is sufficiently high, irrespective of the symbol alphabet. Unfortunately, this is not always the case, since the structure of the detector may be inappropriate for the considered equalization problem.

On the other hand, the estimation error of a zero-forcing equalizer only has a noise component. By definition, all intersymbol and co-channel interference has been rejected. Hence, when the noise variance tends to zero, so will the residual MSE of a zero-forcing equalizer.

However, the residual MSE of the MMSE equalizer cannot exceed the MSE of the zero-forcing (or any other) equalizer with the same structure. Furthermore, the MSE cannot, of course, be less than zero. Hence we conclude that when the residual MSE of the zero-forcing equalizer tends to zero, so must the residual MSE of the MMSE equalizer. *The existence of an equalizer that fulfills the zero-forcing condition* (2.3) *thus guarantees that the corresponding MMSE equalizer will behave well for high SNR*. The existence of a ZF equalizer thus indicates that the equalization problem is well-posed in the sense that a useful solution can be obtained: Good performance is guaranteed when the noise level is sufficiently low. Also, the lack of a zero-forcing equalizer suggests that the corresponding MMSE equalizer may not work well, not even for very high SNR. This effect is particularly apparent when the interfering signals have high power. This is the so-called *near-far problem*, which will be studied in more detail in Chapter 5.

Thus, when a zero-forcing solution exists, good performance can be achieved when the signal-to-noise ratio goes to infinity. The consequences of this fact must, however, be interpreted with some care. When the zero-forcing problem is in some sense well-conditioned, the corresponding MMSE equalizer will work well also at realistic signal-to-noise ratios. However, when the zero-forcing problem is ill-conditioned,[6] the corresponding MMSE solution may not provide adequate performance, despite the fact that a zero-forcing solution does exist. We believe however, that the likelihood for this situation to occur is small.

The simulations in Subsection 4.4.2 demonstrate how the MMSE DFE performs in a mild near-far situation.

4.3.3 Complexity comparison

To compute the MMSE MU- or IR-DFE, we need to solve the system of linear equations (3.22) and determine the feedback filter via (3.25). The number of required complex multiplications are indicated in Table 4.1 for both multiuser and

[6] This would occur for instance if the channels of different users were almost identical.

interference rejecting DFEs.

	MU-DFE	IR-DFE
For the feedforward filter $\boldsymbol{S}$:		
Calculate $\mathcal{F}\mathcal{F}^H + \Psi$	$\frac{1}{4}N^2M(\ell+1)(\ell+2)$	$\frac{1}{4}N^2M^2(\ell+1)(\ell+2)$
Factorize $\mathcal{F}\mathcal{F}^H + \Psi$	$\frac{1}{6}N^3(\delta s+1)^3$	$\frac{1}{6}N^3M(\delta s+1)^3$
Solve for the coefficients	$N^2(\delta s+1)^2M$	$N^2(\delta s+1)^2M^2$
For the feedback filter $\boldsymbol{Q}$:		
Compute the coefficients	$M^2N(L+1)(\delta Q+1)$	$MN(L+1)(\delta Q+1)$
Equalization of one symbol vector:		
Feedforward filtering	$MN(\delta s+1)$	
Feedback filtering	$M^2(\delta Q+1)$	$M(\delta Q+1)$

Table 4.1: The number of complex multiplications necessary to compute and run the MU-DFE and a set of M IR-DFEs for M users and N sensors. The decision delay of the DFEs is ℓ, the degree of the feedforward filter is δs and the delay spread is L. The degree of the feedback filter is $\delta Q = L + \delta s - \ell - 1$.

From Table 4.1, we see that the feedforward filter tuning is more complex for a set of M IR-DFEs than for one MU-DFE, whereas the feedback filter tuning and execution is more complex for one MU-DFE than for M IR-DFEs. To determine which DFE has the higher overall complexity, we have to consider how often the DFE must be retuned.

There is however one important case when the interference rejecting DFE is considerably less complex than the multiuser DFE. If only one of the impinging signals is of interest to us, we can use a single IR-DFE to detect that signal. When using a MU-DFE, we still have to detect all the signals, so the complexity of the multiuser DFE is determined by the total number of impinging signals, not the number of impinging signals of interest. In the uplink, this situation would not be relevant, since the base station must always detect all impinging signals. However, in the downlink the mobile only needs to detect its own signal. In that case, a detector performing interference rejection will be considerably less complex than a multiuser detector.

4.4 Monte Carlo simulations

To explore the performance of the MIMO DFE as a tool for joint multiuser detection, extensive simulation experiments are conducted. The experiments are de-

signed to illustrate several key aspects of a real world implementation of a system employing reuse within a cell. Both uplink and downlink cases are considered. We also compare the performance of a multiuser detection approach with the performance of an interference rejection approach.

In all scenarios, we compare the performance of two MMSE DFEs:

- One MU-DFE, performing multiuser detection on all the signals.
- One IR-DFE, detecting one signal while rejecting the remaining as interference.

4.4.1 The simulation scenario

All the simulations have some properties in common, and we will begin this subsection by describing them.

In all simulations, one, two, three or four transmitters simultaneously send BPSK modulated signals. The signals are received at an array with four elements in the presence of Gaussian noise. The noise is temporally white and uncorrelated at different antenna elements.

The channels are frequency selective with three taps. The taps in each channel fade independently,[7] and the channels from different transmitters to one receiver are uncorrelated.

Both IR and MU DFEs have smoothing lags and feedforward filter lengths equal to the length of the channel impulse response.

In different simulations, the system specified above is investigated under the following additional conditions:

- Known channels (Subsection 4.4.2) with
  - Equal average SNR of all users and uncorrelated antennas.
  - Equal average SNR of all users and correlated antennas.
  - Different average SNR of the users and uncorrelated antennas.
- Estimated channels (Subsection 4.4.3):
  - Estimation using the training sequence only.
  - Estimation using detected data, with a so-called *bootstrap* method [91].

[7] We thus assume uncorrelated scattering [73, p. 706]. See also [42] for an experimental verification. We also neglect the impact of the pulse shaping. In practice, the pulse shaping will introduce some correlation among adjacent taps, but with full-response signalling, this correlation is small, and will not affect the results in the simulations.

4.4.2 Performance with known channel coefficients

In this subsection we shall study the idealized case when all channel coefficients are exactly known. Effects caused by differences in detector structure can here be studied in isolation, since effects of channel estimation errors are avoided.

Equal average SNR for all users and uncorrelated antennas

This is the basic scenario, where all users have the same average SNR, and the channels from a single transmitter to different antenna elements are uncorrelated. In practice, the condition of all users having the same average SNR can be fulfilled by using slow power control that compensates for the propagation loss and the shadow fading, but not for the Rayleigh fading. The condition of uncorrelated antennas presupposes a sufficiently large antenna spacing δ in Figure 4.2.

The above scenario is simulated for an average SNR per bit between 0 and 15 dB, where the average SNR per bit [73, p. 728] for user j, $\bar{\gamma}_b^j$[8], is defined as

$$\bar{\gamma}_b^j = \frac{1}{N} \frac{E[|B_{ij}^0|^2 + |B_{ij}^1|^2 + |B_{ij}^2|^2] E[|d_j(k)|^2]}{E[|v_i(k)|^2]} \tag{4.25}$$

for three-tap channels. We assume that $\bar{\gamma}_b^j$ is equal at different antenna elements and thus independent of i. Note that signals from other users do *not* affect $\bar{\gamma}_b^j$. Adding users will only affect the resulting BER for a fixed $\bar{\gamma}_b^j$ and thereby demonstrate the performance degradation as a function of the system load.

Figure 4.3 shows the estimated BER as a function of the average SNR per bit. With four users, the performance of the multiuser DFE at $\bar{\gamma}_b^j = 15$ dB is around 6 dB better than the performance of the interference rejecting DFE. This difference arises from the fact that the IR-DFE uses up all its degrees of freedom to cancel the interference from the other users. This task is easier for the MU-DFE since its feedback filter takes care of some of the suppression of the co-channel interferers. For fewer users, the difference between the two approaches is smaller. For example, in the case of three users the gain is approximately 3 dB and for two users around 1 dB. This was observed in [20], where a linear receiver was compared to the matched filter bound, which is an upper bound on the detector performance. When the number of antennas is large, the difference between the linear receiver and the matched filter bound is small.

For $\bar{\gamma}_b^j = 15$ dB, the performance degradation when using a MIMO DFE is approximately 1 dB for two users, 3 dB for three users and 5 dB for four users as compared to a single user system. See Table 4.2 for a performance summary.

[8] Thus, we do *not* use the SNR per channel, defined as $\bar{\gamma}_c^j \triangleq N \bar{\gamma}_b^j$. Using $\bar{\gamma}_c^j$ enables a fair comparison among scenarios with different number of antennas.

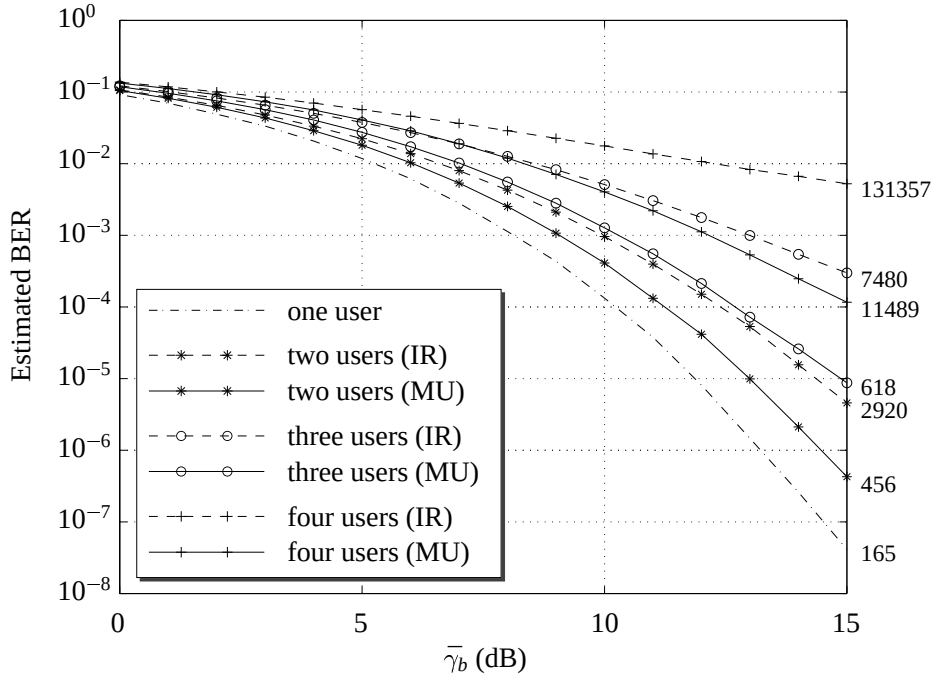

Figure 4.3: Comparison of the MU-DFE and the IR-DFE for known channels, equal transmitter powers and uncorrelated antennas. The numbers to the right of the graph are the number of errors used to estimate the BER for the average SNR per bit $\bar{\gamma}_b$=15 dB.

Equal average SNR for all users and correlated antennas

In a realistic uplink scenario, the channels from a single user to the different antenna elements will be correlated. This makes the system more susceptible to fading. Also, in the corresponding downlink scenario, the channels from different transmitters to a single receiver will be correlated. Separating the different signals then becomes increasingly difficult. However, as we shall see, successful multiuser detection and interference rejection is possible even with correlated base station antennas.

In this simulation, we will assume that a uniform linear array is present at the base station. The correlation between the channels to two adjacent antenna elements is given by (4.14). In the uplink multipath model, each incoming ray from user j will give rise to a column vector $\mathbf{B}_j^p$ at lag p in the impulse response as defined in (4.10). Each of these column vectors originates from a circular distribution of scatterers as depicted in Figure 4.2. The angular locations θ of scatterer distributions corresponding to different column vector taps in the impulse response

are assumed to be independent stochastic variables, uniformly distributed in the interval $[-90°, 90°]$.

The channel correlations (4.14) will depend on the angles θ, which are not under the system designer's control. Therefore, we shall address the performance of the DFE as a function of the correlation coefficient according to (4.14) that would result if the signals would all impinge from an angle $\theta = 0°$, compare with Figure 4.2:

$$\rho(\delta, R, r, \theta = 0) = J_0\left(\frac{2\pi\delta R}{r}\right) \triangleq \tilde{\rho}\left(\frac{\delta R}{r}\right) \ . \tag{4.26}$$

We will call the quantity $\tilde{\rho}$ the *antenna correlation.* It can be measured for a given environment and uniform linear array, and the corresponding performance can be predicted from the simulation results presented below.

To calculate the actual correlation ρ between the channels to two adjacent antenna elements in the impulse response for a given value $\tilde{\rho}_0$ of the antenna correlation, we insert the ratio $R\delta/r$ corresponding to $\tilde{\rho}_0$ and a realization of the stochastic variable θ into (4.14). The resulting value of ρ is used to form the covariance matrix of $\mathbf{B}_n^p$. A realization of $\mathbf{B}_n^p$ is then generated. This procedure is repeated for each of $M(L+1)$ vector taps in the impulse response. The simulation results are presented in Figure 4.4 for a signal-to-noise ratio of 10 dB and antenna correlations between zero and one.

In the downlink, the N receiver antennas are uncorrelated, whereas the transmitter antennas are correlated. The procedure for finding the downlink multipath channel is similar to the uplink case: For a given value of the antenna correlation, we insert the corresponding ratio $R\delta/r$ and a realization of θ into (4.14). The resulting value of ρ is used to form a covariance matrix. Since it is the transmitters that are correlated, this covariance matrix is used to generate one *row* of a tap in the channel impulse response. This procedure is repeated for each of the $N(L+1)$ tap rows in the impulse response. Note that the angle θ is equal for all receiver antennas of a specific mobile. The result is depicted in Figure 4.5.

It is evident from Figures 4.4 and 4.5 that successful multiuser detection and interference rejection are indeed not dependent on uncorrelated antennas. The performance of all algorithms deteriorates when the antenna correlation is increased from zero to one. For the uplink, this is due to the diminished diversity effect, resulting from a decrease in the number of diversity branches from twelve (four uncorrelated antennas and three taps) to three (four perfectly correlated antennas and three taps) per user. For the downlink, the signals transmitted from different base station antennas become increasingly similar, which makes the signal separation more difficult. However, in both links the multiuser detection approach retains its superior performance as compared to the interference rejection approach.

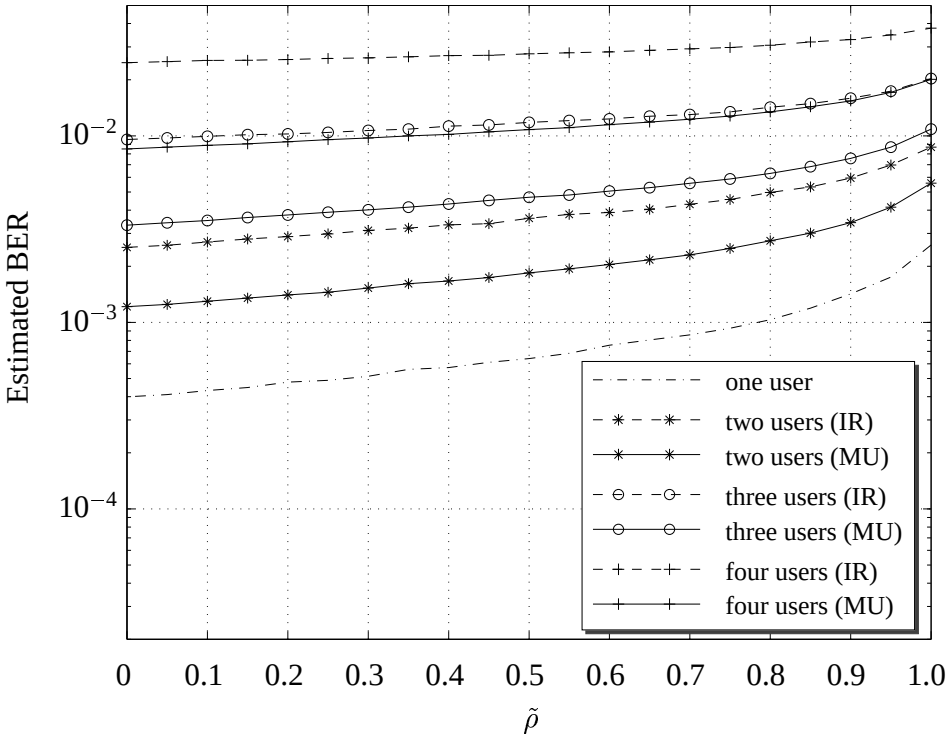

Figure 4.4: Comparison of the MU-DFE and the IR-DFE for uplink transmission, when the base station is equipped with a uniform linear array with correlated antenna elements*. The channels are known and the SNR per bit is $\bar{\gamma}_b = 10$ dB for all users. The estimated BER is shown as a function of the antenna correlation $\tilde{\rho}$.*

Remark 5. Notice that $\tilde{\rho} = 0$ does *not* imply that all channel taps are uncorrelated, only that a signal that impinges from $\theta = 0^\circ$ would result in uncorrelated taps. Therefore, the BER for $\tilde{\rho} = 0$ does not coincide with the BER for $\bar{\gamma}_b = 10$ dB in Figure 4.3, where *all* taps are uncorrelated.

Different average SNR for the users and uncorrelated antennas

In Figure 4.3 and 4.4, we assumed that power control was used to compensate for the propagation loss and the shadow fading. In the scenario investigated in this subsection, we will relax this assumption: Even the average received powers will differ among the users. This will generate the so-called *near-far problem.*

We estimated the BER of a user having an average SNR per bit of 10 dB in a scenario where there are one, two or three additional users, each having an average SNR per bit that is between 0 dB and 10 dB *higher*, that is between 10 dB and 20

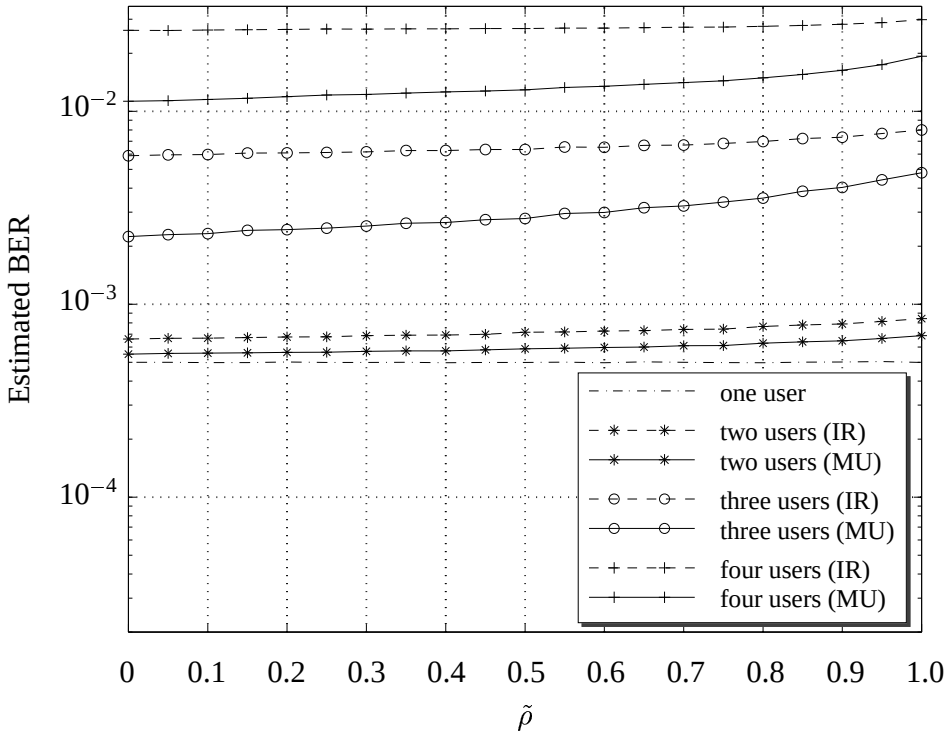

Figure 4.5: Comparison of the MU-DFE and the IR-DFE for downlink transmission, when the base station is equipped with a uniform linear array with correlated antenna elements. *The channels are known and the SNR per bit is* $\bar{\gamma}_b = 10$ *dB for all users. The estimated BER is shown as a function of the antenna correlation* $\tilde{\rho}$.

dB. The result from this simulation is depicted in the *right* half of Figure 4.6.

In a MU-DFE, decisions concerning one user affect future symbol estimates of all users. Incorrect decisions on the symbols from a weak user will thus impair the decisions of other, stronger users. In this case, an IR-DFE may yield better performance since (possibly incorrect) decisions of the weaker users' symbols do not influence the estimates the stronger users' symbols.

To investigate this effect, we estimate the BER of a user having an average SNR per bit of 10 dB in a scenario where there were one, two or three additional users, each having an average SNR per bit that was between 0 dB and 10 dB *lower*, that is the SNR per bit of the remaining users varied between 10 dB and 0 dB. The result from this simulation is depicted in the *left* half of Figure 4.6.

From the leftmost part of Figure 4.6, it is clear that for the investigated differences in power levels, error propagation is not so severe that the BER of a MU-DFE

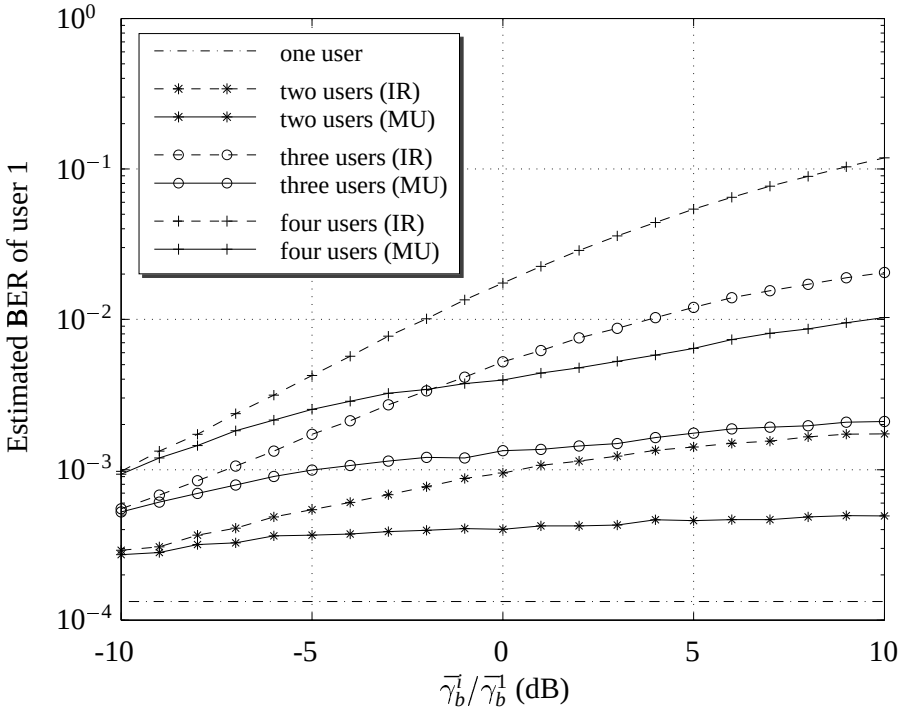

Figure 4.6: Comparison of the BER of user 1 for the MU-DFE and the IR-DFE for known channels, different transmitter powers *and uncorrelated antennas. In this simulation, 25000 channels were randomly selected. Over each channel, 1000 symbols were transmitted. User number 1 has an SNR per bit of* $\bar{\gamma}_b^1 = 10$ *dB, while the SNR per bit* $\bar{\gamma}_b^i$ *of the other users are equal and varies between 0 and 20 dB.*

exceeds the BER of an IR-DFE. On the other hand, from the rightmost part of Figure 4.6, it is evident that for the multiuser DFE, four users can coexist in the cell, even when the received average powers differ substantially. For two users, the BER is hardly affected at all by the power level of the interfering user. However, the performance of the interference rejecting DFE is seriously affected by the increase of the power levels of the interfering users, since the IR-DFE does not comply with the ZF condition (3.29). Inserting numerical values into (3.29) gives the required feedforward filter degree:

$$\begin{aligned} M = 1 &\implies \delta s \geq -1/4 \\ M = 2 &\implies \delta s \geq 2/3 \\ M = 3 &\implies \delta s \geq 2.5 \\ M = 4 &\implies \delta s \geq 8\,. \end{aligned}$$

This means that since we used $\delta s = \ell = L = 2$, complete suppression of all co-

channel interferers is impossible whenever $M \geq 3$. As the powers of these users increase, the estimation error due to residual interference increases, resulting in an increased BER. The multiuser DFE on the other hand is capable of completely removing the interference from the stronger users, at the expense of a slightly increased noise amplification.

4.4.3 Performance with estimated channel coefficients

Estimation using the training sequence only

To demonstrate how the MIMO DFE works in a more realistic case, channel estimation is introduced. The data is transmitted in bursts, with a structure similar to that of GSM: A training sequence of 26 symbols is located in the middle of each burst. Together with data symbols, tail symbols and control symbols, this results in a total burst length of 148 symbols.[9] The channel estimation is performed using the off-line least squares method, and the spatial color of the noise is estimated from the residuals of the channel identification. The temporal color of the noise is not estimated due to the limited amount of data. In the MIMO case, the channels from all users to each antenna element are estimated simultaneously. Apart from this, the simulation conditions are the same as in Subsection 4.4.2. The results are indicated in Figure 4.7 on the following page.

When we compare Figures 4.3 and 4.7, we see that the difference between the MU-DFE and the IR-DFE is greater when the channels have to be estimated. The difference between the multiuser detection approach and the interference rejection approach has now increased to about 4 dB for two users, and to about 7 dB for three users and even more for four users. In this case, the overall penalty for squeezing in four users into one cell is about 7 dB as compared to the single user case. Table 4.2 summarizes the performance loss of the IR-DFE and the MU-DFE for known and estimated channels as compared to the single-user case.

Improving channel estimation using the detected symbols

Since channel estimation errors are a major cause of bit errors in a digital cellular system, there is a great potential for performance improvement in the reduction of the channel estimation errors. One way of accomplishing this would be to use detected symbols as regressors in the estimation algorithm. This approach would thus consist of two passes as follows:

[9] The pulse shaping used in GSM results in a channel with five highly correlated taps. We have not included this feature in the simulation: Only the burst structure resembles the one used in GSM.

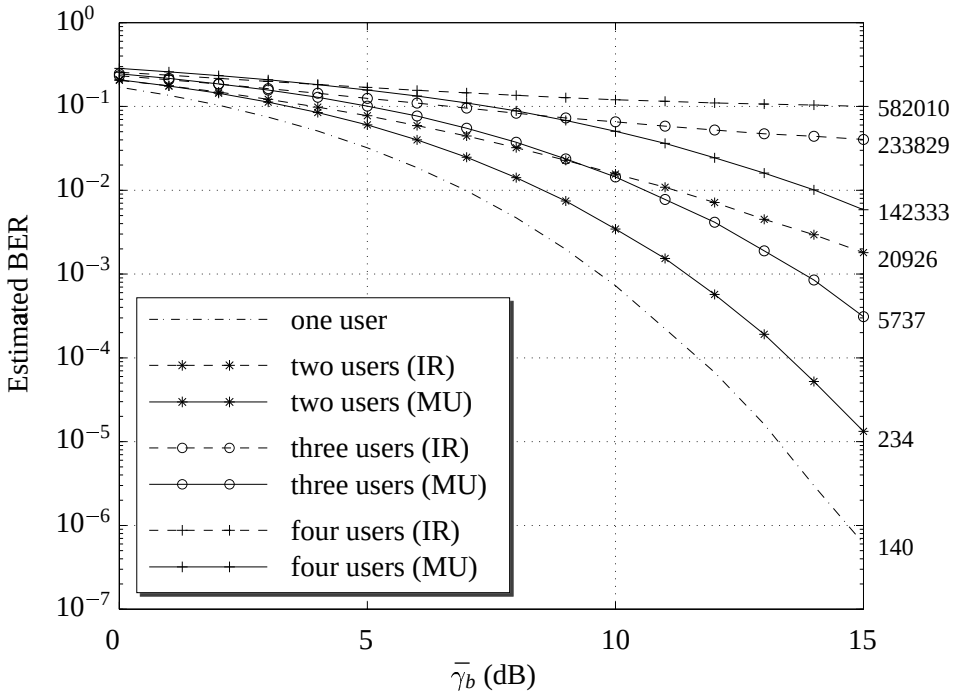

Figure 4.7: Comparison of the MU-DFE and the IR-DFE for estimated channels, equal transmitter powers and uncorrelated antennas. The channel was estimated using only the training sequence*. The numbers at the right edge of the graph are the number of errors used to estimate the BER for an SNR per bit of $\bar{\gamma}_b$=15 dB.*

Pass 1:

1. Estimate the channel using the training sequence.
2. Design an equalizer using these channel estimates.
3. Detect all the symbols in the burst.

Pass 2:

4. Estimate the channel using the training sequence *and* the symbols detected in pass 1.
5. Redesign the equalizer using the updated channel estimates.
6. Repeat the symbol detection.

We thus improve the channel estimates by using detected data that are probably correct. By using these extra regressors we can increase the length of the training

sequence from 26 to 148 symbols in the GSM case. This method — which we call *bootstrap* — is based on the assumption that when the fraction of incorrect decisions from pass 1 is sufficiently small, the channel estimation in pass 2 will provide better accuracy than the channel estimation in pass 1. Bootstrap equalization is discussed in [91] for both decision feedback equalizers and maximum likelihood sequence estimation.

To test this algorithm, we repeat the simulation in Subsection 4.4.3, with the use of the detected symbols to improve the channel estimates, according to the bootstrap algorithm described above. The results from the second pass of the algorithm are shown in Figure 4.8.

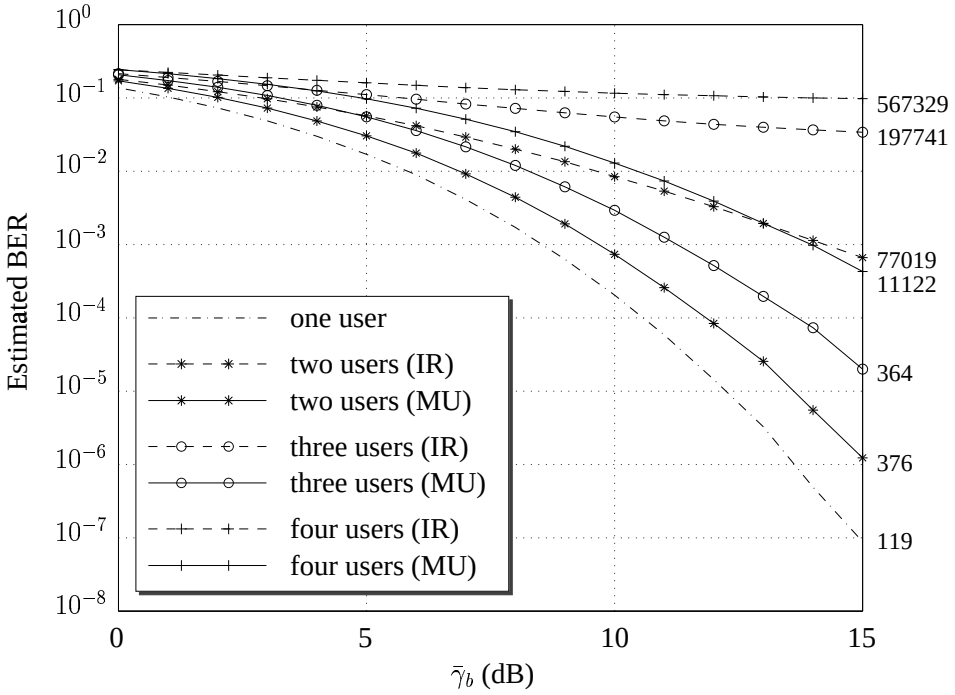

Figure 4.8: Comparison of the MU-DFE and the IR-DFE for estimated channels, equal transmitter powers and uncorrelated antennas. The channel estimates were obtained using both the training sequence and detected symbols*. The numbers at the right edge of the graph are the number of errors used to estimate the BER for an SNR per bit of $\bar{\gamma}_b$=15 dB.*

As can be seen from Figure 4.8, the BER was reduced when the tentative decisions were used to improve the channel estimates. It seems that the performance of the multiuser detector was impaired more by the poor quality of the channel estimates than the performance of the detector performing interference rejection:

The difference between the two approaches is larger when the two pass algorithm is used than when only the training sequence is used to estimate the channel. This is due to the fact that the estimation of the covariance function of the noise and the interferers is still inaccurate, despite the fact that we now have access to a training sequence of 148 symbols. This impairs the performance of the IR algorithm, and largely explains the difference between its performance based on known channels and noise covariances in Figure 4.3 and its performance based on estimates of these quantities in Figure 4.7 and 4.8

The performance at 15 dB of the bootstrap algorithm is summarized in Table 4.2.

	IR-DFE			MU-DFE		
Number of users	2	3	4	2	3	4
Known channels	2.6 dB	5.6 dB	8.9 dB	1.2 dB	3.0 dB	5.0 dB
Estimated channels using						
the training sequence only	6.0 dB	10.5 dB	12.9 dB	1.8 dB	4.2 dB	7.3 dB
the bootstrap algorithm	5.9 dB	11.2 dB	14.0 dB	1.5 dB	3.3 dB	5.6 dB

Table 4.2: The performance loss experienced as compared to a single user system when adding users for the simulations in Figure 4.3, 4.7 and 4.8. All values are estimated at an SNR of 15 dB.

4.5 Application on measured data

The simulations in Section 4.4 indicate that reuse within a cell is indeed possible. But will it work in practice? To investigate this we will apply both the multiuser and the interference rejecting DFE to a set of uplink measurements.

4.5.1 The measurements

The measurements were performed on a testbed designed by Ericsson Radio Systems AB and Ericsson Microwave Systems AB [5]. The testbed implements the air interface of a DCS1800 base station. During all measurements, no other traffic was present and the carrier frequency was 1782 MHz.

The array has four dually polarized ($\pm 45^\circ$) microstrip antennas, resulting in eight antenna outputs. A conventional sector antenna with two branch polarization diversity is also included in the measurement setup for two reasons: to evaluate

the impact of using more antenna elements and to estimate the transmitted signal power.

The measurements were performed in Kista, a suburb north of Stockholm, Sweden.

A single mobile mounted in a van was used for all experiments. The van drove at approximately 30–40 km/h during the measurement period. The mobile transmitted a burst of data in one of the eight time slots in a GSM frame. The base station down-converted and sampled the received signal and the resulting digital baseband signal was recorded for a large number of frames. This procedure was repeated when the mobile traveled the same route but transmitted another data sequence. The two sets of collected digital baseband measurements were added to represent a situation when two mobile users share the same channel. The algorithms investigated in Section 4.4 were then applied, both to the data recorded at the array antenna, and to the data recorded at the sector antenna.

4.5.2 Estimation of the average C/N

We estimate the average *carrier-to-noise ratio* (C/N)[10] indirectly, by measuring the received power at the sector antenna when the mobile is inactive. This provides us with an estimate of the noise level. The received power at the sector antenna during the periods when the mobile is active provides an estimate of the signal-plus-noise power. These power level measurements are averaged over a segment of frames. Due to the shadow fading, this average differs between segments. Thus the performance of the algorithms can be addressed as a function of the average carrier-to-noise ratio.

4.5.3 Results

The frame structure in DCS1800 is identical to the frame structure described in Subsection 4.4.3. In this case, five tap channels are estimated, and $\delta s = \ell = L = 4$ is used.

The MMSE MU-DFE and two MMSE IR-DFEs were used to demodulate the signals from the two users. In both cases, the bootstrap algorithm described in Section 4.4.3 was utilized. The results are shown in Figure 4.9 for the array antenna and in Figure 4.10 for the sector antenna.

When we compare the results in Figures 4.9 and 4.10 with the results from the simulations, we see that the error rate decreases much more slowly with SNR for the experimental data than for the simulations. This is because the number

[10]The carrier-to-noise ratio corresponds to the SNR per channel discussed previously. We use the notation C/N rather than SNR to stress the fact that the quantity has been estimated indirectly.

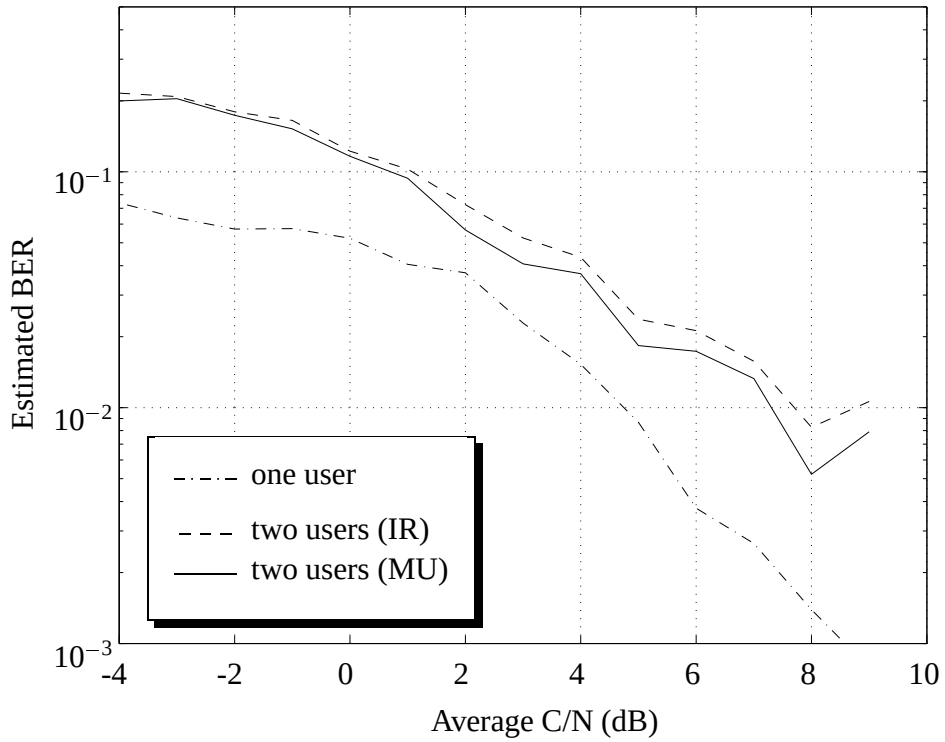

Figure 4.9: Comparison of the MU-DFE and the IR-DFE applied to measurements from a DCS1800 testbed in a flat fading environment. The antenna array had eight outputs and two users were transmitting simultaneously.

of diversity branches is considerably lower in this case: The channel is in fact flat fading and the partial response GMSK modulation causes all the intersymbol interference.

The results from the experiments on the measurements from the array antenna are not surprising. For the lightly loaded system with $N = 8$ and $M = 2$, the performance of a MU-DFE should be only slightly better than the performance of two IR-DFEs.

For the sector antenna, the results are more surprising: A MU-DFE performs slightly *worse* than two IR-DFEs. The reasons for this are twofold:

1. Since the channel is flat fading, the IR-DFE will have adequate degrees of freedom. The intersymbol interference induced by the GMSK modulation will be present in the channels to all antenna elements. Hence, each column of $\boldsymbol{B}(q^{-1})$ will have a common factor of degree L. For $N = 2$ and $M = 2$,

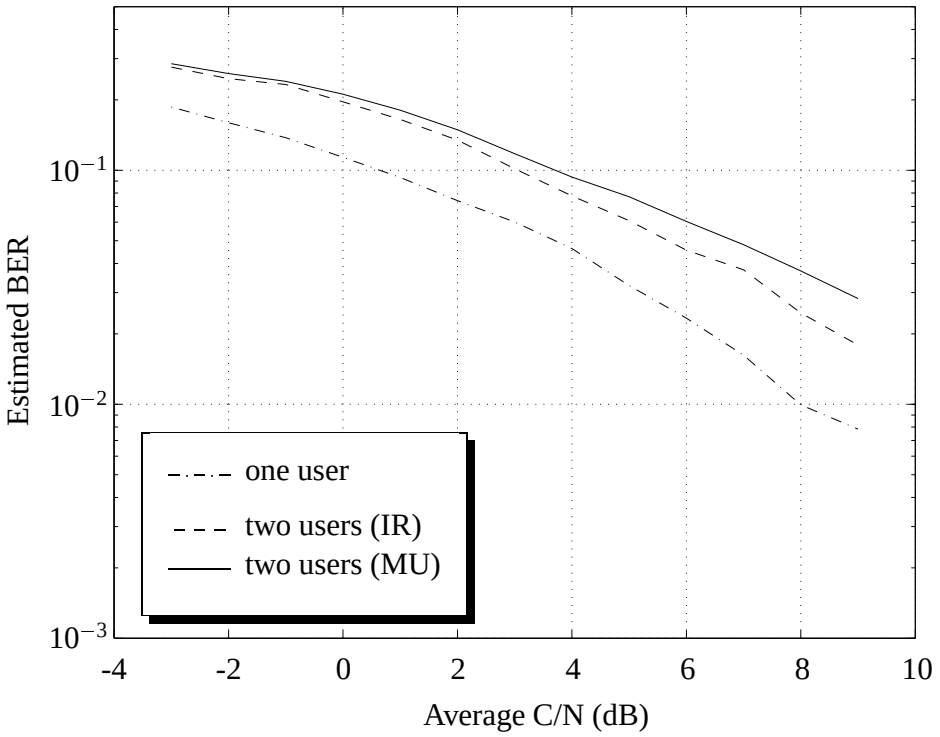

Figure 4.10: Comparison of the MU-DFE and the IR-DFE applied to measurements from a DCS1800 testbed in a flat fading environment. The sector antenna had two outputs and two users were transmitting simultaneously.

the zero-forcing condition (4.22) then reduces to

$$\delta s \geq \frac{\sum_{m=1}^{2} 0 + \ell + 1 - 0 - \Delta_j}{2 + 1 - 2} - 1 = \ell - \Delta_j$$

where ℓ is the decision delay and Δ_j is the propagation delay of user j. Therefore, the choice $\delta s = \ell$ ensures the existence of a ZF IR-DFE for this scenario, and the corresponding MMSE detector will work well.

2. When the amount of intersymbol interference caused by multipath propagation is small, spatial-only interference rejection is sufficient to suppress the interfering user. The multiuser DFE tries to reject co-channel interference by means of an estimate of its spatio-temporal color. This will here lead to *worse* performance, since parameters that do not improve equalization are estimated.

With the array antenna, a few multipath components can be resolved, which leads to a situation where the channels to different antenna elements will have no common factor. In this case, the interference canceller will have to place spatial nulls in several directions, thereby sacrificing some degrees of freedom, which leads to worse performance. In this case, the multiuser detector can use its additional degrees of freedom to cancel the co-channel interference.

It should be noted, that the investigated scenario constitutes a very difficult detection problem: The two mobiles travel exactly the same measurement route. Still, reuse within a cell is possible, using either the array antenna or the sector antenna: The detector performance is approximately 2 dB worse for two users than for one user.

4.6 Discussion

In our investigation of receiver algorithms designed to accomplish reuse within cells, we have compared MIMO DFEs that work as multiuser detectors to the use of interference rejection, implemented by MISO DFEs. In summary, extensive simulations indicate that channel reuse within a cell is indeed a viable option, with multiuser detection providing superior performance. Up to four users could coexist in the same cell if the receivers utilize antenna arrays with only four antenna elements. With multiuser detection, the price paid for this in increased bit error rate is rather small. We have tested the algorithms on experimental measurements from a DCS1800 testbed. For the investigated scenario, reuse within a cell is possible using either an eight-element antenna array or a two-branch diversity sector antenna.

Differences in performance between multiuser detection and interference rejection are partly due to the difference in detector *structure*: A multiuser DFE utilizes feedback from previously estimated symbols from *all* users, while the interference rejecting DFE performs decision feedback from the user of interest only.

The difference also results from the preconditions for *channel estimation*: In the multiuser case, input-output transfer functions from each transmitter to each receiver antenna can, and must, be estimated. For interference rejection, the co-channel interference constitutes colored noise, and multivariate noise models estimated from short data records will have poor accuracy.

These factors will generally result in a higher performance for the multiuser detector. This is particularly apparent when the detectors are applied to heavily loaded systems (with many users/interferers) and when the delay spread in the multipath channel is large.

We have also proposed that the existence of a solution to the zero-forcing prob-

lem can be used as an indication of a well-posed equalization problem. When a zero-forcing equalizer exists, the residual MSE of the corresponding MMSE equalizer will tend to zero as the SNR goes to infinity.

Our conclusions are based on studies and comparisons of symbol-by-symbol decision feedback equalizers. We would expect similar conclusions to hold from a comparison of joint multiuser maximum likelihood detectors [32] to single-user maximum likelihood detectors with spatial interference whitening [14]. The results in [17] confirm this assumption. However, for maximum likelihood detectors the complexity of the two approaches would differ substantially, in contrast to the complexity of the two detectors described here.

Appendix 4.A Proof of Theorem 4.2

We shall here derive the degree condition (4.22). We assume that the conditions in Theorem 4.1 are fulfilled, which implies that a zero-forcing solution exists for some degree of the feedforward filter.

We first need to remove the influence of common factors within each column of $\boldsymbol{B}(q^{-1})$. For this purpose, we insert the factorization (4.18) into (4.17):

$$\boldsymbol{S}^{(i)}(q^{-1})\bar{\boldsymbol{B}}(q^{-1})\boldsymbol{G}(q^{-1})\boldsymbol{\Delta}(q^{-1}) = q^{-\ell}e^{(i)}(1+q^{-1}Q_{ii}(q^{-1}))\ . \tag{4.27}$$

For this equation to have a solution, the right factor $\boldsymbol{G}(q^{-1})\boldsymbol{\Delta}(q^{-1})$ of the left hand side must be a right factor also of the right hand side, that is, we must have

$$q^{-\ell}e^{(i)}(1+q^{-1}Q_{ii}(q^{-1})) = \boldsymbol{X}(q^{-1})\boldsymbol{G}(q^{-1})\boldsymbol{\Delta}(q^{-1}) \tag{4.28}$$

for some matrix polynomial $\boldsymbol{X}(q^{-1})$. We realize that $\boldsymbol{\Delta}(q^{-1})$ cannot be a right divisor of $e^{(i)}(1+q^{-1}Q_{ii}(q^{-1}))$, since the coefficients having the lowest degree differ when the propagation delay Δ_i is non-zero. However, the left hand side of (4.28) can be rewritten as

$$q^{-\ell}e^{(i)}(1+q^{-1}Q_{ii}(q^{-1})) = (1+q^{-1}Q_{ii}(q^{-1}))q^{-\ell}e^{(i)}\ ,$$

which has $\boldsymbol{\Delta}(q^{-1})$ as a right divisor, since $\Delta_i \leq \ell$ for all i. Therefore, we can write

$$\begin{aligned} q^{-\ell}e^{(i)}(1+q^{-1}Q_{ii}(q^{-1})) &= (1+q^{-1}Q_{ii}(q^{-1}))q^{-\ell}e^{(i)} \\ &= \boldsymbol{Y}(q^{-1})\bar{\boldsymbol{\Delta}}(q^{-1})\boldsymbol{\Delta}(q^{-1}) \end{aligned} \tag{4.29}$$

for some matrix polynomial $\boldsymbol{Y}(q^{-1})$ and with

$$\bar{\boldsymbol{\Delta}}(q^{-1}) = \mathrm{diag}\left(q^{-\ell+\Delta_1} \quad \ldots \quad q^{-\ell+\Delta_M}\right)\ .$$

We now choose $\boldsymbol{Y}(q^{-1})$ so that it has $\boldsymbol{G}(q^{-1})$ as a right divisor, or equivalently

$$q^{-\ell}e^{(i)}(1+q^{-1}Q_{ii}(q^{-1})) = \bar{\boldsymbol{Y}}(q^{-1})\boldsymbol{G}(q^{-1})\bar{\boldsymbol{\Delta}}(q^{-1})\boldsymbol{\Delta}(q^{-1})\ . \tag{4.30}$$

The matrix coefficient with the lowest degree on the left hand of (4.30) side must be equal to the matrix coefficient with the lowest degree on the right hand side. Since $\boldsymbol{G}(q^{-1})$ is monic, this can only be satisfied if

$$\bar{\boldsymbol{Y}}(q^{-1}) = e^{(i)}(1+q^{-1}\bar{Q}_{ii}(q^{-1}))$$

for some polynomial matrix $\bar{Q}_{ii}(q^{-1})$. If we insert $\bar{\boldsymbol{Y}}(q^{-1})$ into (4.30), we obtain

$$q^{-\ell}e^{(i)}(1+q^{-1}Q_{ii}(q^{-1}))=e^{(i)}\left(1+q^{-1}\bar{Q}_{ii}(q^{-1})\right)\boldsymbol{G}(q^{-1})\bar{\boldsymbol{\Delta}}(q^{-1})\boldsymbol{\Delta}(q^{-1})\ .$$

Since $\boldsymbol{G}(q^{-1})$ and $\bar{\boldsymbol{\Delta}}(q^{-1})$ are diagonal, they commute. Hence

$$q^{-\ell}e^{(i)}(1+q^{-1}Q_{ii}(q^{-1})) = e^{(i)}\left(1+q^{-1}\bar{Q}_{ii}(q^{-1})\right)\bar{\boldsymbol{\Delta}}(q^{-1})\boldsymbol{G}(q^{-1})\boldsymbol{\Delta}(q^{-1})\ . \tag{4.31}$$

From (4.31) we see that $q^{-\ell}e^{(i)}(1+q^{-1}Q_{ii}(q^{-1}))$ has $\boldsymbol{G}(q^{-1})\boldsymbol{\Delta}(q^{-1})$ as a right factor as required. This factor can thus be removed in our original equation (4.27). We must now solve

$$\boldsymbol{S}^{(i)}(q^{-1})\bar{\boldsymbol{B}}(q^{-1}) = (1+q^{-1}\bar{Q}_{ii}(q^{-1}))\bar{\boldsymbol{\Delta}}(q^{-1}) \tag{4.32}$$

with respect to $\boldsymbol{S}^{(i)}(q^{-1})$ and $\bar{Q}_{ii}(q^{-1})$. The polynomial $Q_{ii}(q^{-1})$ that solves the original Diophantine equation (4.27) can then be obtained from the solution of (4.31).

We now equate the M scalar polynomials in (4.32) to obtain

$$\sum_{k=1}^{N}\bar{B}_{km}(q^{-1})S_{ik}(q^{-1}) = 0 \quad m=1,\ldots,M,\ m\neq i \tag{4.33a}$$

$$\sum_{k=1}^{N}\bar{B}_{ki}(q^{-1})S_{ik}(q^{-1}) = q^{-\ell+\Delta_i}(1+q^{-1}\bar{Q}_{ii}(q^{-1}))\ . \tag{4.33b}$$

In general, equations (4.33a) and (4.33b) can not be solved if there are more equations than there are unknowns. We must assure thus that the number of unknowns equals or exceeds the number of equations.

The feedforward filter of an IR-DFE has $N(\delta s+1)$ scalar taps for each user. Each of these scalar taps can be tuned so that the zero-forcing condition is met.

A system of linear equations is obtained by equating terms with equal powers of q^{-1}. Each of the $M-1$ equations in (4.33a) contribute one equation for each tap in the equalized channel giving a total of

$$\sum_{m \neq i} (\delta s + \bar{L}_m + 1) \tag{4.34}$$

linear equations, whereas the number of equations originating from (4.33b) only equals

$$\ell + 1 - \Delta_i \tag{4.35}$$

since the feedback filter can be determined to fulfill the remaining equations. This means that we have to satisfy

$$\begin{aligned} &\sum_{m \neq i} (\delta s + \bar{L}_m + 1) + \ell + 1 - \Delta_i \\ &\qquad = (M-1)(\delta s + 1) + \sum_{m=1}^{M} \left(\bar{L}_m\right) - \bar{L}_i + \ell + 1 - \Delta_i \end{aligned} \tag{4.36}$$

linear equations, with the $N(\delta s + 1)$ unknowns in the feedforward filter. Thus, we require

$$\delta s \geq \frac{\sum_{m=1}^{M} \left(\bar{L}_m\right) + \ell + 1 - \bar{L}_i - \Delta_i}{N - M + 1} - 1 \, . \tag{4.37}$$

To ensure that the zero-forcing condition is fulfilled for every user, we must require

$$\delta s \geq \max_i \frac{\sum_{m=1}^{M} \left(\bar{L}_m\right) + \ell + 1 - \bar{L}_i - \Delta_i}{N - M + 1} - 1 \, . \tag{4.38}$$

The condition (4.38) is generically necessary to fulfill the zero-forcing condition for all M users.

CHAPTER 5

Multiuser detection in DS-CDMA

5.1 Introduction

IN direct-sequence code division multiple-access (DS-CDMA) systems all users concurrently share the same bandwidth. The users are distinguished by assigning to each user a unique code or signature sequence, whose bandwidth is much larger than that of the transmitted information. This code sequence is used to modulate the data stream.

Conventionally, the transmitted information is retrieved at the receiver by cross-correlation with the signature sequence, followed by symbol rate sampling. This matched filter (or conventional) receiver is optimum in the single-user case or when all signature sequences are orthogonal at the receiver. The first case is obviously of no interest, and the second case is practically impossible to achieve.

In practice, the detection will be adversely affected by *multiple-access interference (MAI)*. When the powers received from different users are approximately equal, the detrimental effect of MAI will be relatively small. However, the conventional receiver will be unable to detect weak signals, typically originating far from the receiver, in the presence of strong (near) interferers. This is the so-called *near-far problem.*

The near-far problem can be alleviated by means of *power control*. The transmitter powers of all signals are thus adjusted so that all signals are received with the same power. However, power control occupies bandwidth and requires amplifiers with high dynamic range to be installed in all transmitters.

An alternative to power control is to replace the matched filter receiver with a more advanced detector. Such *multiuser detectors* have gained an enormous in-

terest in the academic literature during the last decade. Multiuser detectors can be divided into two broad classes: those that operate on the sampled output of a bank of matched filters and those that do not. The latter instead operate directly on the received signal, sampled once or several times during a chip period. Examples of detectors in the first class are the optimal detector [99], the decorrelating detector [56, 57, 77], the multistage detector [96] and the MMSE detector [105] and also some schemes based on multivariable decision feedback equalizers [24, 25, 88].[1] The receivers in [2, 16, 58, 61, 70, 74] are examples of detectors in the second category.

Operating on the output of the matched filter bank has some advantages. The sampled signal constitutes a sufficient statistic of the received continuous-time signal. It is thus possible to derive a receiver that optimally demodulates all transmitted signals. Also, with few users active in the system, the matched filter bank reduces the number of measurement signals considerably, resulting in lower complexity. A third advantage is that these detectors can easily be modified to cope with so-called *long* codes, that is, code sequences with a period that is much larger than the symbol period.

However, the timing accuracy required when sampling the matched filter outputs is high. In fact, the performance of these multiuser detectors may drop drastically with synchronization errors [69, 107]. Also, in many cases the signals from all users must be detected even when only one of them is of interest.

During the first part of this decade, it was realized that it was possible to implement an *adaptive* multiuser detector. This multiuser detector operates directly on the received signal, sampled once or several times during each chip period. Such a receiver is relatively insensitive to errors in the estimates of the propagation delay and other system parameters. Another advantage is that is can be implemented in such a way that only signals that are of interest need to be detected.

The adaptive multiuser detector has two major disadvantages. First, it cannot be applied in systems with long codes. Second, in some cases the rate of convergence may be too slow. However, these two issues are not problems that relate to the detector structure, but to the tuning procedure.

In this chapter, we shall describe how this chip-sampled detector can be designed so that it can be used in a system with long codes. Instead of tuning the receiver directly from the received signal, we derive a linear filter model of the DS-CDMA system. This multivariable model has the symbols transmitted by all users as input, and the received chip-sampled signal as output. This model is then used as a basis for the detector design. Both synchronization errors and multi-

[1] The detector in [88] is the MMSE FIR DFE described in Section 3.3, applied to the multivariable channel model outlined in Subsection 1.4.3.

path propagation is incorporated in the model, and unknown parameters can be estimated with relative ease. The filter model will be time-invariant — or slowly time-varying — in a system with short codes. When long codes are used, the filter model will change abruptly from symbol to symbol, even when the multipath channel is time-invariant.

This model will then be used to design a family of MMSE detectors, with or without decision feedback. We will then show that for a given detector structure, the detector obtained by minimizing the MSE will be near-far resistant if and only if it is possible to adjust its parameters so that the zero-forcing criterion is fulfilled. In the last part of the chapter, we will present Monte Carlo simulations that demonstrate how the proposed design method works in different scenarios.

5.2 System model

In this section, we explain how the entire process of transmission and reception in a DS-CDMA system can be described by a discrete-time model. Our final target is a MIMO model, which has two inputs for each user in the system, whereas the number of outputs equals two times the processing gain. Both long and short codes can be incorporated. However, if long codes are used, the model will be time-varying. Frequency selective fading and arbitrary pulse shaping can also be handled.

5.2.1 The DS-CDMA system

Consider a single user in an asynchronous DS-CDMA system. The symbol period is denoted by T_s, whereas T_c represents the duration of a chip. The processing gain, that is, the ratio T_s/T_c, is denoted by N_c.

It is assumed that user i transmits the complex-valued symbol

$$d_i^{IQ}(k) = d_i^I(k) + j d_i^Q(k)$$

during the time period $[kT_s, (k+1)T_s[$. The I- and Q-components of each symbol are spread by two real-valued wideband signature sequences[2], which are given by

$$c_i^I(kN_c + \nu) \text{ and } c_i^Q(kN_c + \nu)$$

[2]This reflects the way the spreading is performed in some systems, for instance in the W-CDMA downlink [22]. The models and detectors discussed in this chapter would be somewhat simplified if the complex-valued QAM symbols were spread directly by complex-valued signature sequences.

respectively, during the time period $[(kN_c+\nu)T_c, (kN_c+\nu+1)T_c[$. The spreading operation results in a complex-valued discrete-time baseband signal

$$s_i^{IQ}(kN_c+\nu) = s_i^I(kN_c+\nu) + js_i^Q(kN_c+\nu)$$

that can be written as

$$s_i^{IQ}(kN_c+\nu) = \begin{pmatrix} c_i^I(kN_c+\nu) & c_i^Q(kN_c+\nu) \end{pmatrix} \begin{pmatrix} d_i^I(k) \\ jd_i^Q(k) \end{pmatrix} . \tag{5.1}$$

Above, k is a running symbol index, whereas $0 \leq \nu \leq N_c - 1$ denotes the chip number within this symbol. The integer $kN_c + \nu$ thus corresponds to a running chip index. We will use this notation throughout the chapter: If a time series is indexed with the expression $kN_c + \nu$, then it indicates that the sampling period of this time series equals the chip period.

To limit the bandwidth of the transmitted signal, $s_i^{IQ}(kN_c + \nu)$ is passed through a pulse-shaping filter, which is causal with impulse response $p(t)$ of duration T_p. The continuous-time baseband signal is then modulated by a high-frequency carrier, and transmitted.

The transmitted signal propagates through a wideband, frequency selective channel with equivalent baseband impulse response $h_i^c(\tau; t)$. This time-varying impulse response consists of $\Lambda_i + 1$ discrete components with different transmission delays:

$$h_i^c(\tau; t) = \sum_{m=0}^{\Lambda_i} h_{im}^c(t)\delta(\tau - \tau_{im}(t)) . \tag{5.2}$$

Above, the complex-valued coefficients $h_{im}^c(t)$ model the possibly time-varying damping and phase shift for each of the $\Lambda_i + 1$ taps, whereas $\tau_{im}(t)$ represents the corresponding propagation delay.

The receiver front end consists of a conventional IQ-stage, where the I- and Q-signals are down-converted to the baseband. The received baseband signal is then passed through a causal *chip-matched filter*, with impulse response $p(T_p - t)$. The signal at the output of the chip-matched filter is then sampled at the chip rate. The receiver front end is depicted in Figure 5.1 on the next page. Note that the I- and Q-channels are handled separately, which makes more flexible detector tuning possible.

5.2.2 A discrete-time single-user channel model

The entire communication system, from the transmitted symbols to the chip-sampled signal, will now be reformulated as a discrete-time linear model. The model

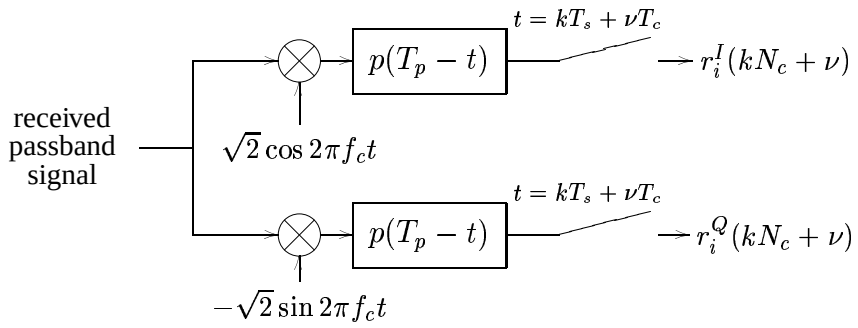

Figure 5.1: The receiver front end.

will include the spreading, as well as the multipath channel and the effects of the pulse shaping and the chip-matched filter.

We begin by relating the spread transmitted signal $s_i^{IQ}(kN_c + \nu)$ to the received signal. The I- and Q- components of the received chip-sampled signal can be modeled as

$$r_i(kN_c + \nu) \triangleq \begin{pmatrix} r_i^I(kN_c + \nu) \\ r_i^Q(kN_c + \nu) \end{pmatrix} = \boldsymbol{b}_i^{kN_c+\nu}(q^{-1}) \begin{pmatrix} s_i^I(kN_c + \nu) \\ s_i^Q(kN_c + \nu) \end{pmatrix} \tag{5.3a}$$

$$= \boldsymbol{b}_i^{kN_c+\nu}(q^{-1}) s_i(kN_c + \nu) \,, \tag{5.3b}$$

where we have defined the equivalent discrete-time impulse response of the *physical channel*

$$\boldsymbol{b}_i^{kN_c+\nu}(q^{-1}) \triangleq \sum_{m=0}^{L_i^c} \mathbf{b}_{im}^{kN_c+\nu} q^{-m} \,. \tag{5.4}$$

The discrete-time physical channel has $L_i^c + 1$ taps, and includes the effects of the pulse shaping, the multipath propagation, and the chip-matched filter. Propagation delays can easily be accommodated by allowing a number of zeros in the beginning of $\boldsymbol{b}_i^{kN_c+\nu}(q^{-1})$. Depending on the pulse shaping employed, the impulse response of the physical channel may be infinite. In practice however, a short FIR filter is sufficient to model the discrete-time physical channel.

We now make the common assumption that the pulse shape is symmetrical, that is, we assume that $p(t) = p(T_p - t)\ \forall\, t$. If $h_{im}^c(t)$ and $\tau_{im}(t)$ are approximately constant over a time interval of length T_p, then the filter taps can be expressed in the form

$$\mathbf{b}_{in}^{kN_c+\nu} \triangleq \sum_{m=0}^{\Lambda_i} \bar{\mathbf{h}}_{im}^c(kT_s + \nu T_c) \mathcal{P}(nT_c - \tau_{im}(kT_s + \nu T_c)) \,. \tag{5.5}$$

Above, we have introduced real-valued 2×2 matrices defined by

$$\bar{\mathbf{h}}_{im}^{c}(t) \triangleq \begin{pmatrix} \mathrm{Re}\, h_{im}^{c}(t) & -\mathrm{Im}\, h_{im}^{c}(t) \\ \mathrm{Im}\, h_{im}^{c}(t) & \mathrm{Re}\, h_{im}^{c}(t) \end{pmatrix}$$

(compare with (1.15)) and the scalar real-valued integral

$$\mathcal{P}(\tau) \triangleq \int_0^{T_p} p(u)p(\tau - u)du \; .$$

A complete derivation of this channel model can be found in Appendix 5.A.

Equation (5.3b) describes a completely discrete-time model. However, as it does not include an explicit model of the spreading, it cannot be directly applied as a basis for design of a DS-CDMA detector. Thus, we would like to include the spreading in the channel model, in such a way that the detector design will be simplified. This can be accomplished by regarding the spreading operation as linear filtering. Designing a DS-CDMA detector will then turn out to be equivalent to designing a fractionally spaced equalizer.

To show that the spreading operation can indeed be interpreted as linear filtering, we study the real part of (5.1)

$$s_i^I(kN_c + \nu) = c_i^I(kN_c + \nu)d_i^I(k) \; , \tag{5.6}$$

over the duration of one symbol period $0 \leq \nu \leq N_c - 1$. Introduce the signals

$$\bar{d}_i^I(kN_c + \nu) \triangleq \begin{cases} d_i^I(k) & \nu = 0 \\ 0 & \nu = 1, \ldots, N_c - 1 \end{cases} \tag{5.7a}$$

$$c_{i,kN_c+\nu}^I(m) \triangleq \begin{cases} c_i^I(kN_c + m) & 0 \leq \nu, m \leq N_c - 1 \\ 0 & \text{otherwise} \end{cases} \; . \tag{5.7b}$$

The chip-sampled signal $\bar{d}_i^I(\cdot)$ is thus equal to $d_i^I(\cdot)$ every N_c chips and zero otherwise, whereas the signal $c_{i,kN_c+\nu}^I(m)$ is the piece of the code that is used to spread the symbol $d_i^I(k)$.[3] Equation (5.6) can then be rewritten as

$$\begin{aligned} s_i^I(kN_c + \nu) &= \sum_{m=0}^{N_c-1} c_{i,kN_c+\nu}^I(m)\bar{d}_i^I(kN_c + \nu - m) \\ &= C_{i,kN_c+\nu}^I(q^{-1})\bar{d}_i^I(kN_c + \nu) \; . \end{aligned} \tag{5.8}$$

[3] With short codes, $c_{i,kN_c+\nu}^I(m)$ is independent of k. This is however not true for long codes.

Above, we have defined a *spreading filter* with impulse response

$$C^I_{i,kN_c+\nu}(q^{-1}) \triangleq \sum_{m=0}^{N_c-1} c^I_{i,kN_c+\nu}(m) q^{-m} \ . \tag{5.9}$$

Analogously, we can write

$$s^Q_i(kN_c+\nu) = C^Q_{i,kN_c+\nu}(q^{-1}) \bar{d}^Q_i(kN_c+\nu) \tag{5.10}$$

where

$$\bar{d}^Q_i(kN_c+\nu) \triangleq \begin{cases} d^Q_i(k) & \nu = 0 \\ 0 & \nu = 1, \ldots, N_c-1 \end{cases} \tag{5.11a}$$

$$C^Q_{i,kN_c+\nu}(q^{-1}) \triangleq \sum_{m=0}^{N_c-1} c^Q_{i,kN_c+\nu}(m) q^{-m} \tag{5.11b}$$

with

$$c^Q_{i,kN_c+\nu}(m) \triangleq \begin{cases} c^Q_i(kN_c+m) & 0 \le \nu, m \le N_c-1 \\ 0 & \text{otherwise} \end{cases} \ .$$

Note that the length of the impulse response of the spreading filter is equal to the processing gain.

When the period of the code sequence is equal to the symbol period, the spreading filters will be *time-invariant,* since the same code is used to spread each symbol. Such codes are known as short codes.

Codes with a period that is much larger than the symbol period are called long or random codes. The spreading in a system with long codes can also be represented as in (5.8), (5.10). In this case, the spreading filter will be *time-varying,* since different symbols are spread with different codes. This means that even if the physical channel is time-invariant (that is, if there is no fast fading), the resulting equivalent channel will vary very rapidly! This time-variation can however be perfectly predicted, since future values of the code sequence are known.

We can now use (5.3a), (5.8) and (5.10) to obtain a combined channel model

$$r_i(kN_c+\nu) = \boldsymbol{b}^{kN_c+\nu}_i(q^{-1}) \begin{pmatrix} C^I_{i,kN_c+\nu}(q^{-1}) & 0 \\ 0 & C^Q_{i,kN_c+\nu}(q^{-1}) \end{pmatrix} \begin{pmatrix} \bar{d}^I_i(kN_c+\nu) \\ \bar{d}^Q_i(kN_c+\nu) \end{pmatrix} \ . \tag{5.12}$$

Note that this model has two real-valued inputs and two real-valued outputs.[4] We can then introduce the complete equivalent channel

$$\bar{\boldsymbol{B}}_i^{kN_c+\nu}(q^{-1}) \triangleq \boldsymbol{b}_i^{kN_c+\nu}(q^{-1}) \begin{pmatrix} C_{i,kN_c+\nu}^I(q^{-1}) & 0 \\ 0 & C_{i,kN_c+\nu}^Q(q^{-1}) \end{pmatrix} \tag{5.13a}$$

$$\triangleq \sum_{m=0}^{L_i^c+N_c-1} \bar{\mathbf{B}}_{im}^{kN_c+\nu} q^{-m} \; . \tag{5.13b}$$

We thus obtain the following model of the received signal from user i:

$$\begin{aligned} r_i(kN_c+\nu) &= \sum_{m=0}^{L_i^c+N_c-1} \bar{\mathbf{B}}_{im}^{kN_c+\nu} q^{-m} \begin{pmatrix} \bar{d}_i^I(kN_c+\nu) \\ \bar{d}_i^Q(kN_c+\nu) \end{pmatrix} \\ &= \sum_{m=0}^{L_i^c+N_c-1} \bar{\mathbf{B}}_{im}^{kN_c+\nu} \begin{pmatrix} \bar{d}_i^I(kN_c+\nu-m) \\ \bar{d}_i^Q(kN_c+\nu-m) \end{pmatrix} \; . \end{aligned} \tag{5.14}$$

Since $\bar{d}_i^I(kN_c+\nu-m)$ and $\bar{d}_i^Q(kN_c+\nu-m)$ are non-zero only when $m-\nu = nN_c$, we realize that (5.14) can be rewritten

$$r_i(kN_c+\nu) = \sum_{n=0}^{L_i} \bar{\mathbf{B}}_{i,nN_c+\nu}^{kN_c+\nu} \begin{pmatrix} \bar{d}_i^I(kN_c-nN_c) \\ \bar{d}_i^Q(kN_c-nN_c) \end{pmatrix} \; ,$$

where we have defined the number of non-zero terms in the sum (5.14):

$$L_i = \left\lfloor \frac{L_i^c+N_c-1}{N_c} \right\rfloor \; . \tag{5.15}$$

We now use the definitions (5.7a) and (5.11a) to express $r_i(kN_c+\nu)$ as

$$r_i(kN_c+\nu) = \sum_{n=0}^{L_i} \bar{\mathbf{B}}_{i,nN_c+\nu}^{kN_c+\nu} \begin{pmatrix} d_i^I(k-n) \\ d_i^Q(k-n) \end{pmatrix} \tag{5.16a}$$

$$= \sum_{n=0}^{L_i} \bar{\mathbf{B}}_{i,nN_c+\nu}^{kN_c+\nu} q^{-n} \begin{pmatrix} d_i^I(k) \\ d_i^Q(k) \end{pmatrix} \; . \tag{5.16b}$$

[4] When a user transmits one-dimensional, for instance BPSK, signals the imaginary part of the input in (5.12) will vanish. The model will then have one real-valued input and two real-valued outputs. In the following, we will however assume that all transmitters utilize two-dimensional signals.

To obtain a collective representation of the signals received during a symbol period, we collect N_c consecutive samples of $r_i(\cdot)$ in the $2N_c$-dimensional vector

$$y_i(k) \stackrel{\triangle}{=} \begin{pmatrix} r_i^T(kN_c) & r_i^T(kN_c+1) & \dots & r_i^T(kN_c+N_c-1) \end{pmatrix}^T . \tag{5.17}$$

The vector-valued stochastic process $y_i(\cdot)$ has a sampling rate that is equal to the symbol rate $1/T_s$. To model $y_i(k)$, we introduce the multiple-input multiple-output transfer function

$$\boldsymbol{B}_i^k(q^{-1}) \stackrel{\triangle}{=} \begin{pmatrix} \sum_{n=0}^{L_i} \bar{\mathbf{B}}_{i,nN_c}^{kN_c} q^{-n} \\ \sum_{n=0}^{L_i} \bar{\mathbf{B}}_{i,nN_c+1}^{kN_c+1} q^{-n} \\ \vdots \\ \sum_{n=0}^{L_i} \bar{\mathbf{B}}_{i,nN_c+N_c-1}^{kN_c+N_c-1} q^{-n} \end{pmatrix} \tag{5.18a}$$

$$= \sum_{n=0}^{L_i} \begin{pmatrix} \bar{\mathbf{B}}_{i,nN_c}^{kN_c} \\ \bar{\mathbf{B}}_{i,nN_c+1}^{kN_c+1} \\ \vdots \\ \bar{\mathbf{B}}_{i,nN_c+N_c-1}^{kN_c+N_c-1} \end{pmatrix} q^{-n} = \sum_{n=0}^{L_i} \mathbf{B}_{in}^k q^{-n} \tag{5.18b}$$

with

$$\mathbf{B}_{in}^k \stackrel{\triangle}{=} \left((\bar{\mathbf{B}}_{i,nN_c}^{kN_c})^T \quad (\bar{\mathbf{B}}_{i,nN_c+1}^{kN_c+1})^T \quad \dots \quad (\bar{\mathbf{B}}_{i,nN_c+N_c-1}^{kN_c+N_c-1})^T \right)^T . \tag{5.18c}$$

In (5.18c), the real-valued matrices $\bar{\mathbf{B}}_{i,nN_c+\gamma}^{kN_c+\nu}$ are defined in (5.13b) whereas the channels $\sum_{n=0}^{L_i} \bar{\mathbf{B}}_{i,nN_c+\nu}^{kN_c+\nu} q^{-n}$ are obtained from (5.16b). The FIR model (5.18b) has two inputs and $2N_c$ outputs, and is of order L_i, as defined in (5.15).

We can now combine (5.17), (5.16b) and (5.18a) to obtain:

$$y_i(k) = \boldsymbol{B}_i^k(q^{-1}) \begin{pmatrix} d_i^I(k) \\ d_i^Q(k) \end{pmatrix} \stackrel{\triangle}{=} \boldsymbol{B}_i^k(q^{-1}) d_i(k) . \tag{5.19}$$

Clearly, this model can be directly used for detector design, since it relates the transmitted symbols to the received (vector) signal, sampled at the symbol rate.

It can be seen from (5.15) that $L_i > 0$ in general. Hence the received signal will suffer from intersymbol interference due to multipath propagation and receiver and transmitter filters. The only exception is when

- the multipath channel is flat fading ($\Lambda_i = 0$ in (5.2)); and
- the synchronization is perfect ($\tau_{i0} = 0$ in (5.2)) .

However, in many cases, the amount of induced intersymbol interference is small and can be ignored. In particular, this is true when the symbol period is large in comparison with the delay spread of the channel. For instance, in a W-CDMA system [22], the symbol period can be as large as 62.5 μs, whereas the delay spread in a typical rural or urban area rarely exceeds 5 μs.

EXAMPLE 5.1

To illustrate the construction of the single-user channel model (5.19), a very simple example is considered. We will build the channel model for one user (user 1) in an asynchronous DS-CDMA system with a processing gain $N_c = 4$ where short codes are used.[5] To simplify the construction further, we make the unrealistic assumption that the taps in the continuous-time baseband channel (5.2) as well as the transmitted signal are real-valued. Thus, $r_i^Q(kN_c + \nu) \equiv 0$, and we can model the channel as a scalar real-valued filter. We assume that the chip-sampled discrete-time equivalent physical channel (5.4) is given by

$$\boldsymbol{b}_1(q^{-1}) = 0.5q^{-1} + 0.3q^{-2} \, .$$

Note that $L_1^c = 2$ and that we have dropped the superscript $kN_c + \nu$, since the channel is time-invariant. The symbols are spread using the code

$$[+1, -1, -1, +1]/2 \, ,$$

which means that the time-invariant spreading filter (5.9) is given by

$$C_1^I(q^{-1}) = 0.5 - 0.5q^{-1} - 0.5q^{-2} + 0.5q^{-3} \, ,$$

where we have omitted the subscript $kN_c + \nu$ on the spreading filter to simplify the notation. The spreading filter $C_1^I(q^{-1})$ and the channel $\boldsymbol{b}_1(q^{-1})$ can now be inserted into (5.13a) to obtain the time-invariant chip-spaced channel

$$\bar{\boldsymbol{B}}_1(q^{-1}) = \sum_{n=0}^{5} \bar{\mathbf{B}}_{1n} q^{-n} = 0.25q^{-1} - 0.1q^{-2} - 0.4q^{-3} + 0.1q^{-4} + 0.15q^{-5} \, .$$

From (5.15), the order of the symbol rate sampled SIMO channel $L_1 = 1$ and using (5.16b) we obtain

$$r_1(4k + \nu) = \bar{\mathbf{B}}_{1,\nu} d_1^I(k) + \bar{\mathbf{B}}_{1,4+\nu} d_1^I(k-1) \, .$$

[5] The construction becomes much more involved when long codes are used.

By stacking the channel taps for $\nu = 0, 1, 2, 3$ into a column vector, the symbol rate sampled SIMO channel (5.18b) is obtained:

$$\boldsymbol{B}_1(q^{-1}) = \begin{pmatrix} \bar{\mathbf{B}}_{1,0} \\ \bar{\mathbf{B}}_{1,1} \\ \bar{\mathbf{B}}_{1,2} \\ \bar{\mathbf{B}}_{1,3} \end{pmatrix} + \begin{pmatrix} \bar{\mathbf{B}}_{1,4} \\ \bar{\mathbf{B}}_{1,5} \\ \bar{\mathbf{B}}_{1,6} \\ \bar{\mathbf{B}}_{1,7} \end{pmatrix} q^{-1} = \begin{pmatrix} 0 \\ 0.25 \\ -0.1 \\ -0.4 \end{pmatrix} + \begin{pmatrix} 0.1 \\ 0.15 \\ 0 \\ 0 \end{pmatrix} q^{-1} \,. \quad (5.20)$$

Note that the order of this channel equals one.

The channel model (5.20) will be used in Example 5.3 to design a multiuser detector.

5.2.3 A multiple-input multiple-output channel model

According to the preceding subsection, the entire single-user channel, from the real and imaginary parts of the symbol sequence to the symbol rate sampled received baseband vector sequence, can be represented by a discrete-time two-input multiple-output (TIMO) channel model. In a multiuser scenario where the processing gains of all users are equal, each user contributes with one such channel. When the processing gains are different, a user with processing gain $N_{c,i}$ will contribute with $N_c/N_{c,i}$ channels, where N_c is the largest processing gain among the active users.[6] Each of these channels can be determined using the procedure described in the preceding subsection. The only difference is that the symbol stream of the high rate user is converted to $N_c/N_{c,i}$ symbol streams. The first of these symbol streams is spread using a code that is non-zero only during the first $N_{c,i}$ chips, whereas the second is spread with a code that is non-zero only in the interval $[N_{c,i}+1, 2N_{c,i}]$ and so on.[7] Keeping in mind that a user with processing gain $N_{c,i}$ is equivalent to $N_c/N_{c,i}$ users with processing gain N_c, we in the following assume that K "equivalent users" with processing gain N_c are active in the system.

The received signal is thus the sum of the outputs from K of the TIMO channels described in the preceding subsection and some noise, as shown in Figure 5.2 on the following page.

[6] The procedure can also be generalized to the case when the quotient $N_c/N_{c,i}$ is not an integer. In this case, we define $\mathcal{N}_c$ to be the least common multiple of all the utilized processing gains. We then define $y_i(k)$ to contain $\mathcal{N}_c$ consecutive chip-samples, and associate with each user $\mathcal{N}_c/N_{c,i}$ channels.

[7] Providing different data rates by varying the processing gain is thus equivalent to multicode transmission with codes that are non-zero only during parts of the transmission.

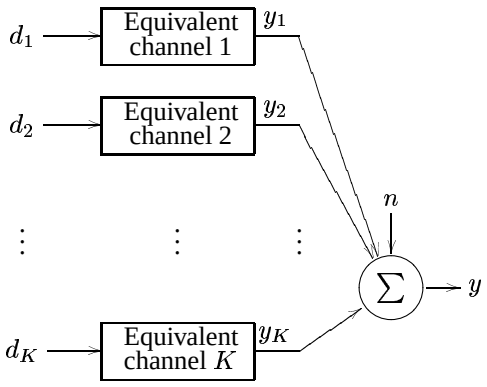

Figure 5.2: A multiple-input multiple-output channel model that relates the symbol sequences transmitted by K users to a symbol rate sampled received vector of dimension $2N_c$.

The entire channel can thus be represented by a linear model with $2K$ inputs and $2N_c$ outputs. To derive this model, we sum the contributions $y_i(k),\ i = 1, \ldots, K$ defined in (5.17) along with some noise $n(k)$ to obtain

$$\begin{aligned} y(k) &\triangleq \sum_{i=1}^{K} y_i(k) + n(k) = \sum_{i=1}^{K} \boldsymbol{B}_i^k(q^{-1}) d_i(k) + n(k) \\ &= \boldsymbol{B}^k(q^{-1}) d(k) + n(k) \end{aligned} \tag{5.21}$$

where

$$\boldsymbol{B}^k(q^{-1}) \triangleq \begin{pmatrix} \boldsymbol{B}_1^k(q^{-1}) & \boldsymbol{B}_2^k(q^{-1}) & \ldots & \boldsymbol{B}_K^k(q^{-1}) \end{pmatrix} \tag{5.22a}$$

$$= \sum_{n=0}^{L} \mathbf{B}_n^k q^{-n} \tag{5.22b}$$

is a $2K$-input $2N_c$-output channel of order

$$L = \max_i L_i \ . \tag{5.23}$$

The I- and Q-components of the symbols for all active users are collected in the vector

$$d(k) \triangleq \begin{pmatrix} d_1^T(k) & d_2^T(k) & \ldots & d_K^T(k) \end{pmatrix}^T \ . \tag{5.24}$$

The noise $n(k)$ is assumed to be zero mean and wide-sense stationary with matrix-valued covariance function

$$E\left[n(i) n^T(j)\right] = \psi_{i-j} \ . \tag{5.25}$$

The noise includes thermal noise and, in a cellular system, out-of-cell interferers.

Equation (5.21) is the desired multiple-input multiple-output channel model, which relates the sequence of symbol vectors to the sampled output sequence. In this multiuser scenario, the conditions for achieving no intersymbol interference become more severe: The fading in *all* channels must be flat, and *all* transmissions have to arrive synchronized at the receiver.

If the coefficients of the impulse response $\boldsymbol{B}^k(q^{-1})$, along with the covariance function ψ_n can be estimated, then we can use these estimates to design an equalizer. In general, this requires that pilot bits are included in all the transmissions.

5.2.4 Model based detector design

A special case of the model (5.19) was used in [70] to analyze the performance of the so-called MMSE detector. Also, the analysis in [58, 61] used a model that is a reformulation of the model (5.21) for the AWGN channel. However, in both cases the model was used only for analysis. For the actual implementation, the authors suggested that the parameters of the detectors be updated directly from the received data using either a training sequence or detected data.

In contrast, we suggest that (5.21) is used for the design of a DS-CDMA detector. In this case, the unknown channel parameters are estimated and the detector is designed using methods described in Section 5.3. This approach has two advantages:

1. The channel estimation is simplified.

2. Long codes can be used.

In the detector implementations suggested in [58, 61, 70], the assumption on short spreading codes is vital. However, with the implementation suggested in this chapter the signature sequences are explicitly modeled and the introduction of long codes “only” implies that the channel will be rapidly time-varying. This will lead to higher complexity, but it is not a fundamental problem, since future values of the code sequence are known.

The benefits for the channel estimation are less obvious and are outlined in the following subsection.

Channel estimation

To use the model (5.21) as a basis for detector design, the channels to the desired users have to be estimated. This can be done if pilot bits are available[8]. We can

[8]When a detector is working in tandem with the channel estimator, some of the pilot bits may be replaced by detected symbols.

then estimate the coefficients of the model (5.21) using the transmitted pilot bits. However, the number of unknown parameters in these models can be large, especially when the processing gain is large. This is true also for the implementation suggested in [2, 58, 61, 70]: The number of parameters to estimate grows with the processing gain.

If we utilize that the spreading codes of the signals we are trying to detect are known, then we can use *spread* pilot bits to reduce the number of unknown parameters. We will now derive a model, where only the taps in the discrete-time impulse response of the physical channel (5.4) has to be estimated.

For this purpose, we use (5.3a) and sum the contributions from all K users along with some noise:

$$\begin{aligned} r(kN_c+\nu) &\triangleq \sum_{i=1}^{K} r_i(kN_c+\nu) + n_{chip}(kN_c+\nu) \\ &= \sum_{i=1}^{K} \boldsymbol{b}_i^{kN_c+\nu}(q^{-1}) s_i(kN_c+\nu) + n_{chip}(kN_c+\nu) \\ &= \boldsymbol{b}^{kN_c+\nu}(q^{-1}) s(kN_c+\nu) + n_{chip}(kN_c+\nu) \end{aligned} \tag{5.26}$$

where

$$\boldsymbol{b}^{kN_c+\nu}(q^{-1}) \triangleq \begin{pmatrix} \boldsymbol{b}_1^{kN_c+\nu}(q^{-1}) & \dots & \boldsymbol{b}_K^{kN_c+\nu}(q^{-1}) \end{pmatrix} \tag{5.27a}$$

$$s(kN_c+\nu) \triangleq \begin{pmatrix} s_1^T(kN_c+\nu) & \dots & s_K^T(kN_c+\nu) \end{pmatrix}^T , \tag{5.27b}$$

and where $n_{chip}(kN_c+\nu)$ constitutes noise. Note that the noise introduced in (5.21) is related to $n_{chip}(kN_c+\nu)$ via

$$n(k) = \begin{pmatrix} n_{chip}^T(kN_c) & \dots & n_{chip}^T(kN_c+N_c-1) \end{pmatrix}^T .$$

The signals $s_i(kN_c+\nu),\ i=1,\dots,K$ can be computed for the duration of the pilot bit transmission. These spread pilot bits can then be used to estimate the parameters of the model (5.26). From the residuals of the channel estimation, the covariance function of the signal $n_{chip}(k)$ can be estimated. We would then use (5.13a), (5.18b), and (5.22a) to compute the complete channel. Finally, we would obtain ψ_n defined in (5.25) from the estimated covariance function of $n_{chip}(kN_c+\nu)$. These entities can then be used for detector design.

If we estimate the coefficients of the model (5.26), only the parameters of the discrete-time physical multipath channel must be estimated. Since this may be only a few coefficients, higher accuracy can be expected, as compared to direct estimation of the parameters of the model (5.21), which has the transmitted *symbols* as

input. The accuracy of the estimate of the covariance function ψ_n defined in (5.25) should also be higher when it is constructed, rather than directly estimated. Moreover, by using the spread pilot bits as regressors in the estimation algorithm, we effectively increase the number of training data by a factor of N_c.

The exact nature of the actual estimation algorithm is not critical. Recursive or block-based methods may be used. Note however that the regressors $s_i(kN_c + \nu)$ in the model (5.26) are white with equal power. This property is of paramount importance if LMS is used for the channel estimation: Since all eigenvalues of the autocorrelation matrix of $s(kN_c+\nu)$ will be equal, a well-conditioned optimization problem is obtained.

We conclude this subsection with an example of the estimation accuracy obtained with the two approaches described above. We thus compare the accuracy of the estimates of the parameters in the model (5.21) when they are

- directly estimated, and
- constructed from estimates of the parameters of the model (5.26).

EXAMPLE 5.2

The system under study is a DS-CDMA system with processing gain $N_c = 8$. Only a single user is active and transmits a BPSK signal using a short BPSK code. The channel (5.4) has four time-invariant Rayleigh fading taps. The channel is estimated using the off-line least-squares method using either 10 or 100 pilot symbols for an SNR between 0 and 15 dB. As a performance measure, we use the MSE between the estimated and true coefficients of the channel (5.19) averaged over 100000 channel realizations. The result is depicted in Figure 5.3 on the next page.

In this scenario, the delay spread equals half the symbol period, which is a large delay spread for a DS-CDMA system. When the impulse response of the discrete-time physical channel is shorter, the difference between direct estimation and channel estimate construction would be even larger.

5.3 Detector description

We will now describe a family of detectors, the members of which are designed based on the models described in the preceding section. The detectors are multivariable equalizers that detect K_1 of the K present signals and feed back K_2 of

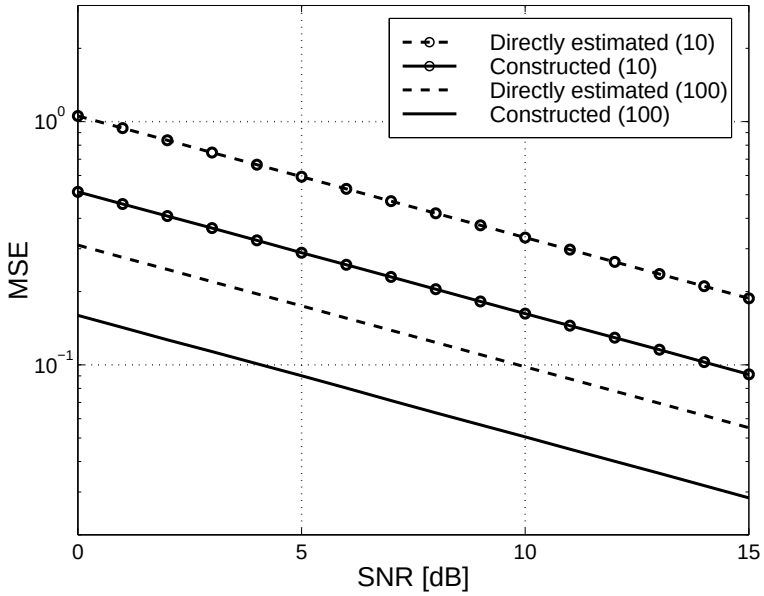

Figure 5.3: The resulting variance of the estimated coefficients of the channel (5.21) *for direct estimation and constructed estimates.*

these K_1 decisions[9], as depicted in Figure 5.4. Without restriction, we assume that the signals to be detected correspond to the first $2K_1$ columns in the channel $\boldsymbol{B}^k(q^{-1})$ and that the decisions fed back correspond to the first $2K_2$ columns in $\boldsymbol{B}^k(q^{-1})$.

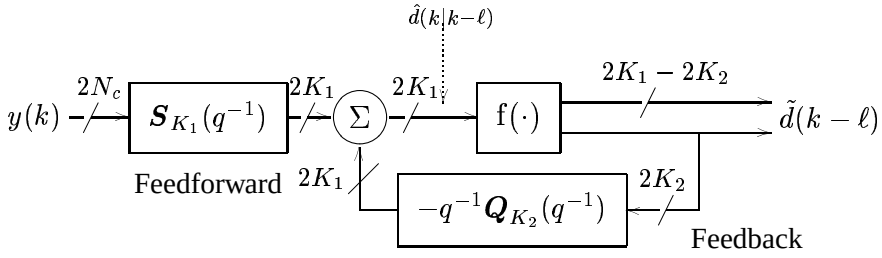

Figure 5.4: The structure of the considered detectors. The feedforward and the feedback filters are transversal filters, which may have multiple inputs and multiple outputs.

With different choices of K_1 and K_2 we obtain different detectors:

[9] We could for instance choose to feed back only the decisions that are considered reliable.

- With $K_1 = 1$ and $K_2 = 0$ we obtain the so-called *MMSE detector*. This linear detector has been suggested for application in a DS-CDMA multiuser scenario by Madhow and Honig in [58] and by Miller in [61]. In both papers, a model related to (5.21) was used for analysis of its performance for the AWGN channel. The analysis was extended to flat fading channels in [62]. Pateros and Saulnier [70] investigated the performance of the linear MMSE detector in a single-user scenario with frequency selective fading and narrowband interference.

- With $K_1 = K_2 = 1$ we obtain the IR-DFE discussed in Subsection 4.3. A detector that is basically equivalent to this DFE has been suggested as a tool for multiuser detection in DS-CDMA systems by Abdulrahman et al. in [2]. See also [1].

- With $K_1 = K_2 = K$, a possibly time-varying version of the multiuser FIR DFE discussed in Section 3.3 is obtained. Such a multiuser DFE has been used in a CDMA system by Rapajic and Vucetic in [74]. The fractionally spaced DFE discussed in [86] is also equivalent to this MIMO DFE.

The detector family we discuss in this chapter is closely related to the detector family introduced by Rapajic and Vucetic in [74]. Unlike those detectors, our detectors will be described by polynomial matrices. Furthermore, since the design is based on a time-varying model, long codes can be handled.

Since this channel model is in general time-varying, so are the detectors discussed in this section. However, to simplify the presentation, the time indices of the detector filters and their parameters have been omitted.

As depicted in Figure 5.4, the estimate at the input of the decision device is given by

$$\hat{d}(k-\ell|k) = \boldsymbol{S}_{K_1}(q^{-1})y(k) - \boldsymbol{Q}_{K_2}(q^{-1})\tilde{d}^{(K_2)}(k-\ell-1)\ , \tag{5.28}$$

where

$$\boldsymbol{S}_{K_1}(q^{-1}) \stackrel{\triangle}{=} \sum_{m=0}^{\delta s} \mathbf{S}_{K_1}^m q^{-m} \tag{5.29a}$$

$$\boldsymbol{Q}_{K_2}(q^{-1}) \stackrel{\triangle}{=} \sum_{m=0}^{L+\delta s-\ell-1} \mathbf{Q}_{K_2}^m q^{-m} \tag{5.29b}$$

and

$$\tilde{d}^{(K_2)}(k) \stackrel{\triangle}{=} \begin{pmatrix} \tilde{d}_1^T(k) & \tilde{d}_2^T(k) & \dots & \tilde{d}_{K_2}^T(k) \end{pmatrix}^T\ . \tag{5.30}$$

Here the feedforward filter $\boldsymbol{S}_{K_1}(q^{-1})$ is a polynomial matrix with $2K_1$ rows and $2N_c$ columns, whereas the feedback filter $\boldsymbol{Q}_{K_2}(q^{-1})$ is a polynomial matrix with $2K_1$ rows and $2K_2$ columns. The degree of the feedforward filter equals δs, and the degree of the feedback filter equals $\delta Q = L + \delta s - \ell - 1$, where L is defined in (5.23). Note that the detector (5.28) uses $N_c(\delta s + 1)$ consecutive chip-samples of the received I- and Q-channels to estimate one transmitted symbol vector.

Remark 1. When $K_2 = 0$, $\boldsymbol{Q}_{K_2}(q^{-1})$ will have no columns. This situation will occur frequently in this chapter and implies that no decision feedback is present.

In the following section, we will present design equations for a detector of the form (5.28) that minimizes the MSE:

$$\mathbf{P}^{K_1} \triangleq E[(d^{(K_1)}(k-\ell) - \hat{d}(k-\ell|k))(d^{(K_1)}(k-\ell) - \hat{d}(k-\ell|k))^T] \quad (5.31)$$

where

$$d^{(K_1)}(k-\ell) \triangleq \begin{pmatrix} d_1^T(k-\ell) & d_2^T(k-\ell) & \dots & d_{K_1}^T(k-\ell) \end{pmatrix}^T . \quad (5.32)$$

The model (5.21) will be used as a basis for the tuning of the detector parameters.

5.3.1 Design equations

We will now describe how to tune the parameters of the MMSE detector (5.28) so that the MSE (5.31) is minimized. As a prerequisite, we need the following definitions:

$$\mathcal{B}_{tot} \triangleq \begin{pmatrix} \mathbf{B}_0^k & \dots & \mathbf{B}_L^k & \dots & 0 \\ \vdots & \ddots & & \ddots & \vdots \\ 0 & \dots & \mathbf{B}_0^{k-\delta s} & \dots & \mathbf{B}_L^{k-\delta s} \end{pmatrix} \quad (5.33)$$

$$\mathcal{B}_{pres} \triangleq \begin{pmatrix} \mathbf{B}_{1\ell}^k & \dots & \mathbf{B}_{K_1\ell}^k \\ \vdots & & \vdots \\ \mathbf{B}_{10}^k & \dots & \mathbf{B}_{K_10}^k \\ \mathbf{0} & \dots & \mathbf{0} \end{pmatrix} \quad (5.34)$$

$$\Psi \triangleq \begin{pmatrix} \psi_0 & \dots & \psi_{\delta s} \\ \vdots & \ddots & \vdots \\ \psi_{-\delta s} & \dots & \psi_0 \end{pmatrix} \quad (5.35)$$

and

$$\hat{\mathbf{B}}_m^k \triangleq \begin{pmatrix} \mathbf{B}_{1m}^k & \dots & \mathbf{B}_{K_2m}^k \end{pmatrix} . \quad (5.36)$$

Note that $\mathbf{B}_{im}^k$ are the matrix coefficients of the two-input $2N_c$-output filter (5.18a), whereas $\mathbf{B}_m^k$ are the matrix coefficients of the filter (5.22a), which has $2K$ inputs and $2N_c$ outputs.

We are now ready to formulate Theorem 5.1:

Theorem 5.1 *Consider the multivariable detector described by* (5.28)*, the channel model* (5.21) *with K transmitters and processing gain N_c and the noise statistics* (5.25)*, with ψ_0 being non-singular. Assume all K signals $d_i^{IQ}(k),\ i = 1, \ldots, K$ to be white and circular with unit variance, to be mutually uncorrelated and uncorrelated with the noise vector $n(k)$. If all past decisions are assumed correct, then the unique matrix polynomials $\boldsymbol{S}_{K_1}(q^{-1})$ and $\boldsymbol{Q}_{K_2}(q^{-1})$ in* (5.29a) *and* (5.29b)*, with which the estimator* (5.28) *minimizes the MSE* (5.31)*, are obtained as follows:*

1. *The coefficients of the feedforward filter $\boldsymbol{S}_{K_1}(q^{-1})$ are obtained as the unique solution to the system of $2N_c(\delta s + 1)$ linear equations*

$$\left(\mathcal{B}_{K_2}\mathcal{B}_{K_2}^T + \Psi\right)\begin{pmatrix}(\mathbf{S}_{K_1}^0)^T\\ \vdots \\ (\mathbf{S}_{K_1}^{\delta s})^T\end{pmatrix} = \mathcal{B}_{pres} \tag{5.37}$$

   Above, $\mathcal{B}_{K_2}$ is the $2N_c(\delta s + 1) \times 2K(\delta s + L + 1)$ matrix, whose (m, n)th element is given by

$$(\mathcal{B}_{K_2})_{m,n} \triangleq \begin{cases}(\mathcal{B}_{tot})_{m,n} & n \le 2K(\ell+1)\\ (\mathcal{B}_{tot})_{m,n} & n = 2K\eta + \gamma,\ \gamma = 2K_2+1, \ldots, 2K\\ & \qquad\qquad \eta = \ell+1, \ldots, \delta s + L\\ 0 & \text{otherwise}\end{cases} \tag{5.38}$$

   where $\mathcal{B}_{tot}$ is defined in (5.33)*. Also, $\mathcal{B}_{pres}$ and Ψ are defined in* (5.34) *and* (5.35)*, respectively.*

2. *When $K_2 > 0$, the coefficients of the feedback filter $\boldsymbol{Q}_{K_2}(q^{-1})$ are given by*

$$\mathbf{Q}_{K_2}^n = \sum_{m=\max(0,n-L+\ell+1)}^{\min(\delta s,\ell+n+1)} \mathbf{S}_{K_1}^m \hat{\mathbf{B}}_{\ell+1-m+n}^{k-m} \tag{5.39}$$

   for $0 \le n \le L + \delta s - \ell - 1$, with $\hat{\mathbf{B}}_m^k$ defined in (5.36)*.*

Proof: See Appendix 5.B. ■

Remark 2. In contrast to the channel parameters, we assume that the covariance function ψ_m is time-invariant over a period of δs symbols. In a cellular DS-CDMA system where long codes are used, this assumption will not be valid, and direct estimation of ψ_m is impossible. Using the noise color to improve the detector performance is in this case very difficult.

Remark 3. When long codes are used, the detector must be retuned for every symbol detection. The detector complexity then becomes very high.

Remark 4. This time-varying DFE is a multi-variable generalization of the SISO DFE derived in [50].

Remark 5. Consider the case $K_2 = 0$. We see from (5.38) and (5.35) that

$$\mathcal{B}_0 \mathcal{B}_0^T + \Psi$$

is independent of K_1. Since each column of $\mathcal{B}_{pres}$ is also independent of K_1, each column of the solution to (5.37) is also independent of K_1. We thus conclude that the tuning of the parameters of a linear detector is not affected by how many signals that are simultaneously detected. Therefore, a linear MMSE multiuser detector is exactly the same detector as a set of linear MMSE interference cancellers.

The resulting MSE when the MMSE detector operates on the output of the channel described by (5.21) can be computed using the following corollary:

Corollary 5.1 *When the MMSE detector designed from Theorem 5.1 is used in the multiuser scenario described by* (5.21)*, the residual MSE is given by*

$$\mathbf{P}^{K_1} = \mathbf{I}_{K_1} - \mathcal{B}_{pres}^T \left(\mathcal{B}_{K_2} \mathcal{B}_{K_2}^T + \Psi \right)^{-1} \mathcal{B}_{pres} \tag{5.40}$$

where $\mathcal{B}_{pres}$, $\mathcal{B}_{K_2}$ and Ψ are defined in (5.34), (5.38) *and* (5.35) *respectively.*

Proof: See Appendix 5.B. ■

As mentioned, when $K_1 = K_2 = K$, this detector reduces to the MMSE FIR MIMO DFE discussed in Subsection 3.3.1. In this case, Theorem 5.1 provides a generalization of Theorem 3.4 to the time-varying case. For a time invariant channel, the DFEs derived from Theorem 5.1 and Theorem 3.4 are identical.

EXAMPLE 5.3

We will now use Theorem 5.1 to design

- the linear MMSE detector ($K_1 = 1, K_2 = 0$),
- the interference rejecting DFE ($K_1 = K_2 = 1$) and
- the multiuser DFE ($K_1 = K_2 = K$)

for the CDMA system with short codes and processing gain $N_c = 4$ discussed in Example 5.1.

Two users are transmitting BPSK signals, the first of which has the channel (5.20). The second user uses the signature sequence

$$[+1, +1, -1, -1]/2$$

and the spread signal travels through the chip-sampled multipath baseband channel

$$\boldsymbol{b}_2(q^{-1}) = -0.8q^{-2} + 0.4q^{-3} + 0.1q^{-4} .$$

As in Example 5.1, we have assumed that the continuous-time channel (5.2) for the second user is real-valued, which means that the single-user channel can be modeled by a scalar, real-valued filter. Proceeding as in Example 5.1, we obtain the symbol rate sampled SIMO channel

$$\boldsymbol{B}_2(q^{-1}) = \begin{pmatrix} 0 \\ 0 \\ -0.4 \\ -0.2 \end{pmatrix} + \begin{pmatrix} 0.65 \\ 0.25 \\ -0.25 \\ -0.05 \end{pmatrix} q^{-1} . \tag{5.41}$$

Combining (5.20) and (5.41) as in (5.22a), we obtain the MIMO model

$$\boldsymbol{B}(q^{-1}) = \mathbf{B}_0 + \mathbf{B}_1 q^{-1} = \begin{pmatrix} 0 & 0 \\ 0.25 & 0 \\ -0.1 & -0.4 \\ -0.4 & -0.2 \end{pmatrix} + \begin{pmatrix} 0.1 & 0.65 \\ 0.15 & 0.25 \\ 0 & -0.25 \\ 0 & -0.05 \end{pmatrix} q^{-1} . \tag{5.42}$$

This channel model will be used to design the three detectors mentioned above. For the linear MMSE detector and the IR-DFE, only the first signal will be detected. All three detectors have $\ell = \delta s = L = 1$. We begin by building the

matrix $\mathcal{B}_{tot}$, defined in (5.33). This matrix is used as a basis for the design of all three detectors. Keeping in mind that $\delta s = 1$ and $L = 1$, we obtain

$$\mathcal{B}_{tot} = \begin{pmatrix} 0 & 0 & 0.10 & 0.65 & 0 & 0 \\ 0.25 & 0 & 0.15 & 0.25 & 0 & 0 \\ -0.10 & -0.40 & 0 & -0.25 & 0 & 0 \\ -0.40 & -0.20 & 0 & -0.05 & 0 & 0 \\ 0 & 0 & 0 & 0 & 0.10 & 0.65 \\ 0 & 0 & 0.25 & 0 & 0.15 & 0.25 \\ 0 & 0 & -0.10 & -0.40 & 0 & -0.25 \\ 0 & 0 & -0.40 & -0.20 & 0 & -0.05 \end{pmatrix} . \tag{5.43}$$

The noise $n(k)$ is white and has covariance matrix $0.03\,\mathbf{I}_4$, which implies that

$$\Psi = 0.03\,\mathbf{I}_8 . \tag{5.44}$$

This will give a signal-to-noise ratio of 9.5 dB and 14.0 dB for users 1 and 2, respectively.

To determine the linear detector and the IR-DFE, we also need

$$\mathcal{B}_{pres} = \begin{pmatrix} \mathbf{B}_{11} \\ \mathbf{B}_{10} \end{pmatrix} = \begin{pmatrix} 0.10 & 0.15 & 0 & 0 & 0 & 0.25 & -0.10 & -0.40 \end{pmatrix}^T , \tag{5.45}$$

where $\mathbf{B}_{10}$ and $\mathbf{B}_{11}$ were obtained from (5.20). Note that $\mathcal{B}_{pres}$ corresponds to column three in (5.43). For the linear detector, we have $K_2 = 0$, and we see from (5.38) that $\mathcal{B}_0 = \mathcal{B}_{tot}$. Inserting (5.43), (5.45) and (5.44) into (5.37), we obtain the feedforward filter for the linear detector

$$\begin{aligned} \boldsymbol{S}_1(q^{-1}) = &\begin{pmatrix} -0.4488 & 0.2393 & 0.0238 & 0.1011 \end{pmatrix} \\ &+ \begin{pmatrix} -0.3784 & 0.7934 & 0.1268 & -1.6861 \end{pmatrix} q^{-1} . \end{aligned}$$

From Corollary 5.1, we then obtain the residual MSE for the linear detector:

$$\mathbf{P}^1 = 0.1489 .$$

For the interference rejecting DFE, we obtain with $K_2 = 1$

$$\mathcal{B}_1 = \begin{pmatrix} 0 & 0 & 0.10 & 0.65 & 0 & 0 \\ 0.25 & 0 & 0.15 & 0.25 & 0 & 0 \\ -0.10 & -0.40 & 0 & -0.25 & 0 & 0 \\ -0.40 & -0.20 & 0 & -0.05 & 0 & 0 \\ 0 & 0 & 0 & 0 & 0 & 0.65 \\ 0 & 0 & 0.25 & 0 & 0 & 0.25 \\ 0 & 0 & -0.10 & -0.40 & 0 & -0.25 \\ 0 & 0 & -0.40 & -0.20 & 0 & -0.05 \end{pmatrix} . \tag{5.46}$$

The only difference between $\mathcal{B}_0$ and $\mathcal{B}_1$ is in the elements $(5,5)$ and $(5,6)$, which are zero in $\mathcal{B}_1$. Inserting (5.46), (5.45), and (5.44) into (5.37), we obtain

$$\begin{aligned}\boldsymbol{S}_1(q^{-1}) = &\begin{pmatrix}-0.3753 & 0.2381 & 0.0162 & 0.1035\end{pmatrix} \\ &+ \begin{pmatrix}-0.4020 & 1.0107 & 0.2063 & -1.5748\end{pmatrix} q^{-1} .\end{aligned}$$

Using $\hat{\mathbf{B}}_1 = \begin{pmatrix}0.10 & 0.15 & 0 & 0\end{pmatrix}^T$, we can determine the feedback filter from equation (5.39):

$$\boldsymbol{Q}_1(q^{-1}) = 0.1114 .$$

Finally, we obtain the residual MSE for a DFE with decision feedback from only signal one from (5.40):

$$\mathbf{P}^1 = 0.1398 .$$

For the multiuser DFE we have

$$\mathcal{B}_2 = \begin{pmatrix} 0 & 0 & 0.10 & 0.65 & 0 & 0 \\ 0.25 & 0 & 0.15 & 0.25 & 0 & 0 \\ -0.10 & -0.40 & 0 & -0.25 & 0 & 0 \\ -0.40 & -0.20 & 0 & -0.05 & 0 & 0 \\ 0 & 0 & 0 & 0 & 0 & 0 \\ 0 & 0 & 0.25 & 0 & 0 & 0 \\ 0 & 0 & -0.10 & -0.40 & 0 & 0 \\ 0 & 0 & -0.40 & -0.20 & 0 & 0 \end{pmatrix} . \tag{5.47}$$

Note that the two last columns now contain only zeros. Since we are now detecting both signals, we have another right hand side in (5.37):

$$\mathcal{B}_{pres} = \begin{pmatrix} \mathbf{B}_{11} & \mathbf{B}_{21} \\ \mathbf{B}_{10} & \mathbf{B}_{20} \end{pmatrix} = \begin{pmatrix} 0.10 & 0.65 \\ 0.15 & 0.25 \\ 0 & -0.25 \\ 0 & -0.05 \\ 0 & 0 \\ 0.25 & 0 \\ -0.10 & -0.40 \\ -0.40 & -0.20 \end{pmatrix} . \tag{5.48}$$

We now insert (5.47), (5.48) and (5.44) into (5.37) to obtain

$$\begin{aligned}\boldsymbol{S}_2(q^{-1}) = &\begin{pmatrix} -0.4178 & 0.2105 & 0.0233 & 0.0880 \\ 1.0339 & 0.1993 & -0.1272 & 0.1413 \end{pmatrix} \\ &+ \begin{pmatrix} 0 & 1.1139 & 0.0857 & -1.5166 \\ 0 & -0.3321 & -0.5851 & 0.1723 \end{pmatrix} q^{-1} .\end{aligned}$$

Using

$$\hat{\mathbf{B}}_1 = \begin{pmatrix} 0.10 & 0.65 \\ 0.15 & 0.25 \\ 0 & -0.25 \\ 0 & -0.05 \end{pmatrix}$$

we can determine the feedback filter from (5.39):

$$\boldsymbol{Q}_2(q^{-1}) = \begin{pmatrix} 0.1671 & 0.3329 \\ -0.0498 & 0.0547 \end{pmatrix} .$$

Finally, we obtain the residual MSE from (5.40):

$$\mathbf{P}^2 = \begin{pmatrix} 0.1337 & -0.0398 \\ -0.0398 & 0.0538 \end{pmatrix} .$$

The residual MSE for user two is smaller than the residual MSE for user one, since the two users have different SNRs.

We see that in this example, the residual MSE for user one is approximately the same for the three detectors:

K_2	0	1	2
MSE	0.1489	0.1398	0.1337

This is generally the case when only a few users are active in the system.

5.3.2 Near-far resistance and the zero-forcing design

To address the performance degradation in a multiuser scenario due to multiple-access interference when the signal-to-noise ratio is high, Verdú introduced the *asymptotic efficiency* [99, 100], which is defined as

$$\eta_i \triangleq \sup \left\{ 0 \le r \le 1;\ \lim_{\sigma \to 0} P_i(\sigma) / Q\left(\frac{\sqrt{r w_i}}{\sigma} \right) < \infty \right\} \tag{5.49}$$

where

$$Q(x) \triangleq \frac{1}{\sqrt{2\pi}} \int_x^\infty e^{-u^2/2}\, du .$$

Above, $P_i(\sigma)$ is the error probability of user i for the considered multiuser detector when the power spectral density of the additive white Gaussian noise is σ^2 and the bit energy of user i is w_i.

The asymptotic efficiency relates the performance of a multiuser detector operating in a multiuser scenario to the performance of an optimum single-user detector, operating in an AWGN channel. When the asymptotic efficiency is equal to one, the performance of the multiuser detector is unaffected by the presence of multiple-access interference.

Intuitively, the asymptotic efficiency of the MMSE detectors discussed in Subsection 5.3 is related to the increase in the residual MSE when multiple-access interference is added: If the MSE only increases marginally with the introduction of MAI, then the asymptotic efficiency is high. A graphical illustration of asymptotic efficiency is given in Figure 5.5.

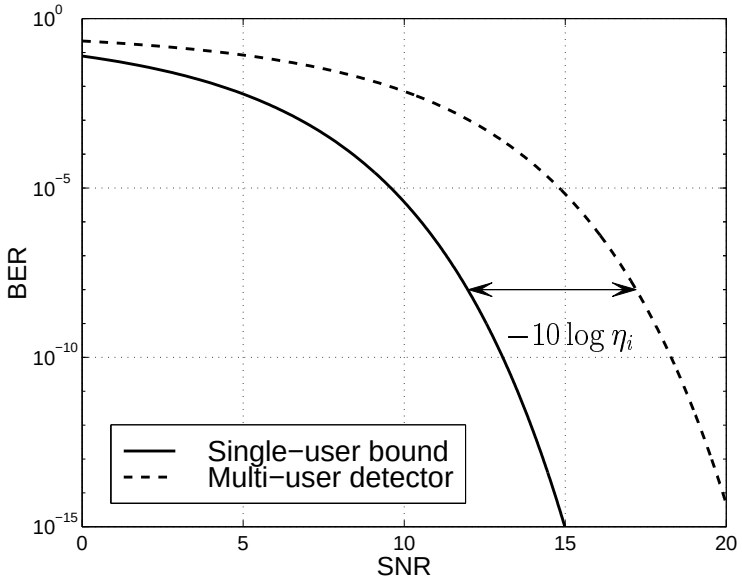

Figure 5.5: An illustration of asymptotic efficiency. The performance of a detector with asymptotic efficiency η_i operating in a multiuser environment degrades by $-10\log\eta_i$ dB as compared to the performance of an optimum single-user detector, operating in a scenario without MAI.

However, the exact mapping from MSE to asymptotic efficiency is complicated.[10] Still, the asymptotic efficiency can, in principle, be evaluated from the

[10]This is mainly because the noise at the input to the decision device is not Gaussian, since the

statistics of the soft symbol estimate $\hat{d}$. Naturally, the choice of codes, the exact multipath channel and the propagation delays will affect this stochastic variable along with the detector structure. However, there is another performance measure that can be used to describe the performance degradation of a multiuser detector relative to the optimum performance of a single-user detector: the *near-far resistance.*

The near-far resistance is defined [57] as the worst-case asymptotic efficiency for any interference power. We will investigate under what conditions the discussed MMSE detectors have a near-far resistance that is greater than zero. When this situation occurs, the detector is said to be *near-far resistant.*

To determine if the considered MMSE detectors are near-far resistant, the residual MSE (5.40) could be evaluated for the current scenario for all transmitter powers of the interfering users. However, since the residual MSE often varies smoothly with the number of users, the results would be non-conclusive. We need a sharper instrument.

For this purpose, we will use the multivariable zero-forcing criterion.[11] To be able to use the zero-forcing criterion to prove near-far resistance of the MMSE detectors in Subsection 5.3.1, we formulate a condition that involves the matrices introduced in Theorem 5.1. This condition is sufficient and necessary for the fulfillment of the zero-forcing condition, and is stated in the following lemma.

Theorem 5.2 *Consider the multivariable detector* (5.28) *and the MIMO channel model* (5.21) *with K users and processing gain N_c. Assume that all previous decisions are correct, and that all K signals $d_i^{IQ}(k),\ i = 1, \ldots, K$ are white, circular with unit variance, and mutually uncorrelated. Then there exist an estimator* (5.28) *that fulfills the zero-forcing condition* (2.3) *if and only if the coefficients of the feedforward filter $\boldsymbol{S}_{K_1}(q^{-1}) = \mathbf{S}_{K_1}^0 + \mathbf{S}_{K_1}^1 q^{-1} + \cdots + \mathbf{S}_{K_1}^{\delta s} q^{-\delta s}$ satisfy*

$$\mathcal{B}_{K_2}^T \begin{pmatrix} (\mathbf{S}_{K_1}^0)^T \\ \vdots \\ (\mathbf{S}_{K_1}^{\delta s})^T \end{pmatrix} = \mathcal{I}\,. \tag{5.50}$$

MMSE detectors balance MAI rejection against noise amplification. The decision statistic will thus have contributions from residual (non-Gaussian) MAI, as well as from (Gaussian) noise. The contributions from all interfering users must then be considered individually.

[11] Since the detector structure discussed in this chapter closely resembles the one discussed in Section 3.3, we are actually investigating a variant of the Diophantine equation (3.28).

Here $\mathcal{B}_{K_2}$ is defined in (5.38)*, and*

$$\mathcal{I} \stackrel{\triangle}{=} \underbrace{\begin{pmatrix} \left.\begin{matrix} 0 & \dots & 0 \\ \vdots & & \vdots \\ 0 & \dots & 0 \end{matrix}\right\} 2K\ell \\ \mathbf{I}_{2K_1} \\ \left.\begin{matrix} 0 & \dots & 0 \\ \vdots & & \vdots \\ 0 & \dots & 0 \end{matrix}\right\} 2K(\delta s + L + 1 - \ell) - 2K_1 \end{pmatrix}}_{2K_1} \tag{5.51}$$

Proof: See Appendix 5.C. ■

Remark 6. As previously mentioned, when $K_1 = K_2 = K$ and the channels are time-invariant, the detector is identical to the FIR DFE introduced in Section 3.3. Also, for $K_1 = K_2 = 1$ and time-invariant channels, the detector is identical to the IR-DFE discussed in Section 4.3. For these situations, equation (5.50) will thus lack a solution whenever the conditions in Theorem 3.5 ($K_1 = K_2 = K$) or Theorem 4.1 ($K_1 = K_2 = 1$) are violated.

We showed in Chapter 3, that a zero-forcing solution *never* exists when $n_d > n_y$, that is, when the number of channel inputs exceeds the number of channel outputs. By imposing this condition on the channel model (5.21), we realize that a zero-forcing CDMA detector with the structure described above cannot exist[12] when

- $K > 2N_c$ (real symbol constellation)
- $K > N_c$ (complex symbol constellation) .

These conditions will be relaxed when the received signal is oversampled. However, excessive oversampling of a bandlimited signal will lead to high correlation among consecutive channel taps, which in turn may lead to an ill-conditioned problem.

To ensure that a solution to (5.50) exists, we have to assure that the number of unknowns equals or exceeds the number of equations. We thus derive a condition corresponding to (3.29) and (4.22), which states the necessary degree of the feedforward filter of the zero-forcing CDMA detector:

[12] Strictly speaking, we have only shown this for $K_1 = K_2 = K$ (Theorem 3.5) and $K_1 = K_2 = 1$ (Theorem 4.1), but formulating and proving the corresponding conditions for any other K_1 and K_2 is straightforward.

Corollary 5.2 *There exists a zero-forcing CDMA detector with the structure* (5.28) *only if*

$$\delta s \geq \frac{(K-K_2)L + K_2(\ell+1)}{N_c - K + K_2} - 1 \; . \tag{5.52}$$

Proof: See Appendix 5.D ■

This condition can be rewritten as

$$K \leq \frac{N_c(\delta s + 1) + K_2(\delta s - \ell + L)}{\delta s + L + 1} \; . \tag{5.53}$$

Since we require $\delta s \geq \ell$, the number of users that can be accommodated in a system with N_c, δs, L and ℓ fixed decreases with decreasing K_2. In this respect, it is of great value to feed back as many detected signals as possible. We also see that the limit increases with increasing N_c.

Remark 7. The most common version of the linear receiver uses $\delta s = 0$. If we insert $\delta s = 0$ and $K_2 = 0$ into (5.53), we obtain

$$K \leq \frac{N_c}{L+1} \; . \tag{5.54}$$

Consider a case without multipath propagation, that is, $\Lambda_i = 0 \; \forall i$ in (5.2). In the synchronous case, no intersymbol interference will then occur ($L = 0$), provided that the synchronization is perfect. In this case, the inequality (5.54) reduces to

$$K \leq N_c \; .$$

In the asynchronous case, we need $L = 1$ to model the resulting intersymbol interference. In this case, a zero-forcing linear receiver with $\delta s = 0$ exists when

$$K \leq N_c/2 \; .$$

Again, these conditions are relaxed if oversampling is used.

We can now use Theorem 5.2 and Corollary 5.2 along with the following theorem to determine if one of the MMSE detectors above is near-far resistant:

Theorem 5.3 *Assuming correct past decisions, the MMSE detector* (5.28) *designed from* (5.37) *and* (5.39) *is near-far resistant if and only if it is possible to tune its parameters so that* (5.50) *is fulfilled.*

Proof: See Appendix 5.E. ■

Remark 8. When the detector employs decision feedback, that is, when $K_2 > 0$, we assume that all previous decisions are correct. We are thus investigating the *ideal near-far resistance* [25].

The theorem is intuitive: If no solution to the zero-forcing condition exists, all multiple-access and intersymbol interference cannot be removed from the signal at the input of the decision device. In situations when the power of the interfering signals is large, the symbol estimates may easily become useless.

It is not surprising that the condition for non-zero near-far resistance becomes milder when more decision feedback is introduced, since the feedback filter helps to suppress MAI. The results in [74] can be predicted from Corollary 5.2: For any given feedforward filter degree, a decision feedback receiver can reject more interferers.

5.4 Monte Carlo simulations

In this section, the results from several Monte Carlo simulations will be presented. In the simulation experiments, the model based design procedure proposed in this chapter is compared to the traditional adaptive approach [58, 61, 70], which is discussed in Subsection 5.2.4. We also evaluate the near-far properties of the considered detectors, and compare these properties with the predictions obtained from consideration of the zero-forcing conditions introduced in Subsection 5.3.2. Finally, we will apply the considered multiuser detectors to the downlink in a W-CDMA system, and compare their performance to that of the conventional detector.

5.4.1 Application in a system with long codes

In our first scenario, we will demonstrate the performance of the proposed model based design in a system with long codes. The considered system is asynchronous with a processing gain $N_c = 8$. The modulation scheme is BPSK, and the pulse shaping employed is a raised cosine with roll-off 0.35.

The transmitted signals pass through a Rayleigh fading channel with four time-invariant taps. These taps are independent and assumed to be known. The channels from different transmitters are independent, as would be the case for uplink transmission. We assume that slow power control ensures that the signals from different transmitters are received with the same average power.

At the receiver, white Gaussian noise is added to obtain an SNR between 0 and 15 dB. We evaluate the BER when three or six users are present in the system and consider three different MMSE detectors:

- The linear receiver described by (5.28) with $K_2 = 0$.
- The multivariable DFE with $K_1 = K_2 = 1$, which is related to the interference rejecting FIR DFE discussed in Subsection 4.3. As in Chapter 4, this DFE will be called the interference rejecting (IR-)DFE.
- The multivariable DFE with $K_1 = K_2 = K$, which closely resembles the FIR DFE discussed in Section 3.3. This DFE will be called the multiuser (MU-)DFE.

For all three detectors, we use $\delta s = \ell = 2$. This is in accordance with the rule of thumb in Subsection 3.3.1, since we must use $L = 2$ in (5.22b) to model the multipath channel, the spreading, and a propagation delay that may be equal to $N_c - 1$. The results are depicted in Figure 5.6.

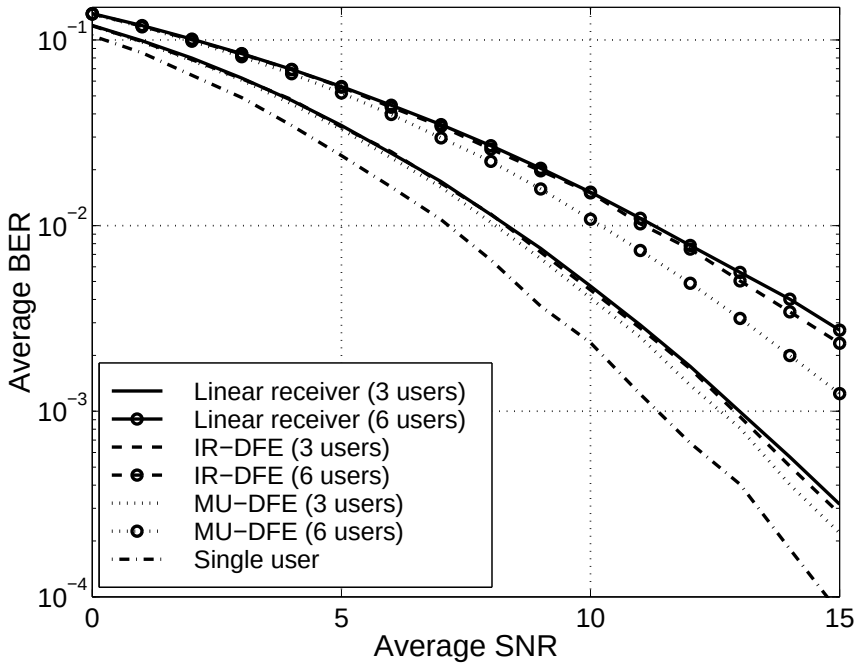

Figure 5.6: Performance of the three detectors in an asynchronous system using long codes. The processing gain is eight, and the channel has four Rayleigh fading taps.

The main objective of this simulation is to show that chip-spaced MMSE detectors *can* be implemented in a system with long codes. The results demonstrate

exactly that. We also see that the difference between the three investigated detectors is small, in particular for the three-user case. This is in agreement with the results obtained in Chapter 4: With few users, the advantage of introducing additional decision feedback is small.

5.4.2 Convergence comparison

In this simulation, we will demonstrate how the improved conditions for parameter estimation affect the performance of the detectors. The proposed model based tuning will be compared to the traditional adaptive setup where the receiver is recursively adjusted to minimize the MSE. This method is proposed in [58, 61, 70], and will be called the *direct* approach.

We investigate the residual MSE for the linear MMSE detector ($K_2 = 0$) for two different parameter adjustment procedures:

1. Indirect adjustment, when the design is based on an estimated channel model and the known code sequences as described in Subsection 5.2.4.

2. Direct adjustment, when the receiver is tuned directly from the received data.

In both cases, the unknown parameters are estimated recursively using the recursive least squares (RLS) algorithm with an increasing data window, that is, with the forgetting factor equal to one.

The comparison between the two approaches is not completely fair: The model based design assumes knowledge of the code sequence whereas the direct method does not. Actually, this is exactly our point: We want to show how much can be gained by using this knowledge.

The considered system is asynchronous. Kasami sequences of length 15 are used to spread BPSK symbols, which are subsequently passed through a raised cosine filter with roll-off factor 0.35.

The transmitted signal propagates through a Rayleigh fading channel with four time-invariant taps. The channels from different transmitters are independent, and slow power control is assumed to ensure that signals from different transmitters are received with the same average power.

At the receiver, the signals from four, eight or twelve users are added together with white Gaussian noise to give an average SNR of 15 dB. We estimate the transient MSE for user 1, whose signal arrives at the receiver with zero delay, using a linear detector with $\delta s = \ell = 1$. Again, this is in accordance with the rule of thumb in Subsection 3.3.1: Since only the signal from user 1 is detected, we can use $\delta s = \ell = L_1 = 1$. The MSE is averaged over 100 noise realizations, in each of 1000 channel realizations. The result is depicted in Figure 5.7.

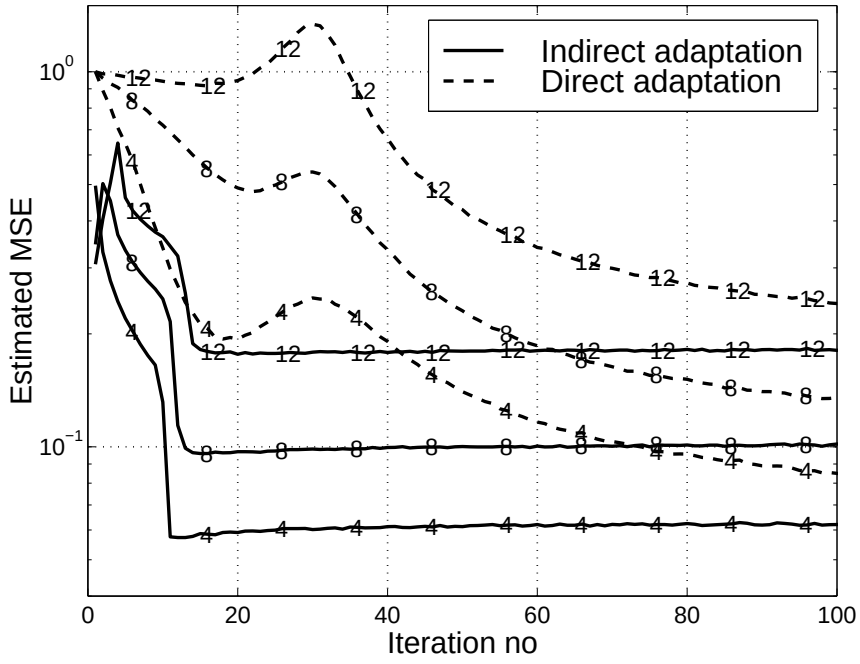

Figure 5.7: Comparison of the rate of convergence for model based (indirect) design and direct estimation of the equalizer parameters for an asynchronous system with processing gain $N_c = 15$. The residual MSE has been estimated for 1000 channel realizations, each of which comprises 100 noise realizations.

From Figure 5.7, we observe that the initial convergence is much faster for the model based approach than for the direct approach. This is quite natural: In the model based approach, much fewer parameters have to be estimated than for the direct approach. The parameters estimated in the indirect approach describe the channel well enough so that a powerful detector can be designed. In this case, sufficient accuracy is obtained with five taps that model the multipath channel and the "interchip" interference that results from the asynchronous sampling of the pulse shaping function $p(t)$.

For the direct approach, the capability to reject interference is directly tied to the number of parameters we have to estimate. In this simulation scenario, a detector that is powerful enough is described by $N_c(\delta s + 1) = 30$ parameters, and all of them must be estimated.

At iteration 30, the MSE of the direct approach has a local maximum. Before this iteration, the estimated covariance matrix of the regressor vector does not have full rank. The parameters then tend to drift off in any direction in the nullspace of this matrix estimate. However, as the convergence proceeds, this nullspace be-

comes smaller and smaller, until it vanishes at iteration 30 and the parameters start moving towards the optimum setting.

Remark 9. Note that the advantage of the model based design lies in the initial convergence. For very long training sequences, better performance is obtained if the channel model has more than five taps, a property that the direct, but not the indirect, method utilizes.

5.4.3 Performance comparison in a near-far situation

We now turn our attention to the near-far properties of the considered detectors as a function of the number of active users. Still, the considered system is asynchronous with processing gain $N_c = 15$. Each QPSK modulated signal is spread by a real-valued Kasami sequence, and raised cosine filtering with roll-off 0.35 is used for pulse shaping. The transmitted signal propagates through a Rayleigh fading channel with four time-invariant taps. These taps are independent and are assumed to be known. Different users have uncorrelated channels, as would be the case for uplink transmission. To model the multipath channel, the spreading, and a propagation delay that may be equal to $N_c - 1$, we must use $L = 2$ in (5.22b).

At the receiver, white Gaussian noise is added to give user 1 an average SNR of 20 or 30 dB, whereas the remaining users have an average SNR of 60 or 70 dB. The near-far ratio is thus 40 dB.

We estimate the residual MSE of user 1 for the linear MMSE detector, the interference rejecting DFE and the multiuser DFE when the number of users vary between 1 and 20. Note that we for the detectors with decision feedback use *correct* decisions. For all three detectors, we use $\delta s = \ell = L = 2$ in accordance with the rule of thumb in Subsection 3.3.1. The result is depicted in Figure 5.8.

In this scenario, the performance of the linear equalizer and the IR-DFE are still approximately equal, whereas the performance of the MU-DFE is clearly better. This conclusion could be predicted if we study the conditions for the existence of a zero-forcing solution for the present scenario. If we insert the system parameters ($L = \ell = \delta s = 2, N_c = 15$) into (5.53) we obtain

$$\begin{array}{ll} \text{Linear:} & K \leq 9 \\ \text{IR-DFE:} & K \leq 9 \\ \text{MU-DFE:} & K \leq 15 \end{array} .$$

We could thus predict that the performance of the linear detector and the IR-DFE would be similar. However, the results in the simulations indicate that a few more than nine users can be accommodated in a system where the linear detector or the IR-DFE are employed. The reasons for this discrepancy are twofold:

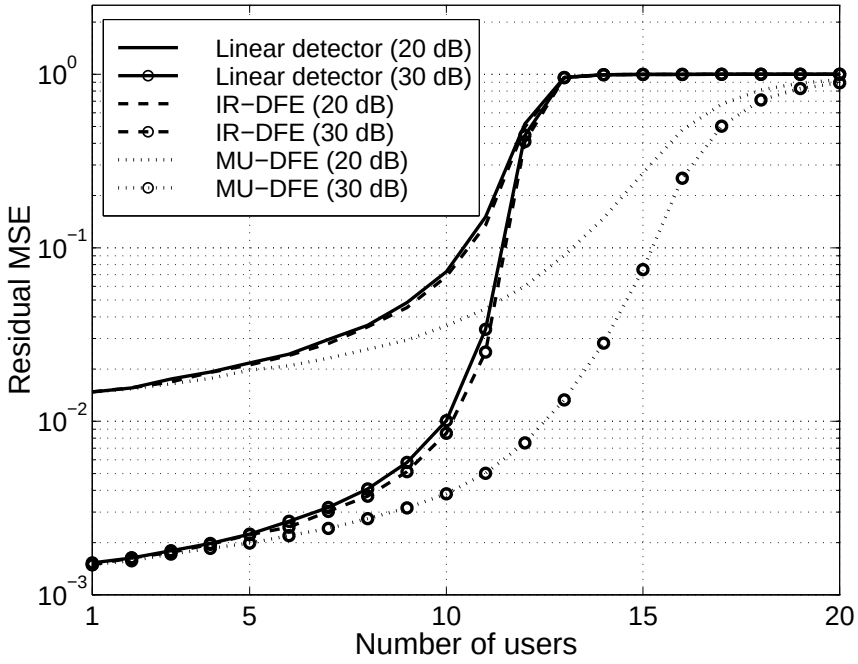

Figure 5.8: The performance of the three detectors in a near-far scenario with processing gain $N_c = 15$. The graph shows the estimated residual MSE for user one, who has an SNR of 20 or 30 dB. The remaining users have an SNR that is 40 dB higher.

1. The system in the simulation has more constraints than is assumed in the discussion on near-far resistance in Subsection 5.3.2:

   - In the definition of near-far resistance, time-varying signal powers are allowed. This feature is not included in the simulation.
   - The discussion in Subsection 5.3.2 is based on a completely general discrete-time channel model, described by the $KN_c(L+1)$ complex coefficients of the multivariable impulse response. In the simulation, we use a realistic CDMA model, where several of these complex coefficients are zero. In the impulse response (5.18b), the first part of the first tap $\mathbf{B}_{i0}^{k}$ is zero to model a propagation delay, whereas the last part of the last tap $\mathbf{B}_{iL_i}^{k}$ is zero to pad the impulse response. For instance, when the channel (5.2) only has a single tap with a propagation delay that is an integer multiple of the chip-period, that is, if $\Lambda_i = 0$ and $\tau_{i0}(t) = nT_c$, the equivalent discrete-time impulse response of the physical channel has $(n+1)$ taps, where only the last one is non-

zero. When the equivalent discrete-time physical channel is convolved with the spreading filters (5.9) and (5.11b), we obtain a two-input two-output channel with $n + N_c$ taps, where the first n are still zero. When we form the two-input $2N_c$-output channel using (5.18b), we obtain a two-tap channel that is described by $(L+1) \times 2 \times 2N_c = 8N_c$ parameters. However, *only* $4N_c$ *of them are non-zero.* The presence of these zeros makes it easier to fulfill the zero-forcing criterion.

2. The system parameters are stochastic variables: One realization may yield a system for which a zero-forcing solution exists, whereas for another realization, such a solution may not exist.

The first point is more important. A closer examination of the number of equations and unknowns should give a more reliable prediction on the near-far resistance of the different detectors.

If the degree of the feedforward filter is increased, then the performance of the linear detector and the IR-DFE should improve. If we insert numerical values into (5.52), we find that a zero-forcing linear equalizer may exist for $K = 14$ if $\delta s \geq 27$ and that a zero-forcing IR-DFE may exist for $K = 15$ whenever $\delta s \geq 31$.

As a final comment, we remark that investigations on near-far resistance are mainly of theoretical interest. In an interference limited cellular system, the "noise" is caused by MAI from other cells. Therefore, it is very unlikely that the weakest user has an SNR of 20 or 30 dB. This is true in particular for a near-far scenario, where power control is *not* used to reduce the power of strong interferers.

5.4.4 Performance of the multiuser detectors in a W-CDMA system

As a final test, the performance of the multiuser detectors in a more realistic scenario will be investigated: the downlink in a wideband CDMA system, according to the UTRA W-CDMA proposal [22].[13]

In this simulation, all users have processing gain $N_c = 16$.[14] The codes used in the W-CDMA downlink are so called OVSF codes, combined with a long code. In this case, when all users have the same processing gain, the OVSF codes are simply Walsh functions. The modulation is QPSK and raised cosine filtering with a roll-off of 0.22 is used.

Each frame contains 160 symbols, and eight of those are pilot symbols. In this simulation, we assume that the frame boundaries for different users are aligned,

[13] The UTRA W-CDMA standard is still evolving. However, the description in [22] is accurate enough for the purpose of this simulation.

[14] This assumption is unrealistic: In a real system, different users will have different processing gains to allow different data rates.

and that the signals to different users are transmitted with the same power. We also assume that the propagation delay has been estimated with an accuracy of one chip period.

The signals from the base station passes through a Rayleigh fading channel with three time-invariant taps.[15] Since the propagation delay has been accurately estimated, it is sufficient to use a channel model (5.22b) with $L = 1$.

The channel is estimated using the off-line least squares method using the spread pilot bits. The transmitted symbols are then detected using the linear MMSE detector, the interference rejecting DFE and the multiuser DFE. For all three detectors, we choose $\delta s = \ell = L = 1$. The BER was then evaluated for an average SNR of 5 and 10 dB, and compared to the BER of the conventional detector with a RAKE receiver. The result is depicted in Figure 5.9.

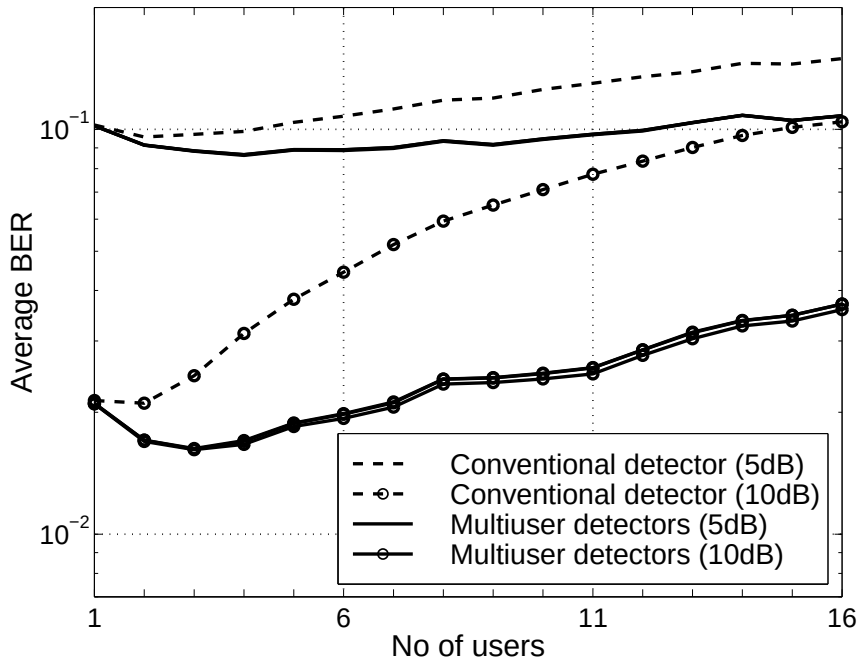

Figure 5.9: The performance of the three multiuser detectors and the conventional receiver in a downlink W-CDMA scenario. The processing gain is 16 and all signals are transmitted with the same power.

A downlink scenario is different from an uplink scenario in a few important

[15] The frame length in W-CDMA is only 0.625ms, so the channel is approximately time-invariant for the duration of a W-CDMA frame.

aspects:

- All the transmitted signals pass through the same channel.
- There is a possibility to receive all signal synchronously.
- The codes can be almost orthogonal at the receiver.

These facts cause the small performance difference between the investigated multiuser detectors to disappear. Furthermore, the difference between the multiuser detectors and the conventional detector is relatively small, in particular when the SNR equals 5 dB. This is a remarkable fact: In a downlink situation with a lot of noise, the potential for improvement in the system capacity by introducing multiuser detectors is small! Only in situations where uplink performance limits the system capacity can it be advantageous to deploy multiuser detectors!

Finally, we note a small anomaly in the results: When the number of active users is small, the BER is *decreased* when the number of users increases. This is because in this situation, the performance is limited by the quality of the channel estimates, and as we increase the number of users, the preconditions for channel estimation are *improved*. To see this we insert $\boldsymbol{b}_1^{kN_c+\nu}(q^{-1}) = \boldsymbol{b}_2^{kN_c+\nu}(q^{-1}) = \cdots = \boldsymbol{b}_K^{kN_c+\nu}(q^{-1})$ into (5.26) to obtain

$$\begin{aligned} r(kN_c+\nu) &= \boldsymbol{b}_1^{kN_c+\nu}(q^{-1}) \sum_{i=1}^{K} s_i(kN_c+\nu) + n_{chip}(kN_c+\nu) \\ &= \boldsymbol{b}_1^{kN_c+\nu}(q^{-1}) u(kN_c+\nu) + n_{chip}(kN_c+\nu) \end{aligned}$$

with

$$u(kN_c+\nu) \stackrel{\triangle}{=} \sum_{i=1}^{K} s_i(kN_c+\nu) \ .$$

We see that the variance of the input signal u increases as the number of users increases, leading to higher accuracy in the channel estimates. As the number of users keeps increasing, the detector performance no longer becomes limited by the accuracy of the channel estimates. When this happens, the performance begins to degrade as the number of users increases.

5.5 Discussion

We have proposed a new methodology for the design of DS-CDMA detectors. The design is based on a linear filter model, which has the transmitted symbols as

input and the chip-sampled signal as output. This model is *constructed* from an estimate of the multipath channel and the known signature sequences. Multipath propagation and propagation delays can be easily handled in this framework.

Similar models have been used previously to analyze CDMA detectors [58, 61, 70]. In contrast, we propose that the model be used also for detector implementation. Since the number of unknown parameters is kept low, the accuracy obtained when estimating these parameters becomes high. Moreover, it is conceptually simple to modify the detector to be used in a system where long codes are used.

The linear model can be used to design MMSE detectors with or without decision feedback, as demonstrated in Section 5.3. The detectors will be time-invariant when the multipath channel is time-invariant and short codes are used. Otherwise, it will be time-varying.

We have also introduced a tool for analyzing the near-far properties of the MMSE detectors: existence of a zero-forcing solution. We have shown that an MMSE detector with a certain structure is near-far resistant if and only if the detector parameters can be tuned so that the zero-forcing condition is fulfilled. A simple condition that is necessary for the existence of a zero-forcing solution has also been derived. The condition provides a relation between important system parameters and detector parameters. In particular, the condition predicts that the near-far properties of a linear MMSE detector and an MMSE detector with decision feedback from only a single user are very similar.

For the case with long signature sequences, the model and the resulting detector are rapidly time-varying. In fact, the detector has to be recalculated for every symbol. The complexity for the design then becomes very high.

Simulations in the preceding section demonstrate that:

- The detector can be implemented in a system with long codes.
- The implementation makes rapid adaptation possible.
- The detector is near-far resistant under conditions that are outlined in Subsection 5.3.2.
- The gains obtained when implementing the detector in the *downlink* of a W-CDMA system are relatively modest.

The final point is alarming, since the system capacity may often be limited by the downlink capacity. It appears that the implementation of a multiuser detector is not worth-while if the downlink is the limiting link. This property is also the most important topic for future research: *How large is the gain in system capacity when multiuser detection is introduced?*

Appendix 5.A Derivation of the channel model (5.4)

In this appendix, we will derive the expression (5.5). To simplify the notation, we will drop the user index i, and derive the expression for the channel from the real part of the transmitted chip sequence to the received chip-sampled in-phase component. The extension to the other three components in the poynomial matrix (5.4) is straightforward.

We will assume that the pulse shaping filter has a time-invariant impulse response $p(\tau)$ that is non-zero only in the interval $[0, T_p[$, where T_p is allowed to be infinite. The receiver filter is matched to the pulse shaping filter. To obtain a causal filter, its impulse response is assumed to be given by $p(T_p - \tau)$. We also assume that the pulse shape is symmetrical, that is, we assume that

$$p(T_p - \tau) = p(\tau) \quad \forall \tau \; . \tag{5.55}$$

The situation is depicted in Figure 5.10.

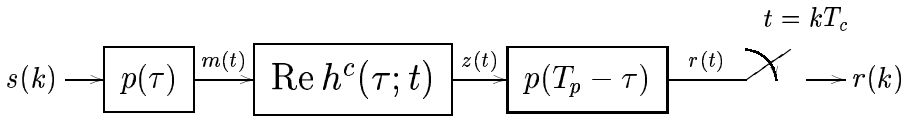

Figure 5.10: The components of the equivalent baseband channel model from the real part of the transmitted symbol to the received in-phase component.

Referring to Figure 5.10, we define the following signals

$s(k) \triangleq$ the real part of the transmitted chip sequence
$m(t) \triangleq$ the real part of the transmitted baseband signal
$z(t) \triangleq$ the received in-phase component prior to chip-matched filtering
$r(t) \triangleq$ the received in-phase component after the chip-matched filtering
$r(k) \triangleq$ sampled in-phase component .

Throughout this appendix, all discrete time time-series are sampled at the chip-rate, and we use the single letter k as an index in these time-series.

At time t, the continuous time baseband representation of the transmitted signal is given by

$$\begin{aligned} m(t) &= p(t)s(0) + p(t - T_c)s(1) + p(t - 2T_c)s(2) + \ldots \\ &= \sum_{n=0}^{N} p(t - nT_c)s(n) \; . \end{aligned} \tag{5.56}$$

The number of non-zero terms in this sum depends on the relation between T_p and T_c.

Each term in the sum (5.56) is attenuated and phase shifted by the $\Lambda + 1$ time-varying multipaths in the impulse response (5.2), which we repeat for ease of reference:

$$\operatorname{Re} h^c(\tau; t) = \sum_{m=0}^{\Lambda} \operatorname{Re} h_m^c(t)\delta(\tau - \tau_m(t)) \; .$$

The received signal prior to the chip-matched filtering is then given by the double sum

$$\begin{aligned} z(t) &= \sum_{m=0}^{\Lambda} \operatorname{Re} h_m^c(t)p(t - \tau_m(t))s(0) + \sum_{m=0}^{\Lambda} \operatorname{Re} h_m^c(t)p(t - T_c - \tau_m(t))s(1) + \ldots \\ &= \sum_{n=0}^{N}\sum_{m=0}^{\Lambda} \operatorname{Re} h_m^c(t)p(t - nT_c - \tau_m(t))s(n) \; . \end{aligned}$$

The received signal is passed through a filter matched to the pulse shaping filter (5.55). The resulting output from the convolution is given by

$$\begin{aligned} r(t) &= \int_0^{T_p} p(u)z(t-u)\,du \\ &= \int_0^{T_p} p(u) \sum_{n=0}^{N}\sum_{m=0}^{\Lambda} \operatorname{Re} h_m^c(t-u)p(t - u - nT_c - \tau_m(t-u))s(n)\,du \; . \end{aligned}$$

Note that the integration only takes place over the interval $[0, T_p[$, since $p(t)$ is non-zero only in this interval.

Finally, the signal $r(t)$ is sampled at the time instant $t = kT_c$, and we obtain

$$\begin{aligned} r(k) = \int_0^{T_p} p(u) \sum_{n=0}^{N}\sum_{m=0}^{\Lambda} &\operatorname{Re} h_m^c(kT_c - u) \times \\ &p(kT_c - u - nT_c - \tau_m(kT_c - u))s(n)\,du \; . \end{aligned}$$

The order of integration and summation can now be exchanged to obtain

$$\begin{aligned} r(k) = \sum_{n=0}^{N} \Bigg\{ \int_0^{T_p} p(u) \sum_{m=0}^{\Lambda} &\operatorname{Re} h_m^c(kT_c - u) \times \\ &p(kT_c - u - nT_c - \tau_m(kT_c - u))\,du \Bigg\} s(n) \; . \end{aligned}$$

With the aid of the definition

$$b_{k-n}^k \triangleq \int_0^{T_p} p(u) \sum_{m=0}^{\Lambda} \operatorname{Re} h_m^c(kT_c - u) \times p((k-n)T_c - u - \tau_m(kT_c - u))\, du \quad (5.57)$$

the received signal can be expressed as

$$r(k) = \sum_{n=0}^{N} b_{k-n}^k s(n) = \sum_{\gamma=0}^{L^c} b_\gamma^k s(k-\gamma) = b^k(q^{-1})s(k)\ , \quad (5.58)$$

where we have substituted γ for $n-k$. We also assumed that $b_\gamma^k = 0$ for $\gamma < 0$ or $\gamma > L^c$. Note that (5.58) coincides with element (1,1) in (5.3a). We thus see that $r(k)$ can be modeled as the output of a linear filter, whose coefficients are given by (5.57).

If we assume that $\operatorname{Re} h_m^c(\cdot)$ and $\tau_m(\cdot)$ are approximately constant over a time interval of length T_p, we can further simplify the expression (5.57). With this assumption we obtain the following approximations of the factors in the integrand:

$$\operatorname{Re} h_m^c(kT_c - u) \approx \operatorname{Re} h_m^c(kT_c)$$
$$\tau(kT_c - u) \approx \tau(kT_c)$$

since $0 \le u \le T_p$. The factor $\operatorname{Re} h_m^c(kT_c)$ can then be moved outside the integration and (5.57) becomes

$$\begin{aligned} b_\gamma^k &= \sum_{m=0}^{\Lambda} \operatorname{Re} h_m^c(kT_c) \int_0^{T_p} p(u)p(\gamma T_c - \tau_m(kT_c) - u)du \\ &= \sum_{m=0}^{\Lambda} \operatorname{Re} h_m^c(kT_c)\mathcal{P}(\gamma T_c - \tau_m(kT_c)) \end{aligned} \quad (5.59)$$

with

$$\mathcal{P}(\tau) = \int_0^{T_p} p(u)p(\tau - u)du\ . \quad (5.60)$$

To return to the notation used in the rest of the chapter, we replace k by $kN_c + \nu = k(T_s/T_c) + \nu$. Equation (5.59) then becomes

$$b_\gamma^{kN_c+\nu} = \sum_{m=0}^{\Lambda} \operatorname{Re} h_m^c(kT_s + \nu T_c)\mathcal{P}(\gamma T_c - \tau_m(kT_s + \nu T_c))$$

which coincides with element (1,1) in (5.5).

Appendix 5.B Proof of Theorem 5.1 and Corollary 5.1

Suppose that a linear finite impulse response channel of order L is given by (5.21) and assume that

$$\begin{aligned} E[d(k)d^T(m)] &= \delta_{km} I \\ E[n(k)n^T(m)] &= \psi_{k-m} \\ E[d(k)n^T(m)] &= 0 \end{aligned} . \tag{5.61}$$

The objective is to estimate the symbol vector

$$d^{(K_1)}(k-\ell) \triangleq \begin{pmatrix} d_1^T(k-\ell) & \dots & d_{K_1}^T(k-\ell) \end{pmatrix}^T \tag{5.62}$$

by means of the equalizer (5.28), which we repeat for ease of reference:

$$\begin{aligned} \hat{d}(k-\ell|k) &= \boldsymbol{S}_{K_1}(q^{-1})y(k) - \boldsymbol{Q}_{K_2}(q^{-1})\tilde{d}^{(K_2)}(k-\ell-1) && (5.63) \\ &= \mathbf{S}_{K_1}^0 y(k) + \mathbf{S}_{K_1}^1 y(k-1) + \dots + \mathbf{S}_{K_1}^{\delta s} y(k-\delta s) \\ &\quad - \mathbf{Q}_{K_2}^0 \tilde{d}^{(K_2)}(k-\ell-1) - \dots - \mathbf{Q}_{K_2}^{\delta Q} \tilde{d}^{(K_2)}(k-\ell-1-\delta Q) \\ &= \Theta_S^T \mathrm{y}_k - \Theta_Q^T \tilde{\mathrm{d}}_{k-\ell-1}^{(K_2)} && (5.64) \\ \tilde{d}_i^{(K_2)}(k-\ell) &= \mathrm{f}(\hat{d}_i(k-\ell|k)) \quad i = 1, 2, \dots, 2K_2 && (5.65) \end{aligned}$$

where $\boldsymbol{S}_{K_1}(q^{-1})$ of order δs and $\boldsymbol{Q}_{K_2}(q^{-1})$ of order δQ are polynomial matrices of dimensions $2K_1 \times 2N_c$ and $2K_1 \times 2K_2$, respectively and $\mathrm{f}(\cdot)$ is the decision non-linearity. Also,

$$\Theta_S^T = \begin{pmatrix} \mathbf{S}_{K_1}^0 & \mathbf{S}_{K_1}^1 & \dots & \mathbf{S}_{K_1}^{\delta s} \end{pmatrix} \tag{5.66a}$$

$$\Theta_Q^T = \begin{pmatrix} \mathbf{Q}_{K_2}^0 & \mathbf{Q}_{K_2}^1 & \dots & \mathbf{Q}_{K_2}^{\delta Q} \end{pmatrix} \tag{5.66b}$$

and

$$\mathrm{y}_k = \begin{pmatrix} y^T(k) & y^T(k-1) & \dots & y^T(k-\delta s) \end{pmatrix}^T \tag{5.67a}$$

$$\tilde{\mathrm{d}}_{k-\ell-1}^{(K_2)} = \begin{pmatrix} \tilde{d}^{(K_2)}(k-\ell-1) \\ \vdots \\ \tilde{d}^{(K_2)}(k-\ell-1-\delta Q) \end{pmatrix} . \tag{5.67b}$$

The feedback filter should be able to cancel all postcursor taps. The number of postcursor taps equals

$$\underbrace{\delta s + L + 1}_{\substack{\text{number of} \\ \text{taps in } \boldsymbol{S}_{K_1}(q^{-1})\boldsymbol{B}^k(q^{-1})}} - \underbrace{\ell}_{\substack{\text{number of} \\ \text{precursor taps}}} - \underbrace{1}_{\substack{\text{reference} \\ \text{tap}}} .$$

Therefore, we conclude that

$$\delta Q = L + \delta s - \ell - 1 \ .$$

The coefficients $\left\{\mathbf{S}_{K_1}^n\right\}$ and $\left\{\mathbf{Q}_{K_2}^n\right\}$ are to be determined so that the mean-square error of the estimate $\hat{d}(k-\ell|k)$ is minimized. Proceeding as in Appendix C, we obtain the normal equations

$$\begin{pmatrix} E\mathrm{y}_k\mathrm{y}_k^T & -E\mathrm{y}_k\left(\tilde{\mathrm{d}}_{k-\ell-1}^{(K_2)}\right)^T \\ -E\tilde{\mathrm{d}}_{k-\ell-1}^{(K_2)}\mathrm{y}_k^T & E\tilde{\mathrm{d}}_{k-\ell-1}^{(K_2)}\left(\tilde{\mathrm{d}}_{k-\ell-1}^{(K_2)}\right)^T \end{pmatrix} \begin{pmatrix} \Theta_S \\ \Theta_Q \end{pmatrix} = \begin{pmatrix} E\mathrm{y}_k(d^{(K_1)}(k-\ell))^T \\ -E\tilde{\mathrm{d}}_{k-\ell-1}^{(K_2)}(d^{(K_1)}(k-\ell))^T \end{pmatrix} \ . \quad (5.68)$$

Assume that all previous decisions affecting the current estimate are correct, that is,

$$\tilde{d}^{(K_2)}(k-n) = d^{(K_2)}(k-n) \quad \forall \ \ell+1 \le n \le L+\delta s$$

with

$$d^{(K_2)}(k) \triangleq \left(d_1^T(k) \quad \ldots \quad d_{K_2}^T(k)\right)^T \ .$$

Define

$$\mathrm{d}_{k-\ell-1}^{(K_2)} \triangleq \begin{pmatrix} d^{(K_2)}(k-\ell-1) \\ \vdots \\ d^{(K_2)}(k-\delta s-L) \end{pmatrix} \ . \quad (5.69)$$

Due to the assumption of uncorrelated symbols made in (5.61), and the assumption of correct past decisions, equation (5.68) can then be simplified to

$$\begin{pmatrix} E\mathrm{y}_k\mathrm{y}_k^T & -E\mathrm{y}_k\left(\mathrm{d}_{k-\ell-1}^{(K_2)}\right)^T \\ -E\mathrm{d}_{k-\ell-1}^{(K_2)}\mathrm{y}_k^T & \mathbf{I}_{2K_2} \end{pmatrix} \begin{pmatrix} \Theta_S \\ \Theta_Q \end{pmatrix} = \begin{pmatrix} E\mathrm{y}_k(d^{(K_2)}(k-\ell))^T \\ 0 \end{pmatrix} \ . \quad (5.70)$$

To evaluate the expectations in (5.70), we invoke the channel model (5.21) to write y_k as

$$\mathrm{y}_k = \begin{pmatrix} \mathbf{B}_0^k & \ldots & \mathbf{B}_L^k & \ldots & 0 \\ \vdots & \ddots & & \ddots & \vdots \\ 0 & \ldots & \mathbf{B}_0^{k-\delta s} & \ldots & \mathbf{B}_L^{k-\delta s} \end{pmatrix} \begin{pmatrix} d(k) \\ \vdots \\ d(k-\delta s-L) \end{pmatrix} + \begin{pmatrix} n(k) \\ \vdots \\ n(k-\delta s) \end{pmatrix} \ . \quad (5.71)$$

The only difference between this equation and equation (C.13) in the proof of Theorem 3.4 is that the channel coefficients are time-varying. To obtain a more compact expression of (5.71), we introduce the vector of stacked noise vectors

$$\mathrm{n}_k = \begin{pmatrix} n^T(k) & n^T(k-1) & \dots & n^T(k-\delta s) \end{pmatrix}^T \tag{5.72}$$

and the vector of stacked symbol vectors

$$\bar{\mathrm{d}}_k = \begin{pmatrix} d^T(k) & d^T(k-1) & \dots & d^T(k-\delta s-L) \end{pmatrix}^T \ . \tag{5.73}$$

The measurement vector y_k is affected by the symbol vectors $d(k-n),\ n = 0,1,\dots,\delta s+L$. Some of the symbols in these vectors have already been detected. We will now separate the influence of these symbols from that of the remaining symbols.

To do this, we will rewrite (5.71) with the aid of the definitions (5.33) and (5.38). Introduce the matrix

$$\tilde{\mathcal{B}}_{K_2} \stackrel{\triangle}{=} \mathcal{B}_{tot} - \mathcal{B}_{K_2} \ , \tag{5.74}$$

where $\mathcal{B}_{tot}$ and $\mathcal{B}_{K_2}$ are defined in (5.33) and (5.38), respectively. Equation (5.71) can then be rewritten

$$\mathrm{y}_k = \mathcal{B}_{tot}\bar{\mathrm{d}}_k + \mathrm{n}_k = \mathcal{B}_{K_2}\bar{\mathrm{d}}_k + \tilde{\mathcal{B}}_{K_2}\bar{\mathrm{d}}_k + \mathrm{n}_k \ . \tag{5.75}$$

Of course, the columns in $\tilde{\mathcal{B}}_{K_2}$ that are non-zero are the columns of $\mathcal{B}_{K_2}$ that are zero. The indices of those columns can be obtained from (5.38):

$$n = 2K\eta + \gamma \qquad \eta = \ell+1,\dots,\delta s+L, \quad \gamma = 1,\dots,2K_2 \ .$$

If we pick out the elements in d_k corresponding to these indices, we obtain the first $2K_2$ elements in $d(k-\eta),\ \eta = \ell+1,\dots,\delta s+L$, that is, $d^{(K_2)}(k-\eta),\ \eta = \ell+1,\dots,\delta s+L$. Comparing with (5.69), we realize that (5.75) can be rewritten as

$$\mathrm{y}_k = \mathcal{B}_{K_2}\bar{\mathrm{d}}_k + \tilde{\bar{\mathcal{B}}}_{K_2}\mathrm{d}^{(K_2)}_{k-\ell-1} + \mathrm{n}_k \ , \tag{5.76}$$

where

$$\tilde{\bar{\mathcal{B}}}_{K_2} \stackrel{\triangle}{=} \text{A matrix with the non-zero columns of } \tilde{\mathcal{B}}_{K_2}. \tag{5.77}$$

Using (5.76) and (5.61), we can evaluate the expectations in (5.70):

$$\begin{aligned} E[\mathrm{y}_k\mathrm{y}_k^T] &= \mathcal{B}_{K_2}\mathcal{B}_{K_2}^T + \tilde{\bar{\mathcal{B}}}_{K_2}\tilde{\bar{\mathcal{B}}}_{K_2}^T + \Psi \\ E[\mathrm{y}_k\left(\mathrm{d}^{(K_2)}_{k-\ell-1}\right)^T] &= \tilde{\bar{\mathcal{B}}}_{K_2} \\ E[\mathrm{y}_k(d^{(K_1)}(k-\ell))^T] &= \mathcal{B}_{pres} \end{aligned}$$

where Ψ and $\mathcal{B}_{pres}$ are defined in (5.35) and (5.34), respectively. To evaluate these expectations, we have used

$$\mathcal{B}_{K_2} E[\bar{\mathrm{d}}_k (\mathrm{d}_{k-\ell-1}^{(K_2)})^T] = 0 \,,$$

which holds since the indices of the non-zero columns of $\mathcal{B}_{K_2}$ are equal to the indices of the zero rows in $E[\bar{\mathrm{d}}_k (\mathrm{d}_{k-\ell-1}^{(K_2)})^T]$.

These computed expectations can then be inserted into (5.70):

$$\begin{pmatrix} \mathcal{B}_{K_2}\mathcal{B}_{K_2}^T + \tilde{\tilde{\mathcal{B}}}_{K_2}\tilde{\tilde{\mathcal{B}}}_{K_2}^T + \Psi & -\tilde{\tilde{\mathcal{B}}}_{K_2} \\ -\tilde{\tilde{\mathcal{B}}}_{K_2}^T & \mathbf{I}_{2K_2} \end{pmatrix} \begin{pmatrix} \Theta_S \\ \Theta_Q \end{pmatrix} = \begin{pmatrix} \mathcal{B}_{pres} \\ 0 \end{pmatrix} \,. \tag{5.78}$$

By observing that $\Theta_Q = \tilde{\tilde{\mathcal{B}}}_{K_2}^T \Theta_S$ from the second block row of (5.78) and inserting this into the first block row, we obtain

$$(\mathcal{B}_{K_2}\mathcal{B}_{K_2}^T + \Psi)\Theta_S = \mathcal{B}_{pres} \tag{5.79a}$$

$$\Theta_Q = \tilde{\tilde{\mathcal{B}}}_{K_2}^T \Theta_S \,. \tag{5.79b}$$

Here (5.79a) coincides with (5.37) and if we transpose both sides of (5.79b) and evaluate for each matrix element $\mathbf{Q}_{K_2}^n$, we obtain (5.39).

Proof of Corollary 5.1

To determine the residual MSE at the output of the detector described in Theorem 5.1, we use the expression (5.64) for the estimator and the expression (5.79b) for its feedback filter coefficients:

$$\hat{d}(k-\ell|k) = \Theta_S^T \left(\mathrm{y}_k - \tilde{\tilde{\mathcal{B}}}_{K_2} \tilde{\mathrm{d}}_{k-\ell-1}^{(K_2)} \right)$$

We now assume that all previous decisions are correct. We thus replace $\tilde{\mathrm{d}}_{k-\ell-1}^{(K_2)}$ by $\mathrm{d}_{k-\ell-1}^{(K_2)}$, defined in (5.69). We also use the expression (5.76) for y_k to obtain

$$\hat{d}(k-\ell) = \Theta_S^T \left(\mathcal{B}_{K_2} \bar{\mathrm{d}}_k + \mathrm{n}_k \right) \,. \tag{5.80}$$

From (5.80) we obtain an expression for the estimation error, which can be used to determine the estimation error covariance matrix (5.31):

$$\begin{aligned} \mathbf{P}^{K_1} = E \Big[& \left(d^{(K_1)}(k-\ell) - \Theta_S^T \left(\mathcal{B}_{K_2} \bar{\mathrm{d}}_k + \mathrm{n}_k \right) \right) \\ & \times \left(d^{(K_1)}(k-\ell) - \Theta_S^T \left(\mathcal{B}_{K_2} \bar{\mathrm{d}}_k + \mathrm{n}_k \right) \right)^T \Big] \,. \end{aligned}$$

The covariance matrix can be evaluated to yield

$$\begin{aligned}\mathbf{P}^{K_1} &= Ed^{(K_1)}(k-\ell)(d^{(K_1)}(k-\ell))^T - Ed^{(K_1)}(k-\ell)\bar{\mathrm{d}}_k^T\mathcal{B}_{K_2}^T\Theta_S \\ &\quad - \Theta_S^T\mathcal{B}_{K_2}E\bar{\mathrm{d}}_k(d^{(K_1)}(k-\ell))^T + \Theta_S^T\mathcal{B}_{K_2}E\bar{\mathrm{d}}_k\bar{\mathrm{d}}_k^T\mathcal{B}_{K_2}^T\Theta_S + \Theta_S^TE\mathrm{n}_k\mathrm{n}_k^T\Theta_S\ ,\end{aligned}$$

where we have used (5.61). Again making use of (5.61) and also of (5.35) we readily obtain

$$\begin{aligned}\mathbf{P}^{K_1} &= \mathbf{I} - Ed^{(K_1)}(k-\ell)\bar{\mathrm{d}}_k^T\mathcal{B}_{K_2}^T\Theta_S - \Theta_S^T\mathcal{B}_{K_2}E\bar{\mathrm{d}}_k(d^{(K_1)}(k-\ell))^T \\ &\quad + \Theta_S^T\mathcal{B}_{K_2}\mathcal{B}_{K_2}^T\Theta_S + \Theta_S^T\Psi\Theta_S\ .\end{aligned} \tag{5.81}$$

It remains to evaluate the expectation $Ed^{(K_1)}(k-\ell)\bar{\mathrm{d}}_k^T$. Since the symbols are white, we obtain

$$\begin{aligned}Ed^{(K_1)}(k-\ell)\bar{\mathrm{d}}_k^T &= \begin{pmatrix} 0 & \dots & 0 & Ed_1(k-\ell)d^T(k-\ell) & 0 & \dots & 0 \\ \vdots & & \vdots & \vdots & \vdots & & \vdots \\ \underbrace{0 & \dots & 0}_{2K\ell} & Ed_{K_1}(k-\ell)d^T(k-\ell) & \underbrace{0 & \dots & 0}_{2K(\delta s+L-\ell)} \end{pmatrix} \\ &= \begin{pmatrix} 0 & \dots & 0 & & 0 & \dots & 0 \\ \vdots & & \vdots & \mathbf{I}_{2K_1} & \vdots & & \vdots \\ \underbrace{0 & \dots & 0}_{2K\ell} & & \underbrace{0 & \dots & 0}_{2K(\delta s+L+1-\ell)-2K_1} \end{pmatrix} = \mathcal{I}^T\end{aligned}$$

where $\mathcal{I}$ is defined in (5.51). The effect of premultiplying $\mathcal{B}_{K_2}^T$ with $\mathcal{I}^T$ is to pick out the rows $2K\ell+1$ to $2K\ell+2K_1$ from $\mathcal{B}_{K_2}^T$. Comparing with (5.34), we realize that the product $Ed^{(K_1)}(k-\ell)\bar{\mathrm{d}}_k^T\mathcal{B}_{K_2}^T$ becomes

$$Ed^{(K_1)}(k-\ell)\bar{\mathrm{d}}_k^T\mathcal{B}_{K_2}^T = \mathcal{I}^T\mathcal{B}_{K_2}^T = \mathcal{B}_{pres}^T\ , \tag{5.82}$$

which can be inserted into (5.81) to yield

$$\mathbf{P}^{K_1} = \mathbf{I} - \mathcal{B}_{pres}^T\Theta_S - \Theta_S^T\mathcal{B}_{pres} + \Theta_S^T\left(\mathcal{B}_{K_2}\mathcal{B}_{K_2}^T + \Psi\right)\Theta_S\ . \tag{5.83}$$

If we insert (5.37) into (5.83), we finally obtain

$$\mathbf{P}^{K_1} = \mathbf{I} - \mathcal{B}_{pres}^T\left(\mathcal{B}_{K_2}\mathcal{B}_{K_2}^T + \Psi\right)^{-1}\mathcal{B}_{pres}\ . \tag{5.84}$$

Appendix 5.C Proof of Theorem 5.2

Suppose that a linear finite impulse response channel of order L is given by (5.21) and assume that

$$E[d(k)d^T(m)] = \delta_{km} I \qquad E[d(k)n^T(m)] = 0\,. \tag{5.85}$$

The objective is to adjust the coefficients of the equalizer (5.28) so that the zero-forcing condition (2.3) is fulfilled. For this purpose, we insert (5.76) into (5.64) to obtain

$$\begin{aligned}\hat{d}(k-\ell|k) &= \Theta_S^T \left(\mathcal{B}_{K_2}\bar{\mathrm{d}}_k + \tilde{\bar{\mathcal{B}}}_{K_2}\mathrm{d}_{k-\ell-1}^{(K_2)} + \mathrm{n}_k\right) - \Theta_Q^T\tilde{\mathrm{d}}_{k-\ell-1}^{(K_2)} \\ &= \Theta_S^T\mathcal{B}_{K_2}\bar{\mathrm{d}}_k + \Theta_S^T\tilde{\bar{\mathcal{B}}}_{K_2}\mathrm{d}_{k-\ell-1}^{(K_2)} + \Theta_S^T\mathrm{n}_k - \Theta_Q^T\tilde{\mathrm{d}}_{k-\ell-1}^{(K_2)}\,.\end{aligned}$$

Assume that all decisions that affect the current estimate are correct, that is, assume that $\tilde{\mathrm{d}}_{k-\ell-1}^{(K_2)} = \mathrm{d}_{k-\ell-1}^{(K_2)}$. The expression above can then be rearranged to yield

$$\hat{d}(k-\ell|k) = \Theta_S^T\mathcal{B}_{K_1}\bar{\mathrm{d}}_k + \left(\Theta_S^T\tilde{\bar{\mathcal{B}}}_{K_2} - \Theta_Q^T\right)\mathrm{d}_{k-\ell-1}^{(K_2)} + \Theta_S^T\mathrm{n}_k\,.$$

We thus obtain an expression for the estimation error

$$\begin{aligned}\varepsilon(k-\ell) &= d^{(K_1)}(k-\ell) - \hat{d}(k-\ell|k) \\ &= d^{(K_1)}(k-\ell) - \Theta_S^T\mathcal{B}_{K_2}\bar{\mathrm{d}}_k - \left(\Theta_S^T\tilde{\bar{\mathcal{B}}}_{K_2} - \Theta_Q^T\right)\mathrm{d}_{k-\ell-1}^{(K_2)} - \Theta_S^T\mathrm{n}_k\,.\end{aligned}$$

To proceed, note that

$$d^{(K_1)}(k-\ell) = \mathcal{I}^T\bar{\mathrm{d}}_k$$

where $\mathcal{I}$ is defined in (5.51). The estimation error $d^{(K_1)}(k-\ell) - \hat{d}(k-\ell)$ can then be simplified to

$$\varepsilon(k-\ell) = \left(\mathcal{I}^T - \Theta_S^T\mathcal{B}_{K_2}\right)\bar{\mathrm{d}}_k - \left(\Theta_S^T\tilde{\bar{\mathcal{B}}}_{K_2} - \Theta_Q^T\right)\mathrm{d}_{k-\ell-1}^{(K_2)} - \Theta_S^T\mathrm{n}_k\,. \tag{5.86}$$

The expression (5.86) can be inserted into the zero-forcing condition (2.3). After rearrangement we obtain

$$\begin{aligned}E[\varepsilon(k-\ell)d^T(\kappa)] = &\left(\mathcal{I}^T - \Theta_S^T\mathcal{B}_{K_2}\right)E[\bar{\mathrm{d}}_k d^T(\kappa)] \\ &- \left(\Theta_S^T\tilde{\bar{\mathcal{B}}}_{K_2} - \Theta_Q^T\right)E[\mathrm{d}_{k-\ell-1}^{(K_2)}d^T(\kappa)] \\ &- \Theta_S^T E[\mathrm{n}_k d^T(\kappa)]\,.\end{aligned} \tag{5.87}$$

Since $n(k)$ and $d(m)$ are assumed uncorrelated for all k and m, the last term vanishes, and by appropriate choice of Θ_Q, we can also make the second term equal to zero. Also, for $\kappa < k - \delta s - L$ and $\kappa > k$, the first term vanishes. However, to ensure that the expected value is equal to zero also for $k - \delta s - L \leq \kappa \leq k$, we must have

$$\mathcal{I}^T - \Theta_S^T \mathcal{B}_{K_2} = 0$$

or, equivalently

$$\mathcal{B}_{K_2}^T \Theta_S = \mathcal{I} \,,$$

which coincides with (5.50).

Appendix 5.D Proof of Corollary 5.2

We will derive what degree of the feedforward filter is necessary to fulfill the zero-forcing condition (5.50). The proof is based simply on comparing the number of equations with the number of unknowns in (5.50).

Consider a single column of the right hand side of (5.50). To fulfill these equations, a single column of the unknown matrix

$$\begin{pmatrix} (\mathbf{S}_{K_1}^0)^T \\ \vdots \\ (\mathbf{S}_{K_1}^{\delta s})^T \end{pmatrix}$$

must be used. A single column of this matrix has

$$2N_c(\delta s + 1) \tag{5.88}$$

elements. The number of equations we have to fulfill is equal to the number of rows in $\mathcal{B}_{K_2}^T$, which is equal to $2K(\delta s + L + 1)$. However, we see from the definition (5.38), that $2K_2(\delta s - \ell + L)$ of these rows are identically zero. Equations that correspond to rows that contain nothing but zeros are fulfilled automatically. Hence, we only have to fulfill

$$2K(\delta s + L + 1) - 2K_2(\delta s - \ell + L) \tag{5.89}$$

equations. For solvability, we must thus require

$$2N_c(\delta s + 1) \geq 2K(\delta s + L + 1) - 2K_2(\delta s - \ell + L) \,,$$

or, equivalently

$$\delta s \geq \frac{(K - K_2)L + K_2(\ell + 1)}{N_c - K + K_2} - 1 \,, \tag{5.90}$$

which coincides with (5.52).

Appendix 5.E Proof of Theorem 5.3

We will now prove that the MMSE detectors described in Section 5.3 are near-far resistant if and only if the equalizer coefficients can be adjusted so that the corresponding zero-forcing condition (5.50) is satisfied.

We begin by showing sufficiency. To this end, we evaluate the symbol estimate at the output of the MMSE detector, given by (5.64):

$$\hat{d}(k-\ell|k) = \Theta_S^T \mathrm{y}_k - \Theta_Q^T \tilde{\mathrm{d}}_{k-\ell-1}^{(K_2)} ,$$

where Θ_S, Θ_Q, y_k, and $\tilde{\mathrm{d}}_{k-\ell-1}^{(K_2)}$ are defined in (5.66a), (5.66b), (5.67a) and (5.67b), respectively. We now assume that all previous decisions are correct, that is, we assume that

$$\tilde{\mathrm{d}}_{k-\ell-1}^{(K_2)} = \mathrm{d}_{k-\ell-1}^{(K_2)}$$

where $\mathrm{d}_{k-\ell-1}^{(K_2)}$ is defined in (5.69). We also insert the expression (5.79b) for the feedback filter coefficients into the expression for the symbol estimate:

$$\hat{d}(k-\ell|k) = \Theta_S^T \left(\mathrm{y}_k - \tilde{\bar{\mathcal{B}}}_{K_2} \mathrm{d}_{k-\ell-1}^{(K_2)} \right) .$$

This can be simplified using the channel model (5.76):

$$\hat{d}(k-\ell|k) = \Theta_S^T \left(\mathcal{B}_{K_2} \bar{\mathrm{d}}_k + \mathrm{n}_k \right) . \tag{5.91}$$

We will now evaluate the first term in (5.91) with the aid of the expression (5.79a) for the feedforward filter coefficients:

$$\hat{d}(k-\ell|k) = \mathcal{B}_{pres}^T (\mathcal{B}_{K_2} \mathcal{B}_{K_2}^T + \Psi)^{-1} \mathcal{B}_{K_2} \bar{\mathrm{d}}_k + \Theta_S^T \mathrm{n}_k .$$

Since we are investigating the asymptotic efficiency, we assume that the noise is white and Gaussian with variance σ^2. This implies that $\Psi = \sigma^2 \mathbf{I}$, which can be inserted into the expression for the symbol estimate:

$$\hat{d}(k-\ell|k) = \mathcal{B}_{pres}^T (\mathcal{B}_{K_2} \mathcal{B}_{K_2}^T + \sigma^2 \mathbf{I})^{-1} \mathcal{B}_{K_2} \bar{\mathrm{d}}_k + \Theta_S^T \mathrm{n}_k . \tag{5.92}$$

To proceed, we note that

$$\begin{pmatrix} d_1^T(k-\ell) & d_2^T(k-\ell) & \dots & d_{K_1}^T(k-\ell) \end{pmatrix}^T = \mathcal{I}^T \bar{\mathrm{d}}_k = d^{(K_1)}(k-\ell)$$

as defined in (5.62). We now add and subtract $d^{(K_1)}(k-\ell)$ from (5.92):

$$\begin{aligned} \hat{d}(k-\ell|k) = {} & d^{(K_1)}(k-\ell) \\ & + \left(\mathcal{B}_{pres}^T (\mathcal{B}_{K_2} \mathcal{B}_{K_2}^T + \sigma^2 \mathbf{I})^{-1} \mathcal{B}_{K_2} - \mathcal{I}^T \right) \bar{\mathrm{d}}_k + \Theta_S^T \mathrm{n}_k . \end{aligned} \tag{5.93}$$

We can now use equation (5.82):

$$\hat{d}(k-\ell|k) = d^{(K_1)}(k-\ell) + \mathcal{I}^T \left(\mathcal{B}_{K_2}^T (\mathcal{B}_{K_2}\mathcal{B}_{K_2}^T + \sigma^2\mathbf{I})^{-1}\mathcal{B}_{K_2} - \mathbf{I} \right) \bar{\mathrm{d}}_k + \Theta_S^T \mathrm{n}_k \,. \quad (5.94)$$

Since there exists a zero-forcing solution, there must exist a matrix Θ_{ZF} such that

$$\Theta_{ZF}^T \mathcal{B}_{K_2} = \mathcal{I}^T \,.$$

This can be inserted into (5.94) to yield

$$\hat{d}(k-\ell|k) = d^{(K_1)}(k-\ell) + \Theta_{ZF}^T \left(\mathcal{B}_{K_2}\mathcal{B}_{K_2}^T (\mathcal{B}_{K_2}\mathcal{B}_{K_2}^T + \sigma^2\mathbf{I})^{-1}\mathcal{B}_{K_2} - \mathcal{B}_{K_2} \right) \bar{\mathrm{d}}_k + \Theta_S^T \mathrm{n}_k \,. \quad (5.95)$$

In this expression, the factor $(\mathcal{B}_{K_2}\mathcal{B}_{K_2}^T + \sigma^2\mathbf{I})^{-1}\mathcal{B}_{K_2}$ can be extracted to the right. After simplification, equation (5.95) becomes

$$\hat{d}(k-\ell|k) = d^{(K_1)}(k-\ell) \underbrace{-\sigma^2 \Theta_{ZF}^T (\mathcal{B}_{K_2}\mathcal{B}_{K_2}^T + \sigma^2\mathbf{I})^{-1}\mathcal{B}_{K_2}\bar{\mathrm{d}}_k}_{\triangleq \varepsilon^{if}(k-\ell)} + \underbrace{\Theta_S^T \mathrm{n}_k}_{\triangleq \varepsilon^{noise}(k-\ell)} \,. \quad (5.96)$$

We will now prove that every element of $|\varepsilon^{if}(k-\ell)|$ is smaller than one for σ^2 sufficiently small. To this end, we define

$$\mathbf{X} = \mathcal{B}_{K_2}\mathcal{B}_{K_2}^T + \sigma^2\mathbf{I} \,.$$

We now make an eigenvalue decomposition of $\mathbf{X}$ to obtain

$$\mathbf{X} = \begin{pmatrix} E_1 & E_2 \end{pmatrix} \begin{pmatrix} \lambda_1 + \sigma^2 & & & & & \\ & \ddots & & & \mathbf{0} & \\ & & \lambda_r + \sigma^2 & & & \\ & & & \sigma^2 & & \\ & \mathbf{0} & & & \ddots & \\ & & & & & \sigma^2 \end{pmatrix} \begin{pmatrix} E_1^T \\ E_2^T \end{pmatrix} \,,$$

where E_1 contains the eigenvectors that correspond to the r non-zero eigenvalues $\lambda_1, \ldots, \lambda_r$ of $\mathcal{B}_{K_2}$. (The matrix $\mathcal{B}_{K_2}\mathcal{B}_{K_2}^T$ may have full rank. In this case, E_2 is empty.) We can now invert $\mathbf{X}$:

$$\mathbf{X}^{-1} = \begin{pmatrix} E_1 & E_2 \end{pmatrix} \begin{pmatrix} \Lambda_r & 0 \\ 0 & \frac{1}{\sigma^2}\mathbf{I} \end{pmatrix} \begin{pmatrix} E_1^T \\ E_2^T \end{pmatrix} \,,$$

where

$$\Lambda_r \stackrel{\triangle}{=} \begin{pmatrix} \frac{1}{\lambda_1+\sigma^2} & & \\ & \ddots & \\ & & \frac{1}{\lambda_r+\sigma^2} \end{pmatrix} .$$

This can be used to simplify $\varepsilon^{if}(k-\ell)$ in (5.96):

$$\varepsilon^{if}(k-\ell) = -\sigma^2 \Theta_{ZF} \begin{pmatrix} E_1 & E_2 \end{pmatrix} \begin{pmatrix} \Lambda_r & 0 \\ 0 & \frac{1}{\sigma^2}\mathbf{I} \end{pmatrix} \begin{pmatrix} E_1^T \\ E_2^T \end{pmatrix} \mathcal{B}_{K_2} \bar{\mathrm{d}}_k$$

Since E_1 contains the eigenvectors of $\mathcal{B}_{K_2}$, the following relation holds

$$\mathcal{B}_{K_2} = E_1 v_B$$

for some matrix v_B. Due to the orthonormality of the eigenvectors, we then obtain

$$\varepsilon^{if}(k-\ell) = -\sigma^2 \Theta_{ZF} E_1 \Lambda_r v_B \bar{\mathrm{d}}_k \, .$$

We realize that every element in $|\varepsilon^{if}(k-\ell)|$ becomes arbitrarily small when σ^2 tends to zero.

We will now study element i in $\hat{d}(k-\ell|k)$. With obvious notations, we have

$$\hat{d}_i(k-\ell|k) = d_i(k-\ell) + \varepsilon_i^{if}(k-\ell) + \varepsilon_i^{noise}(k-\ell) \, . \tag{5.97}$$

For σ^2 small enough, we have

$$|\varepsilon_i^{if}(k-\ell)| \leq \gamma$$

for some $\gamma < 1$. We will now show that the conditional probability $P(\hat{d}_i(k-\ell|k) > 0 | d_i(k-\ell) = -1)$ is upper-bounded by the probability of error for a single-user detector in a single-user scenario, but with a higher noise level. We begin by using $|\varepsilon_i^{if}(k-\ell)| \leq \gamma$:

$$\begin{aligned} P(\hat{d}(k-\ell|k) > 0 | d(k-\ell) = -1) &= P(\varepsilon_i^{noise}(k-\ell) > 1 - \varepsilon_i^{if}(k-\ell)) \\ &\leq P(\varepsilon_i^{noise}(k-\ell) > 1-\gamma) \, . \end{aligned}$$

The stochastic variable $\varepsilon_i^{noise}(k-\ell)$ is Gaussian distributed with zero mean and variance σ_{MMSE}^2. To obtain a normed Gaussian distribution, we divide by σ_{MMSE}:

$$P(\varepsilon_i^{noise}(k-\ell) > 1-\gamma) = P(\frac{\varepsilon_i^{noise}(k-\ell)}{\sigma_{MMSE}} > \frac{1-\gamma}{\sigma_{MMSE}}) \, . \tag{5.98}$$

Unfortunately, the limit $(1-\gamma)/\sigma_{MMSE}$ depends on σ in a rather complex way. Therefore, we upper-bound σ_{MMSE} with the estimation error variance at the output of the zero-forcing equalizer. Since a zero-forcing equalizer removes all inter-symbol and co-channel interference, the estimation error is only a linear combination of noise terms:

$$\varepsilon_i^{ZF}(k-\ell) = \theta_{ZF}^T \mathrm{n}_k$$

where

$$\theta_{ZF} \stackrel{\triangle}{=} \text{column } i \text{ in } \Theta_{ZF} \ ,$$

that is, column i in the solution to (5.50). The estimation error of the zero-forcing detector is thus Gaussian distributed with a variance σ_{ZF}^2 that is proportional to σ^2:

$$\sigma_{ZF}^2 \stackrel{\triangle}{=} E[|\varepsilon_i^{ZF}(k-\ell)|^2] = \mu\sigma^2 \ , \tag{5.99}$$

for some constant $\mu \geq 1$. Since the MSE of the zero-forcing equalizer is always larger than or equal to the MSE of the MMSE equalizer, we have

$$\sigma_{ZF}^2 \geq E|\varepsilon_i^{if}(k-\ell)|^2 + \sigma_{MMSE}^2 \geq \sigma_{MMSE}^2 \ .$$

This implies that

$$\frac{1-\gamma}{\sigma_{MMSE}} \geq \frac{1-\gamma}{\sigma_{ZF}}$$

since $1-\gamma > 0$. Using this, we can upper-bound the probability of error in (5.98) with

$$\begin{aligned} P\left(\frac{\varepsilon_i^{noise}(k-\ell)}{\sigma_{MMSE}} > \frac{1-\gamma}{\sigma_{MMSE}}\right) &\leq P\left(\frac{\varepsilon_i^{noise}(k-\ell)}{\sigma_{MMSE}} > \frac{1-\gamma}{\sigma_{ZF}}\right) \\ &= P\left(\frac{\varepsilon_i^{noise}(k-\ell)}{\sigma_{MMSE}} > \frac{1-\gamma}{\sigma\sqrt{\mu}}\right) \ , \end{aligned}$$

where we in the last equality used (5.99). The conditional probability $P(\hat{d}(k-\ell|k) > 0 | d(k-\ell) = -1)$ can thus be upper-bounded by

$$Q\left(\frac{1-\gamma}{\sigma\sqrt{\mu}}\right) \ . \tag{5.100}$$

Using the same argument, we can show that

$$P(\hat{d}_i(k-\ell|k) < 0 | d_i(k-\ell) = +1) \leq Q\left(\frac{1-\gamma}{\sigma\sqrt{\mu}}\right) \ . \tag{5.101}$$

Assuming BPSK modulation, we can combine (5.100) and (5.101) to obtain

$$P\left(\tilde{d}_i(k-\ell) \neq d_i(k-\ell)\right) \leq Q\left(\frac{1-\gamma}{\sigma\sqrt{\mu}}\right) \tag{5.102}$$

where

$$\tilde{d}_i(k-\ell) = \operatorname{sgn} \hat{d}_i(k-\ell|k)$$

is the binary decision made on the symbol estimate $\hat{d}_i(k-\ell|k)$. If we compare (5.102) with (5.49), we realize that the quotient

$$\frac{P_i(\sigma)}{Q\left(\frac{\sqrt{rw_i}}{\sigma}\right)} = \frac{P(\tilde{d}_i(k-\ell) \neq d_i(k-\ell))}{Q\left(\frac{\sqrt{rw_i}}{\sigma}\right)}$$

is finite if

$$\sqrt{w_i r} = \frac{1-\gamma}{\sqrt{\mu}}$$

for $\gamma < 1$. Since $w_i = E[|d_i(k-\ell)|^2] = 1$, this can be simplified to yield

$$r = \frac{(1-\gamma)^2}{\mu} \, .$$

Since the probability of error for the MMSE detector is upper-bounded by (5.102), we obtain the following bound for the asymptotic efficiency:

$$\eta_i \geq \frac{(1-\gamma)^2}{\mu} \, .$$

Since $\gamma < 1$ and $\mu \geq 1$ is finite, we realize that the near-far resistance of the MMSE detector is always greater than zero. Hence the MMSE detector is near-far resistant.

We now turn our attention to the proof of necessity. We will thus assume that the zero-forcing condition (5.50) cannot be fulfilled for all users, and show that in this case, the corresponding diagonal element in $\mathbf{P}^{K_1}$, defined in (5.31), will tend to one as the interference power goes to infinity. The MSE for user i can only be equal to one when

$$\hat{d}_i(k-\ell|k) = 0 \, . \tag{5.103}$$

For BPSK modulation, the probability of error for this detector is 0.5 irrespective of the noise level. We realize that the quotient

$$\frac{0.5}{Q\left(\frac{\sqrt{rw_i}}{\sigma}\right)}$$

in (5.49) will be finite only for $r = 0$. Thus we conclude that

$$\hat{d}_i(k-\ell|k) = 0 \;\Rightarrow\; \eta_i = 0\;. \tag{5.104}$$

The asymptotic efficiency of a detector that produces the estimate $\hat{d}_i(k-\ell|k) = 0$, irrespective of the noise level and transmitted symbols, is thus zero.

We will now show that the residual MSE at the output of the MMSE equalizer indeed tends to one when no zero-forcing equalizer exists. Consider column n of the right hand side in (5.50). We realize that in column n of $\mathcal{I}$, only element $2K\ell + n$ is non-zero. We define

$$g \stackrel{\triangle}{=} \text{column } 2K\ell + n \text{ in } \mathcal{B}_{K_2} = \text{column } n \text{ in } \mathcal{B}_{pres} \tag{5.105a}$$

$$\mathcal{G} \stackrel{\triangle}{=} \text{the remaining columns in } \mathcal{B}_{K_2}\;. \tag{5.105b}$$

Column n of (5.50) can then be written as

$$\mathcal{G}^T\theta_s = \mathbf{0} \tag{5.106a}$$

$$g^T\theta_s = 1\;, \tag{5.106b}$$

where θ_s is column n in

$$\begin{pmatrix} (\mathbf{S}^0_{K_1})^T \\ \vdots \\ (\mathbf{S}^{\delta s}_{K_1})^T \end{pmatrix}\;.$$

We also define

$$J_{MMSE} \stackrel{\triangle}{=} \text{element } n, n \text{ in } \mathbf{P}^{K_1}\;. \tag{5.107}$$

Since g is equal to column n in $\mathcal{B}_{pres}$, we can use Corollary 5.1 to express J_{MMSE} as

$$\begin{aligned} J_{MMSE} &= 1 - g^T\left(\mathcal{B}_{K_2}\mathcal{B}^T_{K_2} + \Psi\right)^{-1} g \\ &= 1 - g^T\left(\mathcal{G}\mathcal{G}^T + gg^T + \Psi\right)^{-1} g\;. \end{aligned} \tag{5.108}$$

To fulfill the zero-forcing condition, equations (5.106a) and (5.106b) must have a common solution θ_s. A situation where no such common solution exists may arise for the following two reasons:

1. The only solution to (5.106a) is $\theta_s = 0$. This happens when $\mathcal{G}$ has full rank, $\operatorname{rank} \mathcal{G} = 2(\delta s + 1)N_c$.
2. Every solution $\theta_s \neq 0$ to (5.106a) results in $g^T \theta_s = 0$. This happens when
$$g^T = w\mathcal{G}^T \tag{5.109}$$
for some vector w.

These two cases will be discussed next.

Case 1

We will now let the power of the MAI and ISI increase, that is, we will study the case
$$\mathcal{G} \triangleq \alpha \mathcal{G}_0, \quad \alpha \geq 1 \tag{5.110}$$
with $\mathcal{G}_0$ fixed. Insert (5.110) into (5.108):
$$\begin{aligned} J_{MMSE}(\alpha^2) &= 1 - g^T \left(\alpha^2 \mathcal{G}_0 \mathcal{G}_0^T + gg^T + \Psi\right)^{-1} g \\ &= 1 - \frac{1}{\alpha^2} g^T \left(\mathcal{G}_0 \mathcal{G}_0^T + \frac{gg^T}{\alpha^2} + \frac{\Psi}{\alpha^2}\right)^{-1} g \\ &= 1 - \frac{1}{\alpha^2} g^T \mathbf{X}^{-1}(\alpha^2) g \ , \end{aligned}$$
where we have defined
$$\mathbf{X}(\alpha^2) \triangleq (\mathcal{G}_0 \mathcal{G}_0^T + \frac{gg^T}{\alpha^2} + \frac{\Psi}{\alpha^2}) \ .$$
But
$$\lambda_{min}^{\mathbf{X}} \leq \frac{g^T \mathbf{X}^{-1}(\alpha^2) g}{g^T g} \leq \lambda_{max}^{\mathbf{X}}$$
where $\lambda_{min}^{\mathbf{X}}$ and $\lambda_{max}^{\mathbf{X}}$ are the smallest and largest eigenvalues of $\mathbf{X}^{-1}(\alpha^2)$, respectively. Thus
$$J_{MMSE}(\alpha^2) \geq 1 - \frac{\lambda_{max}^{\mathbf{X}} g^T g}{\alpha^2} \ .$$
Since the full rank matrix $\mathcal{G}_0$ has more columns than rows, $\mathcal{G}_0 \mathcal{G}_0^T$ has full rank. Every eigenvalue to $\mathbf{X}(\alpha^2)$ is then strictly positive, which implies that every eigenvalue of $\mathbf{X}^{-1}(\alpha^2)$ is limited for any α. Hence
$$\lim_{\alpha \to \infty} J_{MMSE} \geq 1 \ .$$

But $J_{MMSE} \leq 1$, which leads to the conclusion that

$$\lim_{\alpha \to \infty} J_{MMSE} = 1 \ .$$

When the MSE tends to one, the symbol estimate $\hat{d}_i(k-\ell|k)$ tends to zero. Referring to (5.103) and (5.104), we conclude that the near-far resistance of the MMSE detector is zero.

Case 2

In this case, the rank of the matrix $\mathcal{G}$ is less than $2N_c(\delta s + 1)$, and there exists a non-zero solution to equation (5.106a). We will once again examine the expression for the MSE (5.108). We will now introduce a factorization of the matrix $gg^T + \Psi$:

$$gg^T + \Psi \stackrel{\triangle}{=} \mathcal{L}\mathcal{L}^T \ .$$

Since Ψ has full rank, so has $\mathcal{L}$. We now insert this factorization into (5.108), and rearrange

$$\begin{aligned} J_{MMSE} &= 1 - g^T(\mathcal{G}\mathcal{G}^T + \mathcal{L}\mathcal{L}^T)^{-1}g \\ &= 1 - g^T\mathcal{L}^{-T}(\mathcal{L}^{-1}\mathcal{G}\mathcal{G}^T\mathcal{L}^{-T} + \mathbf{I})^{-1}\mathcal{L}^{-1}g \ . \end{aligned}$$

Again, we allow the power of all interfering signals to increase, that is, we insert (5.110) into the expression for J_{MMSE}:

$$\begin{aligned} J_{MMSE} &= 1 - g^T\mathcal{L}^{-T}(\mathcal{L}^{-1}\alpha^2\mathcal{G}_0\mathcal{G}_0^T\mathcal{L}^{-T} + \mathbf{I})^{-1}\mathcal{L}^{-1}g \\ &= 1 - g^T\mathcal{L}^{-T}\mathbf{Y}^{-1}(\alpha)\mathcal{L}^{-1}g \ , \end{aligned} \tag{5.111}$$

with

$$\mathbf{Y}(\alpha^2) \stackrel{\triangle}{=} \alpha^2\mathcal{L}^{-1}\mathcal{G}_0\mathcal{G}_0^T\mathcal{L}^{-T} + \mathbf{I} \ .$$

Note that g remains fixed, that is,

$$g^T = w_0\mathcal{G}_0^T \ . \tag{5.112}$$

To proceed, we make an eigenvalue decomposition of the matrix $\mathbf{Y}(\alpha^2)$. We realize that

$$\mathbf{Y}(\alpha^2) = \begin{pmatrix} E_1 & E_2 \end{pmatrix} \begin{pmatrix} \alpha^2\Lambda_r + \mathbf{I} & \mathbf{0} \\ \mathbf{0} & \mathbf{I} \end{pmatrix} \begin{pmatrix} E_1^T \\ E_2^T \end{pmatrix} \ , \tag{5.113}$$

where

$$\Lambda_r = \begin{pmatrix} \lambda_1 & & 0 \\ & \ddots & \\ 0 & & \lambda_r \end{pmatrix}$$

contains the r non-zero eigenvalues of the matrix $\mathcal{L}^{-1}\mathcal{G}_0\mathcal{G}_0^T\mathcal{L}^{-T}$. Equation (5.111) can then be expressed as

$$J_{MMSE} = 1 - g^T\mathcal{L}^{-T}\begin{pmatrix} E_1 & E_2 \end{pmatrix}\begin{pmatrix} (\alpha^2\Lambda_r + \mathbf{I})^{-1} & \mathbf{0} \\ \mathbf{0} & \mathbf{I} \end{pmatrix}\begin{pmatrix} E_1^T \\ E_2^T \end{pmatrix}\mathcal{L}^{-1}g \; .$$

But according to (5.112), $g^T = w_0\mathcal{G}_0^T$. Since E_1 forms a basis of eigenvectors of $\mathcal{L}^{-1}\mathcal{G}_0$, we must have

$$g^T\mathcal{L}^{-T} = \tilde{w}_0 E_1^T \tag{5.114}$$

for some row vector $\tilde{w}_0$. We thus obtain

$$J_{MMSE} = 1 - \tilde{w}_0 E_1^T\begin{pmatrix} E_1 & E_2 \end{pmatrix}\begin{pmatrix} (\alpha^2\Lambda_r + \mathbf{I})^{-1} & \mathbf{0} \\ \mathbf{0} & \mathbf{I} \end{pmatrix}\begin{pmatrix} E_1^T \\ E_2^T \end{pmatrix}E_1\tilde{w}_0^T \; . \tag{5.115}$$

We now use the orthonormality of the eigenvector basis: $E_1^TE_2 = 0$ and $E_1^TE_1 = \mathbf{I}$ to simplify (5.115):

$$J_{MMSE} = 1 - \tilde{w}_0(\alpha^2\Lambda_r + \mathbf{I})^{-1}\tilde{w}_0^T \; .$$

The matrix inverse can be evaluated to yield

$$J_{MMSE} = 1 - \tilde{w}_0\begin{pmatrix} \frac{1}{\alpha^2\lambda_1+1} & & 0 \\ & \ddots & \\ 0 & & \frac{1}{\alpha^2\lambda_r+1} \end{pmatrix}\tilde{w}_0^T \; . \tag{5.116}$$

Keeping in mind that the vector $\tilde{w}_0$ is independent of α, we now let α tend to infinity in (5.116) to obtain

$$\lim_{\alpha\to\infty} J_{MMSE} = 1 \; .$$

Again, this implies that

$$\lim_{\alpha\to\infty} \hat{d}(k-\ell|k) = 0 \; .$$

Finally, by using (5.104), we realize that the MMSE detector cannot be near-far resistant, which completes the proof of the necessity.

CHAPTER 6

Concluding remarks

THE heart of this thesis is the three DFE structures introduced in Chapter 3. The first DFE is a generalization of the non-realizable multivariable DFE presented by Duel-Hallen in [23], variants of which were presented in [11, 12, 28]. In contrast to these DFEs, the multivariable MMSE DFE presented in this thesis handles colored noise, and can be straightforwardly implemented in channels with any number of inputs and outputs.

The second multivariable DFE is a multivariable generalization of the realizable DFE in [79]. Both minimum mean-square error and zero-forcing solutions have been derived. The MMSE DFE has optimum structure, and its coefficients can be obtained from closed-form linear design equations. It is noteworthy that this DFE contains no matched filter.

The third DFE has multivariable transversal filters in both the feedforward and the feedback paths. Such a multivariable DFE was first suggested by Voois and Cioffi in [101] for the magnetic recording channel, and by Tidestav et al. in [88] for application in cellular systems with multiple receiver antennas. See also [85]. We have presented design equations for both the MMSE and the ZF criterion.

The performance of a minimum mean-square equalizer is superior to that of a zero-forcing equalizer. However, studies of zero-forcing solutions provide information about the performance of the corresponding MMSE solutions. A desirable property of any MMSE equalizer is that the residual estimation error at its output tends to zero when the noise variance tends to zero. In situations when no zero-forcing solution exists, *this will not happen.* The lack of a zero-forcing equalizer thus suggests that the problem is in some sense ill-posed. This intuition was formalized in Chapter 5, where it was shown that for a time-varying version of the

MMSE FIR DFE, near-far resistance can be guaranteed if and only if the DFE coefficients can be tuned so that the zero-forcing condition is fulfilled. This is true also for equalizers that use decision feedback from only a subset of the detected signals.

A numerical example in Chapter 3 indicates that the difference in performance between the three DFEs is rather small: The optimum non-realizable DFE performs only slightly better than an FIR DFE with appropriate smoothing lag and feedforward filter degree. The exact relative performance of the three structures of course depends on the scenario. Actually obtaining appropriate values of the design variables of the FIR DFE may be difficult, and improved rules of thumb for the selection of both smoothing lag and feedforward filter degree should be derived.

One property that is interesting is that the sensitivity to incorrect decisions is larger the longer the feedback filter is. Since the length of the feedback filter is linked to the length of the feedforward filter, a longer feedforward filter may not lead to better performance when the error propagation is taken into account. This conclusion is confirmed in the numerical example presented in Figure 3.4: With real decisions, the smallest MSE is not obtained for the largest feedforward filter degree.

Possible generalizations and extensions to the multivariable DFE include

- Decision feedback from present signals belonging to other users. This feature was implemented in the DFE in [23]. This feature would give small performance improvements when the number of DFE outputs is small, whereas the extent of the impulse response is large.

- Different smoothing lags for different users. With decision feedback, the interference from symbols already detected is in theory completely rejected. On the other hand, the impact of symbols that are not already detected are only partly suppressed. The deviation from complete suppression is conveyed in the first ℓ taps of the filter $\boldsymbol{L}_1(q^{-1})$. If one signal is detected using a smaller smoothing lag, additional coefficients in $\boldsymbol{L}_1(q^{-1})$ will be zero, leading to a smaller residual MSE and a lower error rate.

- Dependent symbols decisions. When the transmitted symbols corresponding to different channel inputs are correlated, the proposed DFE design is suboptimum. Not only must the filters be retuned to take into account the correlation among the transmitted signals: The decision device must also be redesigned.

In addition to these enhancements, extensions that are applicable to the scalar DFE are of course of interest also for the multivariable DFE. For instance, designs that are robust to incorrect decisions should be investigated.

All the designs are based on models of the channel and the noise that are assumed to be exactly known. When channels and models are estimated, these estimates are used in place of the true parameters. Of course, the estimates are prone to error, and better average performance may be obtained if the parameter uncertainty is taken into account already in the design.

Developing methods that improve the quality of the parameter estimates is also very important. In particular, this is true for the unstructured multivariable noise model introduced in Subsection 2.3.2. One alternative is to approximate the multivariable noise process by an autoregressive model, even though the noise may be more adequately described by a moving average model. This approach was investigated in [9] and [51]. With such a model, the optimum DFE structure has transversal filters in both feedforward and feedback links, which leads to a lower sensitivity to error propagation.

The study of the decision feedback equalizer was motivated by its low complexity as compared to the MLSE and its high performance relative to a linear equalizer. In this thesis, no explicit comparisons has been made with the MLSE, and such a comparison should be made in the future. Deriving guidelines for when a DFE or a linear equalizer should be preferred as a tool for multiuser detection is also an important topic for future research. Regarding the linear equalizer, simulation results in Chapters 4 and 5 indicate that the difference in performance is small when the number of transmitters is small relative to the number of measurement sensors. The difference in complexity between the MIMO linear equalizers and DFEs is also small.

Chapters 4 and 5 are applications of the DFE to two specific scenarios. In Chapter 4, the multivariable DFE is applied to the outputs of an antenna array to accomplish reuse within cell. In addition, interference rejection and multiuser detection is compared. The results confirm that reuse within cell is indeed possible, and indicate in what situations multiuser detection provides better performance than interference rejection. Some issues remain to be addressed however. The two most important are

- What is the impact on the capacity of the cellular system as a whole? How is the frequency plan affected?
- How large is the cost for additional hardware? In particular, the proposed approach assumes there are several receivers at the mobile terminal. Is this technically and economically feasible?

In Chapter 5, the multivariable DFE was applied to a DS-CDMA system. As a basis, we used a possibly time-varying linear filter model. By using this explicit model, it becomes possible to design a detector that can handle long codes, multi-

path propagation and synchronization in a systematic way. The linear model can also be used to investigate under what conditions an MMSE detector is near-far resistant. Near-far resistance is in fact guaranteed if and only if a zero-forcing solution to the equalization problem can be obtained. As in Chapter 4, the impact on the system performance of the proposed detector is not addressed. In fact, one of the simulations indicates that the benefits of using a multiuser detector may not be as large as is usually claimed in the literature on multiuser detection.

Summing up, the multivariable DFE is a versatile tool for multiuser detection. It can be used to detect digital signals, which have been distorted by any linear dispersive multivariable channel. However, the difference in performance between the multivariable DFE and the multivariable linear equalizer seems to be smaller than expected. When compared to the MLSE, the performance difference remains to be investigated whereas the difference in complexity is even larger than in the single-user case.

APPENDIX A

Proof of Theorem 3.1

We will now derive the design equations (3.4a), (3.4b) and (3.4c). We will also show that a bank of matched filters can constitute a part of the MSE optimum MIMO DFE if we allow the smoothing lag ℓ to tend to infinity. For this purpose, we insert (3.1) into the expression (2.5) for the estimation error. To simplify the notation, we will omit the polynomial arguments throughout this appendix.

Assuming correct past decisions, that is, $\tilde{d}(m) = d(m)$ for $m \leq k-1$, and using the expression for the estimator (3.1) and the channel model (2.6) the estimation error can be expressed as

$$\begin{aligned}\varepsilon(k) &= d(k) - \hat{d}^{\infty}(k) \\ &= (\mathbf{I} - \boldsymbol{\mathcal{R}}^{\infty}\boldsymbol{A}^{-1}\boldsymbol{B} + q^{-1}\boldsymbol{\mathcal{F}}^{\infty})d(k) - \boldsymbol{\mathcal{R}}^{\infty}\boldsymbol{N}^{-1}\boldsymbol{M}v(k)\ . \end{aligned} \tag{A.1}$$

For this proof and the proof in Appendix B, we will use the *variational approach* first developed in [3] for scalar problems and extended to the multivariable case in [4].

We begin by introducing the alternate estimate $\hat{d}_a^{\infty}(k)$

$$\hat{d}_a^{\infty}(k) \stackrel{\triangle}{=} \hat{d}^{\infty}(k) + n(k)\ .$$

The variation $n(k)$ is based on all signals the estimate $\hat{d}^{\infty}(k)$ may be based upon:

$$n(k) \stackrel{\triangle}{=} n_1(k) + n_2(k)$$

with

$$n_1(k) \stackrel{\triangle}{=} \boldsymbol{\mathcal{G}}_1^{\infty}y(k) \tag{A.2a}$$

$$n_2(k) \stackrel{\triangle}{=} \boldsymbol{\mathcal{G}}_2^{\infty}d(k-1)\ . \tag{A.2b}$$

Above, $\boldsymbol{\mathcal{G}}_1^\infty$ is an arbitrary stable linear operator whereas $\boldsymbol{\mathcal{G}}_2^\infty$ is an arbitrary stable and causal linear operator. If the estimation error obtained with (3.1) is orthogonal to any admissible variation (A.2a), (A.2b), that is, if

$$E\varepsilon(k)n_1^H(k) = 0 \tag{A.3a}$$

$$E\varepsilon(k)n_2^H(k) = 0 \tag{A.3b}$$

then $\hat{d}_a^\infty(k) = \hat{d}^\infty(k)$ or equivalently $n(k) \equiv 0$ minimizes the MSE (2.4). We must thus assure that (A.3a) and (A.3b) are fulfilled.

To evaluate the cross-correlations (A.3a) and (A.3b), we will use Parseval's relation for complex signals [66] and evaluate the expressions in the frequency domain. The procedure is outlined below.

Consider two complex-valued stochastic processes $x(k) = \boldsymbol{\mathcal{T}}_1(q^{-1})e(k)$ and $w(k) = \boldsymbol{\mathcal{T}}_2(q^{-1})e(k)$, where $\boldsymbol{\mathcal{T}}_1(q^{-1})$ and $\boldsymbol{\mathcal{T}}_2(q^{-1})$ are two stable and causal rational matrices. We can then express the cross-correlation between $x(k)$ and $w(k)$ as [3, 66]

$$Ex(k)w^H(k) = \frac{\lambda_e}{2\pi j}\oint_{|z|=1} \boldsymbol{\mathcal{T}}_1(z^{-1})\left(\boldsymbol{\mathcal{T}}_2\left(\frac{1}{z^{-*}}\right)\right)^H \frac{dz}{z}\,.$$

where $\lambda_e\mathbf{I} = Ee(k)e^H(k)$. By using its Markov parameters, the second factor in the integrand can be simplified to:

$$\left(\boldsymbol{\mathcal{T}}_2\left(\frac{1}{z^{-*}}\right)\right)^H = \left(\sum_{n=0}^{\infty}\mathbf{T}_{2n}\left(\frac{1}{z^{-*}}\right)^n\right)^H = \sum_{n=0}^{\infty}\mathbf{T}_{2n}^H z^n = \boldsymbol{\mathcal{T}}_{2*}(z)\,.$$

The cross-correlation can thus be expressed as

$$Ex(k)w^H(k) = \frac{\lambda_e}{2\pi j}\oint_{|z|=1} \boldsymbol{\mathcal{T}}_1(z^{-1})\boldsymbol{\mathcal{T}}_{2*}(z)\frac{dz}{z}\,.$$

We now insert (A.1) and (A.2a) into (A.3a) and use Parseval's relation to obtain

$$E\varepsilon(k)n_1^H(k) = \frac{\lambda_d}{2\pi j}\oint\big\{(\mathbf{I} - \boldsymbol{\mathcal{R}}^\infty\boldsymbol{A}^{-1}\boldsymbol{B} + z^{-1}\boldsymbol{\mathcal{F}}^\infty)\boldsymbol{B}_*\boldsymbol{A}_*^{-1} - \lambda_e\boldsymbol{\mathcal{R}}^\infty\boldsymbol{N}^{-1}\boldsymbol{M}\boldsymbol{M}_*\boldsymbol{N}_*^{-1}\big\}\,\boldsymbol{\mathcal{G}}_{1*}^\infty\frac{dz}{z}\,. \tag{A.4}$$

Since $\boldsymbol{A}$ and $\boldsymbol{N}$ are both diagonal, we can express (A.4) as

$$E\varepsilon(k)n_1^H(k) = \frac{\lambda_d}{2\pi j}\oint\big\{(\mathbf{I} - \boldsymbol{\mathcal{R}}^\infty\boldsymbol{A}^{-1}\boldsymbol{B} + z^{-1}\boldsymbol{\mathcal{F}}^\infty)\boldsymbol{B}_*\boldsymbol{N}_* - \lambda_e\boldsymbol{\mathcal{R}}^\infty\boldsymbol{N}^{-1}\boldsymbol{M}\boldsymbol{M}_*\boldsymbol{A}_*\big\}\,\boldsymbol{A}_*^{-1}\boldsymbol{N}_*^{-1}\boldsymbol{\mathcal{G}}_{1*}^\infty\frac{dz}{z}\,. \tag{A.5}$$

To find the conditions under which the integral (A.5) vanishes, we need the following lemma:

Lemma A.1 *The integral*

$$V_1 \stackrel{\triangle}{=} \oint_{|z|=1} \boldsymbol{\mathcal{H}}(z, z^{-1}) \boldsymbol{\mathcal{G}}_*(z) \frac{dz}{z} \tag{A.6}$$

is zero for all stable and causal $\boldsymbol{\mathcal{G}}(z^{-1})$ *if and only if*

$$z^{-1}\boldsymbol{\mathcal{H}}(z, z^{-1}) \text{ is analytic within } |z| = 1.$$

The integral

$$V_2 \stackrel{\triangle}{=} \oint_{|z|=1} \boldsymbol{\mathcal{H}}(z, z^{-1}) \boldsymbol{\mathcal{G}}_*(z^{-1}, z) \frac{dz}{z} \tag{A.7}$$

is zero for all stable $\boldsymbol{\mathcal{G}}(z, z^{-1})$ *if and only if*

$$\boldsymbol{\mathcal{H}}(z, z^{-1}) \equiv 0 \, .$$

Proof: Since V_1 should be zero for all stable and causal $\boldsymbol{\mathcal{G}}(z^{-1})$, it should be zero in particular for

$$\boldsymbol{\mathcal{G}}(z^{-1}) = \text{diag} \big(\underbrace{0 \quad \dots \quad 0}_{j-1} \quad z^{-m} \quad 0 \quad \dots \quad 0 \big) \quad , \tag{A.8}$$

where $m = 0, 1, \dots,$. If we insert (A.8) into (A.6), we obtain the condition

$$\oint_{|z|=1} z^{-1} \mathcal{H}_{ij}(z, z^{-1}) z^{m+1} \frac{dz}{z} = 0$$

for element (i, j) in V_1. If this is true for $m = 0, 1, 2, \dots$, then

$$z^{-1}\mathcal{H}_{ij}(z, z^{-1})$$

is analytic within the unit circle, according to Lemma 1 in [108]. Since i and j are arbitrary, we conclude that $z^{-1}\boldsymbol{\mathcal{H}}(z, z^{-1})$ must be analytic inside $|z| = 1$. This proves necessity. Sufficiency follows from the residue theorem.

We now turn our attention to V_2. From the first part of the lemma, we know that V_2 is zero only if $z^{-1}\boldsymbol{\mathcal{H}}(z, z^{-1})$ is analytic inside $|z| = 1$. We now use the residue theorem to evaluate V_2:

$$V_2 = 2\pi j \sum_{k=1}^{N} \operatorname*{Res}_{z=a_k} z^{-1} \boldsymbol{\mathcal{H}}(z, z^{-1}) \boldsymbol{\mathcal{G}}_*(z^{-1}, z) \, , \tag{A.9}$$

where $a_k,\ k = 1, \ldots, N$ are the poles inside the unit circle. Since $\boldsymbol{\mathcal{G}}(z, z^{-1})$ is stable, the only poles of $\boldsymbol{\mathcal{G}}_*(z^{-1}, z)$ that lie inside $|z| = 1$ are those at $z = 0$. Equation (A.9) can thus be rewritten

$$V_2 = 2\pi j \operatorname*{Res}_{z=0} z^{-1}\boldsymbol{\mathcal{H}}(z, z^{-1})\boldsymbol{\mathcal{G}}_*(z^{-1}, z) \ . \tag{A.10}$$

Since $z^{-1}\boldsymbol{\mathcal{H}}(z, z^{-1})$ is analytic at $z = 0$, we can write

$$z^{-1}\boldsymbol{\mathcal{H}}(z, z^{-1}) = \sum_{k=m}^{\infty} \mathbf{H}_k z^k \ ,$$

where $m \geq 0$ is the smallest integer such that $\mathbf{H}_m \neq 0$. We can now evaluate (A.10) for $\boldsymbol{\mathcal{G}}_*(z^{-1}, z) = z^{-m-1}\mathbf{I}$:

$$V_2 = 2\pi j \mathbf{H}_m \ .$$

Since $\mathbf{H}_m \neq 0$, the integral does not vanish. We thus realize that V_2 can be zero for all stable $\boldsymbol{\mathcal{G}}(z, z^{-1})$ only when $\mathbf{H}_k = 0\ \forall\, k$, or equivalently when

$$\boldsymbol{\mathcal{H}}(z, z^{-1}) \equiv 0 \ .$$

This proves necessity. Sufficiency is trivial. ■

Since $\boldsymbol{\mathcal{G}}_1^{\infty}$ is allowed to be non-causal and since $\boldsymbol{A}_*^{-1}$ and $\boldsymbol{N}_*^{-1}$ are obviously non-zero, according to Lemma A.1, the only way to ensure that (A.5) vanishes is to require that

$$(\mathbf{I} - \boldsymbol{\mathcal{R}}^{\infty}\boldsymbol{A}^{-1}\boldsymbol{B} + z^{-1}\boldsymbol{\mathcal{F}}^{\infty})\boldsymbol{B}_*\boldsymbol{N}_* - \lambda_e \boldsymbol{\mathcal{R}}^{\infty}\boldsymbol{N}^{-1}\boldsymbol{M}\boldsymbol{M}_*\boldsymbol{A}_* = 0 \ . \tag{A.11}$$

Proceeding in the same way with (A.3b) gives

$$E\varepsilon(k)n_2^H(k) = \frac{\lambda_d}{2\pi j}\oint \left(\mathbf{I} - \boldsymbol{\mathcal{R}}^{\infty}\boldsymbol{A}^{-1}\boldsymbol{B} + z^{-1}\boldsymbol{\mathcal{F}}^{\infty}\right) z\boldsymbol{\mathcal{G}}_{2*}^{\infty}\frac{dz}{z} \ . \tag{A.12}$$

According to Lemma A.1, the integral vanishes if and only if

$$\mathbf{I} - \boldsymbol{\mathcal{R}}^{\infty}\boldsymbol{A}^{-1}\boldsymbol{B} + z^{-1}\boldsymbol{\mathcal{F}}^{\infty} = \boldsymbol{\mathcal{L}}_{1*} \ . \tag{A.13}$$

for some stable and rational matrix $\boldsymbol{\mathcal{L}}_1$. Insert (A.13) into (A.11):

$$\boldsymbol{\mathcal{L}}_{1*}\boldsymbol{B}_*\boldsymbol{N}_* - \lambda_e \boldsymbol{\mathcal{R}}^{\infty}\boldsymbol{N}^{-1}\boldsymbol{M}\boldsymbol{M}_*\boldsymbol{A}_* = 0 \ .$$

We can now express the feedforward filter as

$$\boldsymbol{\mathcal{R}}^{\infty} = \frac{1}{\lambda_e}\boldsymbol{\mathcal{L}}_{1*}\boldsymbol{B}_*\boldsymbol{N}_*\boldsymbol{A}_*^{-1}\boldsymbol{M}_*^{-1}\boldsymbol{M}^{-1}\boldsymbol{N} \ .$$

If we use the definitions (3.2a) and (3.2b), we obtain

$$\boldsymbol{\mathcal{R}}^{\infty} = \frac{1}{\lambda_e}\boldsymbol{\mathcal{L}}_{1*}\boldsymbol{\tau}_*\boldsymbol{\Gamma}_*^{-1}\boldsymbol{M}^{-1}\boldsymbol{N} \; . \tag{A.14}$$

We now insert (A.14) into (A.13) and rearrange:

$$\begin{aligned}\mathbf{I} + z^{-1}\boldsymbol{\mathcal{F}}^{\infty} &= \boldsymbol{\mathcal{L}}_{1*}\left(\mathbf{I} + \frac{1}{\lambda_e}\boldsymbol{\tau}_*\boldsymbol{\Gamma}_*^{-1}\boldsymbol{\Gamma}^{-1}\boldsymbol{\tau}\right) = \boldsymbol{\mathcal{L}}_{1*}\left(\mathbf{I} + \frac{1}{\lambda_e}\tilde{\boldsymbol{\Gamma}}_*^{-1}\tilde{\boldsymbol{\tau}}_*\tilde{\boldsymbol{\tau}}\tilde{\boldsymbol{\Gamma}}^{-1}\right) \\ &= \boldsymbol{\mathcal{L}}_{1*}\tilde{\boldsymbol{\Gamma}}_*^{-1}\left(\tilde{\boldsymbol{\Gamma}}_*\tilde{\boldsymbol{\Gamma}} + \frac{1}{\lambda_e}\tilde{\boldsymbol{\tau}}_*\tilde{\boldsymbol{\tau}}\right)\tilde{\boldsymbol{\Gamma}}^{-1} = \boldsymbol{\mathcal{L}}_{1*}\tilde{\boldsymbol{\Gamma}}_*^{-1}\boldsymbol{\beta}_*\mathbf{W}\boldsymbol{\beta}\tilde{\boldsymbol{\Gamma}}^{-1}\end{aligned}$$

where we in the second equality used (3.3) and in the last equality the spectral factorization (3.5). We now collect polynomial matrices in z^{-1} on the left hand side and polynomial matrices in z on the right hand side:

$$(\mathbf{I} + z^{-1}\boldsymbol{\mathcal{F}}^{\infty})\tilde{\boldsymbol{\Gamma}}\boldsymbol{\beta}^{-1} = \boldsymbol{\mathcal{L}}_{1*}\tilde{\boldsymbol{\Gamma}}_*^{-1}\boldsymbol{\beta}_*\mathbf{W} \; . \tag{A.15}$$

The left hand side contains only powers of z^{-1} and the right hand side contains only powers of z. The only way for this equality to hold is to require that both sides equal a constant matrix. Since $\boldsymbol{\beta}$ is monic, we see that the constant term of the left hand side equals $\tilde{\boldsymbol{\Gamma}}_0$, the constant term of $\tilde{\boldsymbol{\Gamma}}$. We must thus require

$$\begin{aligned}(\mathbf{I} + z^{-1}\boldsymbol{\mathcal{F}}^{\infty})\tilde{\boldsymbol{\Gamma}}\boldsymbol{\beta}^{-1} &= \tilde{\boldsymbol{\Gamma}}_0 \\ \boldsymbol{\mathcal{L}}_{1*}\tilde{\boldsymbol{\Gamma}}_*^{-1}\boldsymbol{\beta}_*\mathbf{W} &= \tilde{\boldsymbol{\Gamma}}_0 \; ,\end{aligned}$$

or, equivalently

$$\boldsymbol{\mathcal{L}}_{1*} = \tilde{\boldsymbol{\Gamma}}_0\mathbf{W}^{-1}\boldsymbol{\beta}_*^{-1}\tilde{\boldsymbol{\Gamma}}_* \tag{A.16}$$

$$\boldsymbol{\mathcal{F}}^{\infty} = z(\tilde{\boldsymbol{\Gamma}}_0\boldsymbol{\beta}\tilde{\boldsymbol{\Gamma}}^{-1} - \mathbf{I}) \; . \tag{A.17}$$

We can now insert (A.16) into (A.14) to arrive at our final expression for the asymptotic DFE filters:

$$\boldsymbol{\mathcal{R}}^{\infty} = \frac{1}{\lambda_e}\tilde{\boldsymbol{\Gamma}}_0\mathbf{W}^{-1}\boldsymbol{\beta}_*^{-1}\tilde{\boldsymbol{\Gamma}}_*\boldsymbol{\tau}_*\boldsymbol{\Gamma}_*^{-1}\boldsymbol{M}^{-1}\boldsymbol{N} \tag{A.18a}$$

$$= \frac{1}{\lambda_e}\tilde{\boldsymbol{\Gamma}}_0\mathbf{W}^{-1}\boldsymbol{\beta}_*^{-1}\tilde{\boldsymbol{\tau}}_*\boldsymbol{M}^{-1}\boldsymbol{N} \tag{A.18b}$$

$$\boldsymbol{\mathcal{F}}^{\infty} = z(\tilde{\boldsymbol{\Gamma}}_0\boldsymbol{\beta}\tilde{\boldsymbol{\Gamma}}^{-1} - \mathbf{I}) \; . \tag{A.18c}$$

If we replace z and z^{-1} with q and q^{-1} respectively, equation (A.18a) coincides with (3.4a), equation (A.18b) coincides with (3.4b) and equation (A.18c) coincides with (3.4c).

APPENDIX B
Proof of Theorem 3.2

Consider the channel described by (2.6), and the general multivariable decision feedback equalizer (2.2). Insert the expression for the symbol estimate $\hat{d}(k-\ell|k)$ into the expression (2.5) for the estimation error:

$$\varepsilon(k-\ell) = d(k-\ell) - \hat{d}(k-\ell|k) \tag{B.1}$$

$$= d(k-\ell) - \boldsymbol{\mathcal{R}} y(k) + \boldsymbol{\mathcal{F}} \tilde{d}(k-\ell-1) \; . \tag{B.2}$$

Throughout this appendix we will omit the polynomial arguments to simplify the notation.

Assume correct past decisions, that is,

$$\tilde{d}(m) = d(m) \quad m \leq k-\ell-1 \; . \tag{B.3}$$

Insert $\tilde{d}(k-\ell-1)$ from (B.3) and $y(k)$ from (2.6) into (B.2) and rearrange:

$$\begin{aligned}\varepsilon(k-\ell) &= d(k-\ell) - \boldsymbol{\mathcal{R}}(\boldsymbol{A}^{-1}\boldsymbol{B}d(k) + \boldsymbol{N}^{-1}\boldsymbol{M}v(k)) + \boldsymbol{\mathcal{F}}d(k-\ell-1) \\ &= (q^{-\ell}\mathbf{I} - \boldsymbol{\mathcal{R}}\boldsymbol{A}^{-1}\boldsymbol{B} + q^{-\ell-1}\boldsymbol{\mathcal{F}})d(k) - \boldsymbol{\mathcal{R}}\boldsymbol{N}^{-1}\boldsymbol{M}v(k) \; . \end{aligned} \tag{B.4}$$

Introduce the alternative estimate $\hat{d}_a(k-\ell|k) \stackrel{\triangle}{=} \hat{d}(k-\ell|k) + n(k)$, where the variation $n(k)$ is a linear function of all signals that the estimate $\hat{d}(k-\ell|k)$ may be based upon. Thus,

$$n(k) \stackrel{\triangle}{=} n_1(k) + n_2(k)$$

where

$$n_1(k) \stackrel{\triangle}{=} \boldsymbol{\mathcal{G}}_1 y(k) \tag{B.5a}$$

$$n_2(k) \stackrel{\triangle}{=} \boldsymbol{\mathcal{G}}_2 d(k-\ell-1) \; . \tag{B.5b}$$

Above, $\boldsymbol{\mathcal{G}}_1$ and $\boldsymbol{\mathcal{G}}_2$ are arbitrary stable and causal rational matrices. If the estimation error obtained with (2.2) is orthogonal to any admissible variation described by (B.5a) and (B.5b), that is, if

$$E\varepsilon(k-\ell)n_1^H(k) = 0 \tag{B.6a}$$

$$E\varepsilon(k-\ell)n_2^H(k) = 0 \tag{B.6b}$$

then $\hat{d}_a(k-\ell|k) = \hat{d}(k-\ell|k)$ or equivalently $n(k) \equiv 0$ minimizes the estimation error covariance matrix (2.4): For any estimation error covariance matrix $\tilde{\mathbf{P}}$ obtained with $n(k) \neq 0$, $\tilde{\mathbf{P}} - \mathbf{P}$ will be positive definite. We must thus assure that (B.6a) and (B.6b) are fulfilled.

To compute the cross-correlations (B.6a) and (B.6b), we use Parseval's relation. Proceeding as in Appendix A, we thus insert (B.4) and (B.5a) into (B.6a) and use Parseval's relation to rewrite the result as

$$E\varepsilon(k-\ell)n_1^H(k) = \frac{1}{2\pi j}\oint \Big\{(z^{-\ell}\mathbf{I} - \boldsymbol{\mathcal{R}}\boldsymbol{A}^{-1}\boldsymbol{B} + z^{-\ell-1}\boldsymbol{\mathcal{F}})\boldsymbol{B}_*\boldsymbol{A}_*^{-1} - \lambda_e\boldsymbol{\mathcal{R}}\boldsymbol{N}^{-1}\boldsymbol{M}\boldsymbol{M}_*\boldsymbol{N}_*^{-1}\Big\}\boldsymbol{\mathcal{G}}_{1*}\frac{dz}{z}\,. \tag{B.7}$$

Since $\boldsymbol{A}$ and $\boldsymbol{N}$ are both diagonal, we can express (B.7) as

$$E\varepsilon(k-\ell)n_1^H(k) = \frac{1}{2\pi j}\oint \Big\{(z^{-\ell}\mathbf{I} - \boldsymbol{\mathcal{R}}\boldsymbol{A}^{-1}\boldsymbol{B} + z^{-\ell-1}\boldsymbol{\mathcal{F}})\boldsymbol{B}_*\boldsymbol{N}_* - \lambda_e\boldsymbol{\mathcal{R}}\boldsymbol{N}^{-1}\boldsymbol{M}\boldsymbol{M}_*\boldsymbol{A}_*\Big\}\boldsymbol{A}_*^{-1}\boldsymbol{N}_*^{-1}\boldsymbol{\mathcal{G}}_{1*}\frac{dz}{z}\,. \tag{B.8}$$

From Lemma A.1, we know that $E\varepsilon(k-\ell)n_1^H(k) = 0$ if and only if

$$\frac{1}{z}\Big\{(z^{-\ell}\mathbf{I} - \boldsymbol{\mathcal{R}}\boldsymbol{A}^{-1}\boldsymbol{B} + z^{-\ell-1}\boldsymbol{\mathcal{F}})\boldsymbol{B}_*\boldsymbol{N}_* - \lambda_e\boldsymbol{\mathcal{R}}\boldsymbol{N}^{-1}\boldsymbol{M}\boldsymbol{M}_*\boldsymbol{A}_*\Big\}\boldsymbol{A}_*^{-1}\boldsymbol{N}_*^{-1}$$

is analytic inside $|z| = 1$. According to the assumption (2.7), the filters $\boldsymbol{A}^{-1}$ and $\boldsymbol{N}^{-1}$ are stable. This implies that $\boldsymbol{A}_*^{-1}$ and $\boldsymbol{N}_*^{-1}$ are analytic inside the unit circle. Thus, $E\varepsilon(k-\ell)n_1^H(k) = 0$ if and only if

$$(z^{-\ell}\mathbf{I} - \boldsymbol{\mathcal{R}}\boldsymbol{A}^{-1}\boldsymbol{B} + z^{-\ell-1}\boldsymbol{\mathcal{F}})\boldsymbol{B}_*\boldsymbol{N}_* - \lambda_e\boldsymbol{\mathcal{R}}\boldsymbol{N}^{-1}\boldsymbol{M}\boldsymbol{M}_*\boldsymbol{A}_* = z\boldsymbol{\mathcal{L}}_{2*} \tag{B.9}$$

for some rational matrix $\boldsymbol{\mathcal{L}}_{2*}$ with all its poles *outside* the unit circle. Proceeding in the same way with (B.6b) results in a second condition

$$z^{-\ell}\mathbf{I} - \boldsymbol{\mathcal{R}}\boldsymbol{A}^{-1}\boldsymbol{B} + z^{-\ell-1}\boldsymbol{\mathcal{F}} = z^{-\ell}\boldsymbol{\mathcal{L}}_{1*} \tag{B.10}$$

for some rational matrix $\boldsymbol{\mathcal{L}}_{1*}$ with all its poles *outside* the unit circle. However, none of the terms on the left hand side of (B.10) can have poles outside the unit circle. Therefore, we conclude that $\boldsymbol{\mathcal{L}}_{1*}$ must be a polynomial matrix. Thus,

$$z^{-\ell}\mathbf{I} - \boldsymbol{\mathcal{R}}\boldsymbol{A}^{-1}\boldsymbol{B} + z^{-\ell-1}\boldsymbol{\mathcal{F}} = z^{-\ell}\boldsymbol{L}_{1*} \tag{B.11}$$

for some polynomial matrix $\boldsymbol{L}_{1*}$. We can now insert (B.11) into (B.9) to obtain

$$z^{-\ell}\boldsymbol{L}_{1*}\boldsymbol{B}_*\boldsymbol{N}_* - \lambda_e\boldsymbol{\mathcal{R}}\boldsymbol{N}^{-1}\boldsymbol{M}\boldsymbol{M}_*\boldsymbol{A}_* = z\boldsymbol{\mathcal{L}}_{2*}\ . \tag{B.12}$$

We realize that neither of the terms on the left hand side of (B.12) can have any poles outside the unit circle. Therefore, $\boldsymbol{\mathcal{L}}_{2*}$ cannot have any such poles either, and we conclude that $\boldsymbol{\mathcal{L}}_{2*}$ must be a polynomial, rather than a rational, matrix. Hence we can express equation (B.12) as

$$z^{-\ell}\boldsymbol{L}_{1*}\boldsymbol{B}_*\boldsymbol{N}_* - \lambda_e\boldsymbol{\mathcal{R}}\boldsymbol{N}^{-1}\boldsymbol{M}\boldsymbol{M}_*\boldsymbol{A}_* = z\boldsymbol{L}_{2*} \tag{B.13}$$

for some polynomial matrix $\boldsymbol{L}_{2*}$. In the integrand (B.13), the poles contributed by $\boldsymbol{N}^{-1}$ must be canceled by a corresponding factor in $\boldsymbol{\mathcal{R}}$. Also, the polynomial matrix $\boldsymbol{M}$ contributes poles in the origin, which must be canceled by a corresponding factor in $\boldsymbol{\mathcal{R}}$. We therefore insert

$$\boldsymbol{\mathcal{R}} = \boldsymbol{S}\boldsymbol{M}^{-1}\boldsymbol{N}$$

where $\boldsymbol{S}$ is an arbitrary polynomial matrix, into (B.11) and (B.13) and rearrange:

$$\begin{aligned} \mathbf{I} - z^{\ell}\boldsymbol{S}\boldsymbol{M}^{-1}\boldsymbol{N}\boldsymbol{A}^{-1}\boldsymbol{B} + z^{-1}\boldsymbol{\mathcal{F}} &= \boldsymbol{L}_{1*} \\ z^{-\ell}\boldsymbol{L}_{1*}\boldsymbol{B}_*\boldsymbol{N}_* - \lambda_e\boldsymbol{S}\boldsymbol{M}_*\boldsymbol{A}_* &= z\boldsymbol{L}_{2*}\ . \end{aligned} \tag{B.14}$$

We now use that $\boldsymbol{A}^{-1}$ and $\boldsymbol{N}$ are diagonal and hence commute. We also insert (3.2a) and (3.2b) into (B.14):

$$\mathbf{I} - z^{\ell}\boldsymbol{S}\boldsymbol{\Gamma}^{-1}\boldsymbol{\tau} + z^{-1}\boldsymbol{\mathcal{F}} = \boldsymbol{L}_{1*} \tag{B.15a}$$

$$z^{-\ell}\boldsymbol{L}_{1*}\boldsymbol{\tau}_* - \lambda_e\boldsymbol{S}\boldsymbol{\Gamma}_* = z\boldsymbol{L}_{2*}\ . \tag{B.15b}$$

Equation (B.15a) can be further simplified by using the identity (3.3) and multiplying with $\tilde{\boldsymbol{\Gamma}}(q^{-1})$ from the right:

$$\tilde{\boldsymbol{\Gamma}} - z^{\ell}\boldsymbol{S}\tilde{\boldsymbol{\tau}} + z^{-1}\boldsymbol{\mathcal{F}}\tilde{\boldsymbol{\Gamma}} = \boldsymbol{L}_{1*}\tilde{\boldsymbol{\Gamma}} \tag{B.16a}$$

$$z^{-\ell}\boldsymbol{L}_{1*}\boldsymbol{\tau}_* - \lambda_e\boldsymbol{S}\boldsymbol{\Gamma}_* = z\boldsymbol{L}_{2*}\ . \tag{B.16b}$$

Since $\boldsymbol{\mathcal{F}}$ is the only remaining rational matrix in (B.16a), its poles must be canceled by a corresponding factor in $\tilde{\boldsymbol{\Gamma}}$. We thus conclude that

$$\boldsymbol{\mathcal{F}} = \boldsymbol{Q}\tilde{\boldsymbol{\Gamma}}^{-1}$$

where $\boldsymbol{Q}$ is an undetermined polynomial matrix. Note that $\boldsymbol{Q}$ and $\tilde{\boldsymbol{\Gamma}}$ may have common factors. We can now insert this expression into (B.16a) to yield

$$\tilde{\boldsymbol{\Gamma}} - z^{\ell}\boldsymbol{S}\tilde{\boldsymbol{\tau}} + z^{-1}\boldsymbol{Q} = \boldsymbol{L}_{1*}\tilde{\boldsymbol{\Gamma}} \tag{B.17a}$$

$$z^{-\ell}\boldsymbol{L}_{1*}\boldsymbol{\tau}_{*} - \lambda_e \boldsymbol{S}\boldsymbol{\Gamma}_{*} = z\boldsymbol{L}_{2*}\,. \tag{B.17b}$$

If we exchange z for q, equation (B.17a) coincides with (3.8a), whereas (B.17b) coincides with (3.8b).

The Diophantine equations (B.17a) and (B.17b) are *double sided*, that is they contain powers of both z^{-1} and z. Thus, both the powers of z^{-1} and z on the left hand side must match the corresponding powers on the right hand side. For this purpose, we list the degrees in z^{-1} and z for each term in (B.17a) and (B.17b):

Equation (B.17a):

$$z^{-1}: \quad \delta\tilde{\Gamma},\ \delta S + \delta\tilde{\tau} - \ell,\ \delta Q + 1,\ \delta\tilde{\Gamma} \tag{B.18a}$$

$$z: \quad 0,\ \ell,\ 0,\ \delta L_1\,. \tag{B.18b}$$

Equation (B.17b):

$$z^{-1}: \quad \ell,\ \delta S,\ 0 \tag{B.18c}$$

$$z: \quad \delta L_1 + \delta\tau - \ell,\ \delta\Gamma,\ \delta L_2 + 1\,. \tag{B.18d}$$

From (B.18b) and (B.18c) we immediately obtain the conditions for the degrees of $\boldsymbol{L}_1$ and $\boldsymbol{S}$ respectively:

$$\delta L_1 = \ell; \quad \delta S = \ell\,.$$

If we insert $\delta S = \ell$ into (B.18a), we obtain (3.9b). Finally, by inserting $\delta L_1 = \ell$ into (B.18d), we obtain (3.9d).

It remains to show that equations (B.17a) and (B.17b) have a solution with the degrees specified by (3.9a)–(3.9d). For this purpose, we rewrite (B.17a) and (B.17b) as two systems of linear equations. Two matrix polynomials are identical if and only if all the corresponding coefficient matrices are identical. We must thus adjust the coefficients of $\boldsymbol{S}$, $\boldsymbol{Q}$, $\boldsymbol{L}_1$ and $\boldsymbol{L}_2$ so that the expressions for the matrix coefficients for each power of z and z^{-1} are equal on the left and right hand side

of (B.17a) and (B.17b). We thus evaluate the expressions for the matrix coefficients, conjugate, transpose and equate the left and right hand sides. For (B.17a) we obtain

$$\begin{pmatrix} \tilde{\boldsymbol{\tau}}_0^H & & 0 & \tilde{\boldsymbol{\Gamma}}_0^H & & 0 \\ \vdots & \ddots & & \vdots & \ddots & \\ \tilde{\boldsymbol{\tau}}_{\delta\alpha}^H & & \tilde{\boldsymbol{\tau}}_0^H & \tilde{\boldsymbol{\Gamma}}_{\delta\alpha}^H & & \tilde{\boldsymbol{\Gamma}}_0^H \\ & \ddots & \vdots & & \ddots & \vdots \\ 0 & & \tilde{\boldsymbol{\tau}}_{\delta\alpha}^H & 0 & & \tilde{\boldsymbol{\Gamma}}_{\delta\alpha}^H \end{pmatrix} \begin{pmatrix} \mathbf{S}_0^H \\ \vdots \\ \mathbf{S}_\ell^H \\ \mathbf{L}_{1\ell} \\ \vdots \\ \mathbf{L}_{10} \end{pmatrix} = \begin{pmatrix} 0 \\ \vdots \\ \tilde{\boldsymbol{\Gamma}}_0^H \\ \boldsymbol{\alpha}_1^H \\ \vdots \\ \boldsymbol{\alpha}_{\delta\alpha}^H \end{pmatrix} \tag{B.19}$$

where we have defined

$$\boldsymbol{\alpha} = \tilde{\boldsymbol{\Gamma}} + z^{-1}\boldsymbol{Q} \, . \tag{B.20}$$

Note that $\delta\alpha = \max(\delta\tilde{\tau}, \delta\tilde{\Gamma})$ and that the leading coefficient of $\alpha(z^{-1})$ is $\tilde{\Gamma}_0$. In (B.19), $\tilde{\boldsymbol{\tau}}_m = 0$ if $m > \delta\tilde{\tau}$ and $\tilde{\boldsymbol{\Gamma}}_m = 0$ if $m > \delta\tilde{\Gamma}$. Proceeding in the same manner with (B.17b) results in

$$\begin{pmatrix} -\lambda_e\boldsymbol{\Gamma}_{\delta L_2+1} & & 0 & \boldsymbol{\tau}_{\delta L_2+1} & & 0 \\ \vdots & \ddots & & \vdots & \ddots & \\ -\lambda_e\boldsymbol{\Gamma}_0 & & -\lambda_e\boldsymbol{\Gamma}_{\delta L_2+1} & \boldsymbol{\tau}_0 & & \boldsymbol{\tau}_{\delta L_2+1} \\ & \ddots & \vdots & & \ddots & \vdots \\ 0 & \dots & -\lambda_e\boldsymbol{\Gamma}_0 & 0 & \dots & \boldsymbol{\tau}_0 \end{pmatrix} \begin{pmatrix} \mathbf{S}_0^H \\ \vdots \\ \mathbf{S}_\ell^H \\ \mathbf{L}_{1\ell} \\ \vdots \\ \mathbf{L}_{10} \end{pmatrix} = \begin{pmatrix} \mathbf{L}_{2\delta L_2} \\ \vdots \\ \mathbf{L}_{20} \\ 0 \\ \vdots \\ 0 \end{pmatrix} , \tag{B.21}$$

where $\boldsymbol{\Gamma}_m = 0$ if $m > \delta\Gamma$ and $\boldsymbol{\tau}_m = 0$ if $m > \delta\tau$.

Neither (B.19) nor (B.21) can be solved directly, since unknown coefficient matrices appear on their right hand sides. However, we can combine the first $(\ell+1)n_d$ equations from (B.19) with the last $(\ell+1)n_y$ equations from (B.21) to obtain a system with equal number of equations and unknowns

$$\begin{pmatrix} \tilde{\boldsymbol{\tau}}_0^H & & 0 & \tilde{\boldsymbol{\Gamma}}_0^H & & 0 \\ \vdots & \ddots & & \vdots & \ddots & \\ \tilde{\boldsymbol{\tau}}_\ell^H & \dots & \tilde{\boldsymbol{\tau}}_0^H & \tilde{\boldsymbol{\Gamma}}_\ell^H & \dots & \tilde{\boldsymbol{\Gamma}}_0^H \\ -\lambda_e\boldsymbol{\Gamma}_0 & \dots & -\lambda_e\boldsymbol{\Gamma}_\ell & \boldsymbol{\tau}_0 & & \boldsymbol{\tau}_\ell \\ & \ddots & \vdots & & \ddots & \vdots \\ 0 & \dots & -\lambda_e\boldsymbol{\Gamma}_0 & 0 & \dots & \boldsymbol{\tau}_0 \end{pmatrix} \begin{pmatrix} \mathbf{S}_0^H \\ \vdots \\ \mathbf{S}_\ell^H \\ \mathbf{L}_{1\ell} \\ \vdots \\ \mathbf{L}_{10} \end{pmatrix} = \begin{pmatrix} 0 \\ \vdots \\ \tilde{\boldsymbol{\Gamma}}_0^H \\ 0 \\ \vdots \\ 0 \end{pmatrix} , \tag{B.22}$$

where only known coefficient matrices appear on the right hand side. We will now show that this system of linear equations has a unique solution whenever $\lambda_e > 0$. Define

$$\mathbf{T} \triangleq \begin{pmatrix} \boldsymbol{\tau}_0 & \dots & \boldsymbol{\tau}_\ell \\ & \ddots & \vdots \\ 0 & \dots & \boldsymbol{\tau}_0 \end{pmatrix} ; \tilde{\mathbf{T}} \triangleq \begin{pmatrix} \tilde{\boldsymbol{\tau}}_0 & \dots & \tilde{\boldsymbol{\tau}}_\ell \\ & \ddots & \vdots \\ 0 & \dots & \tilde{\boldsymbol{\tau}}_0 \end{pmatrix}$$

$$\mathbf{G} \triangleq \begin{pmatrix} \boldsymbol{\Gamma}_0 & \dots & \boldsymbol{\Gamma}_\ell \\ & \ddots & \vdots \\ 0 & \dots & \boldsymbol{\Gamma}_0 \end{pmatrix} ; \tilde{\mathbf{G}} \triangleq \begin{pmatrix} \tilde{\boldsymbol{\Gamma}}_0 & \dots & \tilde{\boldsymbol{\Gamma}}_\ell \\ & \ddots & \vdots \\ 0 & \dots & \tilde{\boldsymbol{\Gamma}}_0 \end{pmatrix}$$

$$\theta \triangleq \begin{pmatrix} \mathbf{S}_0 & \dots & \mathbf{S}_\ell & \mathbf{L}_{1\ell}^H & \dots & \mathbf{L}_{10}^H \end{pmatrix}^H ; \tilde{\mathbf{g}} \triangleq \begin{pmatrix} 0 & \dots & \tilde{\boldsymbol{\Gamma}}_0 & 0 & \dots & 0 \end{pmatrix}^H .$$

Equation (B.22) can then be written as

$$\underbrace{\begin{pmatrix} \tilde{\mathbf{T}}^H & \tilde{\mathbf{G}}^H \\ -\lambda_e \mathbf{G} & \mathbf{T} \end{pmatrix}}_{\mathbf{W}} \theta = \tilde{\mathbf{g}} .$$

The matrix $\mathbf{W}$ is non-singular since

$$\begin{aligned} \det \mathbf{W} &= (-1)^r \det \tilde{\mathbf{G}}^H \det \left(\lambda_e \mathbf{G} + \mathbf{T} \tilde{\mathbf{G}}^{-H} \tilde{\mathbf{T}}^H \right) \\ &= (-1)^r \det \tilde{\mathbf{G}}^H \det \left(\lambda_e \mathbf{G} + \mathbf{T} (\mathbf{G}^{-1} \mathbf{T})^H \right) \\ &= (-1)^r \det \tilde{\mathbf{G}}^H \det \left(\lambda_e \mathbf{G} \mathbf{G}^H + \mathbf{T} \mathbf{T}^H \right) \det \mathbf{G}^{-H} \end{aligned}$$

where $(\cdot)^{-H} = ((\cdot)^{-1})^H$. Above, the integer r compensates for the sign shifts caused by the elementary operations performed on the determinant. In the second equality, we have used that $\tilde{\mathbf{T}} \tilde{\mathbf{G}}^{-1} = \mathbf{G}^{-1} \mathbf{T}$, which is a consequence of the identity (3.3). Now, since both $\mathbf{G}$ and $\tilde{\mathbf{G}}$ are non-singular, so are $\mathbf{G}^{-H}$ and $\tilde{\mathbf{G}}^H$. Also, $\mathbf{G}\mathbf{G}^H$ is positive definite. Therefore, the matrix $\mathbf{W}$ is non-singular whenever $\lambda_e > 0$.

After having solved (B.22) for $\mathbf{S}_m^H$ and $\mathbf{L}_{1m}$, we use (B.19) to calculate the coefficients of $\boldsymbol{\alpha}$. We then compute the feedback filter $\boldsymbol{Q}$ with the aid of (B.20):

$$\boldsymbol{Q} = z(\boldsymbol{\alpha} - \tilde{\boldsymbol{\Gamma}}) . \tag{B.23}$$

Since the solution to (B.22) is unique, and $\boldsymbol{\alpha}$ and $\boldsymbol{Q}$ are determined explicitly from (B.19) and (B.23), we conclude that there exists a unique solution to (B.17a) and (B.17b).

Remark 1. The system of linear equations (B.22) can be rewritten so that only the coefficients of the feedforward filter is obtained. This leads to lower complexity.

APPENDIX C

Proof of Theorem 3.4 and Corollary 3.3

Suppose that a linear time-invariant finite impulse response channel of order L is given by (2.11) and assume that

$$\begin{aligned} E[d(k)d^H(m)] &= \delta_{km} I \\ E[v(k)v^H(m)] &= \psi_{k-m} \\ E[d(k)v^H(m)] &= 0\ . \end{aligned} \tag{C.1}$$

The objective is to estimate the symbol vector $d(k-\ell)$, by means of the MIMO FIR DFE defined in (3.21), that is

$$\begin{aligned} \hat{d}(k-\ell|k) &= \boldsymbol{S}(q^{-1})y(k) - \boldsymbol{Q}(q^{-1})\tilde{d}(k-\ell-1) && \text{(C.2)} \\ &= \mathbf{S}_0 y(k) + \mathbf{S}_1 y(k-1) + \cdots + \mathbf{S}_{\delta s} y(k-\delta s) \\ &\quad - \mathbf{Q}_0 \tilde{d}(k-\ell-1) - \cdots - \mathbf{Q}_{\delta Q}\tilde{d}(k-\ell-1-\delta Q) \\ &= \Theta_S^H \mathrm{y}_k - \Theta_Q^H \tilde{\mathrm{d}}_{k-\ell-1} && \text{(C.3)} \\ \tilde{d}(k-\ell) &= \mathrm{f}(\hat{d}(k-\ell|k)) && \text{(C.4)} \end{aligned}$$

where $\boldsymbol{S}(q^{-1})$ of order δs and $\boldsymbol{Q}(q^{-1})$ of order δQ are polynomial matrices of dimensions $n_y \times n_d$ and $n_d \times n_d$, respectively and $\mathrm{f}(\cdot)$ is the decision non-linearity. Also,

$$\Theta_S^H = \begin{pmatrix} \mathbf{S}_0 & \mathbf{S}_1 & \ldots & \mathbf{S}_{\delta s} \end{pmatrix} \tag{C.5a}$$

$$\Theta_Q^H = \begin{pmatrix} \mathbf{Q}_0 & \mathbf{Q}_1 & \ldots & \mathbf{Q}_{\delta Q} \end{pmatrix} \tag{C.5b}$$

and

$$\mathrm{y}_k = \begin{pmatrix} y^T(k) & y^T(k-1) & \dots & y^T(k-\delta s) \end{pmatrix}^T \tag{C.6a}$$

$$\tilde{\mathrm{d}}_{k-\ell-1} = \begin{pmatrix} \tilde{d}^T(k-\ell-1) & \dots & \tilde{d}^T(k-\ell-1-\delta Q) \end{pmatrix}^T \ . \tag{C.6b}$$

The feedback filter should be long enough so that all postcursor taps can be canceled. The number of postcursor taps equals

$$\underbrace{\delta s + L + 1}_{\substack{\text{number of} \\ \text{taps in } \boldsymbol{S}(q^{-1})\boldsymbol{B}(q^{-1})}} - \underbrace{\ell}_{\substack{\text{number of} \\ \text{precursor taps}}} - \underbrace{1}_{\substack{\text{reference} \\ \text{tap}}} \ .$$

Therefore, we conclude that

$$\delta Q = L + \delta s - \ell - 1 \ .$$

The coefficients $\{\mathbf{S}_n\}$ and $\{\mathbf{Q}_n\}$ are to be determined so that the mean-square error of the estimate $\hat{d}(k-\ell|k)$ is minimized.

The estimation error

$$\varepsilon(k-\ell) = d(k-\ell) - \hat{d}(k-\ell|k) \tag{C.7}$$

is minimized in the mean-square sense if it is orthogonal to all signals that the estimate $\hat{d}(k-\ell|k)$ may be based upon, that is, y_k and $\tilde{\mathrm{d}}_{k-\ell-1}$. The matrix filter coefficients providing the minimum mean-square estimation error are thus determined by the orthogonality condition

$$E\left[\begin{pmatrix} \mathrm{y}_k \\ -\tilde{\mathrm{d}}_{k-\ell-1} \end{pmatrix} \varepsilon^H(k-\ell)\right] = 0 \tag{C.8}$$

or, with $\varepsilon(k-\ell)$ from (C.7),

$$E\left[\begin{pmatrix} \mathrm{y}_k \\ -\tilde{\mathrm{d}}_{k-\ell-1} \end{pmatrix} \hat{d}^H(k-\ell|k)\right] = E\left[\begin{pmatrix} \mathrm{y}_k \\ -\tilde{\mathrm{d}}_{k-\ell-1} \end{pmatrix} d^H(k-\ell)\right] \ .$$

Next, insert $\hat{d}(k-\ell|k)$ from (C.3):

$$\begin{pmatrix} E\mathrm{y}_k\mathrm{y}_k^H & -E\mathrm{y}_k\tilde{\mathrm{d}}_{k-\ell-1}^H \\ -E\tilde{\mathrm{d}}_{k-\ell-1}\mathrm{y}_k^H & E\tilde{\mathrm{d}}_{k-\ell-1}\tilde{\mathrm{d}}_{k-\ell-1}^H \end{pmatrix} \begin{pmatrix} \Theta_S \\ \Theta_Q \end{pmatrix} = \begin{pmatrix} E\mathrm{y}_k d^H(k-\ell) \\ -E\tilde{\mathrm{d}}_{k-\ell-1} d^H(k-\ell) \end{pmatrix} \ . \tag{C.9}$$

Assume that all previous decisions affecting the current estimate were correct, that is, assume that

$$\tilde{d}(k-n) = d(k-n) \quad \ell+1 \le n \le L+\delta s$$

and define

$$\mathrm{d}_{k-\ell-1} = \begin{pmatrix} d^T(k-\ell-1) & \dots & d^T(k-\delta s-L) \end{pmatrix}^T . \tag{C.10}$$

This can be inserted into (C.9) in place of $\tilde{\mathrm{d}}_{k-\ell-1}$.

Due to the assumption of uncorrelated symbols made in (C.1), equation (C.9) can then be simplified to

$$\begin{pmatrix} E\mathrm{y}_k\mathrm{y}_k^H & -E\mathrm{y}_k\mathrm{d}_{k-\ell-1}^H \\ -E\mathrm{d}_{k-\ell-1}\mathrm{y}_k^H & I \end{pmatrix} \begin{pmatrix} \Theta_S \\ \Theta_Q \end{pmatrix} = \begin{pmatrix} E\mathrm{y}_k d^H(k-\ell) \\ 0 \end{pmatrix} . \tag{C.11}$$

To evaluate the expectations in (C.11), we invoke the channel model (2.11) to write $y(k-n)$ as

$$y(k-n) = \begin{pmatrix} \mathbf{B}_0 & \dots & \mathbf{B}_L \end{pmatrix} \begin{pmatrix} d(k-n) \\ \vdots \\ d(k-n-L) \end{pmatrix} + v(k-n) . \tag{C.12}$$

By inserting (C.12) into (C.6a) for $0 \leq n \leq \delta s$, we will obtain an explicit expression of y_k in terms of the channel coefficient matrices:

$$\mathrm{y}_k = \begin{pmatrix} \mathbf{B}_0 & \dots & \mathbf{B}_L & \dots & 0 \\ \vdots & \ddots & & \ddots & \vdots \\ 0 & \dots & \mathbf{B}_0 & \dots & \mathbf{B}_L \end{pmatrix} \begin{pmatrix} d(k) \\ \vdots \\ d(k-\delta s-L) \end{pmatrix} + \begin{pmatrix} v(k) \\ \vdots \\ v(k-\delta s) \end{pmatrix} . \tag{C.13}$$

To obtain a more compact expression of (C.13), we introduce the vector of stacked noise vectors

$$\mathrm{v}_k = \begin{pmatrix} v^T(k) & v^T(k-1) & \dots & v^T(k-\delta s) \end{pmatrix}^T \tag{C.14}$$

and the vector of stacked symbol vectors

$$\bar{\mathrm{d}}_k = \begin{pmatrix} d^T(k) & d^T(k-1) & \dots & d^T(k-\ell+1) \end{pmatrix}^T . \tag{C.15}$$

Furthermore, we define the following matrices:

$$\begin{aligned} \mathcal{F}_{tot} &\triangleq \left.\begin{pmatrix} \mathbf{B}_0 & \dots & \mathbf{B}_L & 0 & \dots & 0 \\ 0 & \mathbf{B}_0 & \dots & \mathbf{B}_L & \ddots & \vdots \\ \vdots & \ddots & \ddots & \ddots & \ddots & 0 \\ 0 & \dots & \dots & \mathbf{B}_0 & \dots & \mathbf{B}_L \end{pmatrix}\right\} n_y(\delta s+1) \\ &\triangleq \begin{pmatrix} \mathcal{F}_{fut} & \mathcal{F}_{pres} & \mathcal{F}_{past} \end{pmatrix} \end{aligned} \tag{C.16a}$$

where we have defined

$$\mathcal{F}_{fut} \triangleq \text{The first } n_d\ell \text{ columns in } \mathcal{F}_{tot} \tag{C.16b}$$

$$\mathcal{F}_{pres} \triangleq \text{Columns } n_d\ell + 1 \text{ to } n_d(\ell+1) \text{ in } \mathcal{F}_{tot} \tag{C.16c}$$

$$\mathcal{F}_{past} \triangleq \text{Columns } n_d(\ell+1) + 1 \text{ to } n_d(\delta s + L + 1) \text{ in } \mathcal{F}_{tot} \; . \tag{C.16d}$$

Equation (C.13) can then be written as

$$\mathrm{y}_k = \mathcal{F}_{fut}\bar{\mathrm{d}}_k + \mathcal{F}_{pres}d(k-\ell) + \mathcal{F}_{past}\mathrm{d}_{k-\ell-1} + \mathrm{v}_k \tag{C.17}$$

where $\mathrm{d}_{k-\ell-1}$ was defined in (C.10). Using (C.17) and (C.1), we can compute the expectations in (C.11):

$$\begin{aligned} E[\mathrm{y}_k\mathrm{y}_k^H] &= \mathcal{F}_{fut}\mathcal{F}_{fut}^H + \mathcal{F}_{pres}\mathcal{F}_{pres}^H + \mathcal{F}_{past}\mathcal{F}_{past}^H + \Psi \\ E[\mathrm{y}_k\mathrm{d}_{k-\ell-1}^H] &= \mathcal{F}_{past} \\ E[\mathrm{y}_k d^H(k-\ell)] &= \mathcal{F}_{pres} \end{aligned}$$

where Ψ is given by (3.24).

These computed expectations can then be inserted into (C.11):

$$\begin{pmatrix} \mathcal{F}_{fut}\mathcal{F}_{fut}^H + \mathcal{F}_{pres}\mathcal{F}_{pres}^H + \mathcal{F}_{past}\mathcal{F}_{past}^H + \Psi & -\mathcal{F}_{past} \\ -\mathcal{F}_{past}^H & \mathbf{I}_{n_d} \end{pmatrix} \begin{pmatrix} \Theta_S \\ \Theta_Q \end{pmatrix} = \begin{pmatrix} \mathcal{F}_{pres} \\ 0 \end{pmatrix} \; . \tag{C.18}$$

By observing that $\Theta_Q = \mathcal{F}_{past}^H\Theta_S$ from the second block row of (C.18) and inserting this into the first block row, we obtain

$$(\mathcal{F}_{fut}\mathcal{F}_{fut}^H + \mathcal{F}_{pres}\mathcal{F}_{pres}^H + \Psi)\Theta_S = \mathcal{F}_{pres} \tag{C.19a}$$

$$\Theta_Q = \mathcal{F}_{past}^H\Theta_S \; . \tag{C.19b}$$

Now observe that $\begin{pmatrix} \mathcal{F}_{fut} & \mathcal{F}_{pres} \end{pmatrix} = \mathcal{F}$ as defined in (3.23). Thus (C.19a) and (C.19b) can be expressed as

$$(\mathcal{F}\mathcal{F}^H + \Psi)\Theta_S = \mathcal{F}_{pres} \tag{C.20a}$$

$$\Theta_Q = \mathcal{F}_{past}^H\Theta_S \; . \tag{C.20b}$$

Here (C.20a) coincides with (3.22) and if we complex conjugate and transpose both sides of (C.20b) and evaluate for each matrix element $\mathbf{Q}_n$, we readily obtain (3.25).

We will now prove Corollary 3.3. As a starting point, we use the expression (C.3) for the DFE and the expression (C.20b) for its feedback filter coefficients:

$$\hat{d}(k-\ell|k) = \Theta_S^H\left(\mathrm{y}_k - \mathcal{F}_{past}\tilde{\mathrm{d}}_{k-\ell-1}\right) \; .$$

We now assume that all previous decisions are correct. We thus replace $\tilde{\mathrm{d}}_{k-\ell-1}$ with $\mathrm{d}_{k-\ell-1}$, defined in (C.10). We also use the expression (C.17) for y_k to obtain

$$\hat{d}(k-\ell) = \Theta_S^H \left(\mathcal{F}_{fut} \bar{\mathrm{d}}_k + \mathcal{F}_{pres} d(k-\ell) + \mathrm{v}_k \right) . \tag{C.21}$$

From (C.21) we obtain an expression for the estimation error that can be used to determine the estimation error covariance matrix (2.4):

$$\begin{aligned} \mathbf{P} = E \Big[\big(d(k-\ell) - \Theta_S^H \left(\mathcal{F}_{fut} \bar{\mathrm{d}}_k + \mathcal{F}_{pres} d(k-\ell) + \mathrm{v}_k \right) \big) \\ \times \big(d(k-\ell) - \Theta_S^H \left(\mathcal{F}_{fut} \bar{\mathrm{d}}_k + \mathcal{F}_{pres} d(k-\ell) + \mathrm{v}_k \right) \big)^H \Big] . \end{aligned}$$

The covariance matrix can be evaluated to yield

$$\begin{aligned} \mathbf{P} = & E d(k-\ell) d^H(k-\ell) - E d(k-\ell) d^H(k-\ell) \mathcal{F}_{pres}^H \Theta_S \\ & - \Theta_S^H \mathcal{F}_{pres} E d(k-\ell) d^H(k-\ell) + \Theta_S^H \mathcal{F}_{fut} E \bar{\mathrm{d}}_k \bar{\mathrm{d}}_k^H \mathcal{F}_{fut}^H \Theta_S \\ & + \Theta_S^H \mathcal{F}_{pres} E d(k-\ell) d^H(k-\ell) \mathcal{F}_{pres}^H \Theta_S + \Theta_S^H E \mathrm{v}_k \mathrm{v}_k^H \Theta_S , \end{aligned}$$

where we have used (2.9) and (2.13). Again making use of (2.9) and also of (2.12) and (3.24) we readily obtain

$$\begin{aligned} \mathbf{P} &= \mathbf{I} - \mathcal{F}_{pres}^H \Theta_S - \Theta_S^H \mathcal{F}_{pres} + \Theta_S^H \mathcal{F}_{fut} \mathcal{F}_{fut}^H \Theta_S \\ &\quad + \Theta_S^H \mathcal{F}_{pres} \mathcal{F}_{pres}^H \Theta_S + \Theta_S^H \Psi \Theta_S \\ &= \mathbf{I} - \mathcal{F}_{pres}^H \Theta_S - \Theta_S^H \mathcal{F}_{pres} + \Theta_S^H \left(\mathcal{F} \mathcal{F}^H + \Psi \right) \Theta_S \end{aligned} \tag{C.22}$$

where we in the last equality used $\mathcal{F} = \begin{pmatrix} \mathcal{F}_{fut} & \mathcal{F}_{pres} \end{pmatrix}$. If we insert (C.20a) into (C.22), we finally obtain

$$\mathbf{P} = \mathbf{I} - \mathcal{F}_{pres}^H \left(\mathcal{F} \mathcal{F}^H + \Psi \right)^{-1} \mathcal{F}_{pres} , \tag{C.23}$$

which coincides with (3.26).

APPENDIX D

Proof of Corollaries 3.1, 3.2, 3.4, and 3.5

In this appendix, we will prove Corollaries 3.1, 3.2, 3.4, and 3.5. We will thus investigate the solvability conditions for the two Diophantine equations (3.16) and (3.28). For ease of reference, we repeat these equations and the conditions for their solvability:

$$q^{-\ell}\mathbf{I} = \boldsymbol{\mathcal{R}}(q^{-1})\boldsymbol{A}^{-1}(q^{-1})\boldsymbol{B}(q^{-1}) - q^{-\ell-1}\boldsymbol{\mathcal{F}}(q^{-1}) \tag{D.1a}$$

and

$$q^{-\ell}\mathbf{I} = \boldsymbol{S}(q^{-1})\boldsymbol{B}(q^{-1}) - q^{-\ell-1}\boldsymbol{Q}(q^{-1})\ . \tag{D.1b}$$

The Diophantine equation (D.1a) can be solved if and only if every common right divisor[1] of $\boldsymbol{A}^{-1}(q^{-1})\boldsymbol{B}(q^{-1})$ and $q^{-\ell-1}\mathbf{I}$ is a right divisor also of $q^{-\ell}\mathbf{I}$. Equation (D.1b) can be solved if and only if every common right divisor[2] of $\boldsymbol{B}(q^{-1})$ and $q^{-\ell-1}\mathbf{I}$ is a right divisor also of $q^{-\ell}\mathbf{I}$.

We will show that such right factors exist in the situations described in the corollaries. Two facts greatly simplify the proofs:

1. A polynomial matrix in q^{-1} is a special case of a stable and causal rational matrix.

2. A polynomial matrix in q^{-1} that is a right divisor of $\boldsymbol{B}(q^{-1})$ is a right divisor also of the rational matrix $\boldsymbol{A}^{-1}(q^{-1})\boldsymbol{B}(q^{-1})$.

[1] The admissible right divisors are members of the ring of stable and causal rational matrices.
[2] The admissible right divisors are members of the ring of polynomial matrices in q^{-1}.

For each of the proofs in this appendix, we will use the following procedure:

1. Find a polynomial matrix $\boldsymbol{R}(q^{-1})$ that is a right divisor of
   - $\boldsymbol{B}(q^{-1})$ and
   - $q^{-\ell-1}\mathbf{I}$.
2. Show that $\boldsymbol{R}(q^{-1})$ is not a right factor of $q^{-\ell}\mathbf{I}$ in the ring of stable and causal rational functions. In other words, there should not exist any stable and causal rational $\boldsymbol{\mathcal{X}}(q^{-1})$ such that $q^{-\ell}\mathbf{I} = \boldsymbol{\mathcal{X}}(q^{-1})\boldsymbol{R}(q^{-1})$. This will imply that there would, of course, not exist any such $\boldsymbol{\mathcal{X}}(q^{-1})$ that is a polynomial matrix in q^{-1} either, so $\boldsymbol{R}(q^{-1})$ cannot be a right factor of $q^{-1}\mathbf{I}$ in the ring of polynomial matrices.

If we succeed with this, *neither* (D.1b) *nor* (D.1a) *will have a solution.* We are thus able to prove the corollaries "in pairs".

Remark 1. To improve readability, we will omit the polynomial arguments in the remainder of this appendix.

D.1 Proof of Corollaries 3.1 and 3.4

Assume that $\operatorname{rank} \boldsymbol{B} < n_d$. In this case, there exists a *unimodular*[3] matrix $\boldsymbol{U}$ such that

$$\boldsymbol{B}\boldsymbol{U} = \begin{pmatrix} \tilde{\boldsymbol{B}} & 0 \end{pmatrix} \tag{D.2}$$

for some matrix $\tilde{\boldsymbol{B}}$ with n_y rows and $n_d - 1$ columns. Equation (D.2) also holds when $\operatorname{rank} \boldsymbol{A}^{-1}\boldsymbol{B} < n_d$, since

$$\operatorname{rank} \boldsymbol{A}^{-1}\boldsymbol{B} = \operatorname{rank} \boldsymbol{B}\,. \tag{D.3}$$

The above relation holds since $\boldsymbol{A}$ is a diagonal polynomial matrix with finite diagonal elements. The inverse of $\boldsymbol{A}$ will then be a diagonal matrix with non-zero diagonal elements.

We will now show, that when (D.2) holds, the polynomial matrix

$$\boldsymbol{R} \triangleq \begin{pmatrix} \mathbf{I}_{n_d-1} & 0 \\ 0 & q^{-\ell-1} \end{pmatrix} \boldsymbol{U}^{-1} \tag{D.4}$$

is a right divisor of $\boldsymbol{B}$ and $q^{-\ell-1}\mathbf{I}_{n_d}$, but not of $q^{-\ell}\mathbf{I}_{n_d}$.

For $\boldsymbol{R}$ in (D.4), we must thus verify the following three properties:

[3] A square polynomial matrix is said to be unimodular if its determinant equals a non-zero constant.

1. $\boldsymbol{R}$ is a right divisor of $\boldsymbol{B}$
2. $\boldsymbol{R}$ is a right divisor of $q^{-\ell-1}\mathbf{I}$
3. $\boldsymbol{R}$ is *not* a right divisor of $q^{-\ell}\mathbf{I}$.

Property 1

We see that

$$\boldsymbol{B} = \boldsymbol{B}\boldsymbol{U}\boldsymbol{U}^{-1} = \begin{pmatrix}\tilde{\boldsymbol{B}} & 0\end{pmatrix}\boldsymbol{U}^{-1} = \begin{pmatrix}\tilde{\boldsymbol{B}} & 0\end{pmatrix}\begin{pmatrix}\mathbf{I}_{n_d-1} & 0\\ 0 & q^{-\ell-1}\end{pmatrix}\boldsymbol{U}^{-1} = \begin{pmatrix}\tilde{\boldsymbol{B}} & 0\end{pmatrix}\boldsymbol{R}\,,$$

where we in the second equality used the identity (D.2). Hence $\boldsymbol{R}$ is a right factor of $\boldsymbol{B}$.

Property 2

We immediately see that

$$\begin{aligned} q^{-\ell-1}\mathbf{I}_{n_d} = q^{-\ell-1}\boldsymbol{U}\boldsymbol{U}^{-1} &= \boldsymbol{U}\begin{pmatrix}q^{-\ell-1}\mathbf{I}_{n_d-1} & 0\\ 0 & q^{-\ell-1}\end{pmatrix}\boldsymbol{U}^{-1}\\ &= \boldsymbol{U}\begin{pmatrix}q^{-\ell-1}\mathbf{I}_{n_d-1} & 0\\ 0 & 1\end{pmatrix}\begin{pmatrix}\mathbf{I}_{n_d-1} & 0\\ 0 & q^{-\ell-1}\end{pmatrix}\boldsymbol{U}^{-1}\\ &= \boldsymbol{U}\begin{pmatrix}q^{-\ell-1}\mathbf{I}_{n_d-1} & 0\\ 0 & 1\end{pmatrix}\boldsymbol{R}\,. \end{aligned}$$

Hence $\boldsymbol{R}$ is a right factor of $q^{-\ell-1}\mathbf{I}_{n_d}$.

Property 3

We will now try to find a causal and rational matrix $\boldsymbol{\mathcal{X}}$ such that

$$q^{-\ell}\mathbf{I}_{n_d} = \boldsymbol{\mathcal{X}}\begin{pmatrix}\mathbf{I}_{n_d-1} & 0\\ 0 & q^{-\ell-1}\end{pmatrix}\boldsymbol{U}^{-1}\,.$$

This equation can be rewritten

$$q^{-\ell}\boldsymbol{U} = \boldsymbol{\mathcal{X}}\begin{pmatrix}\mathbf{I}_{n_d-1} & 0\\ 0 & q^{-\ell-1}\end{pmatrix}\,. \tag{D.5}$$

Study the last column in (D.5). With $\boldsymbol{U}_{n_d}$ and $\boldsymbol{\mathcal{X}}_{nd}$ being the last columns of $\boldsymbol{U}$ and $\boldsymbol{\mathcal{X}}$, respectively, we obtain:

$$q^{-\ell}\boldsymbol{U}_{n_d} = q^{-\ell-1}\boldsymbol{\mathcal{X}}_{n_d}\,.$$

But since $\boldsymbol{\mathcal{X}}$ is causal, this implies that all elements in $\boldsymbol{U}_{n_d}$ must have q^{-1} as a common factor. However, this is impossible when $\boldsymbol{U}$ is unimodular. Hence we conclude that $q^{-\ell}\mathbf{I}_{n_d}$ cannot have $\boldsymbol{R}$ as a right factor.

This completes the proof of Corollary 3.4. Recalling that $\operatorname{rank} \boldsymbol{A}^{-1}\boldsymbol{B} = \operatorname{rank} \boldsymbol{B}$, the proof of Corollary 3.1 is also complete.

D.2 Proof of Corollaries 3.2 and 3.5

Assume that user ν has a propagation delay that exceeds ℓ. We will now verify that

$$\boldsymbol{R} = \operatorname{diag}\big(\underbrace{1 \quad \dots \quad 1}_{\nu-1} \quad q^{-\ell-1} \quad \underbrace{1 \quad \dots \quad 1}_{n_d-\nu}\big) \tag{D.6}$$

is a right divisor of $\boldsymbol{B}$ and $q^{-\ell-1}\mathbf{I}$, but not of $q^{-\ell}\mathbf{I}$.

With the definition (3.17), we can write

$$\boldsymbol{B} = \tilde{\boldsymbol{B}}\boldsymbol{\Delta} \tag{D.7}$$

where

$$\boldsymbol{\Delta} \stackrel{\triangle}{=} \operatorname{diag}\left(q^{-\Delta_1} \quad q^{-\Delta_2} \quad \dots \quad q^{-\Delta_{n_d}}\right) . \tag{D.8}$$

If we compare (D.6) and (4.19a), we see that

$$\boldsymbol{\Delta} = \tilde{\boldsymbol{\Delta}}\boldsymbol{R} \tag{D.9}$$

with

$$\tilde{\boldsymbol{\Delta}} = \operatorname{diag}\left(q^{-\tilde{\Delta}_1} \quad q^{-\tilde{\Delta}_2} \quad \dots \quad q^{-\tilde{\Delta}_{n_d}}\right)$$

and

$$\tilde{\Delta}_i = \begin{cases} \Delta_i & i \neq \nu \\ \Delta_\nu - \ell - 1 & i = \nu \end{cases} .$$

If we now insert $\boldsymbol{\Delta}$ from (D.9) into (D.7), we obtain

$$\boldsymbol{B} = \tilde{\boldsymbol{B}}\tilde{\boldsymbol{\Delta}}\boldsymbol{R} .$$

Since $\Delta_\nu \geq \ell + 1$, $\tilde{\boldsymbol{\Delta}}$ is a polynomial matrix in q^{-1}, and $\boldsymbol{R}$ is a right divisor of $\boldsymbol{B}$.

We immediately see that $\boldsymbol{R}$ is a right divisor of $q^{-\ell-1}\mathbf{I}$, since

$$q^{-\ell-1}\mathbf{I} = \begin{pmatrix} q^{-\ell-1}\mathbf{I}_{\nu-1} & 0 & 0 \\ 0 & 1 & 0 \\ 0 & 0 & q^{-\ell-1}\mathbf{I}_{n_d-\nu} \end{pmatrix} \boldsymbol{R} .$$

However, if we try to find a stable and causal rational matrix $\boldsymbol{\mathcal{X}}$ such that

$$q^{-\ell}\mathbf{I} = \boldsymbol{\mathcal{X}}\boldsymbol{R}$$

we must require that

$$q^{-\ell}e^{(\nu)} = q^{-\ell-1}\boldsymbol{\mathcal{X}}_{\nu}$$

where $\boldsymbol{\mathcal{X}}_{\nu}$ is column ν in $\boldsymbol{\mathcal{X}}$ and

$$e^{(\nu)} \triangleq \big(\underbrace{0 \quad \dots \quad 0}_{\nu-1} \quad 1 \quad \underbrace{0 \quad \dots \quad 0}_{n_d-\nu}\big)^T \ .$$

Since this equation is impossible to satisfy with a stable and causal $\boldsymbol{\mathcal{X}}$, we conclude that $\boldsymbol{R}$ is not a right factor of $q^{-\ell}\mathbf{I}$.

Since $\boldsymbol{R}$ is a right factor of $\boldsymbol{B}$ and $q^{-\ell-1}\mathbf{I}$, but not of $q^{-\ell}\mathbf{I}$, equations (D.1a) and (D.1b) lack a solution.

APPENDIX E
Proof of Theorem 3.6

We shall here derive the degree condition (3.29). We assume that the condition in Theorem 3.5 is fulfilled, and hence that a zero-forcing solution exists for some choice of feedforward filter degree.

To prove the degree condition (3.29), we first need to remove the influence of pure time delays within each column of $\boldsymbol{B}(q^{-1})$. For this purpose, we define

$$\boldsymbol{\Delta}(q^{-1}) \stackrel{\triangle}{=} \operatorname{diag}\begin{pmatrix} q^{-\Delta_1} & q^{-\Delta_2} & \dots & q^{-\Delta_{n_d}} & . \end{pmatrix} \tag{E.1}$$

We also implicitly define $\bar{\boldsymbol{B}}(q^{-1})$ through the factorization

$$\boldsymbol{B}(q^{-1}) = \bar{\boldsymbol{B}}(q^{-1})\boldsymbol{\Delta}(q^{-1}) \tag{E.2}$$

The factorization (E.2) is inserted into (3.28), which is rearranged to yield:

$$\boldsymbol{S}(q^{-1})\bar{\boldsymbol{B}}(q^{-1})\boldsymbol{\Delta}(q^{-1}) = q^{-\ell}(\mathbf{I}_{n_d} + q^{-1}\boldsymbol{Q}(q^{-1})) \, . \tag{E.3}$$

For this equation to have a solution, we must assure that the right divisor $\boldsymbol{\Delta}(q^{-1})$ of the left hand side is also a right divisor of the right hand side.

To this end, we rewrite the right hand side of (E.3):

$$\begin{aligned} q^{-\ell}\left(\mathbf{I}_{n_d} + q^{-1}\boldsymbol{Q}(q^{-1})\right) &= \left(\mathbf{I}_{n_d} + q^{-1}\boldsymbol{Q}(q^{-1})\right) q^{-\ell}\mathbf{I}_{n_d} \\ &= \left(\mathbf{I}_{n_d} + q^{-1}\boldsymbol{Q}(q^{-1})\right) \bar{\boldsymbol{\Delta}}(q^{-1})\boldsymbol{\Delta}(q^{-1}) \end{aligned}$$

with

$$\bar{\boldsymbol{\Delta}}(q^{-1}) = \operatorname{diag}\begin{pmatrix} q^{-\ell+\Delta_1} & \dots & q^{-\ell+\Delta_{n_d}} \end{pmatrix} \, .$$

Note that $\bar{\boldsymbol{\Delta}}(q^{-1})$ is a polynomial matrix in q^{-1}, since we know from Corollary 3.5 that $\Delta_i \leq \ell \; \forall i$.

We thus see that $q^{-\ell}(\mathbf{I}_{n_d} + q^{-1}\boldsymbol{Q}(q^{-1}))$ has $\boldsymbol{\Delta}(q^{-1})$ as a right factor as required. This factor can thus be removed in equation (E.3). We must now solve

$$\boldsymbol{S}(q^{-1})\bar{\boldsymbol{B}}(q^{-1}) = (\mathbf{I}_{n_d} + q^{-1}\boldsymbol{Q}(q^{-1}))\bar{\boldsymbol{\Delta}}(q^{-1}) \; . \tag{E.4}$$

with respect to $\boldsymbol{S}(q^{-1})$ and $\boldsymbol{Q}(q^{-1})$.

Let us now investigate the equalized channel from sources 1 to n_d to the estimate of source j, that is, let us consider row j in (E.4):

$$\sum_{k=1}^{n_y} S_{jk}(q^{-1})\bar{B}_{km}(q^{-1}) = q^{-\ell+\Delta_m-1}Q_{jm}(q^{-1}) \quad m \neq j \tag{E.5a}$$

$$\sum_{k=1}^{n_y} S_{jk}(q^{-1})\bar{B}_{kj}(q^{-1}) = q^{-\ell+\Delta_j}(1 + q^{-1}Q_{jj}(q^{-1})) \; . \tag{E.5b}$$

In general, equations (E.5a) and (E.5b) can not be solved if the number of equations exceeds the number of unknowns. We must thus assure that the number of unknowns equals or exceeds the number of equations.

The feedforward filter must cancel the precursor taps, and also make the reference tap equal to the identity matrix. In the $n_d - 1$ equations in (E.5a), there are

$$\sum_{m \neq j} (\ell + 1 - \Delta_m) \tag{E.6}$$

precursor taps, which must be canceled. In (E.5b), the $\ell - \Delta_j$ precursor taps must be canceled and the reference tap should be set to unity, giving

$$\ell + 1 - \Delta_j \tag{E.7}$$

additional linear equations. Adding (E.6) and (E.7) gives the total number of conditions (equations) to fulfill:

$$\sum_{m=1}^{n_d} (\ell + 1 - \Delta_m) = n_d(\ell + 1) - \sum_{m=1}^{n_d} \Delta_m \; . \tag{E.8}$$

To satisfy these equations we must use only the feedforward filter. The feedforward filter for user j has $\delta s + 1$ row vector taps, giving a total of

$$n_y(\delta s + 1) \tag{E.9}$$

unknowns. If we compare (E.8) with (E.9), we see that if

$$\delta s \geq \frac{n_d(\ell+1) - \sum_{m=1}^{n_d} \Delta_m}{n_y} - 1 \tag{E.10}$$

all precursor taps can be canceled. Since (E.10) is independent of j, a feedforward filter degree satisfying (E.10) is generically necessary to fulfill the zero-forcing condition (2.3) for all n_d users.

BIBLIOGRAPHY

[1] Majeed Abdulrahman. *DFE for Interference and Multipath Suppression in a CDMA System*, PhD thesis, Department of Systems and Computer Engineering, Carleton University, Ottawa, Canada, January 1994.

[2] Majeed Abdulrahman, Asrar U. H. Sheikh, and David D. Falconer, "Decision feedback equalization for CDMA in indoor wireless communications," *IEEE Journal on Selected Areas in Communications*, vol. 12, no. 4, pp. 698–706, May 1994.

[3] Anders Ahlén and Mikael Sternad, "Wiener filter design using polynomial equations," *IEEE Transactions on Signal Processing*, vol. 39, no. 11, pp. 2387–2399, November 1991.

[4] Anders Ahlén and Mikael Sternad, "Derivation and design of Wiener filters using polynomial equations,", in C T Leondes, editor, *Stochastic Techniques in Digital Signal Processing*, pp. 353–418, Academic Press, New York, NY, 1994.

[5] Sören Andersson, Ulf Forssén, Jonas Karlsson, Tom Witzschel, Peter Fischer, and Andreas Krug, "Ericsson/Mannesmann GSM field-trials with adaptive antennas," in *Proceedings of the IEEE Vehicular Technology Conference*, vol. 3, Phoenix, USA, May 1997, pp. 1587–1591.

[6] Sören Andersson, Mille Millnert, Mats Viberg, and Bo Wahlberg, "An adaptive array for mobile communication systems," *IEEE Transactions on Vehicular Technology*, vol. 40, no. 1, pp. 230–236, February 1991.

[7] Sirikiat Lek Ariyavisitakul, Jack H. Winters, and Inkyu Lee, "Optimum space-time processors with dispersive interference: Unified analysis and required filter span," *IEEE Transactions on Communications*, vol. 47, no. 7, pp. 1073–1083, July 1999.

[8] David Asztély. "On antenna arrays in mobile communication systems, fast fading and GSM base station receiver algorithms," Master's thesis, Royal Institute of Technology, Stockholm, Sweden, February 1995.

[9] David Asztely and Björn Ottersten, "MLSE and spatio-temporal interference rejection combining with antenna arrays," in *Proceedings of the EUSIPCO98*, Rhodos, Greece, September 1998.

[10] M. E. Austin, "Decision-feedback equalization for digital communication over dispersive channels," Technical Report 437, M.I.T. Lincoln Laboratory, Lexington, MA, August 1967.

[11] Philip Balaban and Jack Salz, "Optimum diversity combining and equalization in digital data transmission with applications to cellular mobile radio — Part I: Theoretical considerations," *IEEE Transactions on Communications*, vol. 40, no. 5, pp. 885–894, 1992.

[12] Philip Balaban and Jack Salz, "Optimum diversity combining and equalization in digital data transmission with applications to cellular mobile radio — Part II: Numerical results," *IEEE Transactions on Communications*, vol. 40, no. 5, pp. 895–907, May 1992.

[13] Carlos A. Belfiore and John H. Park, "Decision feedback equalization," *Proceedings of the IEEE*, vol. 67, no. 8, pp. 1143–1156, August 1979.

[14] Gregory E. Bottomley and Karim Jamal, "Adaptive arrays and MLSE equalization," in *Proceedings of the 45th IEEE Vehicular Technology Conference*, vol. 1, Chicago, July 1995, pp. 50–54.

[15] Antonio Cantoni and Paul Butler, "Stability of decision feedback inverses," *IEEE Transactions on Communications*, vol. 24, pp. 970–977, September 1976.

[16] Dao Sheng Chen and Sumit Roy, "An adaptive multiuser receiver for CDMA systems," *IEEE Journal on Selected Areas in Communications*, vol. 12, no. 5, pp. 808–816, June 1994.

[17] Jiunn-Tsair Chen, Jen-Wei Liang, Huan-Shang Tsai, and Young-Kai Chen, "Low-complexity joint MLSE receiver in the presence of CCI," *IEEE Communications Letters*, vol. 2, no. 5, pp. 125–127, May 1998.

[18] John M. Cioffi, Glen P. Dudevoir, M. Vedat Eyuboglu, and G. David Forney, Jr., "MMSE decision-feedback equalizers and coding—Part I: Equalization results," *IEEE Transactions on Communications*, vol. 43, no. 10, pp. 2582–2594, October 1995.

[19] John M. Cioffi, Glen P. Dudevoir, M. Vedat Eyuboglu, and G. David Forney, Jr., "MMSE decision-feedback equalizers and coding—Part II: Coding results," *IEEE Transactions on Communications*, vol. 43, no. 10, pp. 2595–2604, October 1995.

[20] Martin V. Clark, Larry J. Greenstein, William K. Kennedy, and Mansoor Shafi, "Optimum linear diversity receivers for mobile communications," *IEEE Transactions on Vehicular Technology*, vol. 43, no. 1, pp. 47–56, February 1994.

[21] Pedro M. Crespo and Michael L. Honig, "Pole-zero decision feedback equalization with a rapidly converging adaptive IIR algorithm," *IEEE Journal on Selected Areas in Communications*, vol. 9, no. 6, pp. 817–829, August 1991.

[22] Erik Dahlman, Björn Gudmundson, Mats Nilsson, and Johan Sköld, "UMTS/IMT-2000 based on wideband CDMA," *IEEE Communications Magazine*, vol. 36, no. 9, pp. 70–80, September 1998.

[23] Alexandra Duel–Hallen, "Equalizers for multiple input/multiple output channels and PAM systems with cyclostationary input sequences," *IEEE Journal on Selected Areas in Communications*, vol. 10, no. 3, pp. 630–639, April 1992.

[24] Alexandra Duel-Hallen, "Decorrelating decision-feedback multi-user detector for synchronous code-division multiple access channel," *IEEE Transactions on Communications*, vol. 41, no. 2, pp. 285–290, February 1993.

[25] Alexandra Duel-Hallen, "A family of multiuser decision-feedback detectors for asynchronous code-division multiple access channels," *IEEE Transactions on Communications*, vol. 43, no. 2/3/4, pp. 421–434, Feb./Mar./Apr. 1995.

[26] Donald L. Duttweiler, James E. Mazo, and David G. Messerschmitt, "An upper bound on the error probability in decision-feedback equalizers," *IEEE Transactions on Information Theory*, vol. 20, no. 4, pp. 490–497, July 1974.

[27] Richard B. Ertel, Paulo Cardieri, Kevin W. Sowerby, Theodore S. Rappaport, and Jeffrey H. Reed, "Overview of spatial channel models for antenna array communication systems," *IEEE Personal Communications*, vol. 5, no. 1, pp. 10–22, February 1998.

[28] David D. Falconer and Gerard J. Foschini, "Theory of minimum mean-square-error QAM systems employing decision feedback equalization," *Bell Systems Technical Journal*, vol. 52, no. 10, pp. 1821–1849, December 1973.

[29] G. David Forney, Jr., "Maximum-likelihood sequence estimation of digital sequences in the presence of intersymbol interference," *IEEE Transactions on Information Theory*, vol. 18, no. 3, pp. 363–378, May 1972.

[30] G. David Forney, Jr., "The Viterbi algorithm," *Proceedings of the IEEE*, vol. 61, no. 3, pp. 268–278, March 1973.

[31] Tracy Fulghum, Karl Molnar, and Alexandra Duel-Hallen, "The Jakes fading model incorporating angular spread," in *Proceedings of CISS*, Baltimore, USA, March 1997, pp. 364–369.

[32] K. Giridhar, John J. Shynk, Amit Mathur, Sujai Chari, and Richard P. Gooch, "Nonlinear techniques for the joint estimation of co-channel signals," *IEEE Transactions on Communications*, vol. 45, no. 4, pp. 473–484, April 1997.

[33] Alexei Gorokhov and Philippe Loubaton, "Multiple input, multiple output ARMA systems: second order blind identification for signal extraction," in *Proceedings of the 8th IEEE Signal Processing Workshop on Statistical Signal and Array Processing*, 1996.

[34] Alexei Gorokhov and Philippe Loubaton, "Subspace-based techniques for blind separation of convolutive mixtures with temporally correlated sources," *IEEE Transactions on Circuits and Systems—I: Fundamental Theory and Applications*, vol. 44, no. 9, pp. 813–820, September 1997.

[35] Didier Henrion, Martin Hromcik, Huibert Kwakernaak, Sonja Pejchová, Michael Šebek, and Rens C.W. Strijbos, "Polynomial toolbox version 1.6,", 1998, See http://www.math.utwente.nl/polbox.

[36] Michael L. Honig, Kenneth Steiglitz, and B. Gopinath, "Multichannel signal processing for data communications in the presence of crosstalk," *IEEE Transactions on Communications*, vol. 38, no. 4, pp. 551–558, April 1990.

[37] *IEEE Transactions on Information Theory: Special Issue Commemorating Stephen O. Rice*, vol. 34, no. 6, pp. 1365–1537, November 1988.

[38] Jan Ježek and Vladimír Kučera, "Efficient algorithm for matrix spectral factorization," *Automatica*, vol. 21, no. 6, pp. 663–669, 1985.

[39] Rolf Johannesson, *Informationsteori — grundvalen för (tele-)kommunikation*: Studentlitteratur, 1988.

[40] Thomas Kailath, *Linear Systems*: Prentice Hall, 1980.

[41] Jonas Karlsson, *Adaptive Antennas in GSM Systems with Non-Synchronized Base Stations.* Licentiate thesis, Royal Institute of Technology, Stockholm, Sweden, March 1998.

[42] Petri Karttunen, Kimmo Kalliola, Timo Laakso, and Pertti Vainikainen, "Measurement analysis of spatial and temporal correlation in wideband radio channels with adaptive antenna array," in *Proceedings of the 1998 IEEE International Conference on Universal Personal Communications*, Florence, Italy, October 1998, pp. 671–675.

[43] Rodney A. Kennedy and Brian D. O. Anderson, "Recovery times of decision feedback equalizers on noiseless channels," *IEEE Transactions on Communications*, vol. 35, no. 10, pp. 1012–1021, October 1987.

[44] Rodney A. Kennedy, Brian D. O. Anderson, and Robert R. Bitmead, "Tight bounds on the error probability of decision feedback equalizer," *IEEE Transactions on Communications*, vol. 35, no. 10, pp. 1022–1028, October 1987.

[45] Vladimír Kučera, *Analysis and Design of Discrete Linear Control Systems*: Prentice Hall, 1991.

[46] Pierre A. Laurent, "Exact and approximate construction of digital phase modulations by superposition of amplitude modulated pulses (AMP)," *IEEE Transactions on Communications*, vol. 34, no. 2, pp. 150–160, February 1986.

[47] Edward A. Lee and David G. Messerschmitt, *Digital communication*: Kluwer Academic Publishers, 2nd edition, 1994.

[48] Shu Lin and Daniel J. Costello, Jr., *Error Control Coding*: Prentice-Hall, 1983.

[49] Lars Lindbom, *Adaptive Equalization for Fading Mobile Radio Channels.* Licentiate thesis, Uppsala University, Uppsala, Sweden, November 1992.

[50] Lars Lindbom. *A Wiener Filtering Approach to the Design of Tracking Algorithms,* PhD thesis, Uppsala University, Uppsala, Sweden, November 1995.

[51] Erik Lindskog. *Space-Time Processing and Equalization for Wireless Communications,* PhD thesis, Uppsala University, Uppsala, Sweden, 1999.

[52] Erik Lindskog and Claes Tidestav, "Reduced rank space-time equalization," in *Proceedings of the 9th IEEE International Symposium on Personal, Indoor and Mobile Radio Communications*, Boston, MA, September 1998, pp. 1081–1085.

[53] Erik Lindskog and Claes Tidestav, "Reduced rank channel estimation," in *Proceedings of the IEEE Vehicular Technology Conference*, vol. 2, Houston, TX, USA, May 1999, pp. 1126–1130.

[54] Lennart Ljung, *System Identification*: Prentice-Hall, 1987.

[55] Norm K. Lo, David D. Falconer, and Asrar U.H. Sheikh, "Adaptive equalization for a multipath fading environment with interference and noise," in *Proceedings of the IEEE Vehicular Technology Conference*, vol. 1, Stockholm, Sweden, June 1994, pp. 252–256.

[56] Ruxandra Lupas and Sergio Verdú, "Linear multiuser detectors for synchronous code-division multiple-access channels," *IEEE Transactions on Information Theory*, vol. 35, no. 1, pp. 123–136, January 1989.

[57] Ruxandra Lupas and Sergio Verdú, "Near-far resistance of multi-user detectors in asynchronous channels," *IEEE Transactions on Communications*, vol. 38, no. 4, pp. 496–508, April 1990.

[58] Upamanyu Madhow and Michael L. Honig, "MMSE interference suppression for direct-sequence spread spectrum CDMA," *IEEE Transactions on Communications*, vol. 42, no. 12, pp. 3178–3188, December 1994.

[59] Jerry M. Mendel, "Tutorial on higher-order statistics (spectra) in signal processing and system theory: Theoretical results and some applications," *Proceedings of the IEEE*, vol. 79, no. 3, pp. 278–305, March 1991.

[60] John Meurling and Richard Jeans, *Mobil telefoni*: Informationsförlaget, 1994.

[61] Scott L. Miller, "An adaptive direct-sequence code-division multiple-access receiver for multiuser interference rejection," *IEEE Transactions on Communications*, vol. 43, no. 2/3/4, pp. 1746–1755, Feb./Mar./Apr. 1995.

[62] Scott L. Miller and Afonso N. Barbosa, "A modified MMSE receiver for detection of DS-CDMA signals in fading channels," in *Proceedings of the IEEE Military Communications Conference*, vol. 3, 1996.

[63] Peter Monsen, "Feedback equalization for fading dispersive channels," *IEEE Transactions on Information Theory*, vol. 17, no. 1, pp. 56–64, January 1971.

[64] Peter Monsen, "MMSE equalization of interference on fading diversity channels," *IEEE Transactions on Communications*, vol. 32, no. 1, pp. 5–12, January 1984.

[65] Eric Moulines, Pierre Duhamel, Jean-François Cardoso, and Sylvie Mayrargue, "Subspace methods for the blind identification of multichannel FIR filters," *IEEE Transactions on Signal Processing*, vol. 43, no. 2, pp. 516–525, February 1995.

[66] Alan V. Oppenheim and Ronald W. Schafer, *Digital Signal Processing*: Prentice-Hall International, 1975.

[67] Tony Ottosson. *Coding, Modulation and Multiuser Decoding for DS-CDMA systems*, PhD thesis, Chalmers University of Technology, Göteborg, Sweden, December 1997.

[68] Peter van Overschee and Bart L. R. De Moor, *Subspace Identification for linear systems: Theory—Implementation—Applications*: Kluwer Academic Publishers, 1996.

[69] Stefan Parkvall, Erik Ström, and Björn Ottersten, "The impact of timing errors on the performance of linear DS-CDMA receivers," *IEEE Journal on Selected Areas in Communications*, vol. 14, no. 8, pp. 1660–1668, October 1996.

[70] Charles N. Pateros and Gary J. Saulnier, "An adaptive correlator receiver for direct-sequence spread-spectrum communication," *IEEE Transactions on Communications*, vol. 44, no. 11, pp. 1543–1552, November 1996.

[71] Brent R. Petersen and David D. Falconer, "Minimum mean square equalization in cyclostationary and stationary interference—analysis and subscriber line calculations," *IEEE Journal on Selected Areas in Communications*, vol. 9, no. 6, pp. 931–940, August 1991.

[72] H. Vincent Poor, *An Introdution to signal detection and estimation*. UK: Springer-Verlag, 2nd edition, 1995.

[73] John G. Proakis, *Digital Communications*. New York, NY: McGraw–Hill, 2nd edition, 1989.

[74] Predrag B. Rapajic and Branka S. Vucetic, "Adaptive receiver structures for asynchronous CDMA systems," *IEEE Journal on Selected Areas in Communications*, vol. 12, no. 4, pp. 685–697, May 1994.

[75] Jack Salz and Jack Winters, "Effect of fading correlation on adaptive arrays in digital wireless communication," in *Proceedings of the IEEE Vehicular Technology Conference*, St. Louis, May 1993, pp. 1768–1774.

[76] Louis L. Scharf, *Statistical Signal Processing*: Addison-Wesley, 1990.

[77] Kenneth S. Schneider, "Optimum detection of code division signals," *IEEE Transactions on Aerospace and Electronic Systems*, vol. 15, no. 1, pp. 181–185, January 1979.

[78] John J. Shynk and Richard P. Gooch, "The constant modulus array for cochannel signal copy and direction finding," *IEEE Transactions on Signal Processing*, vol. 44, no. 3, pp. 652–660, March 1996.

[79] Mikael Sternad and Anders Ahlén, "The structure and design of realizable decision feedback equalizers for IIR channels with colored noise," *IEEE Transactions on Information Theory*, vol. 36, no. 4, pp. 848–858, July 1990.

[80] Mikael Sternad, Anders Ahlén, and Erik Lindskog, "Robust decision feedback equalizers," in *Proceedings of the IEEE International Conference on Acoustics, Speech and Signal Processing*, vol. 3, Minneapolis, MN, April 1993, pp. 555–558.

[81] Petre Stoica and Mats Viberg, "Maximum likelihood parameter and rank estimation in reduced-rank multivariate linear regressions," *IEEE Transactions on Signal Processing*, vol. 44, no. 12, pp. 3069–3078, December 1996.

[82] Torsten Söderström and Petre Stoica, *System Identification*: Prentice Hall International, 1989.

[83] Shilpa Talwar, Mats Viberg, and Arogyaswami Paulraj, "Blind separation of synchronous co-channel digital signals using an antenna array—Part I: Algorithms," *IEEE Transactions on Signal Processing*, vol. 44, no. 5, pp. 1184–1197, May 1996.

[84] "TIA/EIA/IS-95 Interim Standard, Mobile Station-Base Station, Compatibility Standard for Dual-Mode Wideband Spread Spectrum Cellular System," July 1993.

[85] Claes Tidestav. "Optimum diversity combining in multi-user digital mobile telephone systems," Master's thesis, UPTEC 93094 E, Uppsala University, Uppsala, Sweden, December 1993.

[86] Claes Tidestav, "Designing equalizers based on explicit channel models of DS-CDMA systems," in *Proceedings of the 5th IEEE International Conference on Universal Personal Communications*, Cambridge, MA, October 1996, pp. 131–135.

[87] Claes Tidestav, "Linear baseband modeling of direct-sequence code-division multiple access systems," in *Proceedings of RVK96*, Luleå, Sweden, June 1996, pp. 156–160.

[88] Claes Tidestav, Anders Ahlén, and Mikael Sternad, "Narrowband and broadband multiuser detection using a multivariable DFE," in *Proceedings of the IEEE International Symposium on Personal, Indoor and Mobile Radio Communications*, vol. 2, Toronto, Canada, September 1995, pp. 732–736.

[89] Claes Tidestav, Anders Ahlén, and Mikael Sternad, "A comparison of multiuser detection and interference rejection," in *Proceedings of RVK99*, vol. 1, Karlskrona, Sweden, June 1999, pp. 446–450.

[90] Claes Tidestav, Anders Ahlén, and Mikael Sternad, "Realizable decision feedback equalizers," in *Proceedings of the IEEE International Conference on Acoustics, Speech and Signal Processing*, Phoenix, AZ, USA, March 1999.

[91] Claes Tidestav and Erik Lindskog, "Bootstrap equalization," in *Proceedings of the 1998 IEEE International Conference on Universal Personal Communications*, Florence, Italy, October 1998, pp. 1221–1225.

[92] Claes Tidestav, Mikael Sternad, and Anders Ahlén, "Reuse within a cell—interference rejection or multiuser detection?," *IEEE Transactions on Communications*, vol. 47, no. 10, pp. 1511–1522, October 1999.

[93] Claes Tidestav, Mikael Sternad, and Anders Ahlén, "Reuse within a cell—interference rejection or multiuser detection?," in *Proceedings of the IEEE Vehicular Technology Conference*, vol. 2, Houston, TX, 1999, pp. 1618–1621.

[94] Lang Tong, Guanghan Xu, and Thomas Kailath, "Blind identification and equalization of multipath channels: A time domain approach," *IEEE Transactions on Information Theory*, vol. 40, no. 2, pp. 340–349, February 1994.

[95] Barry D. Van Veen and Kevin M. Buckley, "Beamforming: A versatile approack to spatial filtering," *IEEE ASSP Magazine*, vol. 5, no. 2, pp. 4–24, April 1988.

[96] Mahes K. Varanasi and Behnaam Aazhang, "Multistage detection in asynchronous code-division multiple-access communications," *IEEE Transactions on Communications*, vol. 38, no. 4, pp. 509–519, April 1990.

[97] Alle-Jan van der Veen and Arogyaswami Paulraj, "An analytical constant modululs algorithm," *IEEE Transactions on Signal Processing*, vol. 44, no. 5, pp. 1136–1155, May 1996.

[98] Alle-Jan van der Veen, Shilpa Talwar, and Arogyaswami Paulraj, "Blind estimation of multiple digital signals transmitted over FIR channels," *IEEE Signal Processing Letters*, vol. 2, no. 5, pp. 99–102, May 1995.

[99] Sergio Verdú, "Minimum probability of error for asynchronous Gaussian multiple access channels," *IEEE Transactions on Information Theory*, vol. 32, no. 1, pp. 85–96, January 1986.

[100] Sergio Verdú, "Optimum multiuser asymptotic efficiency," *IEEE Transactions on Communications*, vol. 34, no. 9, pp. 890–897, September 1986.

[101] Paul A. Voois and John M. Cioffi, "Multichannel signal processing for multiple-head digital magnetic recording," *IEEE Transactions on Magnetics*, vol. 30, no. 6, pp. 5100–5114, November 1994.

[102] Ronald K. Wangsness, *Electromagnetic Fields*: Wiley, 2nd edition, 1986.

[103] Jack Winters, "On the capacity of radio communication systems with diversity in a Rayleigh fading environment," *IEEE Journal on Selected Areas in Communications*, vol. 5, no. 5, pp. 871–878, June 1987.

[104] Jack Winters, "Optimum combining for indoor radio systems with multiple users," *IEEE Transactions on Communications*, vol. 35, no. 11, pp. 1222–1230, November 1987.

[105] Zhenhua Xie, Robert T. Short, and Craig K. Rushforth, "A family of suboptimum detectors for coherent multiuser communications," *IEEE Journal on Selected Areas in Communications*, vol. 8, no. 4, pp. 683–690, May 1990.

[106] Per Zetterberg. *Mobile Cellular Communications with Base Station Antenna Arrays: Spectrum Efficiency, Algorithms and Propagation Models*, PhD thesis, Royal Institute of Technology, Stockholm, Sweden, 1997.

[107] Fu-Chun Zheng and Stephen K. Barton, "On the performance of near-far resistant CDMA detectors in the presence of synchronization errors," *IEEE Transactions on Communications*, vol. 43, no. 12, pp. 3037–3045, December 1995.

[108] Karl J. Åström and Torsten Söderström, "Uniqueness of the maximum likelihood estimates of the parameters of an ARMA model," *IEEE Transactions on Automatic Control*, vol. 19, no. 6, pp. 769–773, December 1974.

[109] Kenth Öhrn. *Design of Multivariable cautious discrete-time Wiener filters*, PhD thesis, Signal Processing Group, Uppsala University, Uppsala, Sweden, May 1996.

[110] Kenth Öhrn, Anders Ahlén, and Mikael Sternad, "A probabilistic approach to multivariable robust filtering and open-loop control," *IEEE Transactions on Automatic Control*, vol. 40, no. 3, pp. 405–418, March 1995.